Katholieke Universiteit Leuven
Faculteit Bio-ingenieurswetenschappen

DISSERTATIONES DE AGRICULTURA

Doctoraatsproefschrift nr. 643 aan de faculteit Bio-ingenieurswetenschappen
van de K.U.Leuven

The Discrete Element Method (DEM) to Simulate Fruit Impact Damage during Transport and Handling

Proefschrift voorgedragen tot het
behalen van de graad van
Doctor in de Toegepaste
Biologische Wetenschappen

door

Michael VAN ZEEBROECK

APRIL 2005

Katholieke Universiteit Leuven
Faculteit Bio-ingenieurswetenschappen

DISSERTATIONES DE AGRICULTURA

Doctoraatsproefschrift nr. 643 aan de faculteit Bio-ingenieurswetenschappen
van de K.U.Leuven

The Discrete Element Method (DEM) to Simulate Fruit Impact Damage during Transport and Handling

Promotors:
Prof. H. Ramon, K.U.Leuven
Prof. J. De Baerdemaeker, K.U.Leuven

Leden van de examencommissie:
Prof. J. Delcour, K.U.Leuven, voorzitter
Prof. R. Van Audekercke, K.U.Leuven
Prof. B. Nicolaï, K.U.Leuven
Prof. P. Darius, K.U.Leuven
Dr. E. Tijskens, K.U.Leuven

Proefschrift voorgedragen tot het
behalen van de graad van
Doctor in de Toegepaste
Biologische Wetenschappen

door

Michael VAN ZEEBROECK

APRIL 2005

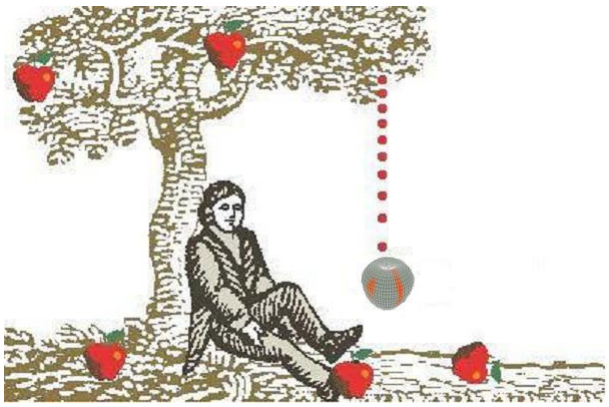

Voorwoord-preface

Mijn oprechte dank gaat uit naar mijn promotors, prof. Herman Ramon en prof. Josse De Baerdemaeker. Hun opmerkingen en suggesties hebben de kwaliteit van dit werk duidelijk verhoogd.
Prof. Herman Ramon wil ik bedanken voor het vertrouwen dat hij in mij stelde, voor de interesse die hij toonde, voor de aanmoedigingen indien het wat minder ging en vooral voor zijn nooit aflatend enthousiasme.

Dr. Bert Tijskens dank ik voor de begeleiding. Zijn ruime wetenschappelijke bagage heeft in belangrijke mate bijgedragen tot het welslagen van het onderzoek. Eveneens gaat mijn dank uit naar Edward Dintwa en Jimmy Loodts dat ik hun kennis over bepaalde domeinen van het onderzoek kon inroepen.

Verder wens ik de juryleden, prof. Jan Delcour, voorzitter, prof. Remy Van Audekercke, prof. Bart Nicolaï, prof. Paul Darius en Dr. Bert Tijskens te bedanken voor het grondig doornemen van de proeftekst, voor de (vele) zinvolle suggesties die de kwaliteit van de tekst duidelijk ten goede kwamen.

Er zijn echter nog vele andere mensen die ik bedanken moet: Veerle Van linden voor de goede samenwerking in sommige aspecten van het onderzoek en Sandra Landahl voor de hulpvaardigheid bij praktische problemen. Vassiliki Deli voor de toffe samenwerking tijdens de uitvoering van het blutsschadeproject. Dr. Bart De Ketelaere om mijn vragen over statistiek met deskundigheid te beantwoorden. Dirk Leroy en Bram Kamers voor de technische bijstand. Johan Verheyen van het fruitteeltcentrum en Jos Meesters van veiling Haspengouw voor het ter beschikking stellen van het onderzoeksmateriaal. Christel Vanfraechem, Petula Latet en Eric Lenaerts voor de goede administratieve zorgen.

De projecten waarbinnen het doctoraat tot stand kwam werden gefinancierd door het voormalige ministerie van Middenstand en Landbouw, het Instituut voor de aanmoediging van innovatie door Wetenschap en Technologie in Vlaanderen (IWT), het Fonds voor Wetenschappelijk Onderzoek in Vlaanderen (FWO) en het Verbond van Belgische Tuinbouwveilingen (VBT).

Mijn collega's in het laboratorium van Landbouwwerktuigkunde bedank ik voor de goede werksfeer en de aangename momenten tijdens de middagpauze en na de werkuren.

Mijn vrienden van Emmaüs en ex-kotgenoten in de ruime zin van het woord dank ik voor de hechte vriendschap van de afgelopen jaren. In alfabetische volgorde noem ik ze hier: Alexander, Arnout en Nele, Bart, Bosco en Jasmin, Dieter, Flip, Geert, Helga, Jeroen en Lotte, Koen, Koen en Mieke, Kristof, Maarten en Leen, Marc en Liesbeth, Pater Marc, Stefaan en Jessie, Stijn.

Mijn ouders wens ik te bedanken voor de interesse en het meeleven tijdens het wel en wee dat de voorbije vier en half jaar met zich meebracht. Ik dank ze ook om mijn zes jaar hogere studies mogelijk te maken. De rest van de familie en schoonfamilie dank ik eveneens voor de aanmoedigingen en interesse, zoals mijn broer Gerbrand, Ilke en oma.

Karine, nu alles bijna achter de rug is, ben ik blij dat ik het doctoraat toch afgemaakt heb. Dit heb ik alleen maar aan jou te danken. Je hebt me het zelfvertrouwen gegeven dat hiervoor nodig was. Bedankt voor je luisterend oor en goede raad. Mijn leven is opengebloeid door jou, ik ben heel blij en fier dat ik je mijn vrouw mag noemen. Ik hoop dat we nog een mooie toekomst tegemoet gaan, te beginnen in Congo… bedankt dat je dit wilt doen voor mij.

Ik draag dit werk op aan de straatkinderen van Lubumbashi en de Salesiaanse missionarissen in Congo.

Michael,
Heverlee, 26 maart 2005, Stille Zaterdag

List of publications

Peer-reviewed journals

Dintwa, E., Van Zeebroeck, M., Tijskens, E., Ramon, H. 2004. Torsional stiffness of viscoelastic spheres in contact. European physical journal B, 39, 77-85.

Dintwa, E., Van Zeebroeck, M., Tijskens, E., Ramon, H. 2005. Torsion of viscoelastic spheres. Granular matter. Accepted.

Dintwa, E., Van Zeebroeck, M., Tijskens, E., Ramon, H. 2005. Determination of parameters of a tangential contact force model for viscoelastic spheroids (fruits) using a rheometer device. Biosystems engineering. Accepted.

Van Zeebroeck, M., Dintwa, E., Tijskens, E., Deli, V., Loodts, J., De Baerdemaeker, J., Ramon, H. 2004. Determining tangential contact force model parameters for viscoelastic materials (apples) using a rheometer. Postharvest biology and technology, 33, 111-125.

Van Zeebroeck, M., Tijskens, E., Van Liedekerke, P., Deli, V., De Baerdemaeker, J., Ramon, H. 2003. Determination of the dynamical behaviour of biological materials using a pendulum device. Journal of sound and vibration, 266, 465-480.

Xing, J., Van linden, V., Van Zeebroeck, M., De Baerdemaeker, J. 2005. Bruise detection on Jonagold apples by visible and near-infrared spectroscopy. Food control, 16(4), 357-361.

Contributions to books

Tijskens, E., Van Zeebroeck, M., Ramon, H., De Baerdemaeker, J., Van Canneyt, T. 2002. DEM modelling for agricultural processes: an overview of recent projects. In: H. Konietzky (Ed) Numerical modelling in micromechanics via particle methods, A.A. Balkema Publishers, Rotterdam, The Netherlands.

Conference proceedings

Dintwa, E., Van Zeebroeck, M., Tijskens, E., Ramon, H. 2004. Determination of parameters of a tangential contact force model for spheroids (fruits) using a rheometer device. Proceedings of AgEng 2004, September 12-16, Leuven, Belgium, paper no 94-w3-564.

Tijskens E, Loodts, J., Van Zeebroeck, M., Van Liedekerke, P., Dintwa, E., Ramon, H. 2004. Particle Based Simulations with DEMeter++. Proceedings of Partec2004 International Conference for Particle Technology, March 16-18, Nuremberg, Germany.

Tijskens, E., Van Zeebroeck, M., Vanlinden, V., Van Liedekerke, P., Ramon, H., De Baerdemaeker, J. 2001. DEM modelling of agricultural processes: an overview of recent projects, M2SABI'01, IMACS/IFAC Fourth International Symposium on Mathematical Modelling and Simulation in Agricultural and Bio-Industries, June 12-14, Haifa, Israel.

Tijskens, E., Loodts, J., Van Zeebroeck, M., Van Liedekerke, P., Dintwa, E., Ramon, H. 2004. Particle simulations with DEMeter++. Proceedings of AgEng 2004, September 12-16, Leuven, Belgium, paper no 04-w3-568.

Tijskens, E., Van Zeebroeck, M., Ramon, H., De Baerdemaeker, J, Van Canneyt. 2002. DEM modelling for agricultural processes: an overview of recent projects. First International PFC Symposium, November 6-8, Gelsenkirchen, Germany.

Van Zeebroeck, M., Dintwa, E., Tijskens, E., Deli, V., Loodts, J., De Baerdemaeker, J., Ramon, H. 2003. Determining tangential contact force model parameters for viscoelastic materials (apples) using a rheometer. Proceedings of the 4th plant biomechanics conference, July 20-25, East Lansing, USA.

Van Zeebroeck, M., Tijskens, E., Dintwa, E., De Baerdemaeker, J., Ramon, H. 2004. The Discrete Element Method (DEM) to simulate fruit mechanical damage during transport: validation by shaking experiments. Proceedings of AgEng 2004, September 12-16, Leuven, Belgium, paper no 04-w4-513.

Van Zeebroeck, M., Tijskens, E., Dintwa, E., Loodts, J., De Baerdemaeker, J., Ramon, H. 2005. The Discrete Element Method (DEM) to simulate fruit mechanical damage during transport: effect of vibrations during transport on bruise damage. Acta horticulturae. Proceedings of Model-it conference, May 29- June 03, Leuven, Belgium, Accepted.

National publications

Van linden, V., Van Zeebroeck M, Deli, V., Ramon, H. De Baerdemaeker, J. 2002. Blutsschade van Jonagold: waar knelt het?, Belgische fruitrevue. Vakblad voor pomologische verenigingen en B.F.O., 54(4), 20-22.

Van linden, V., Van Zeebroeck, M., Deli, V., Ramon, H., De Baerdemaeker, J. 2002. Blutsgevoeligheid: waar knelt het?, Fruitteeltnieuws, Maart 2002.

VOORWOORD – PREFACE I

LIST OF PUBLICATIONS III

TABLE OF CONTENTS VI

SAMENVATTING 1

ABSTRACT 5

CHAPTER 1: INTRODUCTION 7

1.1 Mechanical fruit damage 7

1.2 Causes of mechanical fruit damage 8
1.2.1 The apple and tomato handling chain 8
1.2.2 Parameters affecting mechanical fruit damage 10

1.3 Literature research 11
1.3.1 Apple impact damage 11
1.3.2 Tomato impact damage 14

1.4 The Discrete Element Method (DEM) 15
1.4.1 Benefits of DEM in fruit impact research 15
1.4.2 Literature review of DEM in agriculture and food industry 16

1.5 Problem statement, objectives and outline of the thesis 17
1.5.1 Problem statement 17
1.5.2 Objectives 18
1.5.3 Outline 19

CHAPTER 2: THE DISCRETE ELEMENT METHOD (DEM) TO SIMULATE THE MECHANICAL VISCOELASTIC MATERIALS I.E. FRUITS 21

2.1 Introduction 21

2.2 General description of the Discrete Element Method (DEM) 22

2.3 The DEM software package: DEMeter++ 25

2.4 Contact force models 25

2.5 Normal contact force model 26
2.5.1 Literature review of normal contact force models 26
2.5.1.1 The classical theory of impact: stereomechanics 26
2.5.1.2 Contact mechanics approach 27
2.5.2 Contact force model selection for simulations of viscoelastic bodies like apples and tomatoes 35
2.5.3 Detailed discussion of the Kuwabara and Kono contact force model 39
2.5.3.1 Relationship between the spring parameter k and the material parameters 39
2.5.3.2 Relationship between damping parameter c and the material parameters 42
2.5.3.3 Special case: impact soft sphere - hard sphere or hard flat plate 44

2.6 Tangential contact force model 44

2.7 Conclusions 47

CHAPTER 3: DETERMINATION OF NORMAL CONTACT FORCE MODEL PARAMETERS FOR VISCOELASTIC MATERIALS (FRUITS) USING A PENDULUM DEVICE 49

3.1 Introduction 49

3.2 Development of pendulum device 50
3.2.1 Introduction 50
3.2.2 Description of pendulum device 51
3.2.3 Comparison of displacement during impact measured by the incremental encoder and measured by double integration of the accelerometer signal 57

3.3 Parameter estimation method to extract the parameters of the Kuwabara and Kono contact force model from experimental impact data 58
3.3.1 Introduction 58
3.3.2 Description of the indirect parameter estimation technique 59
3.3.3 Validation of the indirect parameter estimation technique 61
3.3.3.1 Sensitivity of cost function 61
3.3.3.2 Validation of the indirect parameter estimation technique using a Universal Testing Machine (UTS) 64

3.4 Basic analysis of the parameters of the Kuwabara and Kono contact force model for biological materials for impacts below the critical impact energy 66

3.5 Detailed study of the parameters of the Kuwabara and Kono contact force model for apples and tomatoes 70
3.5.1 Introduction 70
3.5.2 Apples 70
3.5.2.1 Materials and methods 70
3.5.2.2 Results and discussion 72
3.5.3 Tomatoes 84
3.5.3.1 Materials and methods 84
3.5.3.2 Results and discussion 85

3.6 Conclusions 96

CHAPTER 4: DETERMINATION OF THE TANGENTIAL CONTACT FORCE MODEL PARAMETERS FOR VISCOELASTIC MATERIALS (APPLES) USING A RHEOMETER 99

4.1 Introduction 99

4.2 Materials and methods 100
4.2.1 Description of the rheometer device 100
4.2.2 Determination of shear modulus G, viscosityη, apparent elastic modulus E 100
4.2.3 Determination of the dynamic friction coefficient μ 102
4.2.4 Validation experiments 104

4.3 Results and discussion 105
4.3.1 Shear modulus and viscosity 105
4.3.2 Friction coefficient 108
4.3.3 Validation experiments 108
4.3.3.1 Quasi-static validation (Validation of the Lubkin model) 108
4.3.3.2 Dynamic validation 111

4.4 Conclusions 117

CHAPTER 5: BRUISE PREDICTION MODELS FOR APPLES AND TOMATOES: STATISTICAL APPROACH 119

5.1 Introduction 119

5.2 Bruise prediction models for apples 121
5.2.1 Introduction 121
5.2.2 Materials and methods 122
5.2.2.1 Experimental setup 122
5.2.2.2 Statistical analysis 126
5.2.3 Results and discussion 127
5.2.3.1 Peak contact force as independent variable 129
5.2.3.2 Bruise volume: Impact energy as independent variable 140
5.2.4 Conclusions 144

5.3 Bruise prediction models for tomatoes 144
5.3.1 Introduction 144
5.3.2 Materials and methods 146
5.3.2.1 Experimental setup 146
5.3.2.2 Statistical analysis 147
5.3.3 Results and discussion 148
5.3.3.1 Models with absorbed energy as dependent and peak contact force as independent variable 149
5.3.3.2 Models with absorbed energy as dependent and impact energy as independent variable 154
5.3.4 Conclusions 159

5.4 Relation between bruising of Jonagold apples and packaging materials 160
5.4.1 Introduction 160
5.4.2 Materials and methods 160
5.4.2.1 Material 160
5.4.2.2 Methods 161
5.4.2.3 Statistical analysis 162
5.4.3 Results and discussion 162
5.4.3.1 Impact energy level 162
5.4.3.2 Peak contact force level 164

5.5 General conclusions 167

CHAPTER 6: VALIDATION OF THE DISCRETE ELEMENT METHOD TO PREDICT BRUISE DAMAGE TO FRUIT 171

6.1 Introduction 171

6.2 Materials and methods 172
6.2.1 Validation experiments: shaking box 173
6.2.2 Determination of the bruise model 175
6.2.3 Determination of the normal contact force model parameters 176
6.2.4 Computer simulations 176
6.2.5 Apple-apple impact vs. apple-hard plate impact 178

6.3 Results and discussion 179
6.3.1 Bruise models 179
6.3.2 Contact force model parameters 182
6.3.3 Comparison of the results of validation shaking box experiments with DEMeter++ simulations 183
6.3.3.1 Introduction 183
6.3.3.2 Comparison of validation experiment and simulation: acceleration signal 1 187
6.3.3.3 Comparison of validation experiment and simulation: acceleration signal 2 188
6.3.3.4 Comparison of validation experiment and simulation: acceleration signal 3 189
6.3.3.5 Comparison of validation experiment and simulation: acceleration signal 4 190

6.4 Conclusions 191

CHAPTER 7: CASE STUDY: DEM SIMULATION OF BRUISE DAMAGE DURING TRANSPORT OF APPLES AND TOMATOES 193

7.1 Introduction 193

7.2 Materials and methods 194

7.3 Simulation of apple bruise damage during transport 195
7.3.1 Effect of vibration frequency on apple bruise damage 195
7.3.2 Effect of stack height on apple bruise damage 199
7.3.3 Effect of apple size on bruise damage 204
7.3.4 Spatial distribution of apple damage in bulk bins 206
7.3.4.1 Introduction 206
7.3.4.2 Simulation of a real size bulk bin used in Belgium 206
7.3.4.3 Detailed study of the relation bruise damage - position 210
7.3.5 Effect of fruit properties on apple bruise damage 214
7.3.5.1 Introduction 214
7.3.5.2 Effect of apple temperature on bruise damage 215
7.3.5.3 Effect of harvest date on bruise damage 218
7.3.5.4 Effect of apple acoustic stiffness on bruise damage 220
7.3.6 Conclusions of the simulations of apple bruise damage during transport 221

7.4 Simulation of tomato bruise damage during transport 222
7.4.1 Introduction 222
7.4.2 Effect of tomato temperature on bruise damage (absorbed energy) 224
7.4.3 Effect of tomato ripeness on bruise damage (absorbed energy) 225
7.4.4 Effect of tomato size on bruise damage (absorbed energy) 225
7.4.5 Effect of vibration frequency on bruise damage (peak contact force) 228
7.4.6 Conclusions of simulations of tomato bruise damage during transport 228

7.5 General conclusions 229

CHAPTER 8: GENERAL CONCLUSIONS AND FUTURE WORK 231

8.1 General conclusions 231

8.2 Future work 236

ABBREVIATIONS 239

NOTATION 241

BIBLIOGRAPHY 245

Samenvatting

In dit doctoraatswerk werd een bijdrage geleverd aan het blutsschadeprobleem van vruchten (appels en tomaten), het meest belangrijke type van mechanische schade tijdens de naoogstbehandeling. Naast het rechtstreekse effect van blutsschade op de vruchtkwaliteit en de visuele appreciatie door de consument, bestaat ook het onrechtstreekse effect van contaminatie doordat pathogene organismen beschadigd weefsel kunnen binnendringen, met een drastische vermindering van de houdbaarheid van de vruchten tot gevolg.

Een computersimulatietechniek, genaamd Discrete-elementen Methode (DEM) of Granulaire Dynamica (GD), werd toegepast om inzichten te verwerven in het blutsschadeprobleem. DEM is in het kort samengevat een numerieke techniek waarmee het kinematische en dynamische gedrag van deeltjes ten gevolge van botsingen wordt gemodelleerd. Een deeltje is bijvoorbeeld een vrucht. In DEM worden alle krachten die op een individueel deeltje inwerken opgeteld. Deze krachten zijn meestal de zwaartekracht en contactkrachten (botsingskrachten). De bewegingsvergelijkingen van Newton en Euler worden geïntegreerd om de snelheden en de posities van de deeltjes in de volgende tijdstap te bekomen. DEM is ontstaan in het onderzoeksdomein van gesteentemechanica en wordt ook intensief gebruikt voor het simuleren van het dynamische gedrag van ingenieursmaterialen. Toepassing van DEM voor biologische materialen zijn tot op heden beperkt gebleven, zeker voor de ‘zachte’ biologische materialen zoals vruchten.

Omwille van het visco-elastische gedrag van de meeste biologische materialen zijn DEM simulaties complexer dan voor de harde elastisch-(plastische) materialen. Een groot deel van het doctoraatswerk werd besteed aan het leren omgaan met het visco-elastische karakter van de vruchten zodat DEM simulaties mogelijk worden. Meer in detail werden experimentele procedures ontwikkeld die het mogelijk maken om de parameters in visco-elastische contactkrachtenmodellen te bepalen. Deze contactkrachtenmodellen vormen een essentieel onderdeel van DEM, daar zij op een kwantitatieve manier de impactkrachten tussen de deeltjes bepalen. Typisch worden de contactkrachten ontleedt in hun normale en tangentiële component.

Een niet-lineaire kleinstekwadraten methode werd gebruikt om de parameters (stijfheid en demping) van het visco-elastische contactkrachtenmodel volgens Kuwabara en Kono voor normale impact tussen bollen te bepalen. Er werd aangetoond dat zowel de effectieve kromtestraal van de botsende deeltjes als de relatieve impactsnelheid een effect heeft op de parameters van het contactkrachtenmodel.

Een slinger werd ontwikkeld om de experimentele impactgrootheden (contactkracht, verplaatsing en verplaatsingssnelheid) van vruchten te bepalen. Er werd aangetoond dat een rechtstreekse meting van de verplaatsing d.m.v. een incrementeel encoder ('digitale hoekmeter') nauwkeuriger is dan de klassieke dubbele integratie van het accelerometersignaal.

Een experimentele procedure werd ontwikkeld om de parameters te bepalen van een visco-elastisch tangentieel contactkrachtenmodel door gebruik te maken van een reometer, een meettoestel normaliter gebruikt om de visco-elastische eigenschappen van vloeistoffen en semi-vaste stoffen te bepalen. Het visco-elastische tangentiële contactkrachtenmodel waarvan de parameters bepaald werden, was een visco-elastische uitbreiding van het klassieke Mindlin en Deresiewicz model voor elastische bollen. De reometer werd eveneens gebruikt om deze visco-elastische uitbreiding te valideren.

Een ander belangrijk deel van het doctoraatswerk handelde over blutspredictiemodellen. Deze modellen zijn weliswaar niet inherent aan DEM, maar wel essentieel voor de bruikbaarheid van DEM in het blutsschadeprobleem. De blutspredictiemodellen koppelen immers de contactkrachten tussen de deeltjes, die gemodelleerd worden door de contactkrachtenmodellen, met de eigenlijke mechanische schade. Meervoudige lineaire en niet-lineaire regressiemodellen werden ontwikkeld om ook vruchteigenschappen zoals rijpheid, stijfheid, vruchttemperatuur, kromtestraal, oogstdatum (enkel appels) en plaats van impact (enkel tomaten: hok of schot) te koppelen met de blutsschade. Blutsvolume werd gebruikt als maat voor blutsschade van appels. Geabsorbeerde energie werd aangewend als maat voor blutsschade van tomaten, omdat een objectieve methode voor het opmeten van de bluts bij tomaten nog niet beschikbaar is. Interessante interacties tussen de vruchteigenschappen onderling maar vooral tussen de piekcontactkracht (of impactenergie) en de vruchteigenschappen werden geïdentificeerd.

De validiteit van de DEM voor het modelleren van de blutsschade werd nagegaan voor Jonagold-appels. 'Blutsschade' werd verkozen als validatieparameter boven het meer gebruikelijke 'traject gevolgd door de deeltjes'. De blutsschade van de appels in kisten, welke werden geschud met een precies bepaald acceleratiesignaal op een electro-hydraulische schudstand, werd vergeleken met de blutsschade berekend uit DEM-computersimulaties met identieke initiële condities als in de reële experimenten. Uit deze validatie experimenten kon worden besloten dat DEM op een voldoende nauwkeurige wijze de blutsschade van appels ten gevolge van trillingen kan modelleren.

Ter afsluiting van het onderzoek werd een 'case studie' uitgevoerd, gebruik makende van de DEMeter++ software en de opgemeten parameters van de contactkrachten- en blutsmodellen. Simulaties tot 1500 deeltjes werden uitgevoerd. De case studie bestond erin dat het effect

van mechanische parameters en van vruchteigenschappen op trillingsschade (impactschade ten gevolge van trillingen) van appels en tomaten werd nagegaan. Het bulktransport van appels (appels getransporteerd in palloxen) en het transport van tomaten in EPS kistjes werd onderzocht. Als acceleratiesignaal werd een verticale sinus aangelegd. De bestudeerde mechanische parameters waren piekacceleratie en frequentie van het trillingssignaal, de stapelhoogte en de grootte van de appels en de tomaten. De bestudeerde vruchteigenschappen bestonden uit de vruchttemperatuur, de rijpheid, de stijfheid en de plukdatum (enkel appels). Er werden grote effecten van de mechanische parameters maar bescheiden effecten van de vruchteigenschappen op de blutsschade opgetekend. Voor de appels werd ook een gedetailleerde studie uitgevoerd van de relatie tussen appelpositie in de stapeling en blutsschade. Zo werd aangetoond dat de positie - blutsschade relatie afhankelijk is van de acceleratie-amplitude, trillingsfrequentie en stapelhoogte. Tenslotte werd ook het bestaan van ‘schadeketens’ in een stapel appels aangetoond, wat in analogie is met de in de literatuur uitvoerig beschreven krachtketens in bulkmaterialen.

Abstract

In this thesis a contribution was made to the fruit (apples and tomatoes) bruising problem, the most important type of postharvest mechanical injury. Besides the direct effect of fruit bruising on fruit quality, and, hence, the visual quality appreciation by the consumer, an important indirect effect can be identified as damaged tissue is a good avenue for entrance of decay organisms, which decrease the shelf-life of the fruit drastically.

A computer simulation technique, named the Discrete Element Method (DEM) or Granular Dynamics (GD) was applied to get insight in the bruising problem. DEM is essentially a numerical technique to model the kinematic and dynamic behaviour of particles interacting with each other through collisions. One fruit, for example, can be considered as a particle. In DEM the forces acting on the particles (gravity force and contact force) are summed and the equations of motion of Newton and Euler are integrated to obtain the velocity and position of the particles in the next time step. DEM originated in the field of rock mechanics and has been used extensively for engineering materials, but its application for biological materials is limited, especially for 'soft' biological materials like fruits.

Due to the viscoelastic nature of biological materials DEM simulation are more complicated than for hard elastic-(plastic) materials. A major part of the research was dedicated to cope with the viscoelastic nature of fruits for its use in DEM. Experimental procedures were developed to determine the parameters of viscoelastic contact force models. Contact force models are an essential part of DEM, because they determine quantitatively the contact (impact) forces between the particles. Contact force models are typically decomposed into normal and tangential components.

A nonlinear least squares technique was used to estimate the parameters (stiffness and damping) of the Kuwabara and Kono viscoelastic contact force models for normal impacts between spheres. It was demonstrated that both the effective radius of curvature of the impacting particles as their relative impact velocity have an effect on the model parameters.

A pendulum device was developed to determine the experimental impact quantities, contact force, displacement and displacement rate of fruit impacts. It was indicated that direct measurement of the displacement by an optical incremental encoder is more accurate than double integration of an acceleration signal.

An experimental procedure was developed to determine the parameters of a viscoelastic tangential contact force model by a rheometer, a device normally intended to measure viscoelastic properties of fluids and semi-fluids. The derived viscoelastic tangential contact

force model is an extension of the Mindlin and Deresiewicz model for elastic spheres. The rheometer was used to demonstrate the validity of this model extension.

Another major part of this thesis was about bruise prediction models. These models are not inherent to DEM, but essential for the utility of DEM for the bruising problem, because they relate contact force during impact, as modelled by the contact force models, with the real bruise damage. Multiple linear and nonlinear regression models were developed to link fruit properties like ripeness, acoustic stiffness, fruit temperature, radius of curvature, harvest date (only apples), location of impact (only tomatoes: partition or compartment of tomato) with the bruise damage. Bruise volume was taken as a measure of apple bruising. Absorbed energy was taken as a measure for tomato bruising, because of the lack of an objective bruise size measurement method for tomatoes. Besides main effects of fruit properties, also some interesting mutual interactions and interactions between fruit properties and peak contact force (or impact energy) were investigated.

The validity of DEM in its prediction of the bruise damage has been validated for Jonagold apples. 'Bruise damage' was preferred above the common 'particle trajectory' as validation parameter. The bruise damage of apples in boxes that were shaken with a well defined acceleration signal on an electro-hydraulic shaker was compared with that calculated from DEM simulations with the same setup and initial conditions. The validations indicated that DEM can predict apple bruise damage in an acceptable way.

At last, a case study was performed by using the DEM++ software and all therefore developed models, in which simulations up to 1500 particles were performed. The influence of mechanical parameters and fruit properties on the vibration damage of apples and tomatoes was investigated. More specifically, the bulk transport of apples in bins and tomatoes in EPS crates was investigated. As acceleration input a sine in the vertical direction was applied. The investigated mechanical parameters were peak acceleration and frequency of the vibration signal, stack height and size of apples and tomatoes. The investigated fruit properties were fruit temperature, ripeness, acoustic stiffness and harvest date (only apples). Major influences of mechanical parameters on the vibration damage were identified, in particular stack height and fruit size, and minor influences of fruit properties. For apples a detailed study was performed in addition to investigate the relation between apple position in the stack and bruise damage. It was demonstrated that the position - bruise damage relation is dependent on acceleration amplitude, vibration frequency and stack height. The existence of damage chains within the core of the apple stack was also identified, which is in accordance with the well-known force chains in bulk materials.

Chapter 1

Introduction

1.1 Mechanical fruit damage

The physical properties of the ancestral fruits were related to the dispersal of their seeds by animals. As a consequence, fruit tissue is often soft and prone to fast decay so that the seeds can be released rapidly after detachment of the tree. Commercial production of fruits requires different mechanical attributes so that the soft tissues survives their journey through the marketing chain in a state suitable for human consumption (the seeds will be discarded). Consumers' demand for high quality products, especially in the Western world, has increased last decades and is still increasing. However, not only the visual aspect of mechanical damage (in the case of apples enzymatic browning) can be mentioned, but also a higher risk of bacterial and fungal invasion, leading to a lower shelf-life of the fruits. In addition, Wilson *et al.* (1999) reported that the moisture loss of a single bruised apple is increased by as much as 400 % compared to that of an intact apple.

For most fruit types, including apples and tomatoes, bruising is the most common type of postharvest mechanical injury. A survey for 12 years on the New York market indicated that 6 % of apples and 1 % of tomatoes were affected by bruising. However, most likely these percentages are underestimated. In the New York market studies mechanical injury was never the most common defect for most fruits (including apples and tomatoes). Usually one or more kinds of fungal disease exceeded mechanical injury. The fungi were often gray mold (*Bortrytis*) or blue mold (*Penicillium*). Like most postharvest pathogens, these organisms cannot infect healthy tissue. Typically they enter through dead or wounded tissue before parasitizing the rest of the fruit. It is likely that minor mechanical injuries were not counted by the market inspectors and were only seen through their consequences in fungal infections.

So, mechanical injury could be the most important cause of defects and disease. If mechanical injury could be avoided there would be less need for fungicides to prevent disease and there would be much less loss of fruit (Knee and Miller, 2002). Studman (1997) indicated that apple bruising can result in product losses up to 50 %, although typically loss levels are in the 10 to 25 % range, depending on consumer's awareness.

The economical cost of mechanical damage to apples in Belgium was estimated. The percentage of degraded apples identified during sorting, from which bruised apples have a major part, was in the years 2000 and 2001 respectively 15 % and 8 %. On the Belgian market the auction price for degraded apples (industrial apples, apples not suitable for fresh market) is 1/3 of the normal price. Knowing the total apple production and the average auction price in these years a reduction of only 10 % in degraded apples could lead to an income increase for the growers by 892 000 € in 2000 and 595 000 € in 2001. Further, some (smaller) bruise damage can not be detected during grading and damage can still be contracted after the visual grading of the apples. This is leading to the presence of bruised apples in the supermarkets and stores. These bruised apples are not sold, leading to an income loss for the supermarkets and traders. Further, if bruising becomes visible after the apple is commercialized, this will lead to a negative appreciation by the consumer that will influence their purchases in the future.

Also for tomatoes an economical drawback of bruising can be mentioned. An economical calculation could not be made because of the lack of data about tomato degrading during sorting.

1.2 Causes of mechanical fruit damage

1.2.1 The apple and tomato handling chain

A distinction has to be made between preharvest and postharvest mechanical damage. Fruits can be injured in several ways while still on the plant. During growth they may come into contact with other fruits or other parts of the plant such as branches causing abrasion, puncture and bruising. Herbivorous animals, slugs, insects, birds and mammals, can puncture the skin and consume a proportion of the tissue. Weather is another important cause of damage: wind can aggravate damage caused by contact with other parts; hail causes impacts bruises that can be locally devastating for fruit production. Apart from predation, preharvest mechanical damage is infrequent or sporadic and not easily controlled. Affected fruit will be culled either on the field or in the packing house (Knee and Miller, 2002).

Further damage to the fruit is caused by human handling. This begins at harvest, which still occurs by hand for most fruits. If the fruit does not detach easily from the plant it can be injured by the force of the hand. This is particularly true when two or three fingertips are used to pull, and so growers plead for the use of a whole hand grip and a bending movement to concentrate the force on the pedicel (Knee and Miller, 2002).

After harvest the fruit begins its long, bumpy ride from the field, greenhouse or orchard to the consumer. It may pass through several containers and modes of transport along the way. Every time there is an unloading of the container a danger exists for impact with other fruits, containers and equipment used to sort and pack the fruit.

In more detail the following stages in handling can be distinguished for apples on the Belgian market (although some adaptations are possible): transfer of the apples from the picking baskets into wooden bulk bins, transport on fork-lift tractor in the orchard, possibly bulk transport (small truck or on tractor trailer) to storage rooms (Controlled Atmosphere, CA)[1], before marketing: transport to the auction, unloading of bulk bins, grading and sorting, transfer to other packaging types (carton-, wooden-, plastic crates, etc.), transport by the seller to the store and at last transport by the customer. For tomatoes the transport chain is somewhat different, the substantial difference is the lack of bulk transport of tomatoes in Belgium. Punctures, cuts, bruises and abrasions can result, depending on how contact is made and on the nature of the surface with which contact is made. Bruising is the major postharvest mechanical damage problem (Knee and Miller, 2002). However, for tomatoes also the puncture of one tomato stalk in the flesh of another tomato is a considerable problem. Research on this topic was recently performed by Desmet *et al.* (2003, 2004ab) and Allende *et al.* (2004).

Dynamic forces during fruit transport and handling are causing by far the most bruise damage, because these forces are higher in incidence and magnitude than static forces (Mohsenin, 1986).

[1] Sometimes a presorting of the apples is executed before CA storage, during this storage apples are also kept in bulk bins

1.2.2 Parameters affecting mechanical fruit damage

The management of fruit quality in distribution begins with understanding the nature of the distribution chain, from production to consumption, and defining the components that make up the chain.
In order to understand the causes and mechanisms of fruit impact and vibration damage, it is necessary to study the following aspects (adapted from Hilton, 1994):

A. The source, magnitude and nature of the impact and vibration input:

- Single fruit impacting against single fruit
- Fruit container subjected to drop impact
- Fruit container subjected to transport vibration
- Vibration response of transport vehicle to road surface

B. The influence of the packaging material and the container itself, for example:

- Cushioning and damping properties of packaging material
- Dynamic response of the box itself
- Friction between the fruit and the container

C. The influence of individual fruit and neighboring fruit in modifying the impact or vibration input, for example:

- Cushioning effect of neighboring fruit
- Interaction between dynamics of fruit and packaging material

D. The susceptibility of the fruit to damage, as a function of maturity, temperature, size, cultivar, etc.

These factors are interrelated and the quality of the fruit at the end of the chain and the cost of maintaining quality are function of all these components and their interactions (Schoorl and Holt, 1982).

1.3 Literature research

.

1.3.1 Apple impact damage

The 40 years of research about apple bruise impact damage was divided in different categories. It can be stated that 90 % of all the research about fruit impact damage was performed on apples.

An overview is given of all the research, subdivided in different categories. In Table 1-1 a schematic overview is presented of the references to the different research categories.

Research *category 1* is about physical impact modelling, either based on elastic theory (Hertz theory) (*1a*) or on viscoelastic theory (*1b*). These models are able to predict to some extent the critical dropt height or bruise size based on the elastic or viscoelastic properties of the apples. In Chapter 5 examples of some theoretical models will be presented.

Research *category 2* can be called 'impact damage energy analysis'. In this research category, bruise damage (mostly bruise volume) is correlated with either impact energy or absorbed energy. The equipment that is used is a drop tester (one apple or column of apples) or pendulum. This category could be divided in three subcategories: *2a*) research on the effect of drop height on bruise damage for one or more cultivars, mostly in association with impact on hard plates, *2b*) the effect of fruit properties (temperature, ripeness, water potential, storage time...) on bruise damage, in other words, research on the bruise sensitivity of the apples and *2c*) research on the effectiveness of packaging materials in diminishing the bruise damage and research on apple-apple impact. All these subcategories will be discussed in Chapter 5.

A new impulse was given to the apple impact damage research with the development of the electronic fruit IS-100 in the USA in the late eighties (research *category 3*). The electronic fruit is in fact a triaxial accelerometer covered by a spherical shaped soft plastic coating (*3a*). The magnitude of the acceleration or deceleration of the sphere during impact is recorded. The development of this device was a breakthrough in identifying critical areas in the fruit handling. Later an electronic fruit was developed in Germany on the basis of force sensors: PMS-60 (*3b*). A lot of research was performed to correlate the acceleration signal of the electronic fruit IS-100 with the actual bruise damage by applying MLRA models (Multiple Linear Regression Analysis) (*3c*).

As an alternative for the use of the electronic fruits, a tactile film, Tekscan®, originally developed to help dentists determine how patient's teeth are contacting, was proposed for measuring contact pressures between fruits (research *category 4*).

Research *category 5* can be called 'study of the effect of vibrations on apple bruise damage', attempts to correlate bruise damage with accelerations during transport either on the field or on the road (*5a*). Pioneer research on vibration was already performed in the sixties-seventies, but for the research no apples were used (*5b*). In Chapter 7 more details about this topic will be discussed.

Research *category 6* handles about characterizing the dynamic stresses. Devices (drop or pendulum design) were developed to characterize the impact on the force, displacement, displacement rate and pressure level. In Chapter 3 more details about this research topic will be discussed.

Research *category 7* involves impact failure mechanisms. Bruising was identified as a consequence of the propagation of cell wall ruptures, breaking of intercellular bonds or cell deflation as a result of loss of cell fluid. Some authors took their analysis down to the cellular level by modelling the cell mechanical response to external load. However, most research about failure mechanism has been done by means of quasi-static compression.

Research *category 8* is about field studies (without electronic fruit, but by direct measuring of the bruise damage) and practical guidelines.

Research *category 9* handles about simulations. Two studies were performed with finite elements (*9a*) and also one study with Discrete Elements (*9b*). The Discrete Element Method will be discussed in Chapters 2, 6 and 7.

Table 1-1: Reference overview of different research categories in apple impact damage

	Research category	*References*	*Chapter*
1	Physical impact modeling 1a: Elastic theory 1b: Viscoelastic theory	1a: Horsfield *et al.* 1972; Mohsenin *et al.*, 1978; Siyama *et al.*, 1988	5
		1b: Hamann, 1970; Peleg, 1984; Gran-mor and Galili, 2000	5
2	Impact damage energy analysis 2a: Effect drop height 2b: Fruit properties	2a: Holt and Schoorl, 1977,1983a,1984a; Schoorl and Holt, 1974,1980,1982b; Diener *et al.,* 1979; Holt *et al.,* 1981; Klein, 1987; Brusewitz and Bartsch, 1989; Bajema and Hyde, 1992; Puchalski and Gorzelany,1992; Blahovec, 1999; Menesatti and Paglia, 2001; Menesatti *et al.*, 2002	5
	2c: Packaging materials	2b: De Baerdemaeker *et al.*, 1978; Schoorl and Holt, 1977; Diener *et al.,* 1979; Holt and Schoorl, 1984; Brusewitz and Bartsch, 1989; Garcia *et al.*, 1995; Verstreken *et al.*, 1995; Studman, 1997; Hyde, 1993, 2001; Baritelle and Hyde, 2000,2001	5

		2c: Hammerle and Mohsenin, 1966; Mohsenin *et al.,* 1978; Holt and Schoorl, 1981; Peleg, 1981; Schoorl and Holt, 1982; Holt and Schoorl, 1983a; Holt and Schoorl, 1984; Chen and Yazdani, 1989,1991; Pang *et al.*, 1992; Pang *et al.*, 1996; Studman *et al.*, 1997	5
3	Electronic fruit research 3a: IS-100 field research 3b: PMS-60 3c: MLRA using IS-100	3a: Brown *et al.,* 1990; Bollen and Dela Rue, 1990 ; Tennes *et al.*, 1990; Sober *et al.,* 1990 ; Zapp *et al.*, 1989, 1990; Schulte-Pason *et al.*, 1989, 1990ab; Pang *et al.,* 1991; Jourdain *et al.,* 1993 ; Garcia *et al.*, 1994 ; Ragni and Berardinelli, 2001	/
		3b: Herold *et al.*, 1993, 1996	5
		3c: Siyama *et al.*, 1988; Timm *et al.*, 1989; Sober *et al.,* 1989, 1990; Chen and Yazdani, 1989,1991; Schulte *et al.,* 1992; Ragni and Berardinelli, 2001	5
4	Tekscan®	Geyer *et al.,* 1999	5
5	Study of the effect of vibrations on apple bruise damage 5a: Apples 5b: Other fruit	5a: Schoorl and Holt, 1982a, 1985; Holt and Schoorl, 1985; Peleg and Hinga, 1986; Schulte-Pason *et al.*, 1989, 1990a; Armstrong *et al.*, 1991; Jones *et al.*, 1991; Hinsch *et al.*, 1993; Singh and Xu, 1993; Timm *et al.*, 1996; Timm *et al.*, 1998; Bollen *et al.*, 2001	7
		5b: O'Brien *et al.*, 1963, 1965, 1969ab, 1972; O'Brien and Guillon, 1969; Chesson and O'Brien, 1971; O'Brien, 1974; Plumbee and Webb, 1974	7
6	Devices characterizing the dynamic impact	Fluck *et al.,* 1973; Finney and Massie, 1975; Jindal and Mohsenin, 1976; Chen *et al.*, 1985; Luan and Rohrbach, 1989; Bajema and Hyde, 1998; Van Zeebroeck *et al.*, 2003	3
7	Impact failure mechanisms	De Baerdemaeker, 1975; Segerlind, 1978; Pitt, 1982; Pitt and Chen, 1983; Holt and Schoorl, 1982, 1983b, 1984b; Van Woensel and De Baerdemaeker, 1983; Vincent, 1990; Gao and Pitt, 1991; Roudot *et al.,* 1991; Khan and Vincent, 1990, 1991, 1993ab; Abbott and Lu, 1996	/
8	Field studies / practical guidelines	Schoorl and Holt, 1982c; 1986; Holt *et al.,* 1983; Sargent *et al.,* 1986; Burton *et al.,* 1989	/
9	Finite/discrete element modeling 9a: Finite element 9b: Discrete element	9a: Rumsey and Fridley, 1977; Wu *et al.*, 1994	/
		9b: Rong *et al.,* 1993	2,6,7

1.3.2 Tomato impact damage

The research about tomato mechanical damage is limited. For tomatoes a distinction has to be made between tomatoes for industrial use, which are sometimes mechanically harvested and are transported in bulk and tomatoes for the fresh market. In Belgium only tomatoes for the fresh market are grown (in green houses). O'Brien *et al.* (1972; 1974) investigated mechanical damage during bulk transport of industrial tomatoes. Besides bruises, defined as soft tissue, also cracks (with or without juice loss) were identified. Sargent *et al.* (1989ab; 1992) investigated mechanical damage of tomatoes for the fresh market. A distinction was made between internal and external bruising. Internal bruising was described by Hatton and Reeder (1963) as a breakdown of the locular gel from the normal clear, pink colour to a cloudy, yellowish stringy, gelatinous tissue. Internal bruising starts at lower impact levels compared to external bruising. This kind of damage can not be identified by inspection in the green house, only the consumer will notice it after slicing of the tomato. Sargent *et al.* (1989ab; 1992) divided the external damage in bruising, cracks and puncture. Bruising was described as a perceptible, permanent deformation of the outer surface. A classification was made in two categories: bruise diameter < 5 mm and bruise diameter > 5 mm. Further, besides research on the prevalence of internal and external bruise damage in practice also drop test of intact tomatoes were performed. In these drop tests, the effect of tomato ripeness on internal and external damage was investigated. Adegoroye and Eniayeju (1988) investigated the effect of container material and shape as used in Nigeria on tomato mechanical damage. Olorunda and Tung (1985) compared the effect on mechanical damage between traditional containers as used in Nigeria with improved ones for different tomato maturity stages.

Sargent *et al.* (1992a) used the electronic fruit IS-100 to investigate impacts on a tomato packing line. Herold *et al.* (2001) investigated with the electronic fruit PMS-60 the forces during mechanical harvesting and bulk transport of tomatoes. Desmet *et al.* (2004b) utilized the PMS-60 to investigate the forces during the production chain of fresh market tomatoes in Belgium. One type of mechanical damage, puncture of tomatoes by their stalks, was investigated in detail by Desmet *et al.* (2003, 2004ab) and Allende *et al.* (2004).

Due to the lack of tissue discolouration no objective method is available to measure the size of external bruising of tomatoes. To some degree the diameter of the flattened soft tissue can be measured, as was done by Sargent *et al.* (1989ab), but only as an approximation, not on a precise and accurate way like it can be done for apples.

1.4 The Discrete Element Method (DEM)

The Discrete Element Method (DEM) is essentially a numerical technique to model the kinematics and dynamics of an assembly of particles interacting with each other through collisions. In Chapter 2 more details about this simulation technique will be provided.

1.4.1 Benefits of DEM in fruit impact research

Several benefits of DEM simulations in the fruit bruising problem can be mentioned:

- DEM can be a *supplement* to the electronic fruit measurements in impact monitoring. Although the benefits of the use of electronic fruits cannot be underestimated, there are also some constraints involved. The electronic fruit dynamic response is different from the fruit itself. Although the recorded forces by the electronic fruit are a measure of the impact environment and may be used to identify locations in the handling chain that require the most urgent attention, the recorded data does not represent the precise forces acting on the fruits. Studman and Pang (1990) admit the considerable difficulty in relating the output of the electronic fruit to the actual level of fruit damage.

- A considerable benefit of DEM simulations is its *completeness*. In a simulation of for example a shaking box of apples, at every moment for every apple in the stack, the forces a particular apple experiences are known. Something that is completely impossible by the use of electronic fruits. This can lead to new insights in the fruit damage problem.

- DEM simulations are *repeatable*. For example a simulation of a shaking box of apples can be repeated with exactly the same stacking and mechanical properties of the apples but at different vibration intensities and frequencies. This is not achievable in practice leading to unwanted variability (experimental and biological), obscuring to conclusions of the effect of acceleration intensity and frequency on bruise damage.

- DEM is a huge *time and money saving* methodology. Two examples can be given to illustrate this. First of all, it is practically almost impossible to measure accurately the bruising spots of ± 1500 apples in a bulk container. Second, improvements in the production chain, like the use of less damaging machine parts, can be simulated to

test its effectiveness, before switching to expensive and time consuming adaptations in practice.

- A last benefit and the ultimate goal is to *optimize* the process and design parameters by minimizing bruise damage. As an example, the design of better packaging materials can be mentioned.

1.4.2 Literature review of DEM in agriculture and food industry

In DEM research a distinction has to be made between soft and firm biological materials. Most research has been done on firm biological materials. *Grain silo behaviour* (Holst *et al.* 1999ab; Rotter *et al.*, 1998; Lu *et al.*, 1997; Negi *et al.*, 1997, Jofriet *et al.*, 1997; Rong *et al.*, 1995 ab) with DEM is mostly investigated. In addition work has been performed on *segregation of rice* (Sakaguchi *et al.,* 1998, 2001), *gravity flow of rice* (Sakaguchi and Favier, 1998; Sakaguchi *et al.*, 1994), *grain flow in a hopper* (Kremmer and Favier, 1999), *compression of oil seed beds* (Raji and Favier, 1998, 1999, 2004) and the effect of *impact on the sugar cane stem* (Schembri and Harris, 1996). More recently the spreading of granular fertilizer grains was investigated (Tijskens *et al.,* 2001).

The research on the DEM for soft biological materials, the research area of this thesis, is very limited. However, outstanding pioneer work has been done by Graham Rong in 1993 on DEM simulation of in transit fruit damage (Rong *et al.,* 1993). A 2D DEM simulation of 12 apples was performed. In the simulation the effect of shocks due to road irregularities on the forces between the disks (apples) was tested. The parameters of the contact force models were not measured but estimated based on literature mechanical property data.

By this Dr. Rong could be considered as the pioneer of DEM simulation in agriculture and food industry. Besides the pioneering work on fruit bruise damage, he did also pioneer DEM research on grain silos (Rong *et al.,* 1995), both topics were part of his PhD thesis “DEM for flow of particulate materials in bins” (1994).

1.5 Problem statement, objectives and outline of the thesis

1.5.1 Problem statement

Forty years of research on the fruit damage problem have been performed, and no doubt the incidence of bruising has decreased compared to forty years ago, the problem is still one of the major problems in the fruit business. The reason for this is that the causes and mechanisms of impact and vibration damage are complex and interrelated (see section 1.2.2). Almost all research done so far was concentrated on one aspect of the causes and mechanisms of impact and vibration. Very few studies were performed using an integrated approach[2]. As a consequence of the ignorance of the interrelated aspects, frequently researchers obtained conflicting results and industry experience of bruising and scientific study also leaded to inconsistent results (reducing the credibility of both groups in the other eyes) (based on Hilton, 1994; Studman, 1997).

The Discrete Element Method (DEM) can be considered as an integrated approach. All aspects of the fruit impact damage problem, as mentioned in section 1.2.2, can be included the modelling technique. Several benefits of the use of the DEM in the fruit impact damage problem, compared to experimental work, were already discussed (see section 1.4.1).

However, the application of the DEM in the fruit impact damage problem is limited. The first step of its application was performed by Rong *et al.* (1993). The complexity of the model was low (2 dimensional model, crude parameter values, number of particles very low). The application of the DEM in problems related to agriculture and food industry is limited in general. In contrast to most engineering materials to which DEM modeling is mainly focused, agricultural and food materials tend to behave like viscoelastic materials when they are subjected to various conditions of stress and strain (Mohsenin, 1986). Although a state of the art nonlinear *viscoelastic* normal contact force model, one of the basic ingredients in DEM, has been described in literature (Kuwabara and Kono, 1987; Brilliantov *et al.,* 1996ab) an experimental method to determine the parameters in the model for viscoelastic materials is still missing. A *viscoelastic* tangential contact force model, another basic ingredient of DEM, was recently developed (Dintwa *et al.,* 2004ab). An experimental method to derive the parameters in this model for viscoelastic materials is also missing.

Statistical bruise prediction models described in literature, which must be used in association with DEM, are restricted to the effect of only two fruit properties (either fruit temperature or fruit ripeness). Besides the statistical bruise models described in literature are inconsistent.

[2] Schoorl and Holt (1982ab) and Jones *et al.* (1991) used an integrated approach for the vibration damage during transport

Probably this is due to the ignorance of some fruit properties in the model like the radius of curvature and the ignorance of interaction effects between the fruit properties and interaction effects between fruit properties and the severity of impact.
Validation of the Discrete Element Method (DEM) for its applicability in predicting fruit bruise damage is another gap in the state of the art.
Advanced application of DEM simulations in the fruit impact damage problem, although a promising technique, were not executed so far.
All the lacuna in the application of DEM for viscoelastic materials in general and fruits in particular lead directly to the objectives of this thesis.

1.5.2 Objectives

The overall objective of the thesis was *the development of the Discrete Element Method (DEM) for the simulation of the impact damage during transport and handling of fruit, more in particular of apples and tomatoes* (two fruits with the highest economical value in Belgium).
This overall objective of the thesis includes five major sub-objectives:

- Development of an efficient experimental methodology to determine the parameters of normal and tangential contact force models suited for DEM simulation of *viscoelastic* materials like fruits.

- The development of bruise prediction models for apples and tomatoes, incorporating different fruit properties and their interactions, which can be used in association with DEM simulations.

- The development of specific DEM application for the fruit bruising problem, utilizing the DEMeter++ software of the laboratory of Agro-Machinery and –processing.

- Validation of the DEM in its ability to simulate real bruise damage of fruits during transport.

- To perform DEM simulations to clarify the factors causing apple and tomato bruising by vibrations during transport.

The following restrictions apply on the work that was performed in this thesis:

- Only postharvest mechanical damage, damage caused by human handling, is considered
- Only bruises as mechanical damage are considered (no cuts, punctures and abrasions)
- Although the DEM can simulate besides dynamic forces also static forces, bruise damage due to static forces was not studied. The reason is that the developed bruise prediction models, using a pendulum device, are only valid for dynamic forces[3].

1.5.3 Outline

In Chapter 2 the Discrete Element Method (DEM) for simulation of viscoelastic materials is discussed. Until present, almost all DEM research was about elastic or elastic-plastic materials. However, agricultural and food materials tend to behave like viscoelastic materials when they are subjected to various conditions of stress and strain (Mohsenin, 1986). The main focus of this chapter is a theoretical discussion of viscoelastic contact force models (both normal and tangential component) and a discussion of their applicability for simulating fruit impact damage.

Unambiguous methods to characterize the mechanical properties of these materials for their use in the DEM, especially to account for their viscosity in the damping parameter in the contact force models, are missing. In Chapter 3 a new measuring technique is described to determine experimentally the parameters of a normal contact force model that is considered most suitable for viscoelastic materials (Kuwabara and Kono model) (Tijskens *et al.,* 2001, 2002ab; Van Zeebroeck *et al.,* 2003b). This measuring technique makes use of a pendulum device that was developed during this work and is described in the same chapter (Van Zeebroeck *et al.,* 2003b).

Chapter 4 describes a technique to measure the parameters of a new tangential contact force model (Van Zeebroeck *et al.,* 2003a; Dintwa *et al.,* 2004ab; Van Zeebroeck *et al.,* 2004a), that is in fact a viscoelastic extension of the Mindlin and Deresiewicz (1953) tangential

[3] Due to increase of the yield stress with deformation rate, fruit bruises at lower peak stress with static compression compared to dynamic compression (Mohsenin, 1986). Therefore static bruise prediction models are mandatory that were not determined in this thesis. Moreover, the static compression damage during storage is also due to fatigue effect of the tissue (the threshold of bruising is lowered in time). A fatigue bruise prediction model was also not determined in this thesis.

contact force model for elastic spheres. To estimate the parameters of this tangential contact force model a commercially available rheometer was used.

Chapter 5 deals with statistical models that link the contact force, modelled by the (normal) contact force model, with the actual impact damage of the apples and the tomatoes, taking in account some fruit properties like the fruit ripeness, temperature, diameter, etc. (Van linden *et al.,* 2002ab).This is the only chapter that is not exclusively linked with the DEM.

Subsequently, Chapter 6 describes the validation of the DEM for its use in predicting the impact damage of apples (Van Zeebroeck *et al.,* 2004b). In this chapter the impact damage of real vibrating boxes of apples, of which the mechanical parameters were measured using the methodologies described in the previous chapters, were compared to DEM simulations.

Chapter 7 handles a case study of a vibrating box of apples and tomatoes simulated with DEM (Van Zeebroeck *et al.,* 2005). The influence of both mechanical parameters (stack height, size of apples and tomatoes, vibration frequency, etc.) and fruit properties on impact damage was investigated.

At last, in Chapter 8 some conclusions and future research topics are outlined.

Chapter 2

The Discrete Element Method (DEM) to simulate the mechanical behaviour of viscoelastic materials i.e. fruits

2.1 Introduction

The objective of this chapter is a brief general discussion of the Discrete Element Method and a profound theoretical discussion of viscoelastic contact force models, one of the basic ingredients of DEM, and their applicability for simulating fruit impact damage

The general aspects of the Discrete Element Method (DEM) are discussed in a first section (section 2.2). Section 2.3 describes briefly the DEM simulation software, named DEMeter++, developed at the laboratory of Agromachinery and –processing. Section 2.4 discusses the contact force model, one of the basic ingredients of DEM. In section 2.5.1 the basic aspects of normal contact force models are discussed and a literature review is presented. In section 2.5.2 the normal contact force model selection for DEM simulation of apples and tomatoes is discussed. In section 2.5.3 the normal contact force model that was argued to be most suitable for DEM simulation of apples and tomatoes (Kuwabara and Kono model) is discussed in more detail. The tangential component of the contact force model is discussed in section 2.6. In section 2.7 some conclusions are drawn.

2.2 General description of the Discrete Element Method (DEM)

The Discrete Element Method (DEM), as it is called by engineers, or Granular dynamics (GD), as it is called by physicians, is a Particle Based Simulation (PBS) technique. Another well-known member of the PBS family is Molecular Dynamics (MD). DEM was pioneered by Cundall and Strack (1979) in the field of rock mechanics. DEM is essentially a numerical technique to model the motion of an assembly of particles interacting with each other through collisions. DEM considers a system as a collection of *discrete* entities; this is in contrast to the Finite Element Method (FEM) which treats a bulk particulate system as a continuum. Therefore DEM provides knowledge of the particle behaviour at the micro scale hence enabling a better prediction an understanding of the macro scale i.e. the bulk system (Raji and Favier, 2004ab).

DEM is quite comparable to Molecular Dynamics (MD), from which it borrows some techniques and experience, but there are also some differences. The particles in MD, are molecules and atoms and in DEM the particles are the grains of a granular material. Granular material can be defined as a form of matter being an assembly of *discrete* macroscopic grains. DEM and MD both sum up the forces acting on the particles and integrate Newton's equation of motion to obtain velocity and position at the next time step. In doing so, the techniques describe the path of every particle in the assembly as time proceeds. Notable differences with MD are the fact that in DEM the particles are not point masses, but necessarily have a finite extent in 2 or 3 dimensions. This implies the possibility of rotational degrees of freedom. In addition the nature of the forces acting on the particles is different. Contrary to *interaction* forces in MD, *contact* forces in granular systems are not conservative due to the inelastic nature of collisions and the presence of friction forces on the contact surfaces. Furthermore, interaction forces between atoms and molecules are determined by continuous long/short range potentials whereas in granular systems the contact force may show discontinuities depending on the contact force model that is applied. Finally, as contact forces act only on particles in mutual contact, a contact detection algorithm is required in DEM programs, something which is absent in MD programs (Tijskens *et al.,* 2003).

Physically, particles in DEM are approximated as rigid bodies and the contacts between them as point contacts. In reality, most particles are more or less deformable. In DEM deformation is accounted for by allowing the particles to overlap slightly. As overlapping particles can of course only exist in a computer model, this overlap is termed *virtual* overlap. The forces resulting from a contact between two particles are related to their virtual overlap by a *contact force model.*

Mathematically, a DEM problem is formulated as a system of ordinary differential equations (ODE) formed by Newton's equation of motion (translation) and Euler equation of motion (rotation) (Haug, 1992):

$$m_i \mathbf{a}_i = \mathbf{g}_i + \sum_c \mathbf{f}_{ci} \qquad (2.1)$$

$$\mathbf{I}'_i \boldsymbol{\alpha}'_i = \mathbf{h}'_i + \sum_c \tilde{\mathbf{r}}'_{ci} \mathbf{f}'_{ci} - \tilde{\boldsymbol{\omega}}' \mathbf{I}' \boldsymbol{\omega}' \qquad (2.2)$$

with :

$\mathbf{a}_i$ and $\boldsymbol{\alpha}_\mathbf{i}$ the i-th particle translational and rotational acceleration vector [m/s^2; rad/s^2]

m_i and $\mathbf{I}_\mathbf{i}$ the i-th particle mass and inertia tensor [kg; kg.m^2]

$\mathbf{g}_i$ and $\mathbf{h}_\mathbf{i}$ the i-th particle body force vector and moment vector [N; N.m]

$\mathbf{f}_\mathbf{ci}$ the contact force vector acting on particle i induced by the c-th contact [N]

$\mathbf{r}_\mathbf{ci}$ the position vector of the c-th contact relative to the i –th particle centre of mass [m]

$\tilde{\mathbf{r}}_{ci}\mathbf{f}_{ci}$ the algebraic notation of the vector product $\vec{r}_{ci} \times \vec{f}_{ci}$

~ is the tilde operator, in case of vector $\mathbf{b} = [b_x b_y b_z]^T$, $\tilde{\mathbf{b}} = \begin{bmatrix} 0 & -b_z & +b_y \\ b_z & 0 & -b_x \\ -b_y & b_x & 0 \end{bmatrix}$

' means with respect to the body coordinate system, the origin coincides with the centre of gravity of the body
"no accent" means to a fixed reference coordinate system
A **bold faced capital letter** represents a second order tensor (matrix) while a **bold faced letter** represents a first order tensor (vector)

Most frequently $\mathbf{g}_i$ and $\mathbf{h}_i$ are:

$$\mathbf{g}_i = \begin{bmatrix} 0 \\ 0 \\ -m_i g \end{bmatrix}, \mathbf{h}_i = \begin{bmatrix} 0 \\ 0 \\ 0 \end{bmatrix} \qquad (2.3)$$

For spheres equation (2.2) can be simplified to (Haug, 1992):

$$\mathbf{I}'_i \boldsymbol{\alpha}'_i = \mathbf{h}'_i + \sum_c \tilde{\mathbf{r}}'_{ci} \mathbf{f}'_{ci} \qquad (2.4)$$

The typical DEM algorithm is organized as follows (Tijskens *et al.,* 2003):

Initialization of the system

Since the ODE system is a system of second order differential equations, two initial conditions are required for every degree of freedom, i.e. for every particle the translational and rotational position and velocity at time $t = 0$ have to be known.

At every time step Δt :

- Contact (or collision) detection. It is detected which particle is in contact with which other particle. Contact detection between pairs of spheres (most used in DEM) can easily verified as:

  $$\delta n = (r_i + r_j) - \| x_i - x_j \| > 0 \quad (2.5)$$

  with x_i the position of the centre of the i-th sphere

  r_i the radius of the i-th sphere

  The most trivial contact detection algorithm is based on a pair wise contact detection resulting in $\frac{N(N-1)}{2}$ contact tests. The quadratic complexity in the number of particles *N* identifies it as a very inefficient algorithm and increases computational time drastically when N increases. Therefore, more efficient contact detection algorithms are described in literature (Tijskens *et al.,* 2003).

- Calculation of the contact forces for every actual contact. Contact forces are typically decomposed into *normal* and *tangential* components, with respect to the contact surface. Therefore, a *normal and tangential contact force model* has to be included in the DEM algorithm.

- Assembly of the forces and moments acting on each individual particle in the equations of motion (equation (2.1) and (2.2))

- Integration of Newton's and Euler's equation of motion over the time step Δt to obtain updated positions and velocities of the particles. Schäfer *et al.* (1996) recommend a minimum of 100 time steps over the time span of a typical collision in the simulation to get accurate results. Different numerical integration schemes are given in Tijskens *et al.* (2003).

2.3 The DEM software package: DEMeter++

As DEM cover a wide range of applications with different number of particles, different particle shapes, different contact physics, a computational framework is needed for efficiently building new DEM applications. Current software systems very often have a restricted application range. An attempt to cope with this problem is the DEMeter++ project at the Laboratory of Agricultural Machinery and Processing (K.U.Leuven). DEMeter++ is a C++ library to be used as an extensible toolkit for efficient development of high performance DEM applications using state of the art algorithms and scientific programming techniques. The central idea was a building brick approach in which all components, like shape representation, contact force models, contact detection, time integration, etc. in the basic DEM algorithm become separate objects that can be easily interchanged and extended or replaced by user-defined objects (Tijskens *et al*., 2003).
The software version that was used for the simulations in this work was DEMeter++3.1, including simulations in three dimensions (*3D*).

2.4 Contact force models

As outlined in the general description of DEM (section 2.2), the forces resulting from a contact between two particles are related to their virtual overlap by a contact force model. The overall contact force can be decomposed into a normal component (perpendicular to the contact surface) and a tangential component (parallel to the contact surface). A separate contact force model describes each component. In DEM the deformation field is simplified to deformation in one point with associated deformation vector. The normal contact force model relates the normal component of the deformation vector to the normal component of the contact force, and the tangential contact force model relates the tangential component of the deformation vector to the tangential component of the contact force. In the most complex form the contact force model is described as presented in Figure 2-1. The normal and tangential forces are both modelled by a spring and a damper placed in parallel. However for the tangential force the spring-damper is modelled in combination with a friction element placed in series. Depending on the model being applied the spring and dampers are linear or nonlinear.

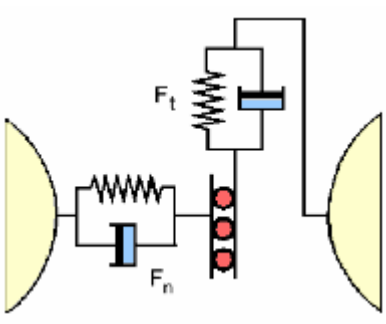

Figure 2-1. Graphical representation of the force scheme. Spring and damper elements are placed in parallel for both the normal and tangential force. The spring-damper element of the tangential force is placed in series with a friction element. F_N denotes the normal force, F_t the tangential force.

2.5 Normal contact force model

2.5.1 Literature review of normal contact force models

The subject of impact attracts the interest of scientists and engineers from different areas of knowledge from astrophysics to biomechanics. The common goal is to develop theories that can predict the behaviour of colliding objects. The two major theories are the stereomechanics approach and contact mechanics approach[4].

2.5.1.1 The classical theory of impact: stereomechanics

The stereomechanics approach (Classic work by Wallis, Wren and Huygens in 1668 and Newton in 1687), involves the application of the fundamental laws of mechanics to predict the velocities after impact. The impulse-momentum law (Huygens) forms the core of this approach. The loss of energy inherent to any real impact process is taken into account by the means of the coefficient of restitution (Newton). The restitution coefficient is not an intrinsic material property. It depends on the material of the bodies, their surface geometry and the impact velocity. The major advantage of the restitution coefficient concept is its mathematical simplicity. However, the engineering value of the information thus obtained remains highly dependent on and very sensitive to an accurate knowledge of the restitution coefficient. Moreover, the restitution coefficient can only be used for perfect normal impacts. For oblique impacts (impacts with tangential relative velocity) the use of a ratio of the

[4] Besides these two theories there exists also the 'elastic wave theory' and the 'plastic deformation theory (including plastic wave theory)'. The first theory is used when energy loss due vibrations is very important and the second theory is used for very high velocity impacts generally associated with explosives and projectiles.

tangential and normal impulse components is mandatory. Again, the determination of this coefficient requires an accurate experimental work.

The highest disadvantage of the stereomechanics approach is that the theory is unable to predict the contact forces between the impacting bodies and the deformations and stresses in them (Faik and Witteman, 2000).

2.5.1.2 Contact mechanics approach

The above mentioned limitations of the classical mechanical approach led many researchers to consider the continuous-dynamics models of collision where bodies deform during impact and the collision dynamics are treated as continuous-time dynamic phenomena. In its general form, the force-displacement relationship may look like:

$$F = F_e(\delta) + F_v(\delta, \dot{\delta}) + F_p(\delta, \dot{\delta}) \qquad (2.6)$$

with F the normal contact force [N]
F_e the elastic (conservative) part of the contact force [N]
F_v the dissipative part due to viscous damping [N]
F_p the dissipative part due to plastic deformation [N]
δ the approach of the colliding objects, displacement [m]
$\dot{\delta}$ the deformation rate [m/s]

Viscous dissipation can be related to the rheological properties of the materials. Plastic dissipation can be determined from the materials' stress-strain curve.

An overview of different types of contact force models is given below.

2.5.1.2.a Elastic contact force models $F_e(\delta)$

The simplest model to model the elastic part is Hooke's law:

$$F_e = k\delta \qquad (2.7)$$

with F_e the normal force pressing the solids together [m]
δ the approach of the objects [m]
k the spring parameter [N/m]

The well known landmark in contact mechanics was the work of Hertz on the elastic contact of spheres published in the year 1882. He demonstrated that the contact force between two elastic spheres is better modelled by:

$$F_e = k\delta^{3/2} \qquad (2.8)$$

with F_e the normal force pressing the solids together [N]
δ the approach of the two spheres, i.e. total of deformation of both spheres [m]
k the spring parameter depending on the sphere radii and elastic properties of the sphere materials [N/m$^{3/2}$]

2.5.1.2.b Viscoelastic contact force models ($F_e(\delta)$; $F_v(\delta,\dot{\delta})$)

The simplest model for the viscous behaviour is the one modelled after Newtonian liquids:

$$F_v = c\dot{\delta} \qquad (2.9)$$

with F_v the viscous damping force [N]
c the damping parameter [kg/s]
$\dot{\delta}$ the deformation rate [m/s]

Together with the linear elastic force it forms the well known Kelvin-Voigt model or linear spring-dashpot model with spring and damper in parallel:

$$F = k\delta + c\dot{\delta} \qquad (2.10)$$

This Kelvin-Voigt model is often used in particle based simulation methods. However, the viscous damping force is unable to describe the material behaviour accurately. Two reasons therefore can be mentioned. The first reason is related to the restitution coefficient. By using the linear spring-dashpot model the restitution coefficient is given by the following equation (Pöschel and Schwager, 2005):

$$e = \exp\left(\frac{-\pi c}{2m_{eff}} \Big/ \sqrt{\frac{k}{m_{eff}} - \left(\frac{c}{2m_{eff}}\right)^2}\right) \qquad (2.11)$$

with m_{eff} the effective mass given by $m_i m_j / (m_i + m_j)$, with $m_{i/j}$ the mass of particles i /j [kg]

As seen in equation (2.11), the linear force law leads to a coefficient of restitution that is independent of the impact velocity. Experiments, however, contradict this assumption of constant coefficient of restitution. Different authors (Kuwabara and Kono, 1987; Falcon *et al.,* 1998; Ramirez *et al.,* 1999) demonstrated that the coefficient of restitution follows the behaviour:

$$e = 1 - f(v_i^{1/5}) \qquad (2.12)$$

with v_i the impact velocity [m/s]

Pöschel and Schwager (2005), claim that the linear spring-dashpot model violates the basic laws of the theory of viscous bodies.

The second reason is that by using the linear model the contact force in the beginning of the impact is different from zero (maximum viscous force due the maximum velocity) what is in contradiction with the reality (Zhang and Whiten, 1996, 1998ab, 1999; Tsuji *et al.,* 1992, 1993). Therefore, different nonlinear spring-dashpots models were proposed by different authors.

As far as known, the first authors describing a nonlinear viscoelastic contact force model were Hunt and Crossley (1975). A hysteresis form of the damping parameter was proposed. Hunt and Crossley (1975) demonstrated that the following nonlinear contact force model better describes the actual force-deformation curve of viscoelastic materials than the linear Kelvin-Voigt model[5]:

$$F = k\delta^{3/2} + c\delta^{3/2}\dot{\delta} \qquad (2.13)$$

with F the contact force [N]
k the spring parameter [N/m$^{3/2}$]
c the damping parameter [kg.m$^{-3/2}$.s^{-1}]
$\dot{\delta}$ the deformation rate [m/s]
δ the deformation [m]

As can be seen, both the elastic and viscous part are nonlinear. By introducing the term $c\delta^{3/2}$ for the damping term, the initial condition of the force being zero at the beginning of impact is met. Using as condition that the dissipated energy during impact is small compared to the elastic energy (restitution coefficient close to one) Hunt and Crossley (1975) calculated the damping parameter as:

$$c = \frac{3}{2}\left(\frac{1-e}{v_i}\right)k \qquad (2.14)$$

Later Lankarani and Nikravesh (1990, 1994) improved the model of Hunt and Crossley, but their model is still based on the condition that the dissipated energy during impact is small

[5] In contrast to the Kuwabara and Kono contact force model (see further) this model is not based on the basic constitutive laws of viscoelasticity

compared to the elastic energy (restitution coefficient close to 1). The relationship between the damping parameter and the restitution coefficient[6] was given by:

$$c = \frac{3k(1-e^2)}{4\mathrm{v}_i} \qquad (2.15)$$

or

$$e = \sqrt{1-\frac{4c\mathrm{v}_i}{3k}} \qquad (2.16)$$

As can be seen, from equation (2.16), the restitution coefficient, in accordance with the empirical equation (2.12), decreases with increasing impact velocity.

Pioneering work in viscoelastic contact force modelling was accomplished by Kuwabara and Kono (1987) and by Brilliantov *et al.* (1996ab). Kuwabara and Kono and Brilliantov *et al.* used a different physical approach to come up with the same physical equations[7]:

$$F = k\delta^{3/2} + c\delta^{1/2}\dot{\delta} \qquad (2.17)$$

with F the contact force [N]
k the spring parameter [N/m$^{3/2}$]
c the damping parameter [kg.m$^{-1/2}$.s^{-1}]
$\dot{\delta}$ the deformation rate [m/s]
δ the deformation [m]

The contact force model (2.17) is a result of a derivation based on basic constitutive laws of elasticity and viscosity. A detailed derivation of the model can be found in Brilliantov *et al.* (1996a).

The damping parameter for the impact of two spheres with identical material properties is described by:

$$c = Ak \qquad (2.18)$$

with A the dissipative material parameter [*s*]

The dissipative material parameter *A* is defined by:

$$A = \frac{1}{3}\frac{(3\eta_2-\eta_1)^2}{3\eta_2+2\eta_1}\frac{(1-\nu)(1-2\nu)}{E\nu^2} \qquad (2.19)$$

with E the elastic modulus [E]
ν the Poisson's ratio [-]
η_1 and η_2 the viscous constants (mathematically they relate the dissipative stress tensor to the deformation rate tensor) [Pa.s]

[6] The effect of effective mass on the restitution coefficient of the colliding objects is neglected
[7] The research group of Brilliantov report the equations of Kuwabara and Kono were guessed, but not derived (Pöschel *et al* 2003). In our opinion, this is far too exaggerated, but the approach of Billiantov's research group can be considered as physically more correct.

A disadvantage of equation (2.19) is that the viscous constants are not known for most materials and are hard to measure.

Rigorous calculations by the Brilliantov research group revealed the following relationship (Schwager and Pöschel, 1998) for the restitution coefficient:

$$e = 1 - C_1 A \kappa^{2/5} \mathrm{v}_i^{1/5} + C_2 A^2 \kappa^{4/5} \mathrm{v}_i^{2/5} \pm \ldots \qquad (2.20)$$

with v_i the impact velocity [m/s]
$C_{1/2}$ empirical constants [-]

where κ can be calculated as:

$$\kappa = \left(\frac{3}{2}\right)^{3/2} \frac{E\sqrt{R^*}}{m_{eff}(1-\nu^2)} \qquad (2.21)$$

with R^* the effective radius of curvature defined as $1/R^* = 1/R_1 + 1/R_2$, $R_{1/2}$ radii of the impacting spheres [m]
E the elastic modulus of the impacting spheres [Pa]
m_{eff} the effective mass [kg]
ν the Poisson's ratio [-]

As can be seen from equation (2.20) the restitution coefficient depends on the impact velocity and also on the effective mass and the radius of curvature of the impacting spheres. Equation (2.20) is the most accurate expression for the restitution coefficient at present for purely viscoelastic materials (Hertzsch *et al.*, 1995; Brilliantov *et al.*, 1996ab; Schwager and Pöschel, 1998; Ramirez *et al.*, 1999; Brilliantov and Pöschel, 2000, 2001; Pöschel and Brilliantov, 2001; Hertzsch, 2002; Pöschel *et al.*, 2003; Pöschel and Schwager, 2005)

The viability conditions of the Kuwabara and Kono and Brilliantov model is summarized by Brilliantov *et al.* (1996ab)[8] and Kuwabara and Kono (1987):

1. The impact velocity has to be much less than the speed of sound in the material of the colliding particles.
2. The colliding materials have to be purely viscoelastic, so there may not be any energy loss due to vibrations or plastic deformation.

[8] In the case of apples and tomatoes the first viability condition is fulfilled. Energy loss due to vibration for apples and tomatoes can be considered negligible. The absence of plastic deformation is only true below the damage threshold (see further).

Unlike the Lankarani and Nikravesh model, this model can still be used when the dissipative loss is considerable, so the model can still be applied when the restitution coefficient is not close to unity.

For completeness, two other viscoelastic contact force models are presented.

A model is described in literature that combines the Hertz model for the elastic force and the linear model for the viscous force, it is called the dissipative Hertz model (Schäfer *et al.*, 1996):

$$F = k\delta^{3/2} + c\dot{\delta} \qquad (2.22)$$

The model was constructed in an *ad hoc* fashion. Taguchi (1992) demonstrated that by applying this model the restitution coefficient increases with an increasing impact velocity, exactly the opposite of what happens in reality. Although this model has been used in DEM simulations, it is not preferred.

Another nonlinear viscoelastic contact force model was proposed by Tsuji *et al.* (1992, 1993):

$$F = k\delta^{3/2} + c\delta^{1/4}\dot{\delta} \qquad (2.23)$$

with F the contact force [N]
k the spring parameter [N/m$^{3/2}$]
c the damping parameter [kg.m$^{-1/4}$.s^{-1}]
$\dot{\delta}$ the deformation rate [m/s]
δ the deformation [m]

The damping parameter is given by:

$$c = \alpha m^{1/2} k^{1/2} \qquad (2.24)$$

with α the empirical constant
m the effective mass [kg]
k the spring parameter [N/m$^{3/2}$]

This model was found heuristically by the authors. However, a physical link is missing[9]. It must be stated that in the Tsuji model it is not specified whether viscous or plastic dissipation is involved. The disadvantage is that the parameter α has to be determined empirically. The model assumed a restitution coefficient independent of the impact velocity and can therefore be considered as less realistic.

[9] In spite of its heuristically derivation, this model has been applied by several authors in DEM simulations

2.5.1.2.c Elasto-plastic contact force model ($F_e(\delta)$; $F_p(\delta,\dot{\delta})$)

Walton and Braun (1986) developed a linear elasto-plastic contact force model. The derivation of the model was distracted from finite element modelling. They assume that there are different spring constants k_1 and k_2, for the loading and unloading part of the contact:

$$F = \begin{cases} k_1\delta & ,\dot{\delta} \geq 0 (loading) \\ k_2(\delta - \delta_0) & ,\dot{\delta} < 0 (unloading) \end{cases} \qquad (2.25)$$

δ_0 is the value of δ where the unloading curve crosses the X-axis, or the permanent deformation.

In this model the restitution coefficient is constant and calculated as:

$$e = \sqrt{k_1 / k_2} \qquad (2.26)$$

So, the Walton and Braun model assumes a restitution coefficient independent of the impact velocity. In reality, as for purely viscoelastic materials, the restitution coefficient of elasto-plastic materials is also decreasing with increasing impact velocity.

Schäfer *et al.* (1996) proposed to make k_2 a function of the maximum force $F_{\max}$ achieved during loading ($k_2 = k_1 + sF^{\max}$), with s an empirical constant. By doing this the restitution coefficient is given by (Schäfer *et al.,* 1996):

$$e = \frac{1}{\sqrt{s\mathrm{v}_i (m_{eff} / k_1)^{1/2} + 1}} \qquad (2.27)$$

As can be seen the restitution coefficient decreases by increasing impact velocity, like it is the case in reality.

Thornton and Ning (1998) developed a nonlinear elasto-perfectly plastic contact force model.

The elasto-perfectly plastic impact is modelled in three phases (Thornton and Ning, 1998; Thornton *et al.*, 2001; Mishra and Thornton, 2002; Wu *et al.*, 2003; Mishra, 2003):

Loading phase 1: In the perfect elastic phase, where no plastic deformation occurs the Hertz law is used (nonlinear elasticity):

$$F = \frac{4}{3} E^* (R^*)^{1/2} \delta^{3/2} \qquad (2.28)$$

Loading phase 2: Above the critical force (yield stress) plastic deformation occurs and a Hertzian pressure distribution is assumed. This leads to the following linear relationship:

$$F = F_y + \pi p_y R^* (\delta - \delta_y) \qquad (2.29)$$

with F_y the critical force, the force above plastic deformation occurs [N]

p_y the critical pressure (=critical force/contact surface) [Pa]

δ_y the displacement (relative approach) at F_y [m]

Unloading phase: If plastic deformation occurred during the loading stage the effective radius of curvature (R_p^*) during unloading is greater than R^*, due to permanent deformation of the contact surfaces (flattening).

During unloading the force-displacement behaviour is assumed to be elastic and is provided by the Hertzian equations but with the effective radius of curvature R_p^*. The contact force is given by the following equation:

$$F = \frac{4}{3} E^* (R_p^*)^{1/2} (\delta - \delta_p)^{3/2} \qquad (2.30)$$

with R_p the effective radius of curvature of the deformed spheres [m]

δ_p the permanent deformation [m]

E^* the equivalent elastic modulus [Pa] defined as $\frac{1}{E^*} = \frac{1}{E_1} + \frac{1}{E_2}$ with $E_{1/2}$ the elastic modulus of the impacting bodies

R_p can be calculated as:

$$R_p^* = \frac{4E^*}{3F^*} \left(\frac{2F^* + F_y}{2\pi p_y} \right)^{3/2} \qquad (2.31)$$

where F^* the maximum force during loading [N]

Thornton and Ning (1998) also proved that the coefficient of restitution behaves realistically and is decreasing with increasing impact velocity:
The restitution coefficient is given by the equation:

$$e=\left(\frac{6\sqrt{3}}{5}\right)^{1/2}\left[1-\frac{1}{6}\left(\frac{\mathrm{v}_y}{\mathrm{v}_i}\right)^2\right]^{1/2}\left[\frac{\left(\frac{\mathrm{v}_y}{\mathrm{v}_i}\right)}{\left(\frac{\mathrm{v}_y}{\mathrm{v}_i}\right)+2\sqrt{\frac{6}{5}-\frac{1}{5}\left(\frac{\mathrm{v}_y}{\mathrm{v}_i}\right)^2}}\right]^{1/4} \quad (2.32)$$

with v_i the impact velocity [m/s]

v_y the critical impact velocity, the velocity above plastic deformation starts to occur [m/s]

The critical impact velocity can be calculated as (Thornton and Ning, 1998):

$$\mathrm{v}_y = 3.194\left(\frac{p_y{}^5 R^{*3}}{E^{*4} m_{eff}}\right)^{1/2} \quad (2.33)$$

Johnson (1985) derived an equation for the critical impact velocity with a prefactor different from 3.194.
Vu-Quoc and Zhang, adapted the model of Thornton and Ning to allow also for strain hardening, i.e nonlinear plastic loading curve (Vu-Quoc and Zhang 1999; Vu-Quoc *et al.* 2000, 2001; Zhang and Vu-Quoc 2002ab). Therefore, new coefficients were introduced. However, until present the link of these coefficients with material properties is missing. Nevertheless, these parameters can be determined from FEM simulations or from experimental impact measurements by parameter estimation techniques (Zhang and Vu-Quoc, 2002a).

2.5.2 Contact force model selection for simulations of viscoelastic bodies like apples and tomatoes

For impact velocities above the critical impact velocity both viscous and plastic dissipation will occur. However, at present no viscoelastic-plastic contact force model has been described in literature[10].
From the literature examination of the contact force models, two models were regarded as state of the art and were considered suitable for describing the real impact behaviour of apples and tomatoes:

[10] There has been accomplished some rheological work on viscoelastic-plastic materials. These models describe on a mathematical way the material behaviour, but these models can not be used as a contact force model.

1. The Kuwabara and Kono (Brilliantov-Pöschel) model for viscoelastic spheres. The model is restricted to impacts where the only energy dissipation mechanism is viscous loss
2. The Thornton (Vu-Quoc) model for elasto-plastic spheres. The model is restricted to impacts where the only energy dissipation mechanism is energy loss due to plastic deformation[11].

A real impact of apples and tomatoes can be divided in two phases:

1. Until the bio-yield pressure, the body can be considered as purely viscoelastic. Bio-yield pressure was defined by Mohsenin (1986) as the pressure above which plastic deformation starts to occur.
2. At contact pressure above the bio-yield pressure, besides viscous dissipation also plastic deformation has to be considered as an energy dissipation mechanism. The body can be allocated viscoelastic-plastic behaviour.

At impact velocity levels where the maximum contact pressure is not exceeding the bio-yield pressure, the Kuwabara and Kono model for viscoelastic spheres can be applied. The critical impact velocity for apples and tomatoes can be calculated using the Thornton and Ning equation (2.33).

One solution for the problem of the absence of a viscoelastic-plastic contact force model could be to use the elastic-plastic Thornton model by totally neglecting the viscous behaviour of the apples and tomatoes. However, for an impact causing clear bruising *grosso modo* half of the energy loss is due to viscous dissipation and the other half to plastic dissipation (Bajema and Hyde, 1998 and own research). It can be expected that by applying the Thornton contact force model for elasto-plastic spheres the errors made by neglecting the viscosity are too high. However, this has not been demonstrated.

The other solution could be to use the Kuwabara and Kono model also for impacts above the critical impact velocity level. One would expect that errors made by neglecting the plastic dissipation ($\cong$ ½ of total energy loss for average impact) are also too high to be justified. However, below it is outlined that this is not the case.

Mathematically, the Kuwabara and Kono equation is describing the hysteresis force-deformation curve of an impact. The dissipated energy can be evaluated trough the work

[11] Both models are neglecting energy loss due the elastic wave propagation (vibration).

done by the damping force $c\delta^{1/2}\dot{\delta}$ in the Kuwabara and Kono equation. The energy loss may be expressed as $\oint c\delta^{1/2}\dot{\delta}d\delta$. $\oint$, the circular integral, refers to the integration around the hysteresis loop. A higher damping parameter c indicates a higher energy loss. Mathematically, with the damping parameter c, no distinction is made between energy losses due to viscous or plastic dissipation. In the case of a viscoelastic-plastic impact the damping parameter c describes energy loss that is a combination of viscous and plastic dissipation. However, physically the combination of viscous and plastic energy loss in one damping term is not correct. The ideal viscoelastic-plastic contact force model breaks down the energy loss in plastic and viscous energy dissipation. At present no such contact force model has been described in literature.

In literature, the method that is most extensively used to determine the damping parameter is the experimental determination of the restitution coefficient. However, a link between the coefficient of restitution and the damping parameter is not known in the case of combined viscous and plastic dissipation, so the restitution coefficient method can not be used. In this work an alternative method is applied to obtain the model parameters, i.e. a parameter estimation technique minimizing the error between measured and modelled contact force, displacement and displacement rate (see Chapter 3).

As a footnote, it must be stated that spring-dashpot contact force models (linear and nonlinear) have been used extensively in DEM, even for non viscoelastic bodies. The pioneers of DEM, Cundall and Strack, used linear spring-dashpots model (Kelvin-Voigt model) to simulate rock deformation what can be considered as an elasto-plastic material. It is just recently that researchers (Thornton, Mishra, Vu-Quoc) argue replacing the classic spring-dashpot models with the Thornton model, for DEM modelling of elasto-plastic materials. The arguments therefore are:

- Linear and nonlinear spring-dashpot models lead to an unrealistic negative contact force at the end of impact.

- The damping parameter c is difficult to determine experimentally[12]. Vu-Quoc and Zhang (1999) argue no solid basis exists for obtaining the coefficient of the dashpot as the dependency of the damping parameter on the collision velocity prevents the use of quasi-static methods. Also Mishra (2003) considers the dependency of the coefficient of restitution on the impact velocity as a difficulty.

[12] All the parameters used in the Thornton model are directly linked to material properties.

Nevertheless, both arguments can be criticized:

- The negative contact force of the spring-dashpot model at the end of the impact was discussed by Tsuji (1992, 1993) and Zhang en Whiten (1996ab, 1998, 1999). The authors attributed this anomaly to the way the dashpot is incorporated in the contact force model. Pöschel and Schwager (2005) give a good explanation for this anomaly: "Real particles do not overlap (like in DEM and Hertz theory), but they deform. In the expansion phase the particles gradually recover their spherical shape. At the time the modelled contact force becomes negative *(real contact force is zero)*, the centers of the particles separate too fast from each other to allow the surfaces to keep touch while recovering their shape. Hence, although $\delta > 0$, the particles do not touch each other. Consequently, the particles stop to interact". The solution of the problem is to replace the contact force model in DEM simulations by (Pöschel and Schwager, 2005):

  $$F = \max\{0, F_{Kuwabara-Kono}\} \qquad (2.34)$$

  In this way the negative, attractive force, leading to an underestimation of the separation velocity of the particles is eliminated. Furthermore, by using the Thornton model, in case it is not stated that the contact is broken when the contact force becomes zero, the contact force can also become negative.

- Using the mathematical relationship between damping and coefficient of restitution is not the only possibility to determine the damping parameter. The damping parameter can also be determined by parameter estimation methods as stated in this work (see Chapter 3).

It can be concluded, the best contact force model to date for use in DEM simulations of apples and tomatoes is the Kuwabara and Kono (Brilliantov-Pöschel) model:

- This model is the best choice to model the exclusive viscoelastic behaviour of the fruit below the critical impact velocity. The model is the most physically correct model available in literature.

- The model is the best choice to model viscoelastic-plastic behaviour, in anticipation of more physically correct contact force models that combine the viscoelastic and plastic behaviour.

2.5.3 Detailed discussion of the Kuwabara and Kono contact force model

In this section the relationship between the parameters of the Kuwabara and Kono model and the material parameters of the impacting objects is discussed.

2.5.3.1 Relationship between the spring parameter k and the material parameters

The relationship between the spring parameter k and the material parameters was derived by Hertz (1892), in his basic work of contact mechanics.
The following assumptions were made by Hertz (Mohsenin, 1986):

- The material of the contact bodies is homogenous (what is in fact never fulfilled)
- The applied loads are static
- The radii of curvature of the contacting solid are very large compared to the radius of the surface of contact
- No tangential forces exist (contacting bodies are sufficiently smooth)

Even with these assumptions, the Hertz model is applied in case some of these conditions are not fulfilled. For example Hertz theory is used by many researchers to model dynamic impacts of non-smooth materials. In these conditions Hertz theory can model the contact force in an acceptable way. Nevertheless, Hertz theory is not applicable when the contact radius of both materials approaches infinity (extreme case impact two flat planes). Caution

has to be taken when the ratio of radius of the contact area/effective radius[13] of curvature is higher then 1/10.

Taking in account the assumptions made by Hertz, the contact radius of the contact area of the impacting spheres can be expressed as (derivation of this formula see Hertz, 1881; Johnson, 1985):

$$a = \left(\frac{3FR^*}{4E^*} \right)^{1/3} \qquad (2.35)$$

with F the contact force [N]
R^* the effective radius of curvature [m]
E^* the equivalent elastic modulus [Pa]

The effective radius of curvature can be defined as:

$$\frac{1}{R^*} = \frac{1}{R_1} + \frac{1}{R_2} \qquad (2.36)$$

with R_1 and R_2 respectively the radius of sphere 1 and 2 [m]

The equivalent elastic modulus can be calculated as:

$$\frac{1}{E^*} = \frac{1-\nu_1^2}{E_1} + \frac{1-\nu_2^2}{E_2} \qquad (2.37)$$

with E_1 and E_2 the elastic modulus of spheres 1 and 2 [Pa]
ν_1 and ν_2 the Poisson's ration of spheres 1 and 2 [-]

The combined deformation (or overlap) δ of the spheres is defined as (Timoshenko and Goodier, 1951; Johnson, 1985)[14]:

$$\delta = \frac{a^2}{R^*} \qquad (2.38)$$

Substituting equation (2.35) in this equation (2.38) yields:

$$\delta = \frac{a^2}{R^*} = \left(\frac{9F^2}{16R^*E^{*2}} \right)^{1/3} \qquad (2.39)$$

[13] Effective radius of curvature is $1/R^* = 1/R_1 + 1/R_2$ with R_1 and R_2 the radii of curvature of the impacting bodies at the place of impact

[14] This relationship between δ and a is derived from the Hertz contact pressure profile in combination with geometry. A derivation can be found in Johnson (1985) and in more detail in Timoshenko and Goodier (1951)

Equation (2.39) can also be written as (Johnson, 1985):

$$F = \frac{4}{3}\sqrt{R^*}E^*\delta^{3/2} \qquad (2.40)$$

By this, the relationship between the spring parameter k (of Hertz nonlinear model) and the material properties (effective radius of curvature and equivalent elastic modulus) is given by:

$$k = \frac{4}{3}\sqrt{R^*}E^* \qquad (2.41)$$

Special case: impact soft sphere - hard sphere or hard flat plate[15]

In the special case of an impact of a soft sphere with a hard sphere or hard flat plate the elastic modulus of the soft sphere can be calculated in case the spring parameter k and the radii of curvature of the impacting bodies are known. This is demonstrated below:
The elastic modulus of a soft sphere (for example an apple or tomato) is much lower than the elastic modulus of the hard sphere or plate (for example a metal impactor)[16]. As a consequence, the elastic modulus of the soft sphere E_1 can be calculated from the equivalent elastic modulus E^*, because E_2 (elastic modulus hard sphere) >>> E_1 (elastic modulus soft sphere):

$$\frac{1}{E^*} = \frac{1-\nu_1^2}{E_1} + \cancel{\frac{1-\nu_2^2}{E_2}} \qquad (2.42)$$

Or

$$E_1 = (1-\nu_1^2)E^* \qquad (2.43)$$

Small corrections to Hertz contact force model by impact of soft elastic spheres with a hard sphere or impact of two soft elastic spheres

Hay and Wolff (2001) calculated that small corrections to the Hertz contact force model are necessary when applied to the impact of soft elastic sphere with a hard elastic sphere or a soft elastic sphere with another soft elastic sphere. The reason for this correction is the penetration of the hard sphere into the soft sphere or the soft spheres into each other. By this the contact radius a is somewhat underestimated by the Hertz theory.

[15] This is the case with the pendulum device where an apple or tomato can be considered as a soft sphere and the round or flat metal impactor respectively as hard sphere and hard flat plate
[16] The elastic modulus of the apple and tomato are respectively in the order of magnitude 10^6 and 10^5 N/m^2 compared to an elastic modulus of hard metal (aluminium) plate in the order of magnitude 10^9

For the contact hard sphere – soft sphere a correction factor can be added to equation (2.40):

$$F = \gamma \frac{4}{3} \sqrt{R^*} E^* \delta^{3/2} \qquad (2.44)$$

With the correction factor γ:

$$\gamma = 1 + \frac{2(1-2\nu)}{3\pi(1-\nu)} \frac{a}{R} \qquad (2.45)$$

As can be seen this correction factor γ depends on $\frac{a}{R}$. The contact radius a varies during impact with the consequence that also correction factor γ is not constant. This makes the correction factor difficult to apply. Hay and Wolf (2001) demonstrated that a slight different correction factor γ is needed for the impact of two soft spheres. However they conclude that in both cases the use of the correction factor γ is a slight improvement of the Hertz model. Nevertheless, an 'average correction factor[17]' was inherent to the parameter estimation method that was used in this work to determine the contact force model parameters (see Chapter 3). The correction factor is incorporated in the value of the spring parameter k of the impact.

2.5.3.2 Relationship between damping parameter c and the material parameters

In this section the relationship between the damping parameter *c* and the material parameters is discussed. The Kuwabara and Kono (1987) and Brilliantov *et al.* (1996) contact force model is recapitulated here:

$$F = k(\delta^{3/2} + A\delta^{1/2}\dot{\delta}) \qquad (2.46)$$

Using the Hertz theory (equation(2.41)) equation (2.46) can also be written as:

$$F = \frac{4}{3} \sqrt{R^*} E^* \left(\delta^{3/2} + A^* \delta^{1/2} \dot{\delta}\right) \qquad (2.47)$$

with A^* some kind of equivalent dissipative parameter, combining the viscous properties of the two impacting bodies [s]

Actually, equation (2.47) was not represented in this form by Brillinatov *et al.* (1996). The equivalent dissipative parameter A^* is a theoretical definition that is introduced as the combined viscous properties of the two impacting spheres.

[17] 'Average' is meaning that a correction factor is applied for the whole impact instead the correction factor is changing during impact

Originally, the model was developed for the impact of viscoelastic spheres with identical material properties (Brilliantov *et al.,* 1996).

For spheres with identical elastic modulus the equivalent elastic moduli E^* becomes:

$$E^* = \frac{E}{2(1-\nu^2)} \qquad (2.48)$$

So, for spheres with identical material properties equation (2.47) can be written as:

$$F = \frac{2E\sqrt{R^*}}{3(1-\nu^2)}\left(\delta^{3/2} + A\delta^{1/2}\dot{\delta}\right) \qquad (2.49)$$

The dissipative parameter A mentioned here, is identical for the two spheres. The weakness in the theory of the viscoelastic impact of spheres of Brillinatov *et al.* (1996) was its limitation to the impact of spheres with identical viscosity. More exactly, it was not indicated how the equivalent dissipative parameter A^* must to be calculated when the viscosity of the two impacting spheres is not identical.

Personal communication with Dr. Thörsten Pöschel (Institute of Biochemistry of the Humboldt-Universität, Berlin) led to early insight in the extension of the viscoelastic model to the impact of spheres with different viscosity (Pöschel and Schwager, 2005).

Pöschel and Schwager (2005) derived heuristically that equation (2.47) can also be written as:

$$F = \frac{4}{3}\sqrt{R^*}\left[E^*\delta^{3/2} + \frac{1}{4}\left(\frac{E_1 A_1}{1-\nu_1^{\,2}} + \frac{E_2 A_2}{1-\nu_2^{\,2}}\right)\delta^{1/2}\dot{\delta}\right] \qquad (2.50)$$

with A_1 and A_2 the dissipative parameters of spheres 1 and 2 [s]

It can be shown that for describing the impact of identical spheres (spheres with identical elasticity and viscosity) equation (2.50) becomes equation (2.49).

2.5.3.3 Special case: impact soft sphere - hard sphere or hard flat plate[18]

In the case of the impact of a soft sphere with an aluminium sphere or a hard flat plate the viscosity of the hard sphere/plate can be taken as zero ($A_2 = 0$)

By doing this, equation (2.50) becomes:

$$F = \frac{4}{3} E^* \sqrt{R^*} \left(\delta^{3/2} + \frac{1}{4} A_1 \delta^{1/2} \dot{\delta} \right) \qquad (2.51)$$

So, from (2.51) it follows:

$$c = \frac{4}{3} E^* \sqrt{R^*} \frac{1}{4} A_1 \qquad (2.52)$$

Further using equation (2.41) equation (2.52) becomes:

$$A_1 = \frac{4c}{k} \qquad (2.53)$$

2.6 Tangential contact force model

Tangential motion can be divided in sliding, spinning and rolling. Sliding and spinning consist of a relative peripheral velocity of the surfaces at their point of contact, and stand respectively for a translational and rotational relative velocity. Rolling involves a relative angular velocity of the two bodies about an axis lying in the tangent plane through the contact point. Rolling and sliding, or spinning, can take place at the same time (Johnson, 1985). Cundall and Strack (1979) developed a theoretical model to describe the tangential contact force for sliding. Mathematically the model can be represented as:

$$F_t = -\min(|k_t \delta|, |\mu F_N|) \qquad (2.54)$$

with k_t the tangential spring parameter [N/m]
μ the dynamic friction coefficient [-]
F_N the normal force [N]
F_t the tangential force [N]
δ the displacement [m]

Sliding involves tangential deformation at small tangential forces and once the tangential force exceeds the static friction force, slipping occurs with a constant dynamic friction force. Later on Walton and Braun (1986) introduced a nonlinear tangential stiffness with a decreasing tangential stiffness with increasing tangential force. This model is far more

[18] The special case of an impact of a soft sphere with a hard sphere or hard flat plate is valid in the case of apple or tomato impact (soft sphere) with the round or flat metal impactor of the pendulum (respectively hard sphere and hard flat plate).

realistic than the previous one. The two drawbacks of these models are that they only apply when the normal force is constant (which in real situations is never the case) and that there exists no physical meaning for the tangential stiffness k_t and as a consequence no experimental method to determine this parameter. To perform DEM simulations with viscoelastic materials, Li *et al.* (2001) added a damping constant (c_t) to the Cundall and Strack model. Mathematically the model can be represented as:

$$F_t = -\min(\left|k_t\delta + c_t\dot{\delta}\right|, \left|\mu F_N\right|) \qquad (2.55)$$

with k_t the tangential stiffness [N/m]

c_t the tangential damping [kg/s]

μ the dynamic friction coefficient [-]

F_N the normal contact force [N]

F_t the tangential force [N]

δ the displacement [m]

$\dot{\delta}$ the displacement rate [m/s]

This model has the same drawbacks as the model for elastic materials: the model is only valid for the case with a constant normal force and no physical meaning can be attributed to the parameters k_t and c_t .For these two reasons it was decided to use physically more realistic models. Mindlin (1949) pioneered a continuum mechanics analysis of the problem of two elastic spheres in torsional tangential contact, later extended by Lubkin (1951). Mindlin and Deresiewicz (1953) developed a more generalized model for elastic spheres in sliding (translation) or torsional contact with varying normal force. These are complicated models based on physical modelling of slip and stick phenomena occurring at the contact area of the spheres. Slip starts at the edge of the contact area and moves to the inner center of the contact surface as the torque (in the case of sliding the tangential force) increases. This leads to the development of an *annulus of microslip* surrounding an inner *region of sticking* in the contact area. Because friction laws are strongly nonlinear, the size and form of the annulus of microslip depend on the loading-unloading history of the contact. This makes the prediction of tangential deformation and friction forces, in a given situation, complicated, but still feasible.

There exists a typical relation between the angular displacement and the torque. The curve monotonically increases to a certain asymptote value. At this asymptote, slip starts to occur.

Because in our applications the materials are not perfectly elastic, an attempt was undertaken to add a viscous term to these continuum mechanical models.

From an analysis of the continuum problem of two viscoelastic spheres in torsional contact, similar to that of Mindlin (1949) and Lubkin (1951), the tangential contact compliance (inverse of the tangential contact stiffness), defined as

$$C_t = \frac{d\beta}{dM_z}, \qquad (2.56)$$

is given by:

$$C_t = \frac{3-W}{16a^3G(1-W)^2}\left[2(4-W)\ A^{-½} - 1\right]$$

$$A = 1 - (W-3)\left(5 - \frac{8M_z}{\mu F_N a}\right) \qquad (2.57)$$

with β the angular displacement [rad]

M_z the applied torque [N.m]

a the radius of the circular contact area [m]

G the shear modulus of the sample material [Pa]

μ the dynamic friction coefficient of the contact [-]

F_N the normal contact force [N]

The factor W, captures the contribution of viscous forces and is given by

$$W = \frac{2\pi\eta\omega a^3}{\mu d} \qquad (2.58)$$

with η the viscosity [Pa.s]

ω the angular velocity [rad/s]

d the deformation depth from the contact plane to a fixed plane in the interior of the spheres where the viscous force becomes zero [m]

The original Lubkin model is achieved from equation (2.57) by putting W=0 (η=0). The material parameters to be determined experimentally are the shear modulus G, the viscosity η and the dynamic friction coefficient μ. Further, the normal force F_N, the contact radius a, the factor d and the angular velocity ω also have to be known. A detailed derivation of this model is presented in Dintwa *et al.* (2004ab). A viscoelastic extension of the Mindlin and Deresiewicz model for translational tangential contact of spheres was recently developed (Dintwa *et al.,* unpublished).

2.7 Conclusions

In this chapter a general description of DEM was presented and the structure of a typical algorithm was outlined. However the main focus of this chapter was on contact force models, an essential part of DEM. It was indicated that the Kuwabara and Kono (1987) normal contact force model for viscoelastic spheres, further developed by Brilliantov *et al. (*1996ab), is the most appropriate normal contact force model for DEM simulation of fruits. The Kuwabara and Kono model for viscoelastic spheres is physically the most correct model for the impact of apples and tomatoes below the bioyield point. Also beyond the bioyield point the Kuwabara and Kono model is still capable to describe the real impact behaviour because the damping parameter can capture besides the viscous dissipation also the plastic dissipation. However in the latter case (combination of viscous and plastic dissipation) a physical link of the damping parameter with material properties is still missing. In addition, in this chapter an extension of the Kuwabara and Kono normal contact force model for impact of spheres with non identical material properties (different elasticity and viscosity) was presented.
The physically most realistic tangential contact force model for elastic spheres of Mindlin and Deresiewicz (1953) was extended to viscoelastic spheres by adding a viscous term. More details of this model are provided in Dintwa *et al.* (2004ab).

Chapter 3

Determination of normal contact force model parameters for viscoelastic materials (fruits) using a pendulum device

3.1 Introduction

In contrast to most engineering materials to which DEM modeling is mainly focused, agricultural and food materials tend to behave like viscoelastic materials when they are subjected to various conditions of stress and strain (Mohsenin, 1986). Although a *viscoelastic* normal contact force model, one of the basic ingredients in DEM, has been described in literature (Kuwabara and Kono, 1987; Brilliantov *et al.,* 1996ab) an experimental method to determine the parameters in the model for viscoelastic materials is still lacking. The viscoelastic Kuwabara and Kono contact force model has been described in detail in the previous chapter (section 2.5.3). The two objectives of this chapter are the description and validation of an experimental procedure to determine the parameters of the Kuwabara and Kono contact force model for viscoelastic materials and the discussion of the contact force model parameters that were obtained for apples and tomatoes using this experimental procedure.

This chapter is divided in four major sections. First, the development of a pendulum device will be discussed in detail (section 3.2). The pendulum was constructed for two main reasons: to make it possible to determine the contact parameters of the normal contact force model of viscoelastic materials (this chapter) and to establish bruise prediction models for apples and tomatoes (see Chapter 5) (Van Zeebroeck *et al.,* 2003b). Subsequently, a nonlinear least squares data fitting technique to estimate the parameters (stiffness and damping) of the

Kuwabara and Kono (1987) viscoelastic contact force model (equation 2.17 and 2.49) will be outlined and will be validated using a rubber ball (section 3.3) (Van Zeebroeck *et al.,* 2003b). Next, a basic analysis of the parameters of the Kuwabara and Kono model for impacts of apples, tomatoes and potatoes for impacts below the critical impact velocity will be presented (section 3.4) (Van Zeebroeck *et al.,* 2003b). In the last section (section 3.5) the effect of the effective radius of curvature and the impact velocity on the parameters of the Kuwabara and Kono contact force model will be discussed in more detail for apples and tomatoes.

3.2 Development of pendulum device

3.2.1 Introduction

During the 40 years of research of fruit impact damage different test equipment was developed to assess the dynamic stresses in fruits. Unlike the equipment used for the measurement of (quasi) static stresses, almost none of the research was executed with commercially available equipment. At present no standard technique for performing impact testing of agricultural products is available and of the variety of methods documented no single technique is reported to be superior and universally used. Probably the main reason for it is that the experimental procedure to use is dictated by a specific problem.

Among the dynamic apparatus there are two main types of design: a drop and pendulum design. During a drop test, either a product is dropped on an instrumented surface (rigid or cushioned) or an instrumented mass is dropped upon the product. To characterize the impact an accelerometer was used by Hammerle and Mohsenin (1966) and Ragni and Berardinelli (2001). However, most researchers used a force transducer (Wright and Splinter, 1967; Fluck and Ahmed, 1972; Diener *et al.*, 1979; Lichtensteiger, 1982; Chen *et al.*, 1985; Brusewitz and Bartsch, 1989; Chen and Yazdani, 1991). In the late eighties commercial impact testing machines, known as impact tables were developed for use in the packaging industry. Siyama *et al.* (1988) used such equipment to characterize apple impact.

Because drop testing methods either lack the possibility of a controllable impact location on the fruit or, when a guide track is used, the friction is introducing errors in the measurements, many researchers preferred the use of a pendulum apparatus (Sarig, 1991). The standard impact testing machines commonly used for Izod and Charpy tests[19] of various non-

[19] Izod and Charpy are two test procedures to determine the amount of energy dissipated during fracture under dynamic loading of metals, polymers and polymers composites. Many commercial pendulums are available (Instron®, Ceast®instruments, Gatha® instruments, etc.) for these tests. None of these instruments can measure within the measuring range (impact velocity, impact energy) suitable for fruits.

biological materials were introduced by Finney and Massie (1975), but mostly special test equipment was developed to attain the specific impact velocities and energies encountered in impact of agricultural products. Simpson (1971) and Srivastava *et al.* (1976) applied the pendulum together with an accelerometer (acceleration during impact). Srivastava *et al.* (1976) also utilized an angular displacement sensor to measure the impact rebound angle. A pendulum device was used by many others (Fridley *et al.*, 1964; Park, 1963; Bilanski, 1966; Nelson and Mohsenin, 1968; Horsfield *et al.*, 1972; Hoag 1972; Jindal and Mohsenin, 1976). Jarimopas *et al.* (1990) employed a pendulum device together with a piezoelectric force transducer. Bajema and Hyde (1992; 1998) constructed a pendulum with a force transducer, a piezoelectric accelerometer, an area sensor and an infrared sensor (to measure impact velocity). Bajema *et al.* (1998) developed a so called tissue pendulum (impact of cylindrical samples of apple flesh). Besides the piezoelectric accelerometer and the force transducer also an angular displacement transducer was used, not only to measure the impact and rebound angle of the pendulum rod, but also to measure its position *during impact*. This is probably the first time an angle sensor (angular displacement transducer in this case) has been utilized to measure displacement during impact of agricultural materials. Before, displacement during impact was measured indirectly by means of double integration of the acceleration signal (Hammerle and Mohsenin, 1966; Wright and Splinter, 1968; Fluck and Ahmed, 1973; Chen *et al.*, 1985; Bajema and Hyde, 1992, 1998) or using an electro-optical device (Finney and Massie, 1975; Jarimopas *et al.,* 1990).

Baheri (1997) developed a pendulum device for his study of potato mechanical damage. Three different sensors were used: accelerometer, force transducer and an analog angle-sensor to measure impact and rebound angle of the pendulum rod.

3.2.2 Description of pendulum device

The pendulum developed by Baheri (1997) was taken as point of departure. An exact duplicate of the pendulum frame was made. The advantage of the pendulum frame is reflected in the ranges of the impact energies (0-2 J) and impact velocities (0-1.6 m/s) that are within the range apples and tomatoes are subjected to in practice in Belgium. However the pendulum is not suited to simulate impact conditions during mechanical harvest of apples and tomatoes and during their rougher handling conditions compared to fruit for the fresh market. In this case impact energies and velocities can exceed 2 J and 1.6 m/s respectively.

The effective mass of the pendulum rod was taken more or less equal to the mass of an average potato (or apple) in practice. The rod was made of pinewood because Baheri (1997) found a pinewood rod minimizes the vibrations during rebound[20] and impact.
The main reason to construct a new pendulum was that Baheri's pendulum was not suited for the objective of the thesis to determine the normal contact force model parameters. This necessitated, besides the measurement of the contact force during impact, also the measurement of displacement and displacement rate (velocity)[21]. To achieve this, the introduction of a new sensor, an incremental optical encoder, was necessary.

The pendulum consists of a 0.515 m long rod with at its tip an aluminium impactor of spherical shape (radius of curvature: 25 mm) (see Figures 3-1 and 3-2). The impactor itself is mounted to a force sensor (Dytran 1051V3, Dytran instruments, Chatsworth, California, US; sensitivity: 11mV/N). At the same location an accelerometer is attached (PCB 352C22, PCB piezotronics, Buffalo, New York, US; sensitivity: 10mV/g). At the hinge of the pendulum rod an incremental optical encoder (Heidenhain RON 275, Heidenhain, Traunreut, Germany) is mounted. The data signals of these three sensors are collected by a National Instrument PCI-MIO-16E-1 card and processed by a LABVIEW (National Instruments Belgium NV, Zaventem, Belgium) program.

[20] However because the elastic energy in the new pendulum configuration is determined from the kinetic energy just after impact and not from the potential energy, vibrations during rebound are not important. The pine wood pendulum arm was remained to minimize the energy loss due to arm vibration *during* impact
[21] Baheri's pendulum is able to measure the impact and absorbed energy and the impact force (acceleration) during impact. These quantities are satisfactory to construct the statistical bruise models (Chapter 5).

Figure 3-1. General view of pendulum device (scheme see figure 3-2)

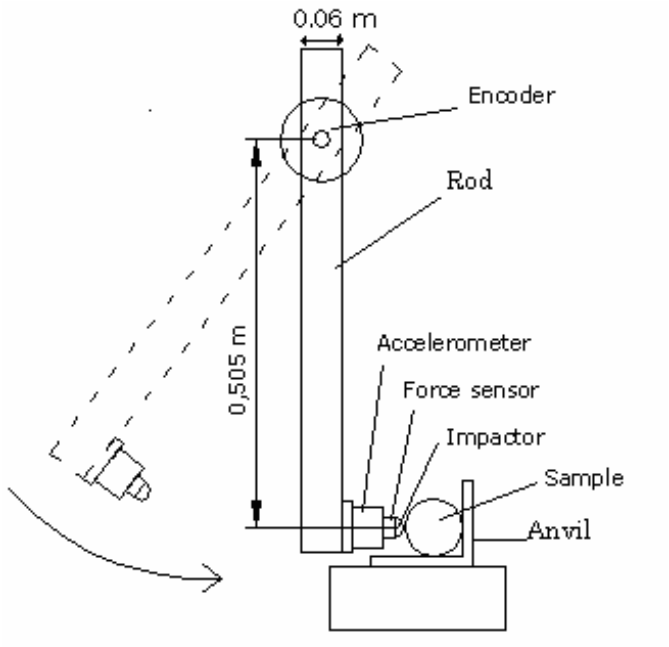

Figure 3-2. Schematic representation of the pendulum rod and anvil. The positions of the different sensors and of the impacted body ("fruit") are indicated.

In our pendulum the displacement during impact is determined in a direct way by using an incremental optical encoder. The encoder sends out two digital signals (block signal) that are 90° phase-shifted. Each signal has a resolution of 18000 cycles/rev (pulses/rev). The resolution of the encoder is increased five times by an electronic interpolation integrated in the encoder itself. After analyzing the digital transitions of the two phase-shifted signals together in the LABVIEW program (procedure known as edge-detection) a resolution of 0.001° is achievable: 18000 cycles/rev x 5 time interpolation x 4 (as a result of the edge detection of the 90° phase shifted A and B signal) = 360000; 360°/360000=0.001°. Taking in account the distance of impactor to encoder shaft, the resolution is 8.7 μm. The accuracy of the encoder, measured in the factory, is 0.0014°. Each signal (force sensor signal, encoder signal A and B) is sampled at a rate of 200 kHz, giving a temporal resolution of 5 μs. The time to switch between signal channels during data acquisition is at most 1 μs. This high sampling rate is necessary to avoid missing of a transition of the encoder signal at the point of maximum velocity (just before impact). Because all the signals are measured at a sampling rate of 5 μs a force-deformation curve can be constructed by plotting force against displacement measurements[22].

The sample to be tested (fruit for example) is mounted to an anvil by an elastic band. The anvil is rigid enough to assume that its deflection or vibration is insignificant during impact. Some samples (apples and potatoes) are cut in two to minimize energy absorption and deformation at the contact surface of the anvil with the sample. By varying the initial angle of the pendulum rod, different impact energies can be created. The contact force $F_c(t_i)$ in de direction normal to the contact surface, displacement $\delta(t_i)$ and displacement rate $\dot{\delta}(t_i)$ of the impactor during impact are measured simultaneously, at the sampling times $t_i = t_0 + i/f$ ($i = 1,...,n$), with f the sampling frequency. t_0 and t_n denote the start and the end of the contact, respectively.

The contact force $F_c(t_i)$ is measured by the force sensor. The acceleration ($\ddot{\delta}(t_i)$), measured by the accelerometer was used as verification for the force sensor signal by taking in account the rotational inertia (I) and length (l) of the pendulum rod ($F_c(t_i) = (I/l^2)\ \ddot{\delta}(t_i)$).

[22] Normally the encoder signal is read with a digital channel of a data acquisition card counting the transitions in the signal (for example 4 V is 1; 0.5 V is 0, depending on the encoder). The channel is called a 'counter'. With the data acquisition card that was used, it seemed not to be possible to couple the time during impact with each transition (for analog channels it is called 'sampling time'). However this is needed because the displacement has to be known on exactly the same time during impact as the force. Therefore the encoder signals were also connected to the analog channels (like the force sensor) of the data acquisition card. It can be argued that this way is preferable (even when the time of measurement can be coupled with the counter signal), because in this way one is absolutely sure the sampling time of the force is maximum 1 µs different from the sampling time of the encoder signals.

Displacement and displacement rate are measured by an optical incremental encoder which in fact measures the angular position of the impactor. The tangential displacement of the impactor is calculated from the displacement angle by taking in account the length of the pendulum rod.

The time of first contact of the impactor with the sample is detected by the force sensor. The rise in voltage (or corresponding force) beyond the noise level of the force sensor is taken as triggering signal. The noise level of the force sensor is quite high (~1 N). As a consequence, no data is available of the impact force below 1 N. The displacement at the point of first contact of the impactor with the sample is set equal to zero. Utilizing the triggering point significantly decreases the calculation time of decoding the digital encoder signal. The displacement rate of the impactor during impact is obtained from the instantaneous position as

$$\dot{\delta}_i = \frac{\delta_{i+1} - \delta_{i-1}}{2dt} \qquad (3.1)$$

with dt the time lapse between successive signals.

Absorbed energy is calculated by subtracting rebound energy of the impact. The impact and elastic energy are obtained from the calculated kinetic energy of the pendulum rod just before and just after impact.

$$E_{impact} = E_{kin}(t_{-1})$$

$$E_{elastic} = E_{kin}(t_{n+1})$$

$$E_{absorbed} = E_{impact} - E_{elastic} \qquad (3.2)$$

t_{-1} and t_{n+1} denote the time of the final signal before impact, and the first signal after the impact, respectively. The kinetic energy is obtained as:

$$E_{kin}(t) = \tfrac{1}{2} I \omega(t)^2 = \tfrac{1}{2} \frac{I \dot{\delta}(t)^2}{l^2} \qquad (3.3)$$

with ω the angular velocity of the impactor [rad/s]
I the moment of inertia of the pendulum rod [kg.m^2]
l the length of the pendulum rod [m]

The moment of inertia I [kg.m^2] was measured by using the equation of Sears and Zemansky (1965), also used by Baheri (1997):

$$I = \frac{T^2 M g r_g}{4\pi^2} \qquad (3.4)$$

with T the oscillation period of the pendulum rod [s]
M the mass of the pendulum rod [kg]
g the gravity [9.81 m/s^2]
r_g the distance of the rotating axis of the pendulum rod to the centre of gravity of the rod [m]

The period of the pendulum rod was determined from the displacement-time signal of the free swinging rod. The centre of gravity was determined by balancing the rod. The calculated moment of inertia was 0.0773 kg.m^2.

The calculation of the impact and elastic energy by means of the kinetic energy is uncommon. Most authors, like Baheri (1997) calculated the impact and elastic energy respectively from the impact and rebound angle, applying the potential energy law (Fluck and Ahmed, 1973; Bajema and Hyde, 1998; Molema, 1999). The authors admit that errors on the value of the impact and elastic energy are made because of the friction at the pivot of the pendulum rod and the energy loss due to rod vibration during rebound. The authors tried to minimize this error by minimizing friction and vibration of the pendulum rod. The application of the kinetic energy instead of the potential energy, in the device described here, has the advantage that the errors made by friction and vibration of the pendulum rod can be excluded.

To test the accuracy of the pendulum device, the impact energy and absorbed energy calculated from the kinetic energy of the pendulum rod was compared to the calculation of the work performed by the pendulum rod by integrating the force-deformation curve. The equations are depicted below. Graphically it is demonstrated in the force-deformation curve of a tomato impact (Figure 3-3). A good agreement was found between impact energy and absorbed energy calculated from the kinetic energy and the performed work.

$$E_{impact} = \int_0^{\delta_m} F d\delta = A_1 + A_2 \qquad (3.5)$$

$$E_{absorbed} = \int_0^{\delta_m} F dx - \int_{\delta_r}^{\delta_m} F dx = A_1 - A_2 \qquad (3.6)$$

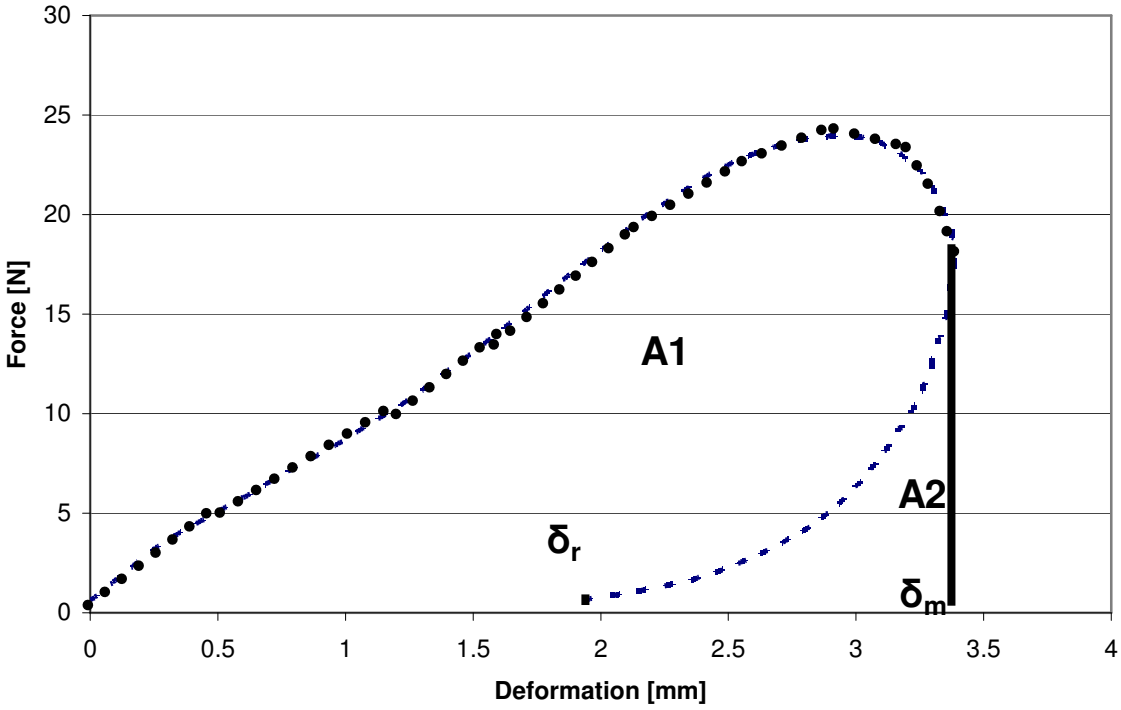

Figure 3-3. Force-deformation curve of a meat tomato impacted with a velocity of 0.7 m/s. δ_m is the maximum deformation during impact, δ_r is the permanent deformation. A1 indicates the surface below the part of the curve indicated by ••••, A2 indicates the surface below the rest of the curve.

3.2.3 Comparison of displacement during impact measured by the incremental encoder and measured by double integration of the accelerometer signal

In the literature displacement rate and displacement are determined respectively by integration and double integration of an accelerometer signal. Several authors however have pointed out the inaccuracy of such numerical integration (Fluck and Ahmed, 1973; Musiol and Harty, 1991). The reason is the uncertainty associated with the individual integration constants of the different frequencies in the signal. The use of highpass filtering can correct this effect to a certain extent. Highpass filtering is satisfactory when there is zero-mean displacement (vibration). When non-zero mean displacement is present, it can only be used for a short time interval (like impact), taking into account that the error on the integration still increases with time (Musiol and Harty, 1991).

Comparison of the force-deformation curve calculated from the accelerometer signal (with high-pass filtering) with the force-deformation curve calculated from the encoder signal indicated that the deformation calculated from the accelerometer signal overestimates the maximum deformation and underestimates the resilience of the tissue at the end of impact

(Figure 3-4). This is in agreement with the fact that the errors made by numerical integration of the accelerometer signal increase with time (Musiol and Harty, 1991).

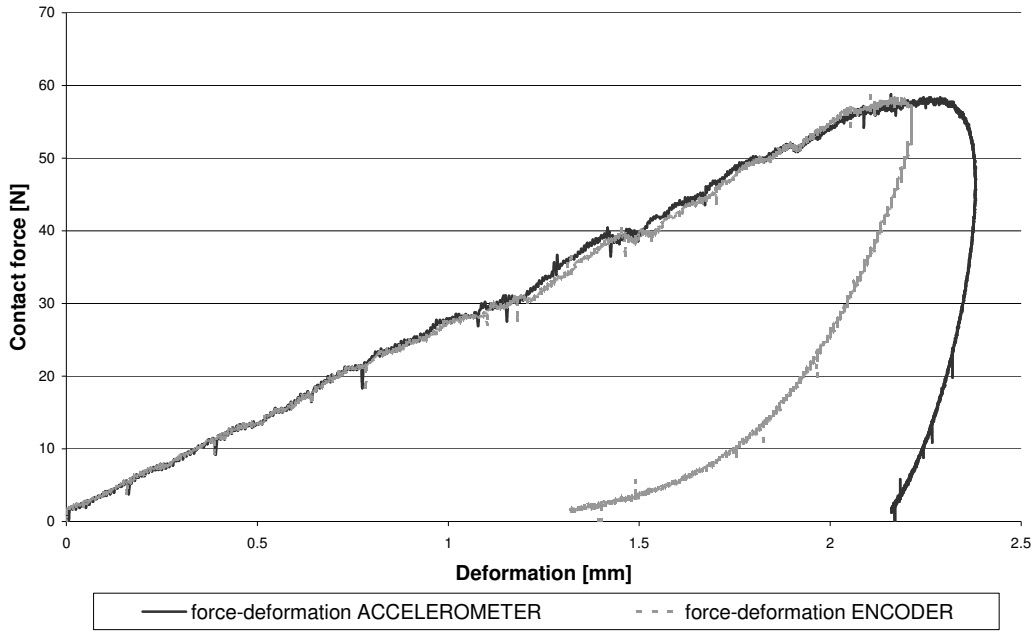

Figure 3-4. Comparison of force-deformation curve obtained from the accelerometer with the force-deformation curve obtained from the encoder for an simultaneously measured apple impact.

3.3 Parameter estimation method to extract the parameters of the Kuwabara and Kono contact force model from experimental impact data

3.3.1 Introduction

In this section an experimental technique will be described to estimate the contact force model parameters of the Kuwabara and Kono contact force model (equation (2.17)). The two impacted bodies will be a piece of fruit and a metal impactor. Principally, the technique can be generalized to impacts of other materials (for example a piece of fruit with packaging materials and machine parts).

The experimental device being used for measuring contact force and displacement during impact is a pendulum. The pendulum simultaneously determines the contact force, the displacement of the surface of the impacted body, and the displacement rate. A pendulum is a classical device to determine bruise susceptibility of fruit and potatoes (Nelson and Mohsenin (1968); Bajema and Hyde (1998); Baheri (1997)). The pendulum has been used in this context for determination of the bruise susceptibility of apples and tomatoes (see

Chapter 5). To a less extent, a pendulum has also been used to determine the parameters of contact force models. The only reference that has been found is Nigg and Liu (1999). They determined the stiffness and damping parameter in a nonlinear viscoelastic contact force model for flat plate impact by least squares data fitting of the experimentally measured force-deformation during impact of shoe-soles with a flat impactor.

3.3.2 Description of the indirect parameter estimation technique

The experimental data of an impact consisted of the normal contact force $F_c(t_i)$, the displacement of the impactor $\delta(t_i)$, the displacement rate $\dot{\delta}(t_i)$, at the sampling times t_i ($i = 1,...,n$).

The parameters, k and c, of the Kuwabara and Kono model were estimated from the experimental data by minimizing an error function that is measuring the difference between the experimental data and predictions based on the Kuwabara and Kono contact force model. The equation of motion for the impactor is given by:

$$I\ddot{\theta} = -mgl\sin\theta - F_c^* l\cos\theta \quad (3.7)$$

with F_c^* the modelled contact force, the asterisk indicates it is the modelled contact force is intended [N]
θ the angle between the rod of the impactor and the direction of gravity [rad]
m the mass of the pendulum rod [kg]
I the inertia of the pendulum rod [kg.m^2]
g the gravitational acceleration [9.81 m/s^2]
l the length of the pendulum rod [m]

The direction of the angle θ was such that $\dot{\theta}$ was positive during loading. The impacted object was positioned so that $\theta(t_0) = 0$. Since $\sin\theta \cong 0$ the influence of the gravity force in equation (3.7) could be neglected. The contact force F_c^* was given by the Kuwabara and Kono contact force model during contact, and vanished after contact was lost. The displacement δ during contact was related to the angle θ by $\delta = l\sin\theta$ and could be approximated by $\theta \cong \delta / l$, since θ was close to zero. The equation of motion (3.7) was easily solved by an explicit Runge-Kutta equation of order 4/5 (Matlab routine ode45 of MATLAB, Mathworks, Natick, Massachusetts, US).

The parameter estimation was carried out using a nonlinear least squares data fitting technique (routine lsqnonlin of the Matlab optimisation toolbox) using the trust region method, based on the interior-reflective Newton method.

The technique minimized the cost function C:

$$C = w_\delta \sum_i \left(\delta(t_i) - \delta^*(t_i)\right)^2 + w_{\dot\delta} \sum_i \left(\dot\delta(t_i) - \dot\delta^*(t_i)\right)^2 + w_F \sum_i \left(F_c(t_i) - F_c^*(t_i)\right)^2 \quad (3.8)$$

with $\delta(t_i); \delta^*(t_i)$ respectively the experimental and modelled displacement [m]

$\dot\delta(t_i); \dot\delta^*(t_i)$ respectively the experimental and modelled displacement rate [m/s]

$F_c(t_i); F_c^*(t_i)$ respectively the experimental and modelled contact force [N]

$w_\delta; w_{\dot\delta}; w_F$ are respectively weight factors for displacement, displacement rate and contact force

The cost function (equation (3.8)) measured the error between experimental data and the solution of the equation of motion (3.7), which is denoted by the asterisk. The weights w_δ, $w_{\dot\delta}$ and w_F could be chosen to vary the relative importance of the corresponding state variables ($\delta(t_i)$, $\dot\delta(t_i)$ and $F_c(t_i)$) and could be put on zero if desired. By putting some weights on zero the cost functions in Table 3-1 were obtained.

Table 3-1. Overview of possible cost functions

State variable	*cost function*
$\delta(t_i)$	$C_\delta = w_\delta \sum_i \left(\delta(t_i) - \delta^*(t_i)\right)^2$
$\dot\delta(t_i)$	$C_{\dot\delta} = w_{\dot\delta} \sum_i \left(\dot\delta(t_i) - \dot\delta^*(t_i)\right)^2$
$F_c(t_i)$	$C_{F_c} = w_F \sum_i \left(F_c(t_i) - F_c^*(t_i)\right)^2$
$\delta(t_i)$, $\dot\delta(t_i)$	$C_{\delta\dot\delta} = w_\delta \sum_i \left(\delta(t_i) - \delta^*(t_i)\right)^2 + w_{\dot\delta} \sum_i \left(\dot\delta(t_i) - \dot\delta^*(t_i)\right)^2$
$\delta(t_i)$, $F_c(t_i)$	$C_{\delta F_c} = w_\delta \sum_i \left(\delta(t_i) - \delta^*(t_i)\right)^2 + w_F \sum_i \left(F_c(t_i) - F_c^*(t_i)\right)^2$
$\dot\delta(t_i)$, $F_c(t_i)$	$C_{\dot\delta F_c} = w_\delta \sum_i \left(\dot\delta(t_i) - \dot\delta^*(t_i)\right)^2 + w_F \sum_i \left(F_c(t_i) - F_c^*(t_i)\right)^2$
$\delta(t_i)$, $\dot\delta(t_i)$, $F_c(t_i)$	$C_{\delta\dot\delta F_c} = w_\delta \sum_i \left(\delta(t_i) - \delta^*(t_i)\right)^2 + w_{\dot\delta} \sum_i \left(\dot\delta(t_i) - \dot\delta^*(t_i)\right)^2 + w_F \sum_i \left(F_c(t_i) - F_c^*(t_i)\right)^2$

3.3.3 Validation of the indirect parameter estimation technique

3.3.3.1 Sensitivity of cost function

To validate the experimental methodology, the use of a test material with predictable behaviour was mandatory. Biological materials are to be avoided, because their behaviour is subject to many factors, which are still poorly understood. They exhibit biological variability. Even when obvious factors[23] are kept constant, material properties can still vary significantly because their state is not constant over time. The material chosen was rubber. Its stiffness is of the same order of magnitude as for the biological materials under study, it does not show biological variability, and it does not yield. A rubber sphere (radius of curvature: 41.5 mm) was cut in two equal parts and one part was mounted on the anvil. A pendulum impact experiment with an initial drop angle of 10° has been repeated 20 times.

The parameters, k and c, of the Kuwabara and Kono model were estimated for each repetition.

In the cost function (Table 3-1) the weights w_δ, $w_{\dot{\delta}}$ and w_{F_c} were chosen to normalize the different terms ($w_q = 1/\langle q \rangle$). $\langle q \rangle$ indicates the average value of the state variable during impact. In this way, each state variable realizes an equal influence on the parameter estimation. Besides the repeatability of the measuring method, differences in the cost function were analyzed.

The results of the parameter estimations for these different cost functions are depicted in Table 3-2. When the parameter estimation was carried out on contact force (C_{F_c} in Table 3-1) or displacement (C_δ in Table 3-1) and respectively the displacement and contact force were calculated according to the estimated parameters, a good fit was found between the experimental and calculated displacement and contact force respectively. The fact that two independent devices (force sensor and encoder) led to approximately the same result was encouraging.

However, quantitatively, the difference between parameter estimation based on displacement (C_δ) and parameter estimation based on contact force (C_{F_c}) seemed to be more pronounced: a difference of 176 $kg.m^{-1/2}.s^{-1}$ in damping parameter (28 %) and 20622 $N.m^{3/2}$ in spring parameter (5 %) between both cost functions was identified.

[23] Obviously, biological materials can generally not be prepared in a controlled way. E.g. apples harvested at the same, even from the same tree, may have a very different history in terms of growth conditions and therefore can exhibit a wide variability for material properties. The obvious factors refer to the conditions which are under the control of the experimenter, such as harvest time, storage conditions, conditions in the experimental setup, etc…

The standard deviation of the damping parameter estimated by the different combinations of the state variables ranged between 1.6 % and 1.8 % (except for the estimation based on experimental displacement C_δ the standard deviation was 4 %, see Table 3-2). The standard deviation of the spring parameter ranged between 0.7 % and 0.8 %. The measurement error of the spring and damping parameters were acceptable.

In the basic analysis of the parameters for biological materials (see section 3.4) the 'triple criterion cost function' was used. The reason therefore was to minimize the measurement error on force sensor and encoder. Figure 3-5, 3-6 and 3-7 compare experimental and optimized displacement, displacement rate and contact force respectively for the estimation using the three state variables together (cost function(3.8)). The conclusion is that the Kuwabara and Kono contact force model can fit accurately the experimental displacement and displacement rate (see Figure 3-6 and 3-7). The prediction of the contact force itself is worse, but still acceptable (see Figure 3-5).

In later analysis of the contact force model parameters of biological materials (section 3.5) 'the double criterion cost function' of contact force and displacement was preferred above 'the triple criterion cost function' as used in section 3.4. The reason for this was that the displacement rate as derived parameter of displacement seemed to be dependent on the applied data processing method (degree of mathematical smoothing or cut-off frequency of low-pass filtering).

The nonlinear parameter estimation procedure presented so far is not the only possible procedure to determine the contact force model parameters. In principle the contact force model parameters could also be estimated using the linear regression procedure:

$$Y = kX_1 + cX_2 \qquad (3.9)$$

with

$$Y = F_c^*$$

$$X_1 = \delta^{*3/2}$$

$$X_2 = \delta^{*1/2}\dot{\delta}^*$$

The difference with the nonlinear parameter estimation method is that the linear regression procedure is only applicable on condition that all three state variables δ , $\dot{\delta}$, and F_c^* are available. The nonlinear parameter estimation method can still be applied if one or two of these state variables are missing. Currently further research is executed on the linear regression procedure as alternative for the nonlinear parameter estimation procedure like it is used in this work.

Table 3-2. Parameter estimation for a rubber ball for the Kuwabara and Kono contact force model (3.40) using different cost functions.

Cost function	$\langle k \rangle \pm \sigma_k$ [N $m^{-3/2}$]	$\langle c \rangle \pm \sigma_c$ [kg $m^{-1/2}$ s^{-1}]	*Residual norm* C^2
C_{δ}	391057 ± 2893	725 ± 29	$0.1*10^{-3} \pm 0.03*10^{-3}$
$C_{\dot{\delta}}$	394933 ± 3001	688 ± 12	111 ± 7
C_{F_c}	411679 ± 2900	549 ± 10	3.17 ± 0.29
$C_{\delta\dot{\delta}}$	394927 ± 3000	688 ± 12	111 ± 7
$C_{\delta F_c}$	411653 ± 2919	549 ± 10	3.17 ± 0.29
$C_{\dot{\delta} F_c}$	394921 ± 2993	681 ± 11	121 ± 7.4
$C_{\delta\dot{\delta} F_c}$	394931 ± 2990	681 ± 11	121 ± 7

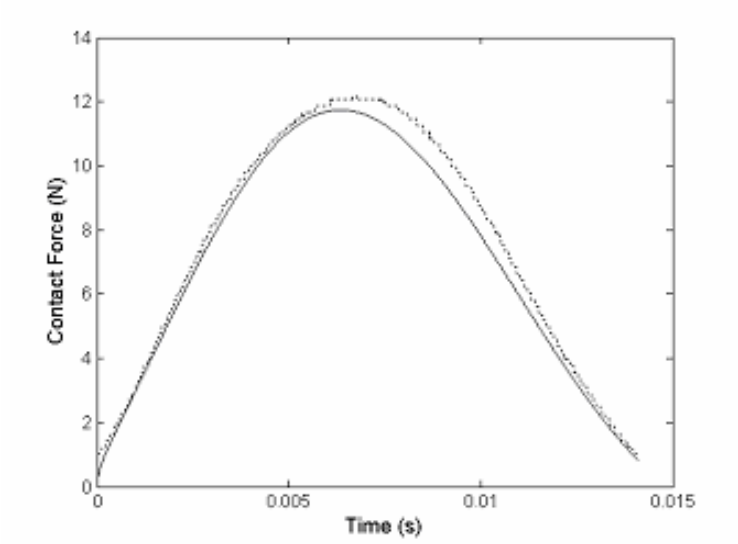

Figure 3-5. Rubber: Experimental and simulated contact force with parameter estimation based on displacement, contact force and displacement rate. Solid line: simulation; Dotted line: experimental

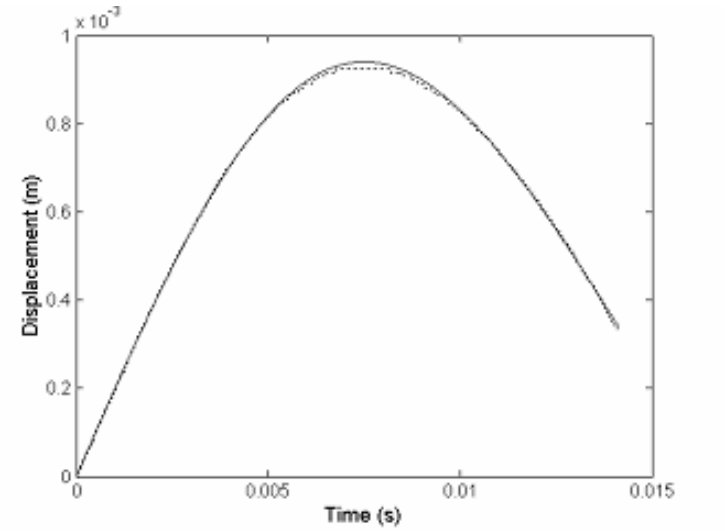

Figure 3-6. Rubber: Experimental and simulated displacement with parameter estimation based on displacement, contact force and displacement rate. Solid line: simulation; Dotted line: experimental

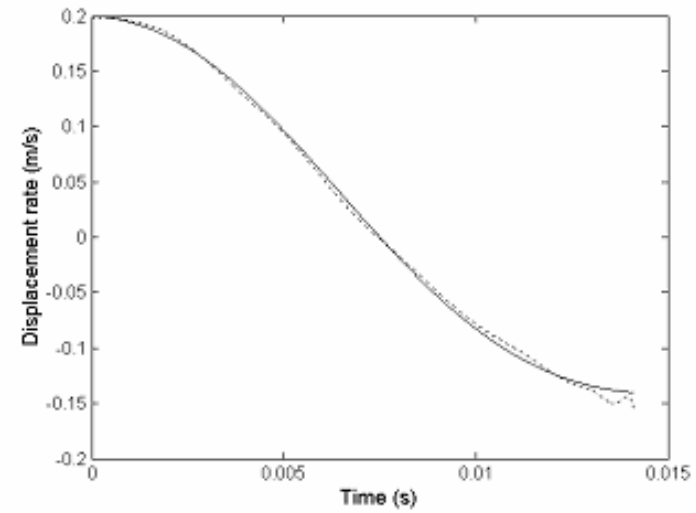

Figure 3-7. Rubber: Experimental and simulated displacement rate with parameter estimation based on displacement, displacement rate and contact force. Solid line: simulation; Dotted line: experimental

3.3.3.2 Validation of the indirect parameter estimation technique using a Universal Testing Machine (UTS)

In order to further validate the estimation procedure using the pendulum device an alternative experimental method based on quasi-static compression was used to measure the state variables. The universal testing machine being used was the UTS-5 (UTS testsystheme GmbH, Ulm, Germany). The rubber ball was placed on a stationary horizontal plate. A horizontal cross-head moved a second horizontal plate downward with a pre-defined speed. A force sensor with a range of 0-200 N and a resolution of 0.001 N was placed between the

cross-head and the second horizontal plate. A computer measured and controlled the speed of the motor. By tracking the measuring time continuously the displacement was calculated at every time-step. By plotting the force and the displacement at the same time-step a force-deformation curve could be constructed.

The rubber ball was compressed at a constant deformation rate of 0.00017 m/s (= 10 mm/min) and 0.0017 m/s (100 mm/min) until the force of 170 N was reached. The maximum deformation was 4.1 mm. Because the noise of the force sensor signal in the low force region was too high, only that part of the force-deformation curve above a deformation of 2 mm was used for further analysis. The force-deformation curves were highly reproducible.

The force-deformation curves of two different measurements with a deformation rate of 0.00017 and 0.0017 m/s were analyzed in MATLAB (Mathworks, Natick, Massachusetts, US). Linear regression was used to determine the parameters k en c in the Kuwabara and Kono model. The parameters obtained were k = 733809 N/m$^{3/2}$ and c = 1078 kg.m$^{-1/2}$.s^{-1} with a coefficient of variation less than 1 %.

To compare these parameters with the parameters estimated with the pendulum device a transformation was necessary because the effective radius of curvature R^* was not identical between pendulum and UTS. In the case of the pendulum a spherical impactor was used to deform the rubber ball and in the case of the UTS a flat plate. As mentioned before the Kuwabara and Kono model can be represented as (Brilliantov *et al.,* 1996):

$$F = \frac{4}{3}\sqrt{R^*}E^*\left(\delta^{3/2} + A^*\delta^{1/2}\,\dot{\delta}\right) \qquad (3.10)$$

Only the effective radius of curvature R^* differs between the pendulum and the UTS measurement. A straightforward computation revealed (with a radius of curvature of rubber ball and impactor respectively 0.0415 and 0.025 m respectively):

$$k_{pendulum} = 0.63 k_{uts} \qquad (3.11)$$

and

$$c_{pendulum} = 0.63 c_{uts} \qquad (3.12)$$

The spring parameter of the rubber ball (k_{uts}) measured with the universal testing machine (UTS) was 733196 N/m$^{3/2}$. The spring parameter measured with the pendulum ($k_{pendulum}$) was 394931 N/m$^{3/2}$ (triple criterion cost function). When the above equation (3.11) is used $k_{pendulum}$ becomes 461913 N/m$^{3/2}$.

The substantial difference between the spring parameter measured with the UTS and the pendulum is probably due to the fact that the impactor was not perfectly spherical. In fact the radius of curvature was varying rapidly from 2.5 cm in the centre of the contact area to approximately 1 cm at the outside. For this reason, in future research a new impactor with well known radius of curvature was used. Another explanation could be the possible deformation rate dependency of the spring parameter k of the rubber ball (like it was proven for apples and tomatoes, see section 3.5).

The damping parameter of the rubber ball (c_{uts}) measured with the universal testing machine (UTS) was 1078 kg $m^{-1/2}$ s^{-1}. The damping parameter measured with the pendulum ($c_{pendulum}$) was 681 $kg.m^{-1/2}.s^{-1}$ (triple criterion cost function). By using the above equation(3.12), $c_{pendulum}$ becomes 673 $kg.m^{-1/2}.s^{-1}$. The difference in the damping parameter between UTS and pendulum measurement is only 4 $kg.m^{-1/2}.s^{-1}$.

These results, may lead to the conclusion that the UTS is a perfect alternative for the pendulum to determine the contact force parameters. This is to some degree true for rubber (as demonstrated here), but it is totally untrue for biological materials like apples and tomatoes. In section 3.5, it will be demonstrated that the damping parameter is highly dependent on the impact velocity (or deformation rate). The maximum deformation rate of the UTS (0.033 m/s) is more than a factor 10 slower than the velocity during dynamic loading with the pendulum device. As a consequence, the UTS is not an alternative for the pendulum for the determination of the parameters of the Kuwabara and Kono contact force model in the case of apples and tomatoes.

3.4 Basic analysis of the parameters of the Kuwabara and Kono contact force model for biological materials for impacts below the critical impact energy

The parameters (damping and stiffness) of the Kuwabara and Kono model are estimated for apples, tomatoes and potatoes, based on the experimentally measured displacement, displacement rate and contact force.

Twenty Jonagold apples, meat tomatoes, and Bintje potatoes were obtained from a local supermarket and were measured the same day. The apples, tomatoes and potatoes were cut in two. Each half was mounted on the anvil and impacted 1 time, resulting in 40 repetitions for each sample.

The impact energy was chosen below the critical impact level of the biological material involved, i.e. the material does not yield. In the derivation of the Kuwabara and Kono model

the most important assumption was the lack of plastic deformation (see Chapter 2). The impact energy for potatoes was 0.024 J, for apples 0.010 J and for tomatoes 0.006 J.

This impact energy level in the experiment was below the critical impact level for apples and potatoes. For the same potato cultivar used in the experiments ('Bintje'), Baheri (1997) stated that the critical impact energy is situated between 0.065 and 0.115 J. For McIntosh apples Studman *et al.* (1997) stated that the critical impact energy level is between 0.010 and 0.017 J. Own research indicated that 0.010 J is below the critical impact energy level for 'Jonagold' apples (see Chapter 5). In literature no data is available about critical impact levels or critical impact height for external bruising of tomatoes. The reason is that bruise detection of tomato fruit is difficult due to a lack of visible tissue discolouration.

The constant height multiple impact (CHMI) method, validated for apples and potatoes (Bajema and Hyde, 1998), was used to estimate the critical impact energy level of tomato fruits used in the experiment. According to the CHMI method no tissue damage has occurred when the force vs. time graph of a repeated impact with the same impact energy on the same spot shows identical force vs. time graph as the first impact. Starting from an impact energy level of 0.0095 J with tomatoes a shift in the force-time curve of the second impact occurred compared to the first one. This is an indication that mechanical damage was present. The impact energy level of 0.0095 J was also the starting point of the sense of a dent on the impacting spot. However, the correlation between the force-time shift and real tomato cell debonding or cell rupture is not known. Further investigation is necessary to correlate cell damage with the force-time shift.

It can be concluded that no clear evidence was found that no cell damage at the impact energy level of 0.006 J occurs, but the starting point of the force-time shift at 0.0095 J can be seen as an indication that this is not the case.

In the cost function (3.8) the weights, w_δ, $w_{\dot{\delta}}$ and w_{F_c} were chosen to normalize the different terms ($w_q = 1/\langle q \rangle$) ('triple criterion cost function'). The results are summarized in Table 3-3.

Figures 3-8, 3-9 and 3-10 compare experimental and simulated contact force, displacement and displacement rate of a typical potato impact (the curves for apples and tomatoes are similar).

The standard deviation of the parameter estimations of the biological materials seemed to be quite high. Two possible explanations could be given. The differences could be caused by geometrical differences or by biological variability in mechanical tissue properties. Concerning the geometrical differences, it was stated before that the contact force (F_c) is also dependent on the radii of curvature of the colliding bodies. In future research the radii of curvature were included in the model (see section 3.5).

The higher standard deviation of the parameter estimations for potatoes than for apples and tomatoes, can be explained by the more irregular shape of potatoes compared to apples and tomatoes. The higher standard deviation (coefficient of variation) of the parameter estimations of tomatoes compared to apples can be explained by the higher anisotropy of tomato internal structure.

Table 3-3. Kuwabara and Kono contact force model parameter estimation of apples, tomatoes and potatoes based on displacement, displacement rate and contact force

Sample	$\langle k \rangle \pm \sigma_k$ $10^3 * N/m^{3/2}$	$\langle c \rangle \pm \sigma_c$ $[kgm^{-1/2}s^{-1}]$	*Residual norm* C^2
Apples	754 ± 133 (18 %)	1524 ± 263 (17 %)	87 ± 41
Tomatoes	141 ± 460 (33 %)	680 ± 200 (29 %)	16 ± 15
Potatoes	654 ± 208 (32 %)	1587 ± 320 (20 %)	77 ± 27

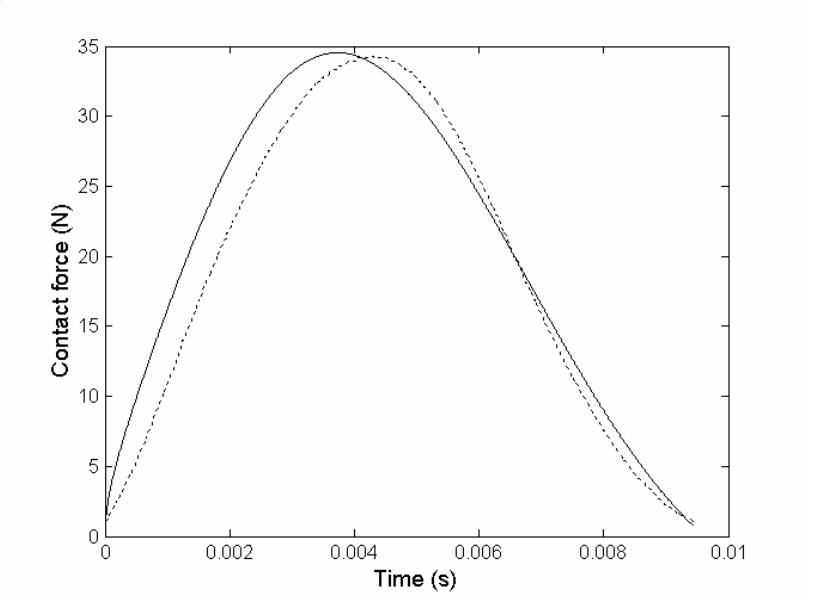

Figure 3-8. One potato: Experimental and simulated contact force with parameter estimation based on displacement, displacement rate and contact force. Solid line: simulation; Dotted line: experimental

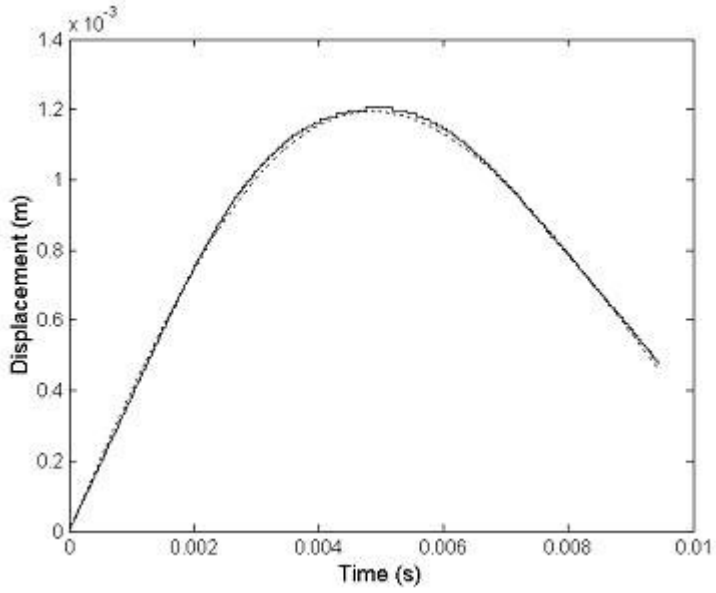

Figure 3-9. One potato: Experimental and simulated displacement with parameter estimation based on displacement, displacement rate and contact force. Solid line: simulation; Dotted line: experimental

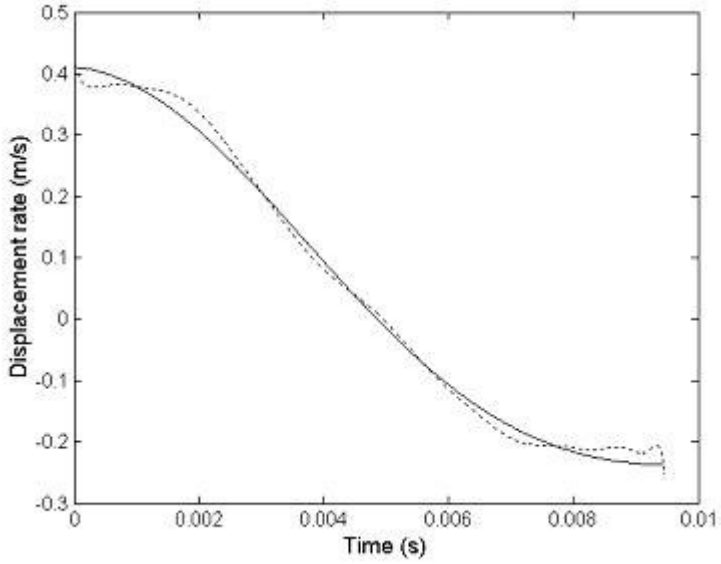

Figure 3-10. One potato: Experimental and simulated displacement rate with parameter estimation based on displacement, displacement rate and contact force. Solid line: simulation; Dotted line: experimental

3.5 Detailed study of the parameters of the Kuwabara and Kono contact force model for apples and tomatoes

3.5.1 Introduction

The first experiments (section 3.4) demonstrated that the pendulum method in combination with the proposed nonlinear parameter estimation method is satisfactory to obtain the contact parameters of the Kuwabara and Kono contact force model. In this section, the dependence of the contact parameters on the effective radius of curvature and impact velocity will be investigated. The dependence of the contact parameters on the radii of curvature of the impacting bodies was described by Kuwabara and Kono (1987), but the dependence on the impact velocity was not. The relationship between the contact parameters and material parameters will also be demonstrated in this section, although the theoretical analysis of this relationship is discussed in Chapter 2.
In contrast to section 3.4 also impacts beyond the critical impact level will be analyzed; i.e. besides viscous energy dissipation also plastic energy dissipation takes place.

3.5.2 Apples

3.5.2.1 Materials and methods

Twenty "Jonagold" apples were utilized to determine the contact parameters of the normal contact force model. The apples were obtained from the Belgian auction "Veiling Haspengouw". All apples were picked in the same orchard and were stored under identical conditions (controlled atmosphere for ± 2 months until the measurement and storage at 3°C, 85% RH during the measurement period in the lab). The acoustic stiffness of the apples was 28.3 ± 1.1 $Hz^2.kg^{2/3}$.
Each apple was divided in a red and green side and mounted on the pendulum was impacted with a flat metal plate ($R = \infty$). Seven velocity levels were applied in the experiment: 0.1; 0.2; 0.3; 0.4; 0.6; 1 and 1.2 m/s. Ten apples were used for the velocity level 0.1-0.4 m/s and ten apples for the velocity level 0.6-1.2 m/s. For the velocity level 0.1-0.4 m/s twenty halves of an apple were repeatedly impacted (on one spot), starting with 0.1 m/s, subsequently 0.2, 0.3 and 0.4 m/s. As a consequence for each impact velocity (0.1; 0.2; 0.3; 0.4 m/s) the impact was measured on twenty halves of an apple. Previous research pointed out that 'Jonagold' apples at room temperature start to bruise starting from 0.35 m/s. Most likely the impact properties of damaged tissue are altered. Integrating the contact parameters of

damaged tissue in the DEM simulations is too far-reaching in this stage of research. To avoid the influence of damaged tissue on the contact force parameters, the impact levels 0.6; 1; 1.2 m/s were not measured on the same halve of an apple. Six halves of an apple were measured at 0.6 m/s, six halves of an apple at 1 m/s and eight halves of an apple at 1.2 m/s.

The local radius of curvature of each half of an apple (at the location of impact) was measured with a radius of curvature meter (details about the radius of curvature meter are given in Chapter 5). Because the apple is not a perfect sphere, the harmonic average was calculated of the circumferential radius of curvature and the meridian radius of curvature (see Figure 3-11), more or less corresponding for Jonagold apples with the minimum radius of curvature (R) and the maximum radius of curvature (R') respectively. The harmonic average ($\frac{2RR'}{R+R'}$), was preferred over the arithmetic average, because the harmonic average privileges the smaller radius of curvature (R) and this radius of curvature contributes more to the peak contact pressure (Hertz theory).

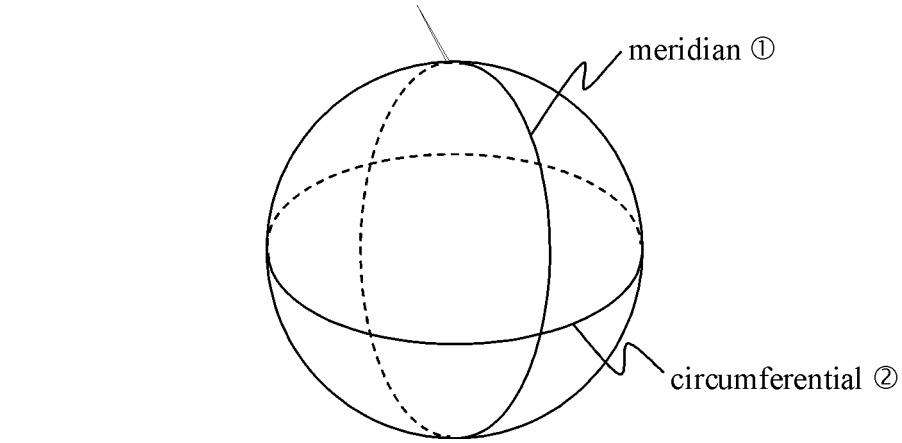

Figure 3-11. Graphical representation of an apple indicating the different directions

For each impact the parameters were determined by performing a nonlinear least squares parameter estimation method minimizing the error between the experimental measured state variables (contact force and displacement) and the predictions by the Kuwabara and Kono contact force model. The data were processed with the statistical software package SAS (SAS version 8.2, The SAS Institute Inc., Cary, NC, U.S.A.). 1-factorial covariance analysis with three concomitant variables was performed (proc GLM). The discrete variable side of apple has two levels: red and green. The concomitant variables (continuous variables in covariance model) are duration of impact t, effective radius of curvature r and impact velocity v.

A backward stepwise (step-down) procedure was used to select the relevant independent variables and their interactions. The significance level for staying in the model was set at 0.05. Sensitivity analysis of the regression equations was performed in EXCEL.

3.5.2.2 Results and discussion

3.5.2.2.a. Contact parameters

All independent variables (side of apple, effective radius of curvature, impact velocity and impact time) had a significant effect (95 % level) on the contact force model parameters. Nevertheless, regression equations without the impact time as independent variable were also constructed because this variable is not known *a priori* (only after the impact) and as a consequence the regression equations including the impact time can not be used in DEM.
In Table 3-4 the statistically significant models with all the independent variables are presented (side of apple, effective radius of curvature, impact velocity and impact time). Figures 3-12 and 3-13 give the predicted value-experimental value plot of the model including the impact time for respectively the damping and spring parameter. In Table 3-5 the statistically significant models are described by elimination of the impact time as independent variable. Figures 3-14 and 3-15 show the predicted value-experimental value plot for the reduced model for respectively the damping and spring parameter. In Figures 3-16 and 3-17 the statistical relationship between the contact parameters and the impact velocity and effective radius of curvature is shown graphically.

Table 3-4. Apple: Treatment regression equations of the models with impact time included

	R^2
$c_R = -10410 + 9279\ v + 303000\ r + 1291794\ t - 134000\ v \times r - 787568\ v \times t - 32419000\ r \times t$ $c_G = -10738 + 9799\ v + 303000\ r + 1291794\ t - 134000\ v \times r - 787568\ v \times t - 32419000\ r \times t$	0.57
$k_{R/G} = 3258994 + 5282475 v + 25762000\ r - 287734236\ t - 81786000\ v \times r - 542201717\ v \times t$	0.89

c: damping parameter [kg $m^{-1/2}$ s^{-1}]; k: spring parameter [$N/m^{3/2}$]; subscript R: red side of apple; subscript G: green side of apple; v: impact velocity [m/s]; r: effective radius of curvature [m]; t: impact time [s]

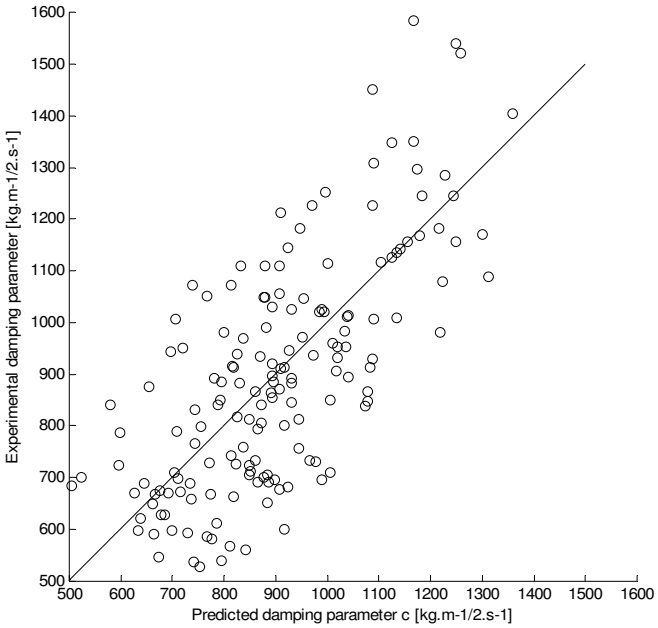

Figure 3-12. Apple: Model with impact time included (Table 3-4): predicted value – experimental value plot of the damping parameter c [kg $m^{-1/2}$ s^{-1}]

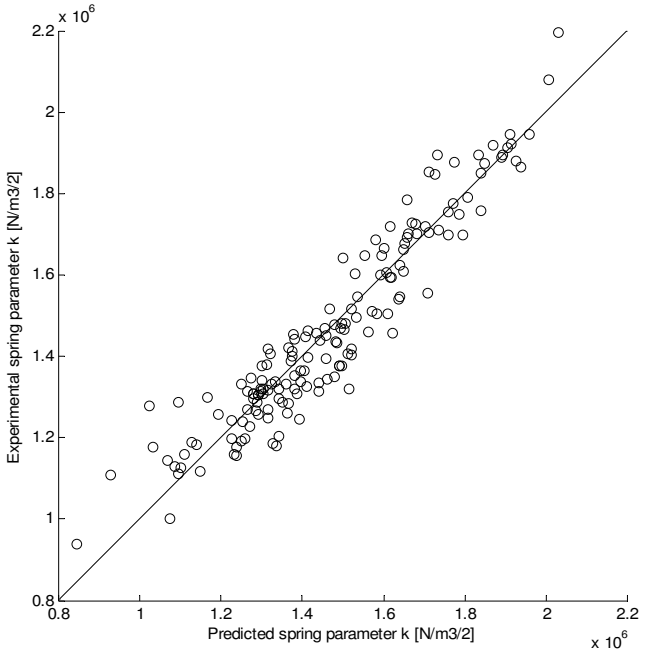

Figure 3-13. Apple: Model with impact time included (Table 3-4): predicted value – experimental value plot of the spring parameter k [N/$m^{3/2}$]

Table 3-5. Apple: Treatment regression equations of the models without impact time

	R^2
$c_R = -612 + 1872\ v + 54000\ r - 76000\ v \times r$ $c_G = 8 + 2187\ v + 27000\ r - 76000\ v \times r$	0.48
$k_R = 865408 - 432426\ v + 23444000\ r$ $k_G = 725855 - 432426\ v + 23444000\ r$	0.31

c: damping parameter [kg $m^{-1/2}$ s^{-1}]; *k*: spring parameter [$N/m^{3/2}$]; subscript *R*: red side of apple; subscript *G*: green side of apple; *v*: impact velocity [m/s]; *r*: effective radius of curvature [m]; *t*: impact time [s]

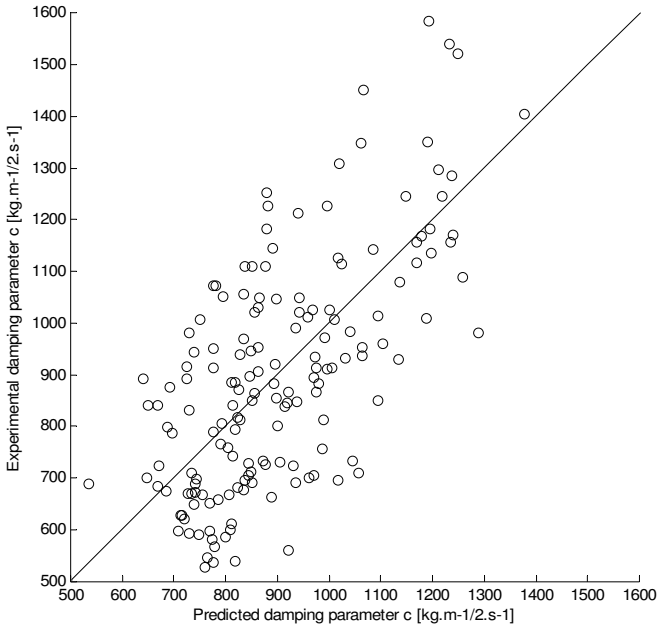

Figure 3-14. Apple: Model without impact time (Table 3-5): predicted value – experimental value plot of the damping parameter *c* [kg $m^{-1/2}$ s^{-1}]

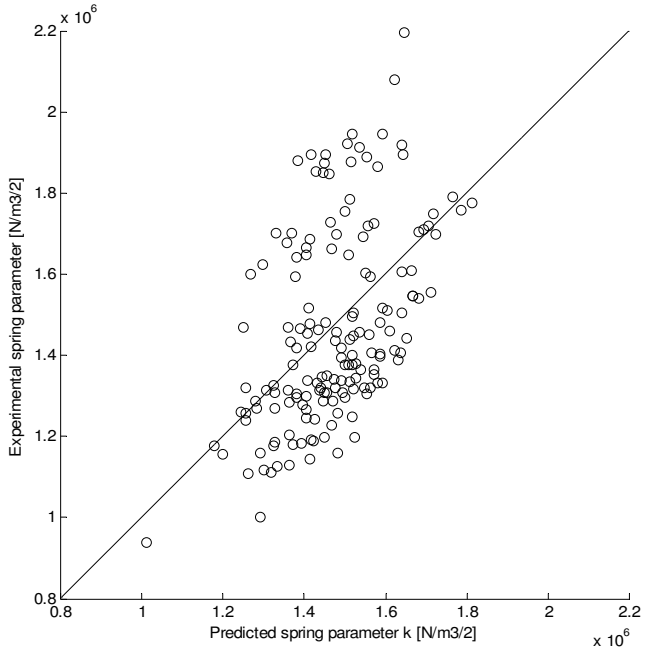

Figure 3-15. Apple: Model without impact time (Table 3-5): predicted value – experimental value plot of the spring parameter *k* [N/m$^{3/2}$]

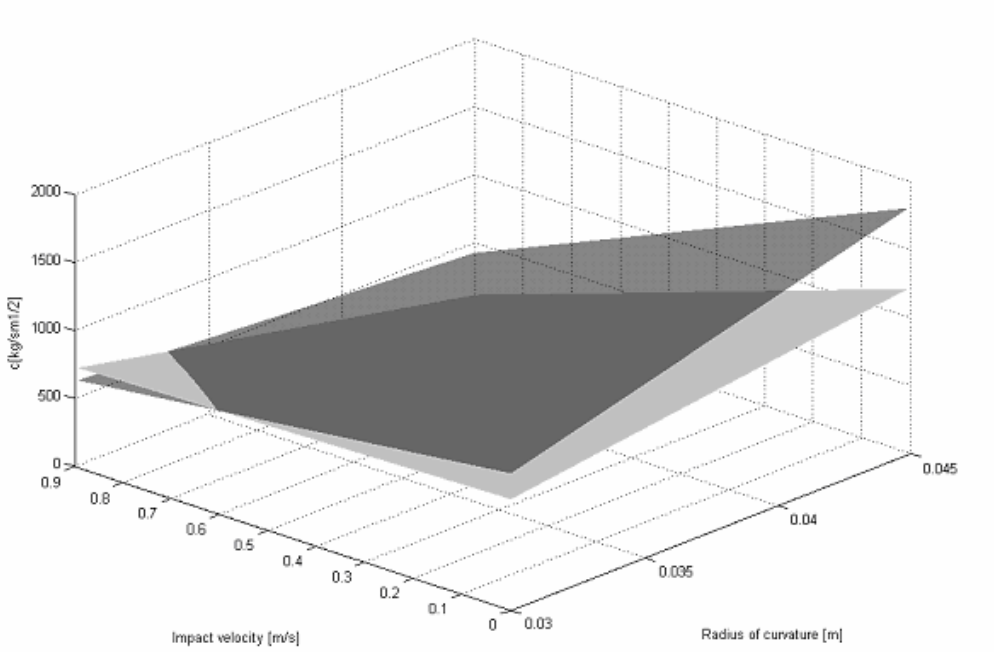

Figure 3-16. Apple: 3-D plot of the effect of the effective radius of curvature and impact velocity on the damping parameter *c* [kg m$^{-1/2}$ s^{-1}], produced from the regression equations of Table 3-5. Upper plane (black) is for the red side of the Jonagold apple. Lower plane (grey) is for the green side of the 'Jonagold' apple.

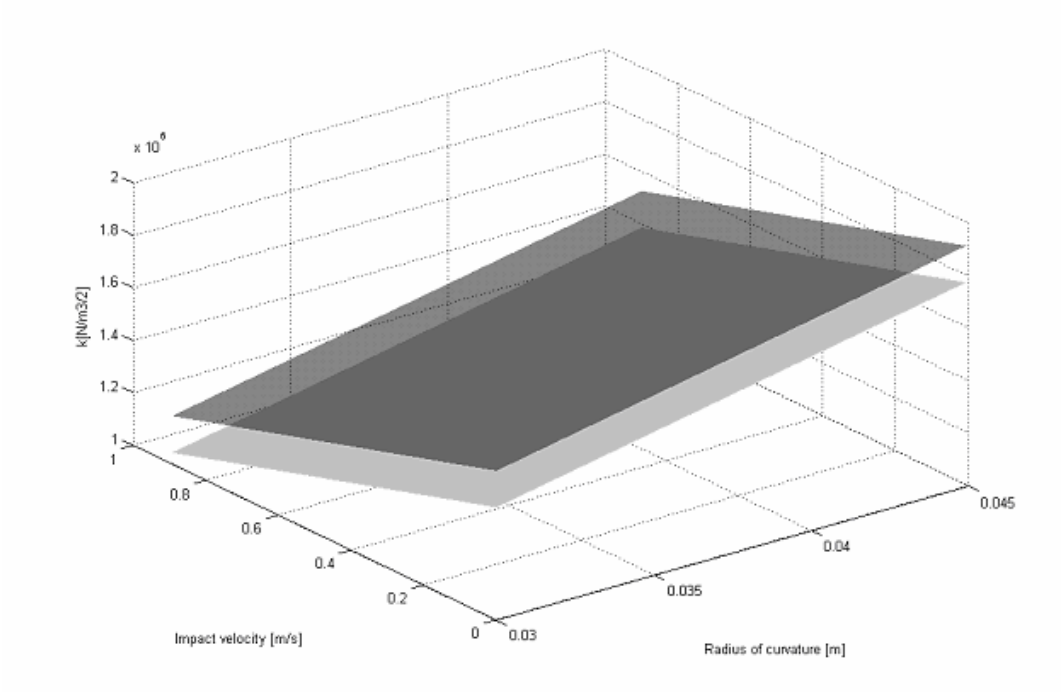

Figure 3-17. Apple: 3-D plot of effect radius of effective radius of curvature and impact velocity on the spring parameter *k* [N/m$^{3/2}$], produced from the regression equations of Table 3-5. Upper plane (black) is for the red side of the Jonagold apple. Lower (grey) plane is for the green side of the 'Jonagold' apple.

In Table 3-6 and 3-7 the extra sum of squares for the regression models without the impact time are given for the spring parameter k and damping parameter c respectively.

Table 3-6. Type I Extra sum of squares for spring parameter k

Type I Extra sum of squares	*Absolute number*	$\left[SSR(X_2, X_2 \times X_1 \middle| X_1) / SSE(X_1)\right]$*100
$SSR(r, r \times side \middle| side)$	$2.08*10^{12}$	18.4
$SSR(r, r \times \mathrm{v} \middle| \mathrm{v})$	$1.37*10^{12}$	13.0
$SSR(\mathrm{v}, \mathrm{v} \times side \middle| side)$	$1.43*10^{12}$	12.6
$SSR(\mathrm{v}, \mathrm{v} \times r \middle| r)$	$9.40*10^{11}$	9.3
$SSR(side, side \times r \middle| r)$	$8.46*10^{11}$	7.2
$SSR(side, side \times \mathrm{v} \middle| \mathrm{v})$	$6.28*10^{11}$	6.0

The third column indicates the coefficient of partial determination multiplied by 100. It indicates with how many percent the error sum of squares when only X_1 is in the model is further reduced when $X_2, X_2 \times X_1$ are added to the model

Table 3-7. Type I Extra sum of squares for damping parameter *c*

Type I Extra sum of squares	*Absolute number*	$\left[SSR(X_2, X_2 \times X_1 \mid X_1) / SSE(X_1)\right]$*100
$SSR(side, side \times r \mid r)$	$2.10*10^6$	19.3
$SSR(side, side \times \mathrm{v} \mid \mathrm{v})$	$1.83*10^6$	18.1
$SSR(\mathrm{v}, \mathrm{v} \times r \mid r)$	$1.92*10^6$	17.7
$SSR(\mathrm{v}, \mathrm{v} \times side \mid side)$	$1.66*10^6$	16.7
$SSR(r, r \times side \mid side)$	$1.19*10^6$	12.0
$SSR(r, r \times \mathrm{v} \mid \mathrm{v})$	$8.24*10^5$	8.1

The third column indicates the coefficient of partial determination multiplied by 100. It indicates with how many percent the error sum of squares when only X_1 is in the model is further reduced when $X_2, X_2 \times X_1$ are added to the model

From the results can be seen that eliminating the impact time decreases the statistical prediction of the contact parameters considerably. The impact time was eliminated because it is not known *a priori* and as a consequence cannot be used in DEM. The reason for the much better fit when the impact time is included, is the mathematical relationship between the impact time and the material parameters (*A* and *E*). For the Kuwabara and Kono contact force model for viscoelastic spheres this relationship is given by (Schwager and Pöschel, 1998):

$$t_i = \left(\frac{\rho}{m_{eff}}\right)^{-2/5} \mathrm{v}_i^{-1/5} \left(D_0 + D_1 \frac{3}{2} A \left(\frac{\rho}{m_{eff}}\right)^{2/5} \mathrm{v}_i^{1/5} + D_2 \left(\frac{3}{2} A\right)^2 \left(\frac{\rho}{m_{eff}}\right)^{4/5} \mathrm{v}_i^{2/5} + \ldots \right) \quad (3.13)$$

with m_{eff} the effective mass [kg]

v_i the impact velocity [m/s]

A the dissipative parameter [s]

ρ can be calculated as $\rho = \frac{2E}{3(1-\nu^2)}\sqrt{R^*}$

The mathematical relationship between the material parameters and the contact parameters has been discussed before (see Chapter 2, section 2.3.3). By interpreting equation (3.13) it can be seen that higher elasticity leads to shorter impact time and higher viscosity leads to longer impact time. By correlation analysis in SAS it could also be shown statistically: $(r_{k,t})$ = -0.64 and $(r_{c,t})$ = 0.20.

From the regression equations (Table 3-5 and Figures 3-16 and 3-17) can also be seen that higher effective radius of curvature leads to higher contact force parameters. This is in accordance with the Kuwabara and Kono contact force model (equation (2.17)). The only

exception was for high impact velocities, where on opposite effect of the effective radius of curvature on the damping parameter c was identified. The negative effect of the impact velocity on both the spring parameter k and the damping parameter c of the Kuwabara and Kono contact force model is remarkable (see Table 3-4 and 3-5). This has not been described in literature before.

The negative effect of the impact velocity on the damping parameter c could be expected. As described before, the damping is correlated with the (mathematical) dissipative parameter *A,* which in turn is correlated with the material bulk and shear viscosity $\eta_{1/2}$. As will be described in chapter 4, the shear viscosity of most materials (like apples) is negatively correlated with the shear rate[24]. Also equation (2.16) describing the relation between damping, stiffness and impact velocity of the Lankarani and Nikravesh model[25] (2.13) predicts a lower damping parameter with increasing impact velocity. As can be seen in Figure 3-16 the effect of the impact velocity on the damping parameter is very strong for high effective radius of curvature. The negative effect of the impact velocity on the spring parameter k was not expected. In preliminary experiments with another batch of Jonagold apples the dependency of the spring parameter on the impact velocity could not be indicated[26]. Also, by applying the Kelvin-Voigt model on the experimental data[27], the opposite was found: an increase in the spring parameter k by increasing the impact velocity (data not shown). The latter result confirms the research of Lichtensteiger *et al.* (1988a) who evaluated the dependency of the coefficients of the Kelvin-Voigt model with the impact velocity for viscoelastic spheres.

It was also found that the spring parameter k and the damping parameter c are not the same for the red or green side of the "Jonagold" apple: the damping parameter and spring parameter were higher for the red side of the "Jonagold" apple.

From the extra sum of squares analysis presented in Table 3-6 and 3-7 can be concluded that most of the variance of the spring parameter k is explained by the effective radius of curvature r at the location of impact, followed by the impact velocity v and the side of the apple (red or green side). However most variance of the damping parameter is explained by the side of the apple, closely followed by the impact velocity v. The effective radius of curvature at the location of impact r has the least effect on the damping parameter c.

[24] At average the shear rate of the deformation of an impact with higher impact velocity can also be considered to be higher.
[25] A nonlinear contact force model close to the Kuwabara and Kono contact force model
[26] The data is not shown due to inaccurate measurement of the radius of curvature at the location of impact
[27] As explained before, the Kelvin-Voigt model is inadequate to predict the impact behaviour; this can be seen from the inaccurate fit of the real impact data (not shown).

A sensitivity analysis of the regression equations in Table 3-5 was performed in EXCEL to obtain a more detailed picture of the effects of the independent variables on the response variables.

From this analysis can be concluded that the effect of the impact velocity (-) and the effective radius of curvature (+) on the spring parameter is comparable: ≅ 20 % change in spring parameter between the highest and lowest value of impact velocity and effective radius of curvature in the experiment. Because of the interaction term in the regression equations for the damping parameter, the interpretation is more complex. A 50 % reduction in the damping parameter was noted between the lowest (0.2 m/s) and highest value of the impact velocity (0.9 m/s) for low effective radius of curvature (0.035 m). For high effective radius of curvature (0.045 m) even a reduction of 90 % was identified for the damping parameter between the lowest (0.2 m/s) and highest (0.9 m/s) value of the impact velocity in the experiment. The effect of the effective radius of curvature for low impact velocity (0.2 m/s) is modest: a 20 % increase in damping parameter between low effective radius of curvature (0.035 m) and high effective radius of curvature (0.045 m). For high impact velocity the opposite effect of the effective radius of curvature on the damping parameter, not according to the Kuwabara and Kono model, was noted. No explanation for this result could be found.

3.5.2.2.b Material parameters

The material parameters were calculated from the contact parameters using equations (2.41) and (2.52). In Table 3-8 the statistically significant models with all independent variables are depicted (side of apple, impact velocity and impact time). Figures 3-18 and 3-19 give the predicted value-experimental value plot of the model including the impact time for respectively the equivalent elastic modulus E^* (E.(1-ν^2)) and the dissipative parameter A for the impact apple-metal (could be noted A^*, equivalent dissipative parameter, but this is not a generally accepted terminology).

In Table 3-9 the statistically significant models are given by elimination of the impact time as independent variable. Figures 3-20 and 3-21 show the predicted value-experimental value plot for the reduced model for respectively the equivalent elastic modulus and the dissipative parameter.

Table 3-8. Apple: Treatment regression equations of the models with the impact time included

	R^2
$E_{R/G}^{*} = 14631167 + 7033963\mathrm{v} - 960852947t - 1568559609\mathrm{v}\times t$	0.73
$A_R = -0,004198 + 0.0100944\mathrm{v} + 0.9366971t - 1.399362675\mathrm{v}\times t$ $A_G = -0.00449972 + 0.011061866\mathrm{v} + 0.9366971t - 1.399362675\mathrm{v}\times t$	0.31

E^*: Equivalent elastic modulus [Pa]; A: Dissipative parameter for impact apple-metal [s]; subscript R: red side of apple; subscript G: green side of apple; v: impact velocity [m/s]; t: impact time [s]

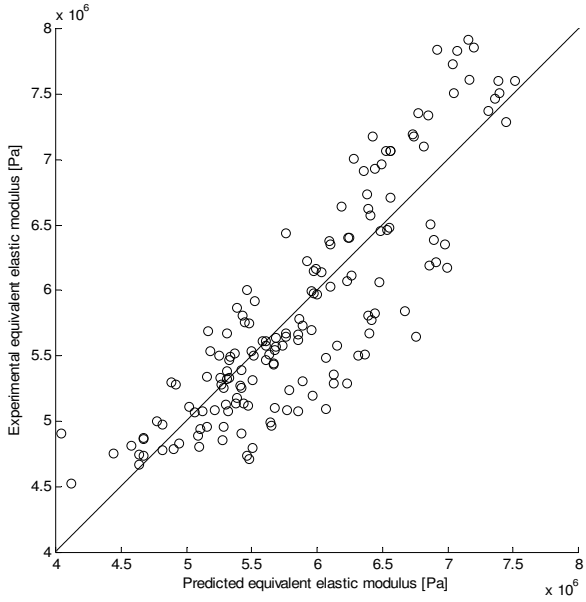

Figure 3-18. Apple: Model with impact time included: predicted value – experimental value plot of the equivalent elastic modulus E^* [Pa]

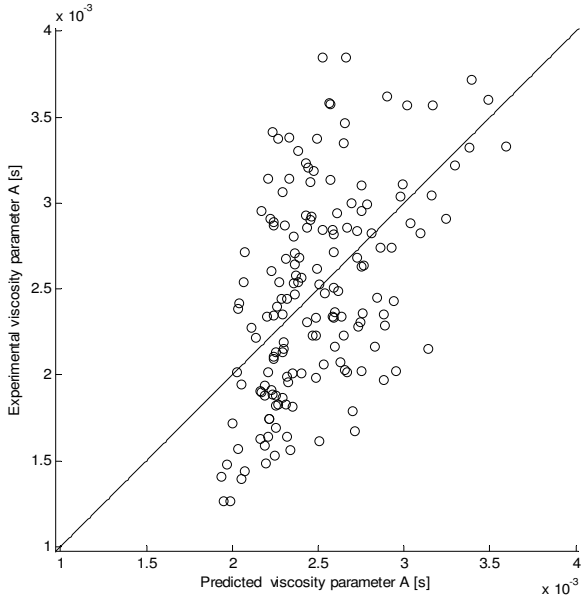

Figure 3-19. Apple: Model with impact time included: predicted value – experimental value plot of the dissipative parameter A [s]

Table 3-9. Apple: Treatment regression equations of the models without the impact time

	R^2
$E_R^* = 6790286 - 1823034\text{v}$ $E_G^* = 6242440 - 1823034\text{v}$	0.20
$A_R = 0.00303 - 0.00102\text{v}$ $A_G = 0.00266 - 0.00102\text{v}$	0.13

E^*: Equivalent elastic modulus [Pa]; A: Dissipative parameter for impact apple-metal [s]; subscript R: red side of apple; subscript G: green side of apple; v: impact velocity [m/s]

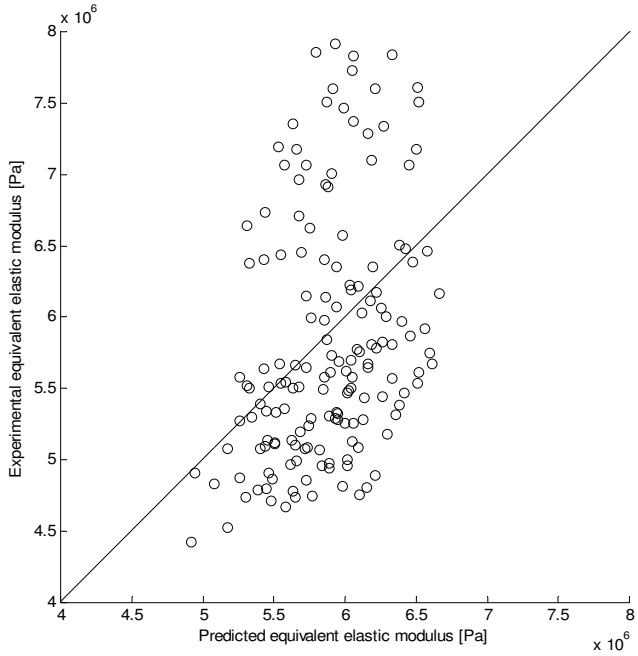

Figure 3-20. Apple: Model without impact time: predicted value – experimental value plot of the equivalent elastic modulus E^* [Pa]

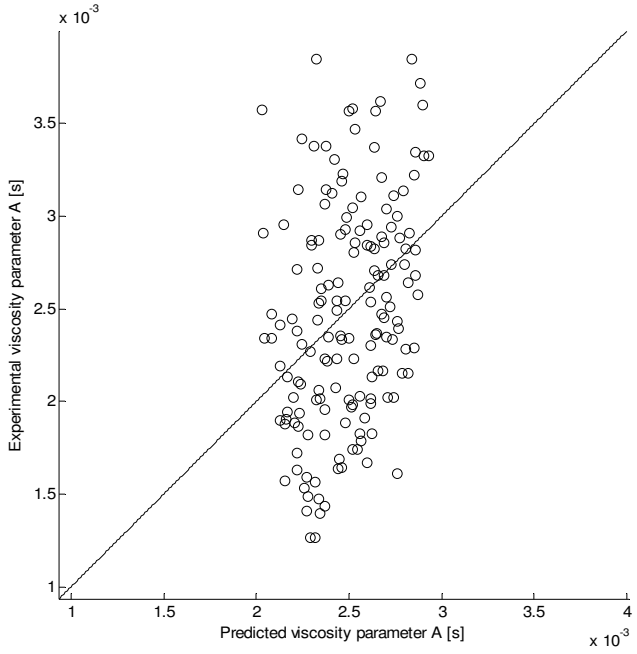

Figure 3-21. Apple: Model without the impact time: predicted value – experimental value plot of the dissipative parameter *A* [s]

Better statistical relationships could be obtained with the impact time included in the statistical model. The explanation of the correlation of the impact time with the material parameters has been discussed in the previous section (section 3.5.2.2.a).

The low coefficient of determination of the statistical models without the impact time indicate that impact velocity and side of impact (red/green side of apple) as only independent variables are insufficient to predict the elastic modulus and dissipative parameter of the apples. In other words other independent variables that were not included in the model (for example the fact the apple was positioned on the tree toward the sun side or not) explain more the variation of the elastic modulus and the dissipative parameter of the apples than the impact velocity (or deformation rate) and the side of impact.

However, especially the dissipative parameter has a low coefficient of determination. Therefore also second reason can be mentioned. To calculate the dissipative parameter in the case of impact tomato-metal plate it was indicated in Chapter 2 (equation 2.53) that the relationship $A_{fruit} = 4c/k$ applies. Dividing the damping parameter by the spring parameter increases the variability of the dissipative parameter compared the variability of the damping- and spring parameter separately.

The negative relationship between the impact velocity and the dissipative parameter was expected and is explained in the previous section (section 3.5.2.2.a).
The elastic modulus of the apples, calculated from the equivalent elastic modulus by multiplying with $1-\nu^2$, with Poisson's ratio ν for Jonagold apples 0.35 (Golacki and Stropek, 2001), was 5.09 ± 0.83 MPa. The order of magnitude of the elastic modulus calculated from the pendulum experiment is comparable with the elastic modulus determined by quasi-static compression tests. Lammertyn *et al.* (1998) measured an elastic modulus of 3.63 ± 0.41 MPa for Jonagold apples, own research (Chapter 4) indicated an elastic modulus of 3.02 ± 0.44 MPa for Jonagold apples (not the same apples were used as for the pendulum experiment).

As for the spring parameter in the previous section, a negative relationship between the (equivalent) elastic modulus and the impact velocity was found. This is in contradiction with preliminary research where a statistical relationship between impact velocity and elastic modulus could not be identified (data not shown). These results were compared with the data about strain rate dependency of the elastic modulus of apples found in literature. However, a direct comparison with the elastic modulus from compression tests (Instron testing machine) is difficult. Firstly, the strain rate during impact is not constant (like it is in compression tests) and secondly due to the curvelinear shape of force-deformation and stress-stain curve the modulus of elasticity is dependent on the deformation. In contrast to the compression tests the elastic modulus calculated from the nonlinear parameter estimation method described above is not measured at a certain deformation (or strain) but must be seen as 'an average elastic modulus' during impact. Besides, with increasing impact velocities both the maximum deformation and the average deformation rate (strain rate) increase. The effect of deformation and deformation rate on the elastic modulus is mixed.

The literature about the effect of strain rate on the elastic modulus by compression of apples is limited. Bajema *et al.* (1999) found there exists no relationship between the strain rate and the apparent elastic modulus (secant elastic modulus at point of failure) for red Delicious apples. In some cases they found an increase of the elastic modulus in other cases a decrease in elastic modulus with strain rate. Maybe this result can be explained by the research results of Pitt and Chen (1983). These authors found that the effect of the strain rate on the stress-strain curve is dependent on the tissue turgor.
A higher elastic modulus and dissipative parameter was found for the red side of the Jonagold apple compared to the green side.

3.5.3 Tomatoes

3.5.3.1 Materials and methods

Fifty meat tomatoes were utilized to determine the contact parameters of the normal contact force model. From each tomato a distinct partition and compartment was identified and impacted by the flat plate of the pendulum device. Eight velocity levels were applied: 0.2; 0.3; 0.4; 0.5; 0.6; 0.7; 0.8 and 1 m/s. For the velocity level 0.2-0.6 m/s. 25 tomatoes were repeatedly impacted with a flat plate ($R = \infty$) at one compartment and one partition, for each impact increasing the impact velocity (starting at 0.2 m/s, subsequently 0.3; 0.4; 0.5. 0.6 m/s). As a consequence for each impact velocity 25 impacts were obtained both for compartment and partition. Additionally for each impact level in the range 0.5-1 m/s the compartment and partition of five tomatoes was single impacted. As a consequence, velocity levels 0.5 m/s and 0.6 m/s were both measured on multi impacted tomatoes (at one spot the velocity increases from 0.2 m/s to 0.5 (0.6) m/s) and single impacted tomatoes. This was done to investigate the influence of already impacted tissue – and the unknown onset of plastic deformation – on the contact parameters.

In contrast to the apple experiment intact tomatoes, enclosed by plasticine, were impacted. Hard fruit, like apples are cut in two when mounted on the pendulum to limit the deformation of the impacted fruit on the location of impact. It has been shown that by dividing the tomato in two the rigidity of the tomato is lost, leading to altered impact behaviour. It can be assumed that enclosing the tomato by the plasticine gives rise to more realistic contact force model parameters than the use of tomato halves.

The local radius of curvature of each partition and compartment was measured by a radius of curvature meter (details about the radius of curvature meter are presented in Chapter 5).

Because the tomato is not a perfect sphere, the harmonic average was calculated of the circumferential radius of curvature and the meridian radius of curvature (see section 3.5.2.1).

For each impact the parameters were determined by performing a nonlinear least squares estimation minimizing the error between the experimental measured quantities (contact force and displacement) and the predictions by the Kuwabara and Kono model.

The data were processed with the statistical software package SAS (SAS version 8.2, The SAS Institute Inc., Cary, NC, U.S.A.). 1-factorial covariance analysis with three concomitant variables was performed (proc GLM). The discrete variable side of tomato has two levels: compartment and partition. The concomitant variables (continuous variables in covariance model) are duration of impact t, effective radius of curvature r and impact velocity v.

A backward stepwise (step-down) procedure was used to select the relevant independent variables and their interactions. The significance level for staying in the model was set at 0.05. Sensitivity analysis of the regression equations was performed in EXCEL.

3.5.3.2 Results and discussion

No significant difference (95 % level) in contact parameters could be identified for multi and single impact tomatoes for the 0.5 and 0.6 m/s impact level. As a consequence, the data was pooled.

3.5.3.2.a. Contact parameters

In Table 3-10 the statistical significant models with all the independent variables are described (side of tomato, effective radius of curvature, impact velocity and impact time). Figures 3-22 and 3-23 show the predicted value-experimental value plot of the model including the impact time for respectively the damping and spring parameter In Table 3-11 the statistical significant models are given by elimination of the impact time as independent variable. Figures 3-24 and 3-25 indicate the predicted value-experimental value plot for the reduced model for respectively the damping and spring parameter. In Figures 3-26 and 3-27 the statistical relationship between the contact parameters and the impact velocity and effective radius of curvature is shown graphically.

Table 3-10. Tomato: Treatment regression equations of the models including impact time

	R^2
$c_P = 2617 - 2258\mathrm{v} - 107779t + 112511\mathrm{v}\times t$ $c_C = 2577 - 2258\mathrm{v} - 107779t + 112511\mathrm{v}\times t$	0.74
$k_P = 677366 - 417215\mathrm{v} + 299662r - 34773750t + 22962260\mathrm{v}\times t$ $k_C = 633157 - 417215\mathrm{v} + 299662r - 31456877t + 22962260\mathrm{v}\times t$	0.91

c: damping parameter [kg $m^{-1/2}$ s^{-1}]; k: spring parameter [$N/m^{3/2}$]; subscript P: tomato partition; subscript C: tomato compartment; v: impact velocity [m/s]; r: effective radius of curvature [m]; t: impact time [s]

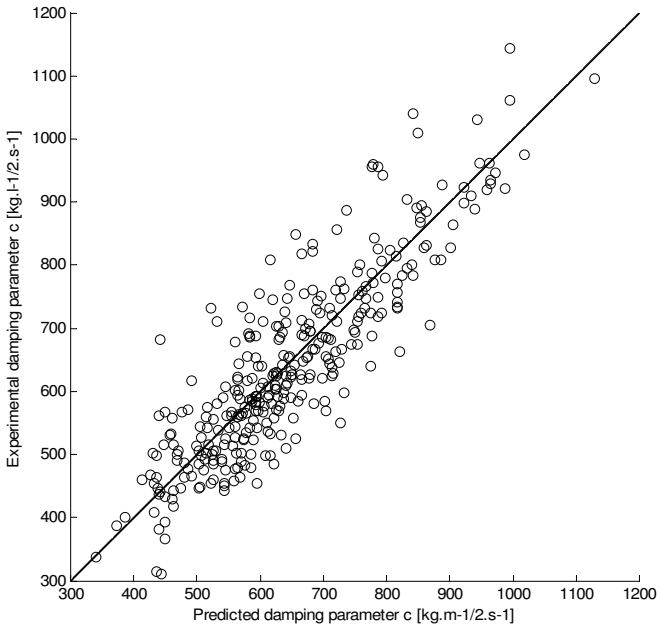

Figure 3-22. Tomato: Model with impact time included (Table 3-10): predicted value – experimental value plot of the damping parameter *c* [kg $m^{-1/2}$ s^{-1}]

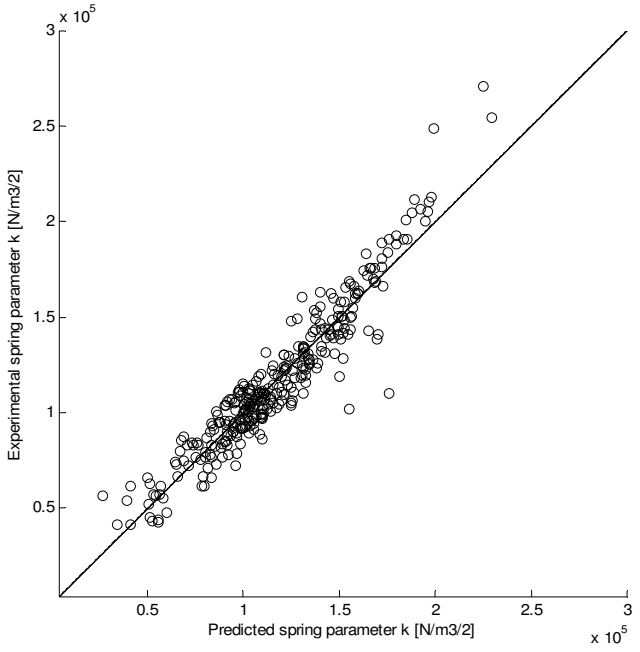

Figure 3-23. Tomato: Model with impact time included (Table 3-10): predicted value – experimental value plot of the spring parameter *k* [N/$m^{3/2}$]

Table 3-11. Tomato: Treatment regression equations of the models without the impact time

	R^2
$c_P = 767 - 549\mathrm{v} + 8949r$ $c_C = 948 - 549\mathrm{v} - 1033r$	0.55
$k_p = 100292 - 115017\mathrm{v} + 3294360r$ $k_C = 142422 - 115017\mathrm{v} + 655983r$	0.42

c: damping parameter [kg $m^{-1/2}$ s^{-1}]; k: spring parameter [$N/m^{3/2}$]; subscript P: tomato partition; subscript C: tomato compartment; v: impact velocity [m/s]; r: effective radius of curvature [m]

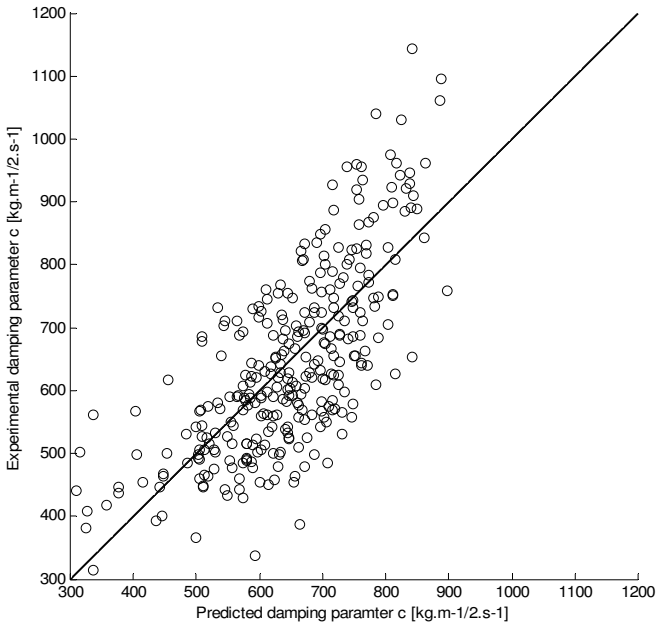

Figure 3-24. Tomato: Model without impact time (Table 3-11): predicted value – experimental value plot of the damping parameter c [kg $m^{-1/2}$ s^{-1}]

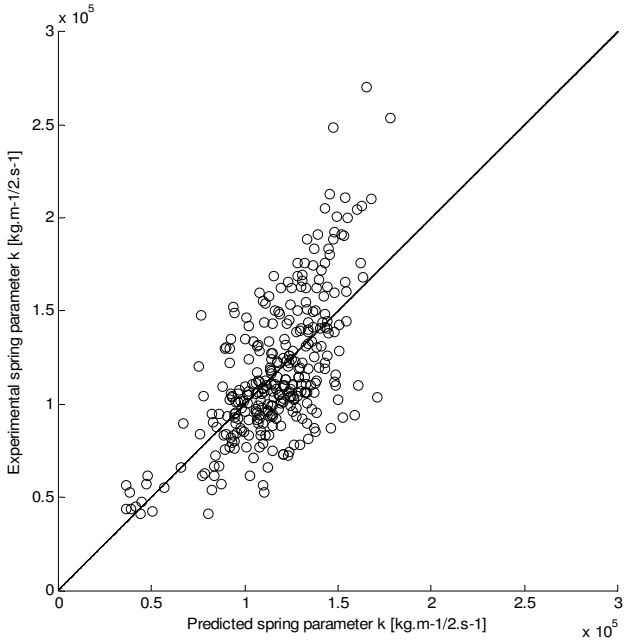

Figure 3-25. Tomato: Model without impact time (Table 3-11): predicted value – experimental value plot of the spring parameter k [N/m$^{3/2}$]

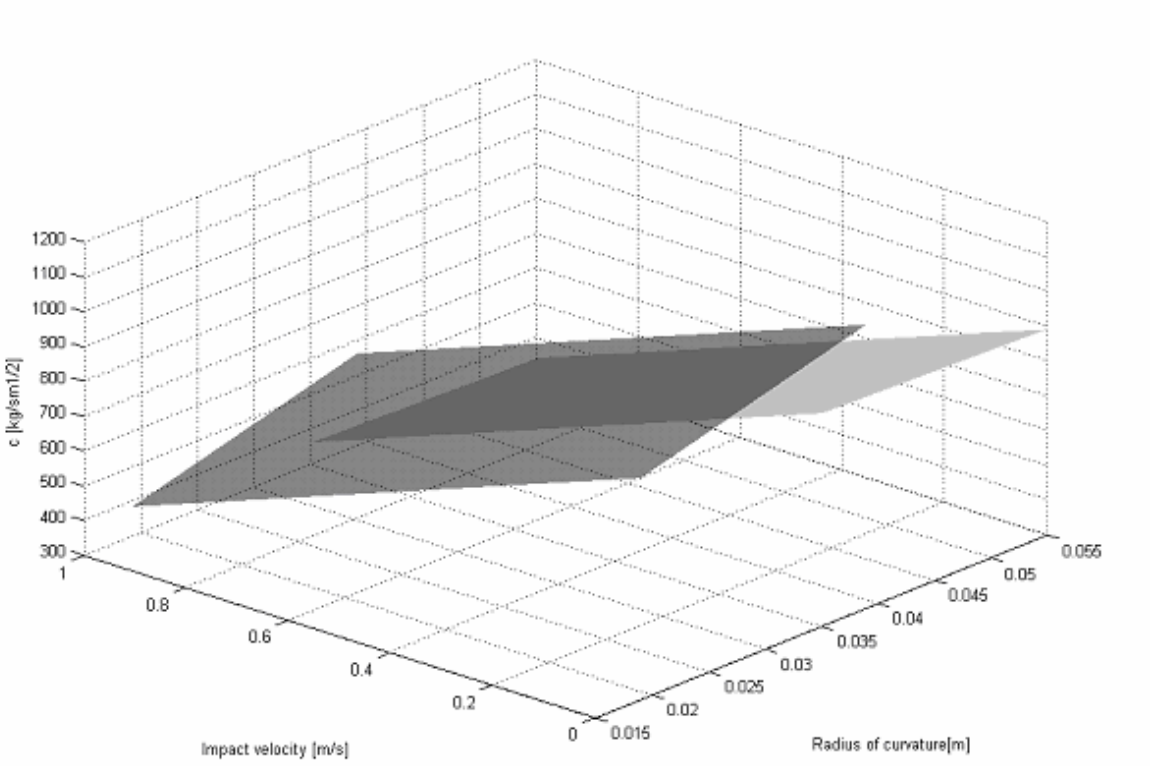

Figure 3-26. Tomato: 3-D plot of the effect of the effective radius of curvature and impact velocity on the damping parameter c [kg m$^{-1/2}$ s^{-1}], produced from the regression equations of Table 3-11. Upper plan (black) indicates tomato partition. Lower plane (grey) indicates tomato compartment.

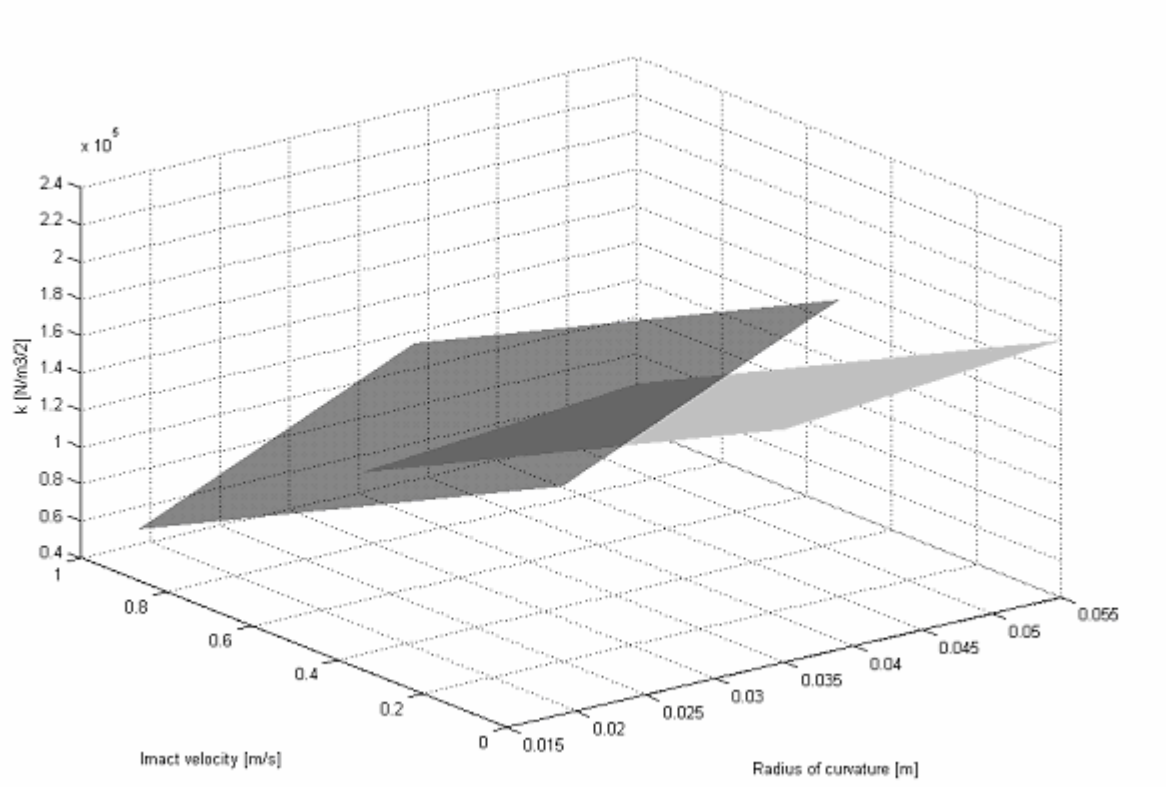

Figure 3-27. Tomato: 3-D plot of the effect of the effective radius of curvature and impact velocity on the spring parameter *k* [N/m$^{3/2}$], produced from the regression equations of Table 3-11. Upper plane (black) indicates tomato partition. Lower plane (grey) indicates tomato compartment.

In Table 3-12 and 3-13 the extra sum of squares for the regression models without the impact time are given for the spring parameter k and damping parameter c respectively.

Table 3-12. Type I Extra sum of squares for spring parameter *k*

Type I Extra sum of squares	*Absolute number*	$\left[SSR(X_2, X_2 \times X_1 \mid X_1) / SSE(X_1)\right]$*100
$SSR(\mathrm{v}, \mathrm{v} \times side \mid side)$	$1.45*10^{11}$	31.1
$SSR(\mathrm{v}, \mathrm{v} \times r \mid r)$	$1.43*10^{11}$	30.3
$SSR(side, side \times r \mid r)$	$3.87*10^{10}$	8.2
$SSR(side, side \times \mathrm{v} \mid \mathrm{v})$	$8.13*10^{9}$	2.5
$SSR(r, r \times side \mid side)$	$3.29*10^{10}$	7.1
$SSR(r, r \times \mathrm{v} \mid \mathrm{v})$	$8.82*10^{8}$	0.3

The third column indicates the coefficient of partial determination multiplied by 100. It indicates with how many percent the error sum of squares when only X_1 is in the model is further reduced when $X_2, X_2 \times X_1$ are added to the model

Table 3-13. Type I Extra sum of squares for spring parameter c

Type I Extra sum of squares	*Absolute number*	$\left[SSR(X_2, X_2 \times X_1 \middle| X_1) / SSE(X_1)\right]*100$
$SSR(\mathrm{v}, \mathrm{v} \times r \middle| r)$	$3.73*10^6$	49.0
$SSR(\mathrm{v}, \mathrm{v} \times side \middle| side)$	$3.66*10^6$	47.9
$SSR(side, side \times \mathrm{v} \middle| \mathrm{v})$	$6.67*10^5$	14.9
$SSR(side, side \times r \middle| r)$	$6.20*10^5$	8.0
$SSR(r, r \times \mathrm{v} \middle| \mathrm{v})$	$4.25*10^5$	9.5
$SSR(r, r \times side \middle| side)$	$3.04*10^5$	4.1

The third column indicates the coefficient of partial determination multiplied by 100. It indicates with how many percent the error sum of squares when only X_1 is in the model is further reduced when $X_2, X_2 \times X_1$ are added to the model

Eliminating the impact time from the model decreases the statistical prediction of the contact parameters considerably. The same explanation can be given as for the apples (section 3.5.2.2).

From the regression equations (Table 3-10 and 3-11) can be seen that higher radii of curvature led to higher contact force model parameters as predicted by the Kuwabara and Kono contact force model. The only exception was for the damping parameter of the tomato compartment where a slight negative effect of the effective radius of curvature was identified. No explanation for this exception could be found.

The negative effect of the impact velocity on spring parameter k and damping parameter c of the Kuwabara and Kono contact force model was also found in the case of tomatoes. The same comments can be made as for the apples (see section 3.5.2.2).

It was identified that the damping and stiffness are higher for the partition compared to the compartment of the tomato.

From the extra sum of squares analysis presented in Table 3-12 and 3-13 can be concluded that by far most of the variance of the spring parameter k and damping parameter c is explained by the impact velocity v. The effect of the side of impact (compartment or partition) and the effective radius of curvature r is much less.

A sensitivity analysis of the regression equations in Table 3-11 was performed in EXCEL to obtain a more detailed analysis of the effect of the independent variables on the response variable. For the tomato partition the effect of the impact velocity (-) on the damping parameter is considerably higher than the effective radius of curvature (+): ≅45 % change in damping parameter between the highest and lowest value of impact velocity compared to ≅25 % change in damping parameter between the highest and lowest effective radius of

curvature in the experiment. For the tomato partition the effect of the impact velocity (-) on the spring parameter is also higher than the effective radius of curvature (+): ≅50 % change in damping parameter between the highest and lowest value of impact velocity and ≅40 % change in damping parameter between the highest and lowest effective radius of curvature in the experiment.

For the tomato compartment a different picture was seen. A reduction of 45 % in the damping parameter was noted between the lowest (0.3 m/s) and highest value of the impact velocity (0.9 m/s). Also a reduction of 50 % was noted for the spring parameter between the lowest (0.3 m/s) and highest (0.9 m/s) value of the impact velocity in the experiment. On the other hand almost no effect of the effective radius of curvature was noted for the damping parameter and only a 13 % increase of the spring parameter was noted for the lowest (0.035 m) and highest (0.055 m) value of the effective radius of curvature in the experiment. It can be concluded that the effect of the impact velocity on both damping and spring parameter for the tomato compartment is much stronger than the effect of the effective radius of curvature.

3.5.3.2.b Material parameters

The material parameters were calculated from contact parameters applying equations (2.41) and (2.52).

In Table 3-14 the statistically significant models with all the independent variables are given (side of tomato, impact velocity and impact time). Figures 3-28 and 3-29 depict the predicted value-experimental value plot of the model including the impact time for respectively the equivalent elastic modulus E^* (E.(1-ν^2)) and the dissipative parameter A. In Table 3-15 the statistically significant models are presented by elimination of the impact time as independent variable. Figures 3-30 and 3-31 give the predicted value-experimental value plot for the reduced model for respectively the equivalent elastic modulus and the dissipative parameter.

Table 3-14. Tomato: Treatment regression equations of the models including the impact time

	R^2
$E_P = 2972109 - 1662007\text{v} - 147221863t + 89933301\text{v}\times t$ $E_C = 2279080 - 1662007\text{v} - 109777078t + 89933301\text{v}\times t$	0.91
$A_P = 0.01285 - 0.03458\text{v} + 0.82284t + 2.07385\text{v}\times t$ $A_C = 0.00884 - 0.03458\text{v} + 0.82284t + 2.07385\text{v}\times t$	0.36

E^*: Equivalent elastic modulus [Pa]; A: Dissipative parameter for impact apple-metal [s]; subscript P: tomato partition; subscript C: tomato compartment; v: impact velocity [m/s]; t impact time [s]

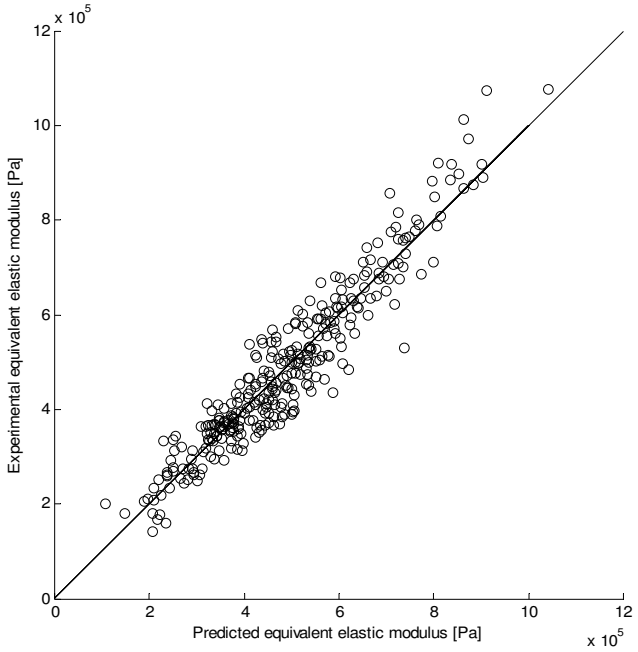

Figure 3-28. Tomato: Model with impact time included (Table 3-14): predicted value – experimental value plot of the equivalent elastic modulus E^* [Pa]

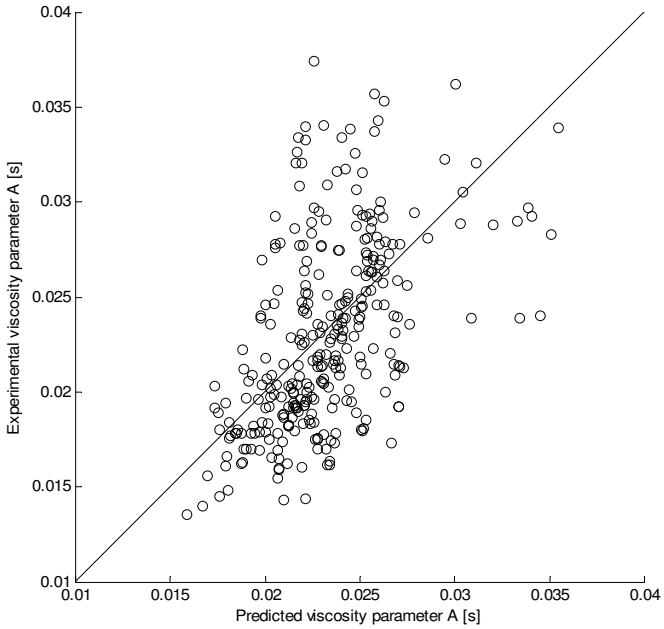

Figure 3-29. Tomato: Model with impact time included (Table 3-14): predicted value – experimental value plot of the dissipative parameter A [s]

Table 3-15. Treatment regression equations of the models without the impact time

	R^2
$E_P^* = 893576 - 609713\text{v}$ $E_C^* = 564008 - 331094\text{v}$	0.55
$A_P = 0.01966 - 0.0089\text{v}$ $A_C = 0.01754 - 0.0089\text{v}$	0.12

E^*: Equivalent elastic modulus [Pa]; A: Dissipative parameter for impact apple-metal [s]; subscript P: tomato partition; subscript C: tomato compartment; v: impact velocity [m/s]; t: impact time [s]

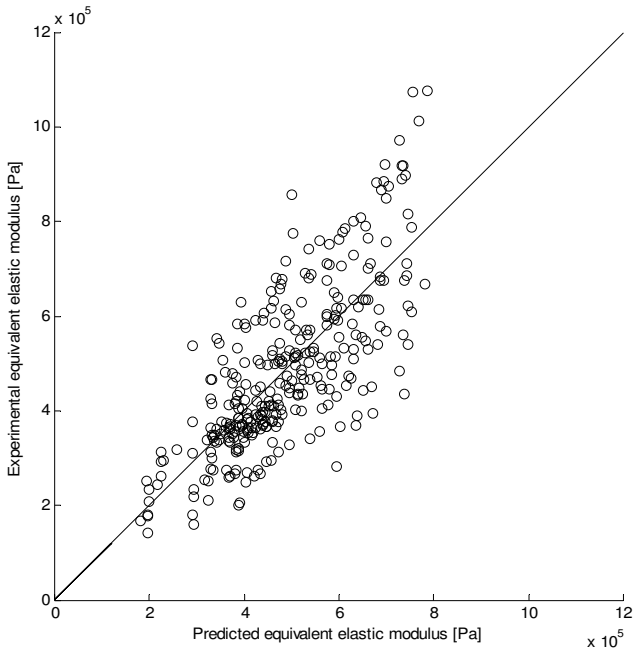

Figure 3-30. Tomato: Model without impact time (Table 3-15): predicted value – experimental value plot of the equivalent elastic modulus E^* [Pa]

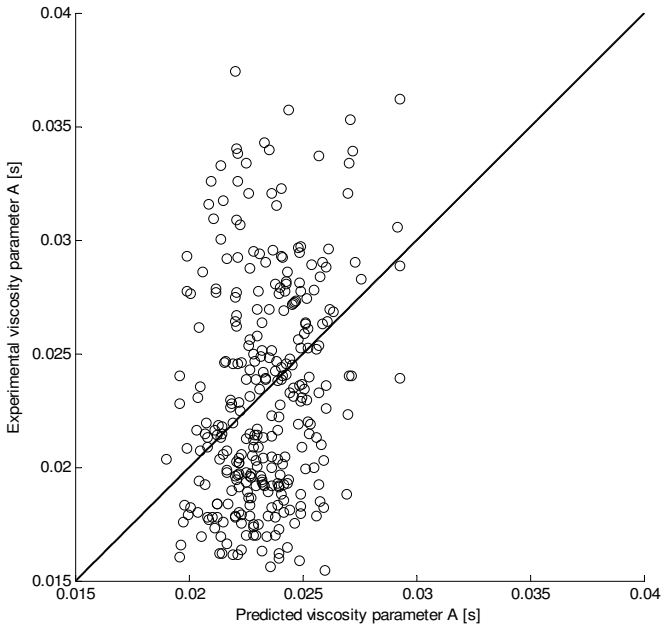

Figure 3-31. Tomato: Model without the impact time (Table 3-15): predicted value – experimental value plot of the dissipative parameter *A* [s]

Better statistical relationships could be obtained with the impact time included in the statistical model. The explanation of the correlation of the impact time with the material parameters has been given in the previous section (section 3.5.2.2) for the Jonagold apples.

The low coefficient of determination of the statistical models without the impact time indicate that impact velocity and side of impact (partition/compartment of tomato) as only independent variables are insufficient to predict the elastic modulus and dissipative parameter of the tomatoes. In other words other independent variables that were not included in the model (for example the ripeness of the tomato) explain more the variation of the elastic modulus and the dissipative parameter of the tomatoes than the impact velocity (or deformation rate) and the side of impact.

However, especially the dissipative parameter has a low coefficient of determination. Therefore also second reason can be mentioned. To calculate the dissipative parameter in the case of impact tomato-metal plate it was indicated in Chapter 2 (equation 2.53) that the relationship $A_{fruit} = 4c/k$ applies. Dividing the damping parameter by the spring parameter increases the variability of the dissipative parameter compared the variability of the damping- and spring parameter separately.

The negative relationship between the impact velocity and the dissipative parameter was expected. This was discussed in section 3.5.2.2 for the apples. The dissipative parameter A for the tomatoes is ≅ 7 times higher than the dissipative parameter for the apples.

The elastic modulus of the tomatoes, calculated from the equivalent elastic modulus by multiplying with $1-\nu^2$, with Poisson's ratio ν for red tomatoes 0.32 (Kopec, 1979), was 0.43 ± 0.16 MPa. The order of magnitude of the elastic modulus calculated from the pendulum experiment is comparable with the elastic modulus determined by quasi-static compression tests. Duprat *et al.* (1997) measured an elastic modulus between 0.2 and 1 MPa for tomatoes of different ripeness (lowest values for red tomatoes like in experiment). Van linden (unpublished) indicated an average elastic modulus of 0.322 ± 0.090 MPa for orange-red tomatoes.

As for the spring parameter in the previous section, a negative relationship between the (equivalent) elastic modulus and the impact velocity was identified. The dependency of the calculated elastic modulus of the tomatoes on the impact velocity was much more pronounced than for the apples. It is important to realize that with increasing impact velocity both the maximum deformation of the tissue and the average deformation rate increase. Most likely the strong heterogeneity of the tomato tissue is responsible for the high dependency of the elastic modulus on the impact velocity. For low impacts the effect of the locular gel on the impact characteristics (contact force, displacement and displacement rate) is less pronounced than for high impacts.

A higher elastic modulus and dissipative parameter was found for the tomato partition compared to the tomato compartment.

3.6 Conclusions

In this chapter an experimental technique was developed to derive the parameters (damping and stiffness) of the Kuwabara and Kono model for viscoelastic spheres (fruits). The technique is a nonlinear least squares data fitting technique, determining the parameters by minimizing the error between the experimental impact quantities (contact force, displacement and displacement rate) and those determined by solving the Kuwabara and Kono equation of motion.

To determine these experimental impact quantities (contact force, displacement and displacement rate) a pendulum was constructed. The pendulum design of Baheri (1997) was taken as a departure point. The main improvements were achieved by application of a high resolution and high accuracy incremental digital encoder ('angle sensor'). The encoder enabled high resolution measurements of the displacement of the pendulum rod during impact. It was indicated that direct measurement of the displacement by means of the encoder gave more accurate results than double integration of the accelerometer signal. By means of differentiation of the displacement signal, i.e. the velocity (displacement rate) of the pendulum rod before, during and after impact was determined. The measurement of the velocity of the pendulum rod before and after impact enabled the calculation of the kinetic energy of the pendulum rod to determine respectively the impact and the elastic energy. The calculation of the impact and elastic energy from the kinetic energy of the pendulum rod can be considered as more accurate than the use of the potential energy because the errors introduced by friction and vibration of the pendulum rod are totally eliminated. All impact quantities (displacement, displacement rate and contact force during impact; impact- and elastic energy; coefficient of restitution, etc.) were logged to the computer for further analysis.

The agreement between the calculation of the work performed by the pendulum rod, derived by integration of the force-deformation curve, and the impact- and elastic energy of the pendulum rod demonstrated the accuracy exerted by the pendulum rod for experimental use.

The nonlinear least squares data fitting technique using the pendulum device was validated by comparing the parameters of the Kuwabara and Kono contact force model of a rubber ball obtained by impact with the parameters obtained by quasi-static compression. Statistical analysis of the spring and damping parameter of apples and tomatoes demonstrated a dependency on the effective radius of curvature at the location of impact, the impact velocity and the location of impact (red or green side of the Jonagold apple and compartment or partition of the tomato). The dependency of the spring and damping parameter on the

effective radius of curvature follows the theoretical relations described by Kuwabara and Kono (1987). The dependency of the parameters of the Kuwabara and Kono model on the impact velocity, not described in literature before, was discussed. Much better statistical models were achieved if besides the effective radius of curvature at the impact location, the impact velocity and the place of impact (red/green side of Jonagold apple or compartment/partition of tomato) also the impact duration was included in the model. However, these statistical models cannot be used in DEM simulations because the impact duration is not known before impact. The theoretical link with the impact time and the contact parameters was indicated. The spring and damping contact parameters were transformed into respectively the (equivalent) elastic modulus and the theoretical dissipative parameter of the Kuwabara and Kono model. The calculated elastic moduli of apples and tomatoes were in agreement with the literature.

Chapter 4

Determination of the tangential contact force model parameters for viscoelastic materials (apples) using a rheometer

4.1 Introduction

A rheometer device was considered to be very promising for determining the tangential contact force model parameters and for its validation. Current rheometers are extremely accurate instruments mostly used to determine the viscoelastic properties of fluids and semi solids by putting the sample material in contact with an object with a well-characterized geometry and monitoring the samples' response to torsion. For fruit, or viscoelastic bodies in general, the response to torsion is a contact force moment acting in the contact plane. As such, it bears a close relationship to tangential contact forces. An additional advantage is that it is possible to control the normal contact force and the contact area of the objects.

Rheology is the study of the manner in which materials respond to applied stress or strain. With regard to fruit, the rheometer is extensively used to determine the viscoelastic characteristics of juices, but is used to a lesser extent for solid tissue. A rheometer has been used to determine the viscoelastic properties of tomato pericarp (Jackman and Stanley, 1995), and apple flesh (Martinéz *et al.,* 2002). As far as known, until the present work, application of a rheometer for the determination of the parameters of a tangential contact force model has not been used.

This chapter proceeds as follows. In the material and methods section (section 4.2) the working principles of the rheometer were described (section 4.2.1). The following sections (section 4.2.2. and section 4.2.3) the description of the experimental procedure is presented to measure the shear modulus, viscosity and dynamic friction coefficient of apple-apple contact with the rheometer device, needed for the viscoelastic extension of Lubkin/Mindlin/Deresiewicz model for torsional contact of spheres equation (2.56)). The material and methods section ends with the description of an experimental procedure for the validation of the above mentioned model (section 4.2.4). In the results and discussion section (section 4.3), first the results of the measurement of the shear modulus, viscosity and dynamic friction coefficient of apple-apple contact are discussed (section 4.3.1 and section 4.3.2) and subsequently the results are presented of quasi-static (section 4.3.3.1) and dynamic experiments (section 4.3.3.2) for respectively the validation of the Lubkin/Mindlin/Deresiewicz model and its viscoelastic extension (equation (2.57)).

4.2 Materials and methods

4.2.1 Description of the rheometer device

The rheometer TA instruments AR-1000N is a controlled stress type rheometer. A rotational stress is applied and the angular displacement is measured. The rheometer contains an electronically-controlled induction motor with an air bearing support for all the rotating parts. The drive motor is equipped with a hollow spindle, with a detachable draw rod inserted through it. The draw rod has a screw-threaded section at the bottom, which allows the geometry to be securely attached. The torque range is between 0.1 μNm and 100 mNm. The measurement of the angular displacement is done by an optical encoder with a resolution of 0.62 μrad. The normal force range of the transducer is between 0.001 N and 49 N with a resolution of 0.01 N.

4.2.2 Determination of shear modulus G, viscosity η, apparent elastic modulus E

In order to measure the (apparent) shear modulus *G,* a torsion test can be used. Although the use of a rheometer to measure the shear modulus is rare, the measurement of the *G* modulus by torsion is not. For example, the *G* modulus of potatoes has been determined by twisting a whole potato (Van Lancker *et al.*, 1975). Because of the inhomogeneity of most materials,

determining the *G* modulus by twisting the whole material and locally twisting of the material, as with a rheometer, are not identical.

The *G* modulus was measured by applying a sinusoidal torsional torque instead of a gradually increasing torque because, besides the *G* modulus, also the dynamic viscosity (η') was determined. A sinusoidal torque (stress) was applied on the apple tissue, while the strain was measured. If the applied sinusoidal stress is within the linear viscoelastic region, a sinusoidal strain will result, phase-shifted by an angle δ. This stress-strain relation can be represented as having a component in phase with stress (G') and a component 90° out of phase with stress (G''). The complex modulus G^* is defined as the ratio of the stress and strain amplitude. The storage modulus G' (representing elasticity) is defined is as

$$G' = G^* \cos\delta \qquad (4.1)$$

The loss modulus G'' (representing viscosity) is defined as

$$G'' = G^* \sin\delta \qquad (4.2)$$

The dynamic viscosity is determined as:

$$\eta' = \frac{G''}{\omega} \qquad (4.3)$$

Because the oscillation program of the rheometer software makes use of stress and strain data, the dimensions of the sample have to be well defined. The parallel plate geometry was used for the experiments. A nearly cylindrical sample, diameter 1 cm, height 1 cm, and skin on one side, was put between the parallel plates. The diameter of the upper parallel plate (1 cm) was small enough to ensure full contact with the curved surface (skin) of the cylindrical apple sample.

The frequency of the sinusoidal oscillation was increased in time using the frequency sweep program of the rheometer software. The shear stress amplitude was kept constant at 200 Pa. This stress amplitude remained within the linear viscoelastic region of the apple and was low enough to avoid slipping of the upper parallel plate on the cylindrical sample. Although it was believed that the effect of slipping was negligible at the applied torque amplitude, torsion clamps (to clamp the cylindrical sample) will be utilized in future experiments. The

samples were compressed with a normal force of 5 N. By selecting this normal force, enough pressure is applied on the sample to avoid slipping and sample damage.
The apparent elastic modulus was measured by quasi-static compression using a universal testing machine (UTS testsystheme GmbH, Ulm, Germany) with the parallel plates configuration, using halves of an apple. The *E* modulus was calculated from the force-deformation curve by applying Hertz contact theory (ASAE standards, 1999, standards for engineering practices and data adopted by the American Society of Agricultural Engineers for compression test of food materials of convex shape).

4.2.3 Determination of the dynamic friction coefficient μ

The rheometer device was also utilized to measure the dynamic friction coefficient. Although it is not a classical instrument to measure the friction coefficient, the application of a rheometer has some advantages compared to more classical methods. Thanks to the rotational instead of translational motion, like it is the case with more classic devices to measure friction coefficients, it becomes very simple to measure friction coefficients between curved materials like apples. Another advantage is that during rotation the normal force and the contact surface can be controlled accurately.
An additional difference with more classical devices like the *inclined plane, rotating disk* or *wagon* method (Mohsenin, 1986) is that the calculation of the friction coefficient is not based on Coulomb's law of friction. Sherwood (Mohsenin, 1986), indicated that some basic assumptions of Coulomb's law do not apply. Due to irregularities at the contact surface, the friction coefficient is dependent on the contact surface. The equation (4.4) to calculate the friction coefficient in rotation incorporates the contact surface, and is based on the physical reality of stick-slip transition at the contact surface. A disadvantage of the rotational method is that only the dynamic friction coefficient, not the static friction coefficient, can be determined. The static friction coefficient can't be determined because the pressure distribution is not equal over the whole contact surface. As a consequence, the static friction force is not equal either. During increase of the torque, the contact zone where the static friction force is exceeded moves from the edge to the center of the contact surface.

The dynamic friction coefficient can be derived from the following relation (Lubkin, 1951):

$$M_s = \frac{3\pi}{16}\mu_d F_N a \qquad (4.4)$$

with M_s represents the critical torque, i.e. the torque at which free sliding starts [N.m]

F_N the normal force [N]

μ_d the dynamic friction coefficient [-]

a the contact radius [m]

The experimental setup is depicted in Figure 4-1. The experiment consists of two halves of an apple put on each other. The bottom half of an apple was attached by a stand clamp, to prevent rotation of the lower half of an apple at high torques. The upper half of an apple was attached to the draw rod of the rheometer by another clamp. Before the test was conducted, the contact surface area between the two apple halves was measured using a tactile film with a spatial resolution of 1.6 mm^2 (5051, see Figure 4-1). The tactile sensors indicated that the contact area could be approximated by a circular surface, at least if the apples were in contact by their equator as in the experiment (maximum and minimum radii of curvature are almost identical). The contact radius was calculated by using the formula $S = \pi r^2$. The rotational test was performed at the same normal force at which the contact surface had been measured. The torque of the apple was gradually increased in time while the angular displacement and angular velocity were measured (continuous stress ramp program of the commercial rheometer software). At the critical torque a sudden increase in angular displacement and angular velocity (10 times increase) occurred.

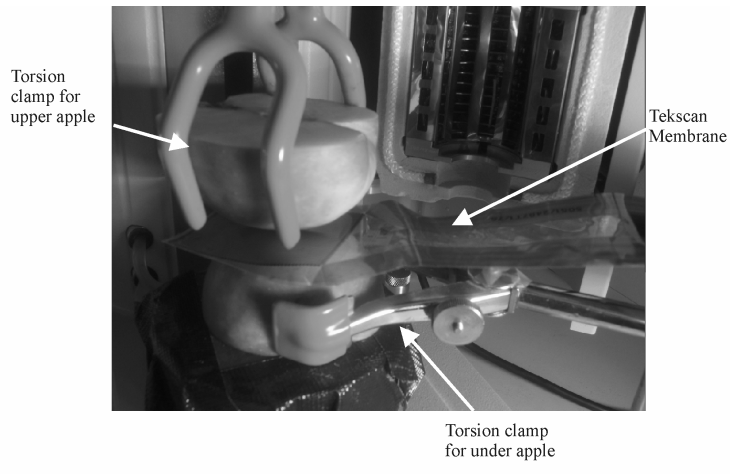

Figure 4-1. Detail of the measurement of the dynamic friction coefficient, with the rheometer. The membrane between the two apples is used to measure the contact area.

4.2.4 Validation experiments

A quasi-static validation was carried out to validate the original Lubkin model (equation (2.56)) for the torsion of apples. A dynamic validation was carried out to evaluate the effect of the viscous term that was added to the Lubkin model by Dintwa *et al.* (2004ab). The validation experiments were performed with five 'Jonagold' apples. The shear modulus, and viscosity and dynamic friction coefficients, were specifically measured for the apples that were also used in the validation experiments. The validation experiment and determination of the friction coefficient experiment were carried out on the intact halves of the apple. In a following experiment, a cylindrical sample, cut from one half of the apple, was used to determine the shear modulus and viscosity. An identical setup and procedure was applied for the quasi-static validation. The torque was increased with time and the angular displacement, angular velocity and normal force were registered.

For the dynamic validation, the same setup was used, but another type of test was performed. Due to constraints of the standard software of the rheometer, high angular velocities can only be reached in oscillation mode. The oscillation program was mandatory to validate the tangential contact force model dynamically. An oscillation at 5 Hz was performed with torque amplitude of 0.010 or 0.025 Nm. In contrast to the oscillation experiments to determine the shear modulus and viscosity, high torque amplitude was desirable because slipping of the upper apple was induced. Unlike the oscillation experiment to determine the shear modulus and viscosity, the rough data, the applied sinusoidal torque and the measured angular displacement, were recorded for further analysis. By plotting the torque and angular displacement data, measured at the same time interval, an angular displacement-torque curve could be obtained.

A nonlinear least squares data fitting technique (routine lsqnonlin of the Matlab optimisation toolbox) using Levenberg-Marquardt method with quadcubic line-search was applied to investigate the influence of the parameters and variables of the tangential contact force model on the tangential force. From the experimentally measured angular deformation-torque curve the stiffness S_t for each data point was calculated from the equation:

$$S_t = (M_z(i) - M_z(i-1)) / (\beta(i) - \beta(i-1)) \qquad (4.5)$$

The inverse of the theoretical compliance (2.56, 2.57) provides the theoretical stiffness. An error function between the measured and theoretical stiffness was minimized for all data points:

$$\min(S_t(i_{theoretical}) - S_t(i_{experimental})) \qquad (4.6)$$

By integrating the theoretical stiffness curve, a theoretical angular displacement-torque curve could be plotted. The estimated parameters were the shear modulus G, the viscosity η and the dynamic friction coefficient μ. The estimated variables were the normal force F_N, the contact radius a and factor d. As an initial guess, the measured parameters and variables were used.

4.3 Results and discussion

4.3.1 Shear modulus and viscosity

By using the measurement method described in section 4.2.2., the shear modulus (G) and viscosity (η) of cylindrical apple samples were measured.

The storage modulus G' was quasi-independent of the frequency (data not shown). Owing to this frequency independency the value of the storage modulus G' is equal to the shear modulus G (Kelvin model; Barnes, 2000, p92).

Since the measurement of the shear modulus by a rheometer device is not common, the results were compared with the apparent elastic modulus measured by quasi-static compression. For isotropic materials the following relationship exists between the shear modulus G and the elastic modulus E:

$$E = 2G(1+\nu) \qquad (4.7)$$

with ν the Poisson's ratio [-]

To determine the elastic modulus the radii of curvature and the Poisson's ratio have to be known. The Poisson's ratio of 'Jonagold' apples was taken from the literature. (0.35, Golacki and Stropek, 2001). Because the Poisson's ratio varies from apple to apple and the relationship between the E and G modulus is valid only for isotropic materials (apples are anisotropic), the calculation of the G modulus from the E modulus can only be regarded as an estimate. In Figure 4-2 the calculated G modulus is compared with the measured G modulus. The difference was on average, 10 % $\pm$ 8 %. Taking into account the assumptions made for the calculation of the G modulus, the difference between measured and calculated values is acceptable.

The measured dynamic viscosity (η') of 'Jonagold' apples is represented in Figure 4-3 (1-10 Hz). As can be seen, the dynamic viscosity of 'Jonagold' apples was strongly dependent on the frequency, with a decreasing dynamic viscosity when the frequency increased (shear-thinning behaviour).

However, the viscosity to be used in the extended Lubkin model (2.57) is not the dynamic viscosity (η'), but the steady shear viscosity (η). The relationship between the dynamic viscosity and the steady shear viscosity (viscosity at a certain shear rate) is complex. Steady shear viscosity is measured by a viscometer or a rheometer in the flow procedure instead of the oscillation procedure. However, the measurement of the steady shear viscosity of apple tissue was not feasible with the flow procedure due to slipping at higher shear rates. For this reason the steady shear viscosity was calculated from the oscillation experiments by applying the extended Cox-Merz rule (Doraiswamy *et al.*, 1991). These authors showed that the plot of the complex viscosity d (G^*/ω) versus the strain amplitude multiplied by the angular frequency ($\gamma_0\omega$) is equivalent to the plot of the steady shear viscosity versus the shear rate. They claim that the extended Cox-Merz rule is valid for a wide range of materials. In Figure 4-4, the extended Cox-Merz rule was applied to the oscillation data of Figure 4-3.

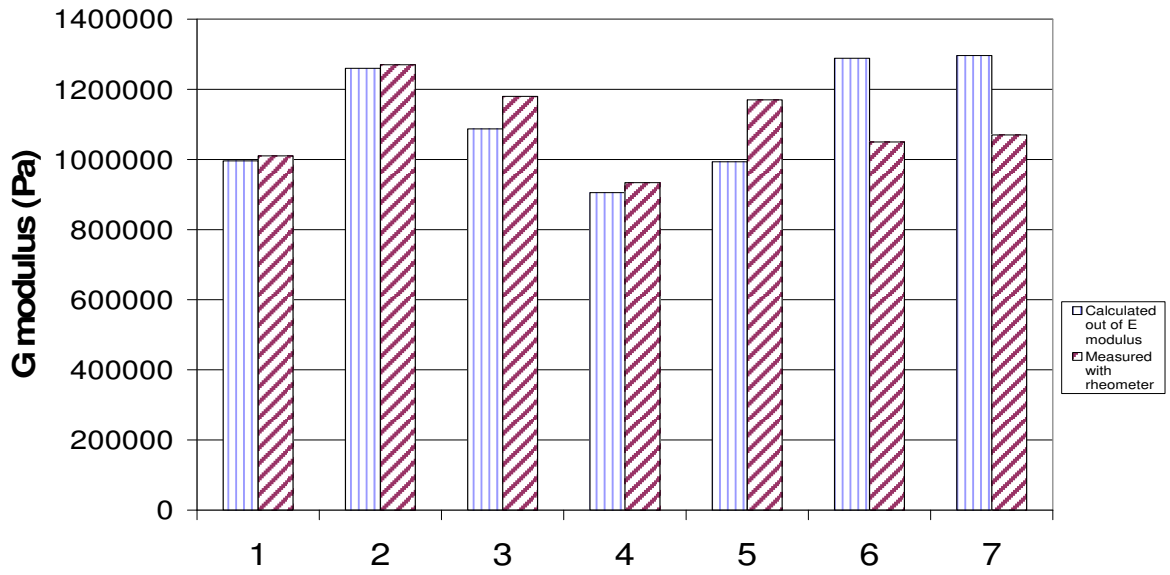

Figure 4-2. Comparison of the G modulus of 7 apples measured with the rheometer and calculated from the E modulus that was measured with the compression machine

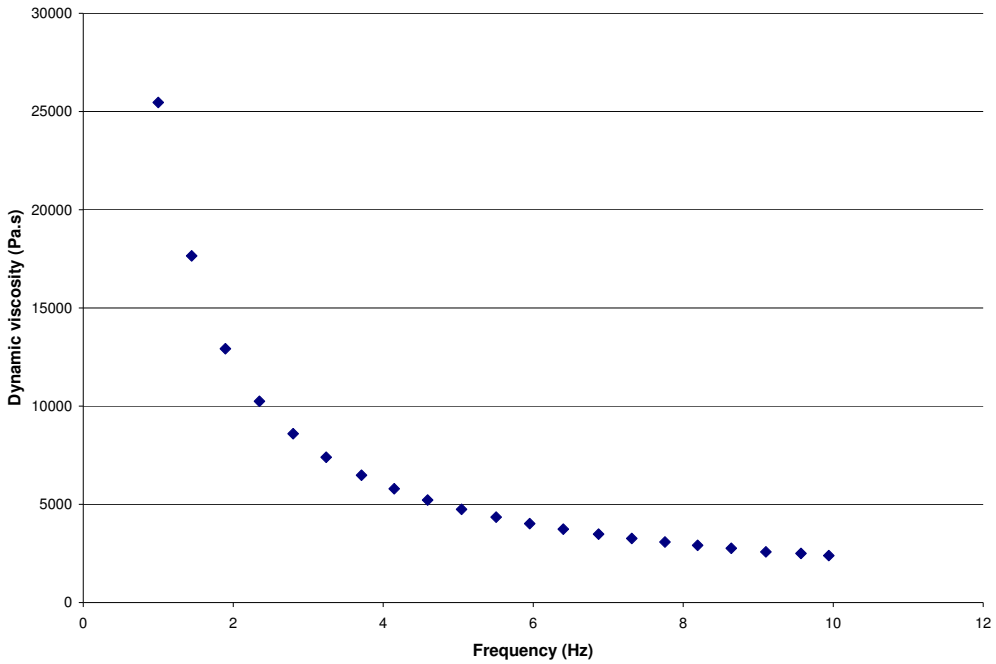

Figure 4-3. The frequency dependency (1-10 Hz) of the dynamic viscosity of 'Jonagold' apples

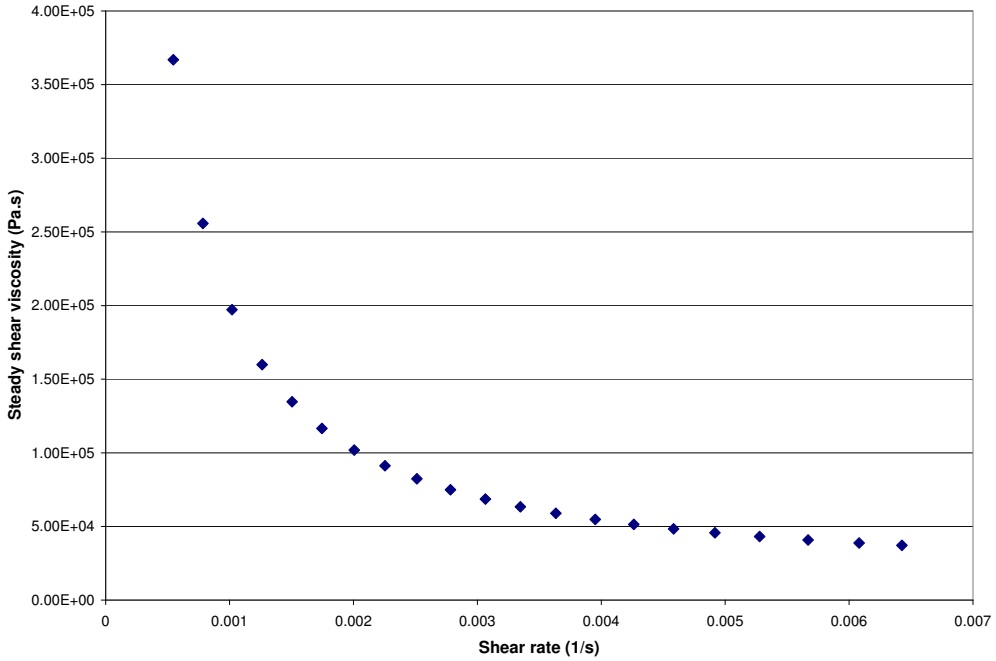

Figure 4-4. Steady shear viscosity as a function of the shear rate after applying the extended Cox-Merz rule on the oscillation data

4.3.2 Friction coefficient

Because a rheometer is not commonly used to determine the dynamic friction coefficient, experiments were designed the make it possible to compare the results with those from the literature. Besides the dynamic friction coefficient of apple-apple contact, the dynamic friction coefficient between apple and aluminium was also determined. In total, the dynamic friction coefficient of 10 apple halves at two normal forces (20 and 40 N) was determined. Because there was no significant difference (95 % significance level)) between the friction coefficient measured at 20 or 40 N, as Coulomb's law of coefficient of friction indicates, all the data were analyzed together to determine the friction coefficient of a 'Jonagold' apple in contact either with another apple or an aluminium plate.

The dynamic friction coefficient for the apple-apple contact was 0.27 ± 0.08 and the dynamic friction coefficient between apple and aluminium was 0.27 ± 0.03. No data could be found in the literature for the friction coefficient for apple-apple contact, but the friction coefficient of aluminium-apple contact was in agreement with that of steel-apple contact found in the literature (0.32, the average of six apple varieties) (Mohsenin, 1986).

4.3.3 Validation experiments

4.3.3.1 Quasi-static validation (Validation of the Lubkin model)

In Table 4-1 the measured parameters and variables are compared with the estimated ones. The parameter estimation procedure that has been used is explained in section 4.2.4. For two out of five validations the results are visualized in Figures 4-5 and 4-6. The experimental angular displacement-torque curve was plotted together with the non-optimized and optimized theoretical angular displacement-torque curves. The curve, which monotonically increases to a certain asymptote, was measured and could be modelled. At the asymptote slip starts to occur. Validations 1 (Figure 4-5) and 2 (Figure 4-6) show respectively the highest and lowest difference between the measured angular displacement-torque curve and the theoretical curve with measured variables and parameters. For all five apples used in the validation experiments, good parameter estimation could be obtained. The contact radius *a,* was the only variable that was significantly changed by the nonlinear least squares estimation routine to obtain a good model fit. The maximum change between measured and optimised contact radius a was 1.2 mm (apple 5). In relative value, this is an overestimation of the contact radius by 23.5 %. Besides the contact radius a, a parameter change between measurement and estimation was found for the dynamic friction coefficient μ. The highest

change in dynamic friction coefficient was noted for apples 1 and 3, but even then it was small, 0.014 (5.5-6 %). For all the other parameters and variables the change between measurement (initial guess) and estimation was negligible.

Remarkably, for all five validations the contact radius was overestimated. This systematic overestimation could be explained by the measuring technique. The tactile films are constructed out of cells with a resolution of 1 mm^2. When electrical wires in the cells sense a pressure beyond the noise level, they count for a 1 mm^2 contact area. Cells at the edge of the contact area between the apples can be electrically stimulated without being in full contact with the apple tissue.

The great importance of the contact radius in the tangential contact force model was obvious from the parameter estimations. This is not surprising, because it is present to the power three in the equation of the tangential contact force model(2.57). It can be concluded that in DEM simulations, for a correct application of the tangential contact force model, accurate estimation of the contact radius between the particles is essential.

Table 4-1. Comparison of the measured and estimated parameters and variables for the quasi-static validation of the Lubkin model

Apple		*Measured variable/parameter*	*Estimated variable/parameter*
1	a [m]	0.0050	0.0045
2	a [m]	0.0053	0.0044
3	a [m]	0.0061	0.0053
4	a [m]	0.0054	0.0052
5	a [m]	0.0057	0.0045
1	μ	0.23	0.216
2	μ	0.31	0.312
3	μ	0.26	0.246
4	μ	0.25	0.251
5	μ	0.27	0.276
1	F_N [N]	19.57	19.55
2	F_N [N]	18.93	18.92
3	F_N [N]	19.09	19.06
4	F_N [N]	17.00	17.00
5	F_N [N]	17.93	17.93

1	*G* [MPa]	3.36	3.36
2	*G* [MPa]	3.90	3.90
3	*G* [MPa]	2.73	2.73
4	*G* [MPa]	2.24	2.24
5	*G* [MPa]	3.42	3.42
1	Resnorm	/	1.09
2	Resnorm	/	0.27
3	Resnorm	/	5.40
4	Resnorm	/	2.79
5	Resnorm	/	4.18

a: contact radius, μ: dynamic friction coefficient, F_N: normal force, *G*: shear modulus

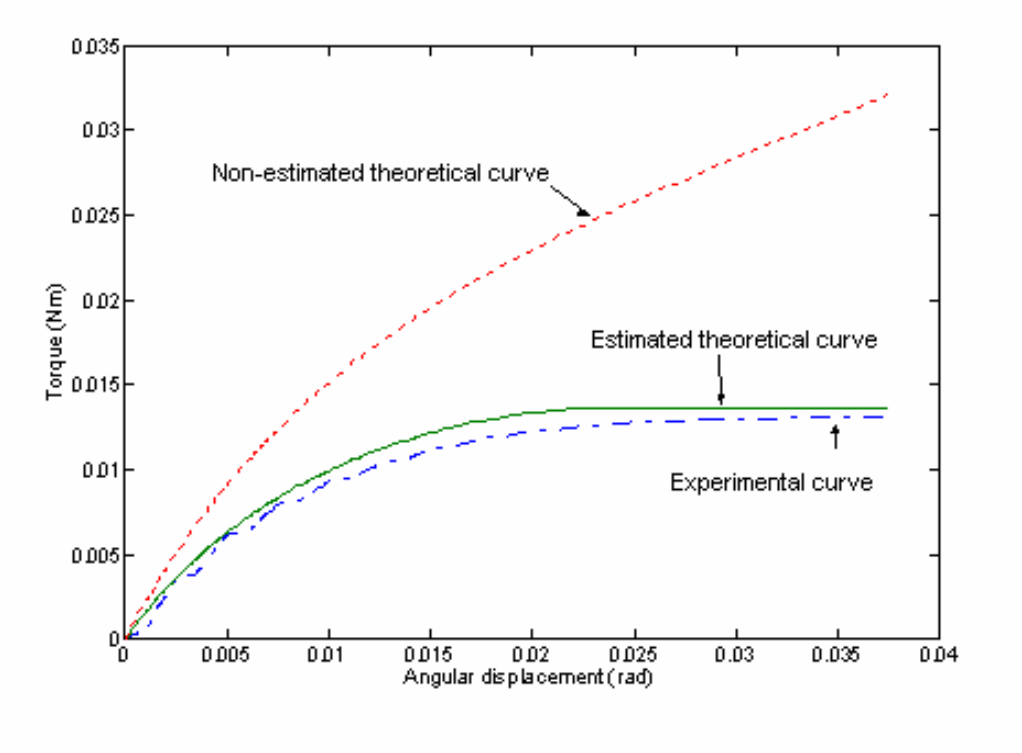

Figure 4-5. Torque vs. angular displacement curve for apple 1.

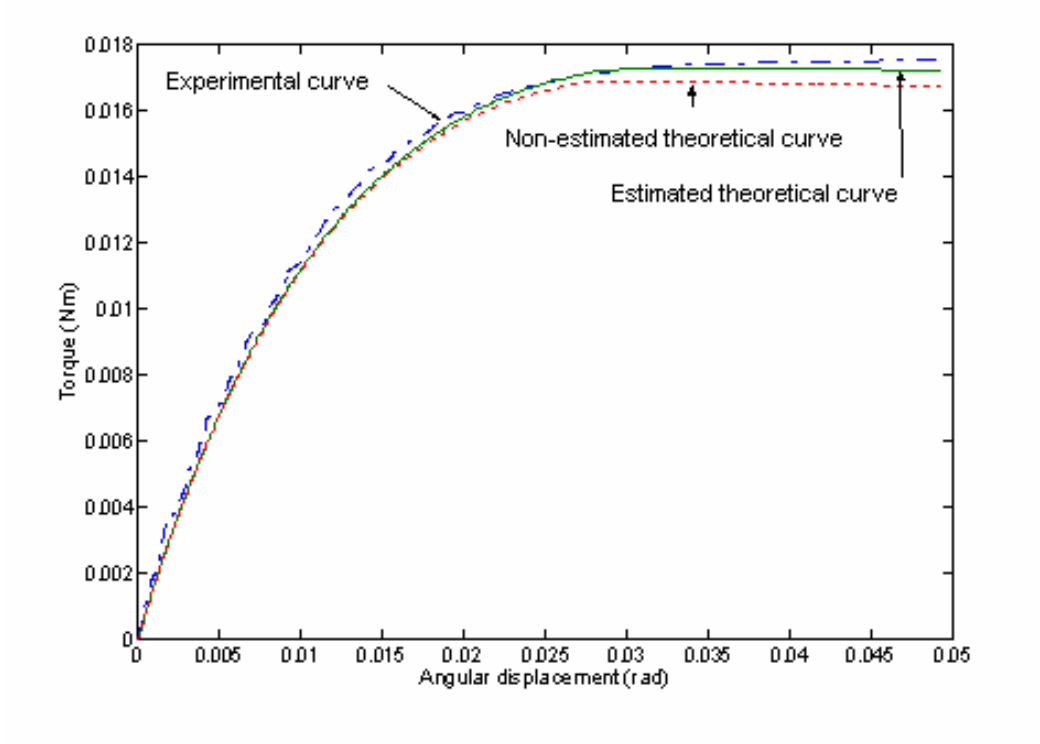

Figure 4-6. Torque vs. angular displacement curve for apple 2.

4.3.3.2 Dynamic validation

The steady shear viscosity was determined from the dynamic viscosity by applying the extended Cox-Merz rule (see section 4.3.1) to the oscillation data of the cylindrical apple samples (used for the validation experiments). It was determined at the average shear rate recorded during the validation experiments. The shear rate was calculated by applying the following equation:

$$\dot{\gamma} = \frac{\omega a}{d} \qquad (4.8)$$

with $\dot{\gamma}$ the shear rate [1/s]
ω the angular velocity [rad/s]
a the contact radius [m]
d the gap, distance between bottom plate and upper plate of the rheometer [m]

The average angular velocity and contact radius during the five validation experiments was used to calculate the (average) shear rate. For factor d the maximum value of 4 cm (height of the half of an apple) was taken.

In Table 4-2 the measured parameters and variables are compared with the estimated ones for the tangential contact force model with and without the viscous term added. For one validation, the results are visualized in Figures 4-7 to 4-10. The experimental angular

displacement-torque curve is plotted along with the non-estimated (=with measured parameters and variables) and estimated theoretical angular displacement-torque curves for the model with and without the viscous term (Figures 4-7 and 4-8). In Figures 4-9 and 4-10 the experimental stiffness vs. angular displacement curve is plotted along with the non-estimated and estimated theoretical stiffness vs. angular displacement curve for the model with and without the viscous term. Unlike the parameter estimations obtained for the quasi-static validations, the best estimations for the dynamic validation were reached with unrealistic values for the dynamic friction coefficient and normal force. By keeping the friction coefficient and normal force unchanged, the estimations were only slightly worse. As a consequence, it can be concluded that the unrealistic friction coefficient and normal force were due to an optimisation artifact rather than a problem with the tangential contact force model itself.

It was demonstrated that by adding a viscous term to the tangential contact force model of Lubkin (2.57), a better model for the dynamic rotation of viscoelastic spheres could be achieved. This is shown by the improvement of the residual error (resnorm) and the clearly better fit of the experimental stiffness vs. angular displacement curve (Figures 4-9 and 4-10), although it's less clear when the (estimated) angular displacement-torque curves are compared to the experimental ones (Figures 4-7 and 4-8). This could be due to the inaccuracy of the applied integration method to obtain the theoretical angular displacement-torque curve from the theoretical stiffness.

The irregular shape of the measured and modelled stiffness vs. angular displacement curve, with viscous term included, is remarkable. It can be explained by the effect of a varying viscous term during the oscillation. The viscous term W in equation (2.57) is given by

$$W = \frac{4\pi\eta\omega a^3}{\mu 2d} \qquad (4.9)$$

The angular velocity ω varies during the oscillation, resulting in a varying viscous term. It can be concluded that the model of Lubkin, in contrast to the Lubkin model with the viscous term included, cannot describe the varying stiffness during oscillation of viscoelastic spheres.

By blocking the friction coefficient (and normal force) at the measured value, the only variables that changed significantly by the nonlinear least squares estimation procedure, were the contact radius a and factor d (Table 4-2). At first, it may look contradictory that for the quasi-static validations the contact radius was overestimated and for the dynamic validations, with the model including the viscous term, the contact radius was underestimated, although this may be due to the sub-optimal conditions in which the

dynamic validation was performed. For the quasi-static validation, the apples were only sliding (free slipping) at the end of the measurement. When free sliding started to occur, the measurement was stopped. For the dynamic validations it was obliged, due to constraints in the rheological software, to perform the test in an oscillative way, given a maximum torque amplitude. The torque amplitude was, based on the quasi-static validations, 0.015 Nm (or 0.010 Nm). During oscillations (torque driven) the apple behaviour changes between a stage of slip-stick (low torque) to a stage of the beginning of free sliding (above critical torque). Because of the irregular shape of the apple, fluctuations can occur in the contact area during oscillation. In contradiction to this explanation, for the model without the viscous term, still an overestimation of the contact radius was observed (Table 4-2). Nevertheless, by taking for the model with the viscous term added, the estimated contact radius of the model without the viscous term, still a better fit of the experimental stiffness with the model including the viscous term was noted (data not shown).

Factor d was defined as the depth from the contact plane to a fixed plane in the interior of the sphere where the viscous force becomes zero. With regard to fluids, factor d is the gap between the upper and bottom plate of the parallel plate geometry. As an initial guess the height of the lower half of an apple (≈ 4 cm) was taken as factor d . Theoretically the value of factor d has to be between 0 and the height of the half of an apple (≈ 4 cm). The estimated value of factor d ranged from 1.1 cm to 4.3 cm (see Table 4-2). This is rather a substantial difference. Further research is needed to find out whether this is an optimisation artifact or factor d is really changing that much from apple to apple. This factor d can be considered as a weak point in the model because of it is a quantity that cannot be measured. In a recent modification, the new equation for the viscous force is lacking the factor d (Dintwa *et al.,* 2004b).

A small change in shear modulus G between measured and estimated shear modulus was noted. Although, for two out of five validations, little improvement in the model fit could be reached with unrealistic high values of shear modulus G (apples 2 and 5). Therefore the value of the shear was fixed on the measured value (see Table 4-2). Also a small change between the measured and estimated viscosity η was noted for all nonlinear least squares estimations.

Table 4-2. Comparison of the measured, estimated parameters and variables for the model with and without the viscous term.

Apple		*Measured Parameters and variables*	*Estimated parameters and variables : Model without viscous term*	*Estimated parameters and variables : Model with viscous term*
1	η [Pa.s]	5714	/	5722
2	η [Pa.s]	5906	/	5921
3	η [Pa.s]	6290	/	6289
4	η [Pa.s]	6506	/	6502
5	η [Pa.s]	6658	/	6660
1	Factor d	0.040	/	0.01725
2	Factor d	0.040	/	0.0107
3	Factor d	0.040	/	0.0319
4	Factor d	0.040	/	0.0431
5	Factor d	0.040	/	0.0274
1	a [m]	0.0052	0.0046	0.0058
2	a [m]	0.0056	0.0046	0.0058
3	a [m]	0.0061	0.0060	0.0067
4	a [m]	0.0056	0.0055	0.0064
5	a [m]	0.0050	0.0051	0.0064
1	μ	0.23	0.23	0.23
2	μ	0.31	0.31	0.31
3	μ	0.26	0.26	0.26
4	μ	0.25	0.25	0.25
5	μ	0.27	0.27	0.27
1	F_N [N]	18.13	18.13	18.12
2	F_N [N]	19.32	19.32	19.32
3	F_N [N]	19.71	19.71	19.71
4	F_N [N]	19.01	19.01	19.01
5	F_N [N]	20.05	20.05	20.05
1	G [MPa]	3.36	3.23	3.42
2	G [MPa]	3.39	3.39 F	3.39 F
3	G [MPa]	2.73	2.61	2.93
4	G [MPa]	2.24	2.39	2.42
5	G [MPa]	3.42	3.42 F	3.42 F
1	Resnorm	/	1.75	0.55
2	Resnorm	/	5.32	2.07
3	Resnorm	/	4.20	1.55
4	Resnorm	/	1.01	0.66
5	Resnorm	/	4.44	1.15

η, viscosity, d, factor d (definition see text), a, contact radius, μ, dynamic friction coefficient, F_N, normal force, G, shear modulus, F stands for fixed on the measured value.

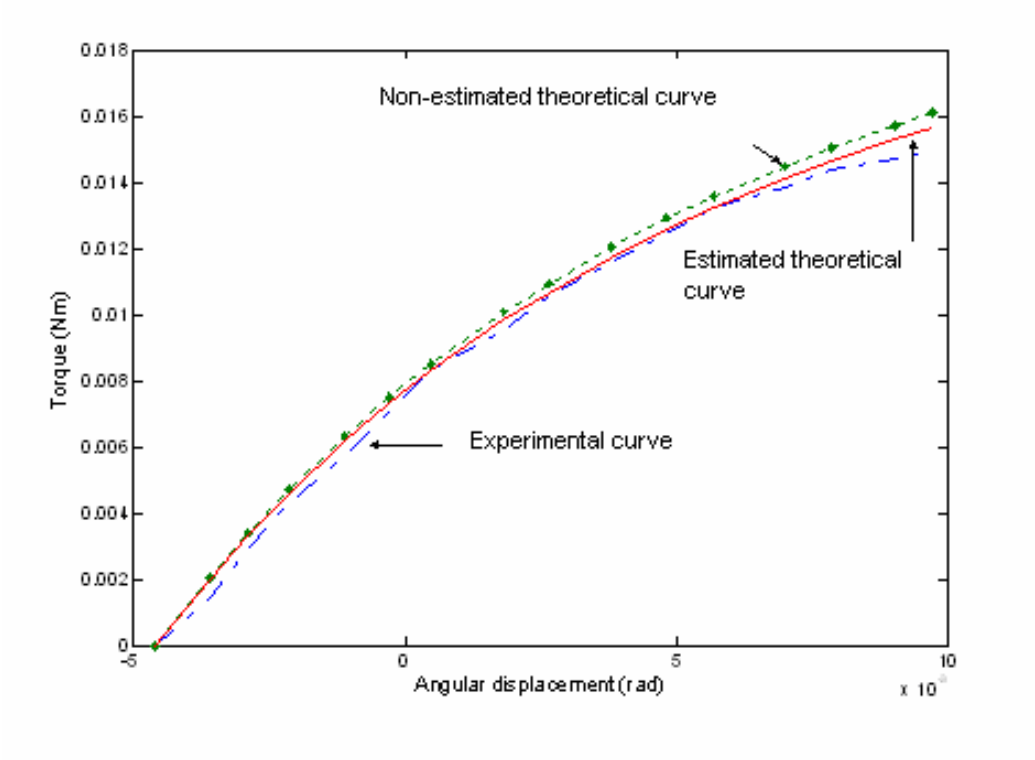

Figure 4-7. Torque vs. angular displacement curve for apple 4 for the model without the viscous term

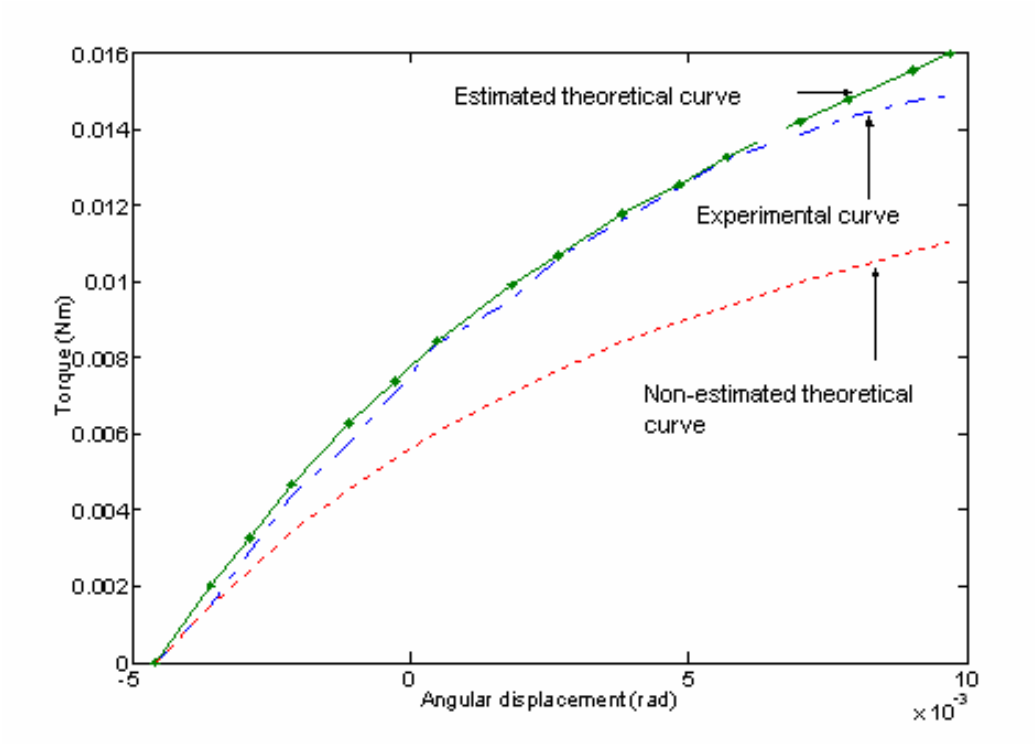

Figure 4-8. Torque vs. angular displacement curve for apple 4 for the model containing the viscous term

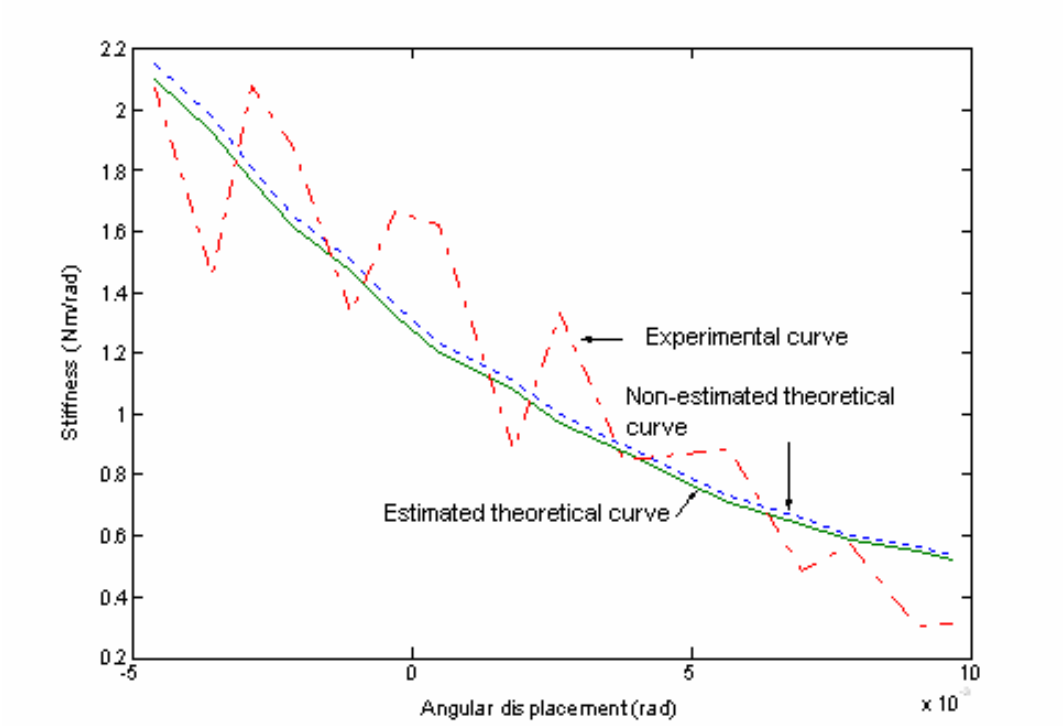

Figure 4-9. Stiffness vs. angular displacement curve for apple 4 for the model without the viscous term.

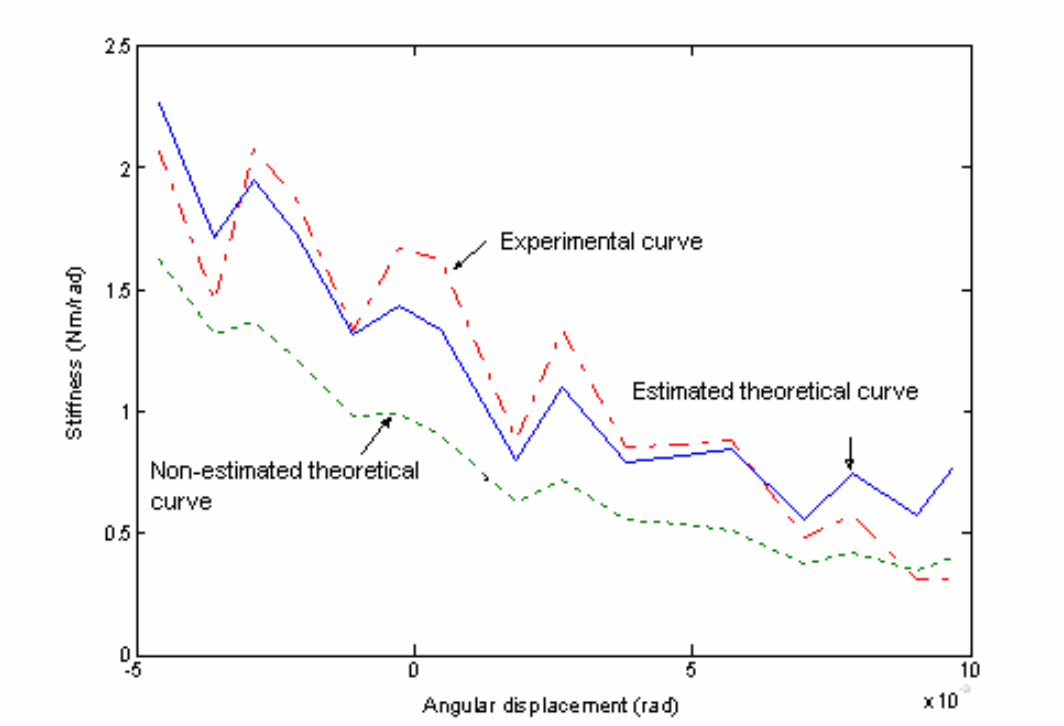

Figure 4-10. Stiffness vs. angular displacement curve for apple 4 for the model containing the viscous term.

4.4 Conclusions

In this chapter it was demonstrated that a rheometer, a device normally intended to measure viscoelastic properties of fluids and semi-solids, can be applied to determine the parameters of the most physical realistic tangential contact force model described in literature: the Lubkin/Mindlin/Deresiewicz model for torsional contact between elastic spheres. Although this model is only valid for rotational tangential contact of spheres, a similar model with identical material parameters exists for translational tangential contact between elastic spheres (Mindlin and Deresiewicz, 1953). The material parameters determined by the rheometer, were the shear modulus of the spheres (apples) and the dynamic friction coefficient of sphere-sphere (apple-apple) contact. Since the determination of the shear modulus and dynamic friction coefficient by means of a rheometer is not a standard method, it was compared with literature. Some advantages of the determination of the shear modulus and dynamic friction coefficient by means of a rheometer device were discussed.
The Lubkin/Mindlin/Deresiewicz tangential contact force model is only valid for elastic spheres. Because of the viscoelastic nature of the fruits, an extension of the Lubkin/Mindlin/Deresiewicz model for viscoelastic spheres was proposed (see Chapter 2).
For the viscoelastic extension of the model, besides the shear modulus and the dynamic friction coefficient, also the viscosity of the spheres (apples) needed to be measured. The viscosity of the spheres (apples) was also determined by use of the rheometer.
The rheometer was not only utilized to determine the material parameters needed for the tangential contact force model but also for its validation. By means of a quasi-static validation procedure it was demonstrated that the Lubkin/Mindlin/Deresiewicz model for elastic spheres is an accurate model to describe the tangential contact behaviour of apple-apple contact. By means of a dynamic validation procedure it was demonstrated that the extension of the Lubkin/Mindlin/Deresiewicz model for viscoelastic spheres improves the modelling of the tangential contact behaviour during dynamic contact of apples.
The nonlinear least squares estimation routine indicated the importance of the contact radius of the contact area between spheres (apples) for accurate modelling results of the tangential contact behaviour. An accurate estimation of the contact radius is also indispensable for DEM simulations.

The tangential contact force model will be incorporated in the discrete element software DEMeter++ to simulate mechanical damage during transport and handling of fruit and vegetables. Not only the rotational, but also the translational version of the tangential contact force model will be included. In this regard, the viscoelastic extension of the Mindlin and

Deresiewicz model for translational tangential contact of spheres was recently developed (Dintwa *et al.,* unpublished).

However, for the DEM simulations in this work (Chapter 6 and 7), in expectation of the incorporation of these models in DEMeter++, a more simplified tangential contact force model was applied.

Chapter 5

Bruise prediction models for apples and tomatoes: statistical approach

5.1 Introduction

In the previous two chapters the normal and tangential contact force model was outlined. For DEM simulations of fruit bruise damage also a bruise prediction model is indispensable. Bruise prediction models are not inherent to DEM itself, but essential for the utility of the DEM for the bruising problem, because they relate the contact force during impact, as modelled by the contact force models, with the real bruise damage. The bruise prediction model connects the impact characteristics (drop height, impact time, peak contact force) with bruise damage taking in consideration some fruit properties (temperature, ripeness, etc.) determining the bruise sensitivity. Apart from DEM these statistical models can provide useful information about the influence of fruit properties (for example ripeness) on bruise susceptibility, leading to recommendations for fruit handling.

Statistical bruise prediction models described in literature are restricted to the effect of only two fruit properties (either fruit temperature or fruit ripeness). Besides the statistical bruise models described in literature are inconsistent. Probably this is due to the ignorance of some fruit properties in the model like the radius of curvature and the ignorance of interaction effects between the fruit properties and interaction effects between fruit properties and the severity of impact.

Bruise prediction models including the effect of packaging materials described in literature are limited. Moreover, in most studies the effect on apple bruise damage of cushioning materials not used in practice (lab designed) was investigated.

The inconsistent and/or limited information about bruise prediction models, for apples but certainly for tomatoes, leads to the objective of this chapter: Development of bruise prediction models for apples and tomatoes, including different fruit properties like fruit temperature, fruit ripeness, harvest date, radius of curvature and for apples also considering the effect of packaging materials used on the Belgian market. The bruise prediction models must be applicable in association with DEM simulations.
Besides statistical modelling also theoretical modelling could be used to connect the impact properties and the bruise damage. However, Siyama *et al.* (1988) demonstrated the superiority of multiple linear statistical models above theoretical models in predicting the bruise damage.

Statistical models in this chapter were made either including *impact energy* or *peak contact force*. Both models have advantages and disadvantages in perspective to DEM. The advantage of the models including the peak contact force is that they can be generalized to impacts of materials with different material properties[28]. An example will make this clear. When an apple falls from the same height on the one hand on another apple and on the other hand on a metal plate, the bruise will be larger in the latter case. The underlying reason is that the impact characteristics are different. For instance, the peak contact force is higher for apple-metal plate contact than for apple-apple contact. The contact force models (Chapter 3) used for DEM consider these differences in material properties to calculate the right (peak) contact force. The statistical models including the peak contact force that were measured for apple-metal impactor contact can be applied (to some degree[45]) for apple-apple contact. On the other hand, the model including the impact energy is useless because in both cases (apple-apple and apple-metal plate) the impact energy is identical. The bruise volume is drastically overestimated in the case the model including the impact energy for apple-metal impactor contact, is used for apple-apple contact. A solution is to build different statistical models including impact energy for each impact pair, demanding a lot of experimental work.
However, a disadvantage of the use of statistical models including the peak contact force is that the peak contact force is most likely to be influenced by the fruit properties itself (temperature, ripeness, etc.). If DEM simulations are performed without adaptation of the parameters of the contact force model to the different fruit properties, the (peak) contact force is (slightly) over or underestimated. As a consequence, statistical models including the peak contact force may over- or underestimate the experimental bruise volume.

[28] The generalization is even more accurate when besides the peak contact force also the impact time is included in the model. It has been demonstrated that impact time is also an important factor in determining bruise damage (Chen and Yazdani, 1991).

An advantage of the models including the impact energy is that the above mentioned problem does not occur: the impact energy is not influenced by the fruit properties. As a consequence, these models are better suited to investigate the effect of fruit properties on bruise susceptibility.

This chapter is divided into three major sections. In section 5.2 statistical bruise prediction models for apples are developed with bruise volume as bruise evaluation parameter. The influence on the bruise susceptibility (bruise volume) of the radius of curvature of the apples, harvest date, acoustic stiffness, and apple temperature is discussed. Bruise prediction models are developed with besides the fruit properties both the impact energy and the peak contact force as independent variables. In section 5.3 statistical bruise prediction models for tomatoes are developed with absorbed energy as bruise evaluation parameter. The influence on bruise susceptibility (absorbed energy) of the radius of curvature of the tomatoes, ripeness and tomato temperature is discussed. Models are developed with besides the fruit properties both the impact energy and the peak contact force as independent variables. Section 5.4 discusses the influence of packaging materials, used on the Belgian market, on the bruise damage of apples. Statistical bruise prediction models are developed with both the impact energy and the peak contact force as independent variable.

5.2 Bruise prediction models for apples

5.2.1 Introduction

Owing to the enzymatic browning of the apple when the tissue is damaged, the measurement of the bruise size is a very objective method to quantify the bruise damage.
To quantify bruise damage, bruise volume has been selected in this research because it is by far the mostly applied bruise quantification method in scientific publications. Nevertheless some critics have been made by Pang *et al.* (1996) that the bruise surface should be used to measure bruise damage. The argument therefore is that only the bruise surface is noticed by consumers when purchasing the apples.
In the experiment to establish the bruise prediction models for apples, besides the bruise volume also dynamic yield pressure (*DYP*) was used as dependent variable. The *DYP* is the minimum pressure at which plastic deformation starts to occur (Mohsenin, 1986). This *DYP* can be calculated based on Hertz theory (Tabor, 1951). The accuracy of this calculation is limited due to the assumptions made in Hertz theory (Chapter 2). Bajema and Hyde (1992, 1998) developed a method to measure this dynamic yield pressure using a pendulum device

in combination with tactile films (pressure membranes). The method is called CHMI (constant height multiple impact). Details about this method are presented in Bajema and Hyde (1998). Although the method has been used in this experiment, the results will be given in reduced form. Several reasons for this can be mentioned. First of all, until present the accuracy of this method is not been determined, neither by literature, nor by us. Secondly, the *DYP* is only a bruise threshold; it does not provide information about degree of bruising once this dynamic yield pressure is exceeded. Thirdly, *DYP* is not the only factor determining the bruise sensitivity (although the most important, see equation (5.9) in this Chapter). Fourthly, the concept of *DYP* is difficult to combine with DEM[29].

Multiple regression models are made and discussed to link fruit properties, acoustic stiffness, apple temperature, radius of curvature, harvest date, with bruise damage. Statistical bruise prediction models are developed with both the impact energy and the peak contact force as independent variable. As dependent variable both *DYP* and bruise volume, as measure of bruise damage, were used. However the results of models with *DYP* as dependent variable are discussed briefly.

5.2.2 Materials and methods

5.2.2.1 Experimental setup

For this experiment 540 Jonagold apples of harvest season 2001 were used. The apples were carefully harvested on three different days (24/09, 4/10 and 14/10) in the orchard of 'K.U. Leuven Fruitteeltcentrum' in Rillaar, Belgium. The apples were harvested at the same hour each day (to minimize turgor fluctuations). No rain was present before and during harvest (important to minimize turgor fluctuations). On each harvesting day, the apples were picked at random from the same four marked trees in the orchard. The apples were stored in optimal conditions (3°C, 85 % RH) during measurement in the lab of Landbouwwerktuigkunde K.U. Leuven. Maximum storage before measurement was 5 days. At least 12 hours before starting the measurements, the apples were stored at the desired temperature for the measurement. The apples at temperature of 1°C were measured within 10 minutes to minimize apple warming up. The apples were cut into two equal pieces and mounted on the pendulum. They were impacted by a round shaped metal impactor (R= 25 mm). No distinction was made between red and green side of the Jonagold apple. One half of an apple was single impacted with the desired impact velocity. The other half of an apple was multi-impacted with the

[29] Using DYP in DEM necessitates the estimation of the contact area for each time step during particle impact

same impact velocity and a tactile film (Tekscan ®9500, Tekscan, Inc., South Boston, US, see Figure 5-1 and 5-2) was placed between apple and impactor. The latter setup was done to determine the Dynamic Yield Pressure[30] (the method is described in detail in Bajema and Hyde, 1998).

Tactile sensor *Tekscan*® measures dynamic and static load (type 9500) or only static load (type 5051) by means of changes in electrical resistance. A network of silverelectrode wires is separated by an interlaying gel. The gel has an electrical resistance that is pressure sensitive. Gel and wires are captured in a thermoplastic polyester material. The sensor is connected by means of a special holder to the computer. The load changes locally the electrical resistance of the gel that is 'sensed' by the network of silverelectrodes. After calibration of the sensor, the commercial software ISCAN® calculates a spatial distribution of the pressure in time. Tekscan® 9500 was used for the dynamic measurements in this chapter because of its rather high measure frequency of 1400 Hz. A technological consequence of this high measure frequency is its rather low spatial resolution (25.7 mm^2)**.** In Chapter 4, for a static application, Tekscan® type 5051 was used, with a higher spatial resolution (1.6 mm^2)**.** The maximum measurable load for 5051 and 9500 type is 1725 kPa and 690 kPa respectively. More details about the Tekcan® membranes to measure contact pressures between fruits are given in Geyer *et al.* (1999).

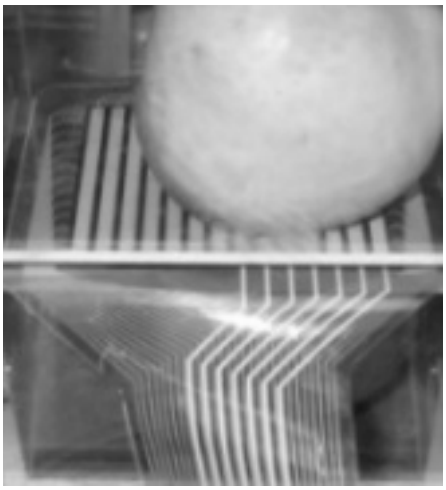

Figure 5-1. Picture of Tekscan membrane

Three impact levels were applied: ≅ 0.3 m/s, ≅ 0.7m/s and ≅ 1.1 m/s. For each impact the exact impact velocity (used to calculate impact energy) was measured and logged to a data file. Impact velocity differences were due to little fluctuations in drop height and apple positioning.

[30] When Dynamic Yield pressure during impact is being exceeded, the apples start to bruise.

The bruise volume was measured (single impact) 24 hours later utilizing the equation by Chen and Sun (1981):

$$BV = \frac{\pi}{6} dD^2 \qquad (5.1)$$

where BV bruise volume [m^3]
d bruise depth [m]
D bruise diameter [m]

Bruise volume (*BV*) and dynamic yield pressure (*DYP*) were the dependent variables in the statistical models.

The independent variables were:

- Impact energy or peak contact force
- 3 harvest dates: optimal harvest date – 10 days, optimal harvest date, optimal harvest date + 10 days
- 3 apple temperatures: 1°C, 15°C and 20°C
- Apple radius of curvature at location of impact
- Apple acoustic stiffness
- Apple mass

Impact energy and *peak contact force* were logged to a data file for each impact. The tree impacts levels that were used were (Table 5-1):

Table 5-1. Overview of different impact levels used in the experiment.

	Impact energy [J]	*Peak contact force [N]*	*Bruise volume [mm^3]*
Level 1	≅ 0.015	≅ 30	≅ 100
Level 2	≅ 0.075	≅ 60	≅ 500
Level 3	≅ 0.18	≅ 100	≅ 1100

Level 1 is situated on the edge of bruise detection ability. Level 2 and 3 are easily detectable bruises, clearly visible. During measurements that were executed with an electronic fruit (PMS-60) in orchards and sorting lines in Flanders, no impacts of level 3 were recorded (Van linden, unpublished). Nevertheless, Brown *et al.* (1990) measured that also impacts of level 3 occur during apple packaging..

To determine the optimal *harvest date* the VCBT (Vlaams Centrum voor Bewaring van Tuinbouwproducten) was consulted. The optimal harvest date for all apple cultivars in Flanders is determined each year by VCBT. Successful storage results for hard fruit are

strongly dependent on an optimal harvest date. Too early harvested fruit will not ripe sufficiently (taste), too late harvested fruit diminishes shelf-life drastically. The parameters that are measured by the VCBT to determine the optimal harvest date are apple size, apple firmness (Magness-Taylor test), starch content, soluble solids and colour. The optimal harvest date for Jonagold apples is a two weeks period. For the orchard in Rillaar (one of the sample orchards in the VCBT research) this was determined more precisely.

For conditioning of the apples on the desired *temperature,* two cooling cells were used (1°C, 85 % RH and 15 °C, 85 % RH). Temporal storage in the measuring room provided the temperature of 20 °C.

The *radius of curvature* was measured locally at the location of impact by a radius of curvature meter. Because the appropriate radius of curvature meter was not commercially available, it was constructed on the basis of a digital Mitutoyo® height meter, Mitutoyo Belgium NV, Kruibeke, Belgium (Figure 5-2 and 5-3). The spring constant of the meter is low enough to avoid damaging soft fruits like tomatoes. The radius of curvature was calculated using the following equation (Mohsenin, 1986):

$$RADIUS = \frac{(AC)^2}{8(BD)} + \frac{(BD)}{2} \qquad (5.2)$$

Because the apple is not a perfect sphere, the harmonic average was calculated of the circumferential radius of curvature and the meridian radius of curvature (see section 3.5.2.1).

Figure 5-2. Radius of curvature meter using a Mitutoyo® height meter.

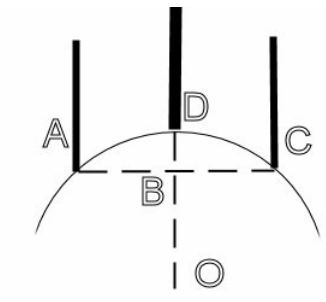

Figure 5-3. Schematic representation of geometry to calculated the radius of curvature of fruit

The apple *acoustic stiffness* was determined by the acoustic impulse technique (De Baerdemaeker *et al.,* 1982; Chen, 1993; Chen and De Baerdemaeker, 1995; Schotte *et al.,* 1999; Landahl *et al.,* 2000; De Ketelaere and De Baerdemaeker, 2001). The commercial AWETA® firmness sensor (AFS, Aweta, Nootdorp, the Netherlands) was utilized. The stiffness was measured acoustically at the same temperature the apple was impacted.

The apple is smoothly impacted and the sound is recorded. The impact energy is partially absorbed by the fruit; the rest is transformed to a damped vibration resulting in a deformation of the fruit. At specific frequencies these deformations (amplitudes) are maximized. These frequencies are called resonance frequencies. The vibrations (resulting in sound) that are being recorded are filtered and amplified. A Fourier analysis is performed resulting in a frequency spectrum from where the resonance frequencies can be extracted. At the same time the apple is automatically weighted.

The acoustic stiffness can be calculated using equation:

$$S \cong f^2 m^{2/3} \qquad (5.3)$$

with S acoustic stiffness [$Hz^2.kg^{2/3}$]
f first resonance frequency [Hz]
m mass of the apple [kg]

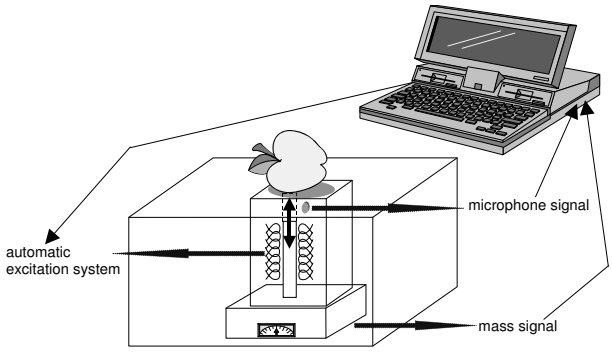

Figure 5-4. Overview of acoustic resonance technique

The 540 apples for the experiment were divided in 27 groups. For each harvest date-temperature-impact level combination, 20 apples were tested.

5.2.2.2 Statistical analysis

The data were processed with the statistical software package SAS (SAS version 8.2, The SAS Institute Inc., Cary, NC, U.S.A.). A multiple linear or nonlinear regression model was setup (proc GLM or proc NLIN). In the case of nonlinear regression a Gauss-Newton

optimisation routine was applied and the coefficient of determination was calculated as: $1-\frac{SSE}{SSTO}$.

A backward stepwise (step-down) procedure was used to select the relevant independent variables and their interactions. The significance level for staying in the model was set at 0.05. Cross-product terms were analyzed up to the three-factorial level. The cross-product term in multiple regression is often called interaction term in accordance with ANOVA, although the interpretation of interaction in multiple regression is less straightforward. From now on 'interaction term' has been utilized to identify the cross-product term. To facilitate the interpretation of the regression models, in particular the interactions in the model, the bruise volume was estimated for different values of the independent variables using EXCEL. The data was also analyzed with analysis of variance (ANOVA) with a class for harvest date (three levels: R1, R2 and R3), a class for temperature (three levels: 1°C, 15°C and 20°C) and a class for impact velocity (three levels: V1, V2 and V3). The impact velocity level can be identified with impact energy level. However the results of the analysis of variance are not integrated in this work.

5.2.3 Results and discussion

As stated in the introduction the result of the *DYP* is given briefly. The overall *DYP* for all apples in the measurements (this means apples at all temperatures, harvest dates and impact levels) was in the range 393 ± 83 kPa. A significant effect of temperature, harvest date and impact energy (impact velocity) on *DYP* could be identified (Van Zeebroeck, unpublished). These results are in agreement with Bajema *et al.* (1999) who found a *DYP* for Red Delicious apples between 320 – 450 kPa, depending on strain rate and apple size.

The results of the analysis of variance (Van Zeebroeck, unpublished) were in agreement with the regression analysis given below. There are three reasons why the analysis of variance was not integrated in this work:

- The results of the analysis of variance are less suitable to be integrated in the DEM simulations.
- Measuring error has been introduced because the real impact velocity differs from the (theoretical/desired) impact velocity of the different levels (0.3 m/s, 0.7m/s and 1.1 m/s). In the regression analysis this error was avoided because the real impact velocity (measured by the encoder) was utilized.

- The part of the bruise volume variance that can be explained by differences in radii of curvature or stiffness of the apples can not be integrated in the ANOVA model.

In Figure 5-5 a schematic overview is presented of all the relations between the variables in the experiment. The grouping of some variables in the figure can be explained by the design of the experiment. Although the variables impact energy and peak contact force are continuous variables they appear in three different data clouds because the pendulum rod was released from three different heights. The control of the impact height was sub-optimal. Nevertheless, this is not introducing errors in the data analysis, because the exact impact energy/peak contact force was measured for each impact and was treated as a continuous variable.

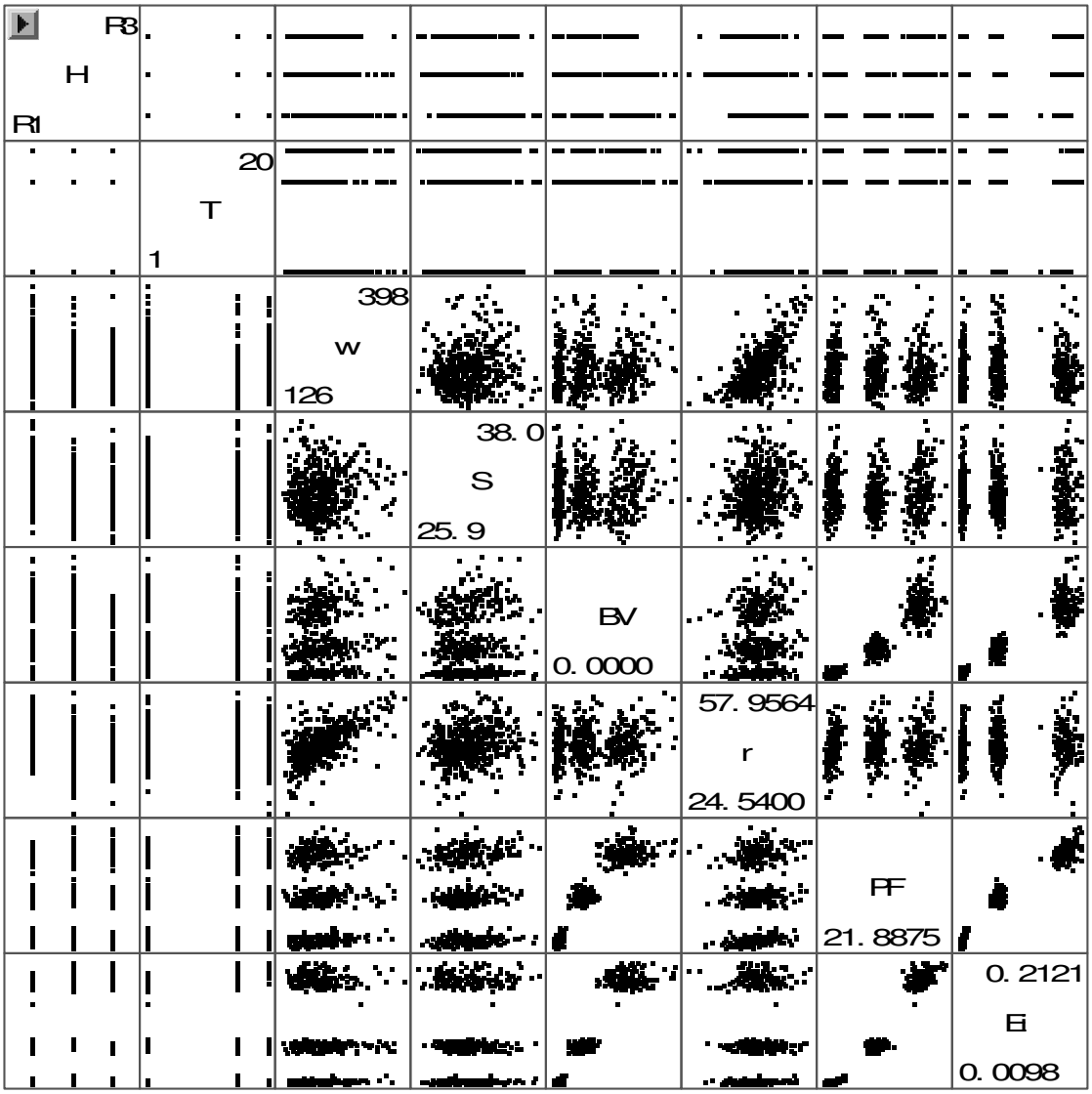

Figure 5-5. Overview of the different relations between the independent/dependent variables

H: Harvest date; *T*: Temperature [°C]; w: Weight [g]; *S*: Stiffness [$Hz^2.kg^{2/3}$]; *BV*: Bruise volume [mm^3]; *r*: radius of curvature at location of impact [mm]; *PF*: Peak force [N] ; *Ei*: Impact energy [J]

5.2.3.1 Peak contact force as independent variable

The discrete variable harvest date was made continuous by introducing dummy variables:

Table 5-2. Dummy variables to make the discrete data continuous

Harvest date	X_1	X_2
Optimal - 10	1	0
Optimal	0	0
Optimal +10	0	1

The significant main effects and interactions (up to three factorial level) between all variables (peak contact force, temperature, harvest date, acoustic stiffness, radius of curvature and mass) were analyzed on the 95 % significance level. Using the backward stepwise (step-down) procedure (model reduction), different linear and nonlinear statistical models were analyzed. Besides, different linear combinations of second and first order interaction terms, also a power law dependency between peak force and bruise volume in combinations with second and first order linear interaction terms were analyzed.

Radius of curvature and apple mass appeared to be complementary variables. No effect was found for the radius of curvature when the mass was in the model and vice versa; therefore it was decided to eliminate the mass in the model. The elimination of the mass was preferred because firstly the only possible effect of the mass on the bruise volume is through the radius of curvature and secondly a higher coefficient of determination was obtained. It is important to realize that in the pendulum experiment the mass of the apple has no effect on the impact energy and impact force (the inertia of the pendulum rod and impact angle do). For an impacting apple in practice or in the DEM simulation the mass of the apple is of course also determining impact energy and contact force.

The following statistical model was identified (P<0.0001):

$$BV = 0.239PF^{1.796} + 43.488X_2 + 3.484T - 1.596X_2 \times PF - 0.112PF \times T - 3.664r + 0.102r \times PF \quad (5.4)$$

$$R^2 = 0.896$$

with BV bruise volume [mm^3]
X_2 dummy variable for harvest date
T temperature [°C]
PF peak contact force [N]
r radius of curvature on location of impact [mm]

In Figure 5-6 the predicted bruise volume- measured bruise volume plot is given.

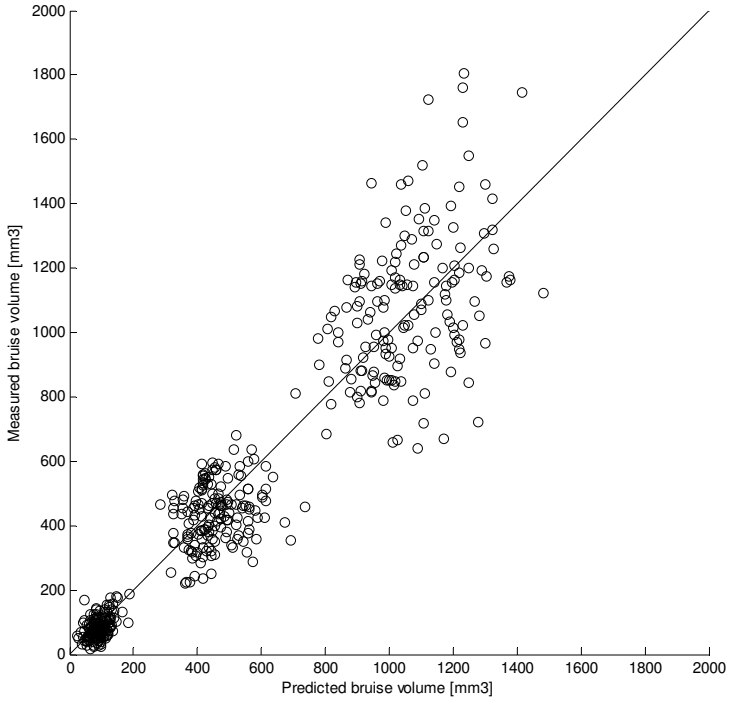

Figure 5-6. Model 5.4: Predicted value (p) – measured value (BV) plot of the bruise volume [mm^3]

The different data clouds that can be seen in Figure 5-6 are a result of the experimental design. The pendulum rod was released from three different heights.

As can be seen in model (5.4), the dummy variable X_1 was not significant. It was identified that by eliminating the radius of curvature, also a significant effect of dummy variable X_2 could be identified (P<0.0001). This is due to the correlation between harvest date and apple size.

$$BV = 0.304PF^{1.794} - 98.040X_1 - 6.166X_2 + 0.518T + 1.966X_1 \times PF - 0.731X_2 \times PF - 0.072PF \times T \quad (5.5)$$

$$R^2 = 0.895$$

In Figure 5-7 the predicted bruise volume- measured bruise volume plot for this model is depicted.

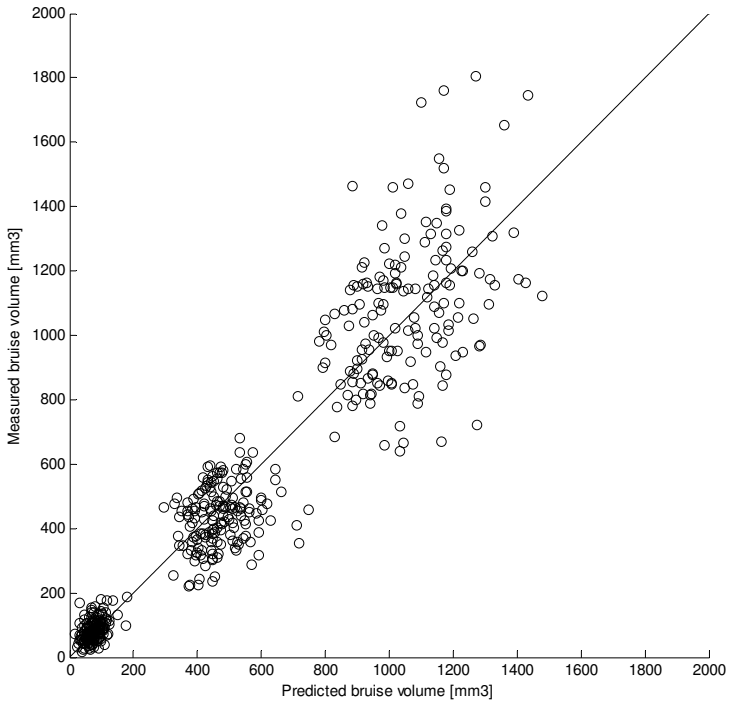

Figure 5-7. Model 5.5: Predicted value (p) – measured value (BV) plot of the bruise volume [mm^3]

The fact that the peak contact force is the most important independent variable in the statistical model can be seen from the coefficient of determination:

$$BV = 0.165 PF^{1.910} \qquad (5.6)$$

$$R^2 = 0.875$$

87.5 % of the variance of the bruise volume in the experiment is explained by the peak contact force.

In Figure 5-8 the predicted bruise volume- measured bruise volume plot for this model is shown.

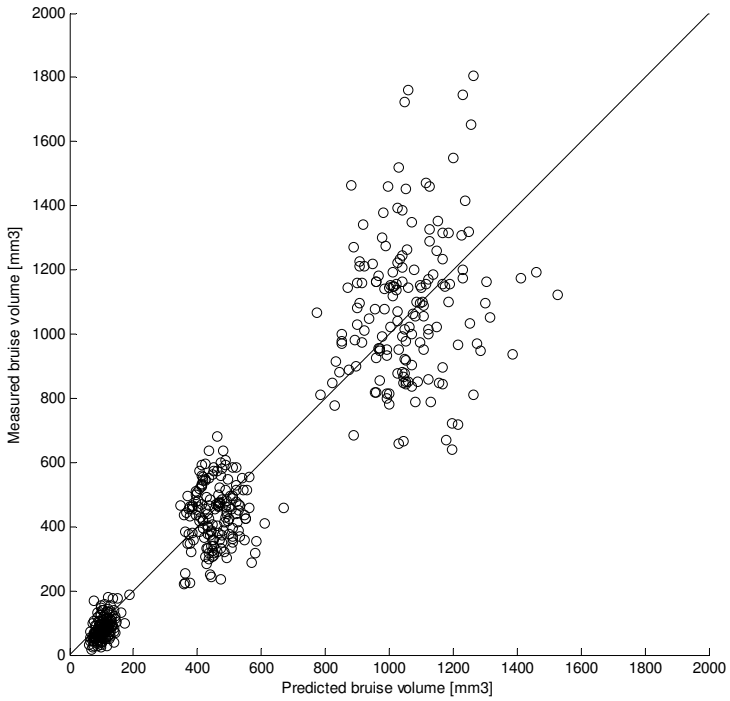

Figure 5-8. Model 5.6: Predicted value (p) – measured value (BV) plot of the bruise volume [mm^3]

Since no significant effect of the acoustic stiffness could be identified when it was analyzed together with harvest date (probably due to the biological relation between acoustic stiffness and ripeness), a statistical significant model is given without considering apple harvest date (P<0.0001):

$$BV = 0.167PF^{1.864} - 4.658S + 3.635T + 0.1415S \times PF - 0.116T \times PF \quad (5.7)$$

$$R^2 = 0.888$$

with S acoustic stiffness [Hz^2.kg$^{2/3}$]

In Figure 5-9 the predicted bruise volume- measured bruise volume plot for this model is depicted.

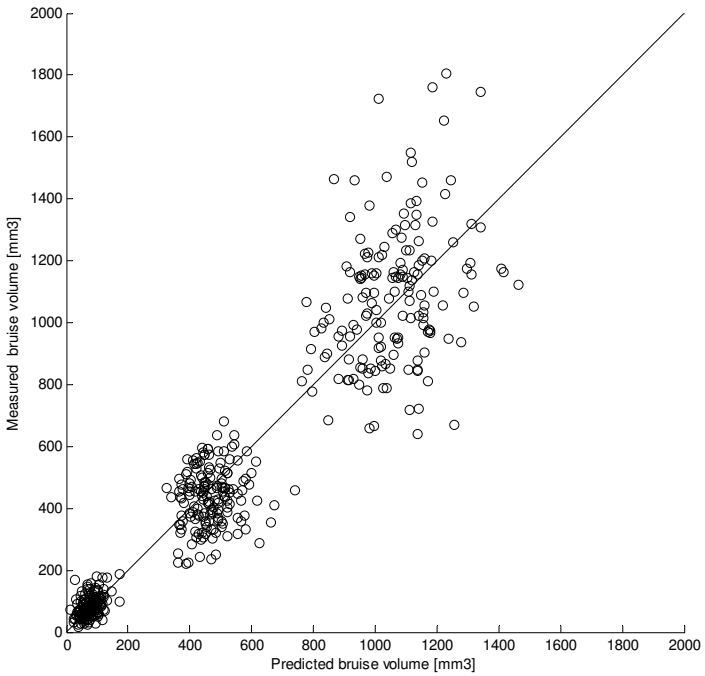

Figure 5-9. Model 5.7: Predicted value (p) – measured value (BV) plot of the bruise volume [mm^3]

In the different predicted bruise volume - measured bruise volume plots can be noticed that the prediction of the bruise volume is inferior for higher bruise volumes. This is due to the increase of the error variance of the bruise volume for higher impact levels. Fortunately, these high bruise volumes are infrequent during postharvest treatment of fruit for the fresh market like it is the case in Belgium.

In Table 5-3 the extra sum of squares of the remaining independent variables are given when the peak contact force is already in the model. To obtain the extra sum of squares also a linear relationship between the peak contact force and the bruise volume was assumed. In the nonlinear regression procedure the extra sum of squares cannot be calculated.

Table 5-3. Extra sum of squares for the remaining independent variables when the peak contact force is already included in the model

Type I Extra sum of squares	*Absolute number*	$\left[SSR(X_2, X_2 \times X_1 \middle\| X_1) / SSE(X_1)\right] * 100$
$SSR(X_2, X_2 \times PF \middle\| PF)$	$8.80 * 10^5$	7.0
$SSR(X_1, X_1 \times PF \middle\| PF)$	$8.01 * 10^5$	6.4
$SSR(r, r \times PF \middle\| PF)$	$7.13 * 10^5$	5.7
$SSR(T, T \times PF \middle\| PF)$	$6.89 * 10^5$	5.5
$SSR(S, S \times PF \middle\| PF)$	$4.98 * 10^5$	4.0

The third column indicates the coefficient of partial determination multiplied by 100. It indicates with how many percent the error sum of squares when only X_1 is in the model is further reduced when $X_2, X_2 \times X_1$ are added to the model

By far the most important factor in predicting the bruise volume is the peak contact force. This can be seen in the high coefficient of determination of the model including the peak contact force as only independent variable (model 5.6) and the low coefficient of partial determination of all the other independent variables if the peak contact force is already included in the model. Nevertheless, a significant effect of all fruit properties was identified.

According to Table 5.3 the following classification of their importance in explaining the overall variance of the bruise volume can be made:

1. Harvest date
2. Radius of curvature at the location of impact
3. Apple temperature
4. Acoustic stiffness

A sensitivity analysis was performed to obtain a more detailed understanding of the effect of the different independent variables on the bruise volume. The results of this analysis are presented below.

Effect of apple harvest date on bruise volume (model 5.4 and 5.5)

A significant interaction effect between peak contact force and harvest date was identified, giving rise to different conclusions for high and low impacts.
The optimal harvest date (defined by VCBT) was taken as a reference. Late harvest (optimal date + 10 days) is leading to less bruise damage compared to harvest at the optimal date. The positive interaction of harvest date with peak contact force caused an increase in the absolute value of the bruise volume reduction with increasing peak contact force. When expressed in relative numbers (percentage), for impacts beyond 37 N a reduction in bruise volume around 10 % was noted for late harvested apples compared to optimal harvested ones. For impacts below 37 *N* less than 10 % reduction in bruise volume was noted for late harvested apples compared to optimal harvested ones.
Due to the same interaction term between harvest date and peak contact force, an opposite effect of *early* harvest date on bruise volume was noted for low and high impacts. Low impacts gave rise to *less* bruise damage; high impacts however gave rise to *more* bruise damage. The transition was around 51.5 N, with of course little effect of harvest date on bruise volume. The positive or negative effect of early harvest date was respectively

increasing with lower and higher peak forces. In relative number the positive effect was up to 50 % bruise volume reduction for low impacts (however, a high reduction in a small bruise volume is not so meaning full) and up to 9 % increase in bruise volume for high impacts. Because large bruises are more visible, the effect of harvest date can be simplified to an overall negative outcome of early harvest date on bruising of the apples. However, it must be stated that no statistical effect of early harvest date on bruise volume could be noticed when the radius of curvature was present in the model (model 5.4).

In literature lots of contradicting results concerning the effect of harvest date on fruit bruise damage are present. Some authors like Johnson and Dover (1990) and Garcia (1995) found an increase in bruise damage with harvest date (contradicting our results). Other authors, like Diener *et al.* (1979) found the opposite effect confirming our results. Garcia (1995) gives an explanation for the contradicting results found in literature. Two processes are associated with ripening: decrease in turgor and decrease in apple firmness. Decrease in turgor leads to less bruise damage. But in contrary, decrease in apple firmness leads to more bruise damage (Garcia *et al.,* 1995). The effect of turgor can be explained as such: cell walls of apple cells with less turgidity experience less stress and therefore, this stress added by the supplementary stress caused by impact will stay longer under the critical level. Garcia *et al.* (1995) states that the effect of maturity on bruise volume (+,= or -) depends on which process (turgor change or firmness change) dominates the ripening process. In this experiment only a slight reduction in apple firmness with increasing harvest date could be identified. This was concluded from the slight reduction in apple acoustic stiffness with increasing ripeness for the apples in the experiment (data not shown)[31]. As a consequence, a hypothesis can be stated that the decrease in turgor with increasing harvest date is the causing factor of the decrease in bruise damage with increasing harvest date for the apples in the experiment (the turgor of the apples was not measured).

More experiments are needed to verify whether the reduction of bruise susceptibility with maturity can be generalized to all Jonagold apples.

Effect of apple temperature on bruise volume (model 5.4 and 5.5)

A significant effect of apple temperature on bruise volume could be identified. Higher apple temperature leads to less bruising. The interaction term with the peak contact force indicates that the effect of temperature on the bruise volume in absolute value increases with higher peak forces. In relative value (percentage) the effect of temperature on bruise volume

[31] Different authors demonstrated a positive correlation between apple stiffness and firmness (Abbott *et al.,* 1996, Galili and De Baerdemaeker, 1996; Duprat *et al.,* 1997; Landahl *et al.*, 2000).

increases with peak impact force: from 0 % more bruise volume for low impacts to 15 % more bruise volume for high impacts for apples of 1°C compared to 20°C.

Temperature might be expected to influence the physical properties of the apples and therefore also bruising, but reports of temperature effects on bruising are inconsistent. Saltveit (1984) reported for two varieties of apple a progressively higher bruise volume from 0 to 30 °C. Other authors found no effect of temperature on bruising of apples (Klein, 1987; Schoorl and Holt, 1977). However, according to Knee and Miller (2002), the data presented by Schoorl and Holt (1977) show that bruise volumes were smaller at 30 °C compared to lower temperatures. Van Lancker (1979) and Hyde *et al.* (2001) both on Golden Delicious apples, showed a decreasing bruise volume with higher temperatures, confirming our results. Also Pang *et al.* (1992) and Mowatt (1997) found a slight higher bruise susceptibility of apples of 1°C compared to apples at room temperature.

It is agreed with Van Lancker (1979) that the elastic modulus decreases with increasing apple temperature and the elastic modulus is positively related to bruise damage. In the data of this study also a decrease in apple acoustic stiffness with increasing temperature was identified (data not shown). The acoustic stiffness is positively related to the apparent elastic modulus, although its degree is depending on the turgor (Landahl *et al.,* 2004). The effect of apple acoustic stiffness on bruise susceptibility is discussed below.

A physical explanation of the effect of temperature on (acoustic) stiffness of tissue is given by Hertog *et al.* (2004): As viscosity of the cell walls will increase with decreasing temperature the cell walls might become more brittle resulting in an increased stiffness. Nevertheless, another explanation, contradicts the effect of temperature on the stiffness given above. With increasing and decreasing temperature, the water inside the fruit expands and contracts in volume. This effect is comparable to the effect of turgor. An increased cell tension due to increased turgor or temperature will increase the acoustic stiffness and the elastic modulus of the tissue (Chen, 1993; Hertog *et al.,* 2004). The overall effect of temperature on stiffness will be the result of the effects temperature has on both tissue tension and cell wall viscosity (Hertog *et al.,* 2004).

Effect of apple radius of curvature on bruise volume (model 5.4)

The interaction term of the radius of curvature with the peak contact force indicates an opposite effect of radius of curvature for low and high impacts. Small apples (low radius of curvature) contract more bruise compared to large apples for small impacts, however the opposite is true for high impacts, there small apples contract less bruise. The transition of both effects is around 35 N, with of course little effect of radius of curvature on bruise

volume. The positive or negative effect of larger radius of curvature on bruise volume is respectively increasing with lower and higher peak forces. In relative value and for two extreme apple sizes that are commercialized, 65 mm diameter compared to 90 mm diameter, the bruise volume is up to 10 % higher for low impacts (30 N) and up to 6 % lower for high impacts (100 N).

Statistical studies describing the effect of the radius of curvature on apple bruise damage are rare. It can be derived from a study by Brown and Segerlind (1975) that the incidence of bruises is higher, but the size of the bruises is smaller, around the apple steel and calyx compared to the rest of the apple. Because the radius of curvature of the apples is lower at steel and calyx, these results are in agreement with our results.

Besides this statistical study, two physical models found in literature based on Hertz theory, are supporting our results:

The first model was derived by Horsfield *et al.* (1972):

$$\sigma_i = C(mgh)^{1/5}\left[\frac{1-\nu_1^2}{E_1}+\frac{1-\nu_2^2}{E_2}\right]^{-4/5}\left[\frac{1}{R_1}+\frac{1}{R_2}\right]^{3/5} \qquad (5.8)$$

with C a constant
σ_i the peak contact stress [Pa]
$\nu_{1/2}$ the Poisson's ratio
$E_{1/2}$ elastic modulus [Pa]
R radius of curvature [m]
m mass of apple [kg]
g 9.81gravity [m/s^2]
h drop height [m]

Baritelle and Hyde (2000) used this equation to calculate the critical impact height by introducing $\sigma_i = \sigma_f$; the peak contact stress becomes the failure stress:

$$h_c = C\sigma_f^{\,5}\frac{1}{mg}\left(\frac{1-\nu_1^2}{E_1}+\frac{1-\nu_1^2}{E_2}\right)^4\left(\frac{1}{R_1}+\frac{1}{R_2}\right)^{-3} \qquad (5.9)$$

with h_c critical drop height [m]
σ_f the failure stress [Pa]
$\nu_{1/2}$ the Poisson's ratio [-]
$E_{1/2}$ elastic modulus [Pa]
$R_{1/2}$ radius of curvature [m]
m mass of apple [kg]
g gravity [m/s^2]

Analyzing both equations states that higher radius of curvature leads to lower peak stress and therefore to higher critical drop height. This is confirming the statistical results for *low* impacts where small radius of curvature leads to more bruise damage.

However, another equation by Siyami (1988), also derived from Hertz theory, shows an opposite effect of apple radius of curvature on bruise diameter (bruise volume). The assumption is that the bruise surface area is similar to the contact area.

$$BD = 4.624\left(\frac{mhR^2}{4F_{mt}}\right)^{1/5} \qquad (5.10)$$

with BD bruise diameter [mm]
m mass of apple [kg]
R radius of curvature [m]
h drop height [mm]
F_{mt} Magness-Taylor force, 11 mm probe [kg]

Equation (5.10) indicates that a higher radius of curvature leads to higher bruise diameter (also higher bruise volume). Equation (5.10) is confirming the statistical result for *high* impacts.

From formula's 5.8 and 5.10 can be distracted that the radius of curvature has a double effect on the bruise damage: a smaller radius of curvature increases the peak stress (5.8), but decreases the contact area (bruise surface area) during impact (5.10).

From our results, it can be postulated that for high impacts it is more important to have more tissue in contact (= high radius of curvature) to get more bruise damage than to induce a higher peak stress, because the peak stress is lowered in the case of high radius of curvature. For small impacts the opposite is true: it is more important to induce a higher peak stress in the case of smaller radius of curvature to obtain more bruise damage than a higher contact area during impact because the latter is lower for apples with a smaller radius of curvature.

A possible explanation for the different effect of the radius of curvature on apple bruise damage for low and high impacts is that once the peak contact stress is sufficiently beyond the tissue failure stress (in the case of high impacts) the contact surface during impact becomes more important in determining the bruise damage.

Another explanation for the effect of radius of curvature on the bruise damage is through the differences in tissue structure between small and large apples. Johnson and Dover (1990) identified that large apples have larger cells and thinner cell walls and this is the reason they contract more bruise damage. However for our results this explains only the larger bruises in the case of high impacts, but not the larger bruises with smaller radius of curvature for low impacts.

Effect of apple acoustic stiffness on bruise volume (model 5.7)

The interaction term of the acoustic stiffness with the peak contact force indicates an opposite effect of apple acoustic stiffness for low and high impacts. Stiffer apples contract less bruise for low impacts, however the opposite is true for high impacts, there they contract more bruise. The transition of both effects is around 34 N, with of course little effect of apple acoustic stiffness on bruise volume. In relative value and for apples of acoustic stiffness 28 $Hz^2.kg^{2/3}$ compared to 35 $Hz^2.kg^{2/3}$ (acoustic stiffness extremes in measurement), the bruise volume is up to 9 % higher for low impacts (30 N) and up to 7 % lower for high impacts (100 N).

A statistical study of the effect of acoustic stiffness, as measured by the acoustic impulse technique has not been published before. Because acoustic stiffness itself is positively correlated with elastic modulus (Duprat *et al.,* 1997; Landahl *et al.,* 2004) the effect of elastic modulus on bruise is given here.

Statistical data in literature about the effect of elastic modulus on bruise susceptibility is rare. Verstreken *et al.* (1995) found a positive correlation between skin modulus of elasticity and bruise volume during storage. Also, from Hertz theory can be seen that higher elastic modulus of apple give rise to more bruise damage (Equation (5.8)). This equation (5.8) indicates that higher elastic moduli of impacting bodies give rise to higher peak stress when dropped from the same height. Bruise damage is positively correlated with this peak stress at the contact area, what explains the higher bruise volume for apples with higher elastic modulus.

However, for very small impacts (<34N), the opposite effect of acoustic stiffness (elastic modulus) was identified. This can be explained as such: Different authors demonstrated a positive correlation between apple acoustic stiffness and firmness[32] (Abbott *et al.,* 1996, Duprat *et al.,* 1997; Galili and De Baerdemaeker, 1996; Landahl *et al.*, 2000). Higher firmness or failure stress σ_f (synonyms) for stiffer apples declares they are more resistant to bruising (for low impacts). The fact that higher firmness of stiffer apples leads only to more bruise damage for low impacts and not for high impacts can be explained as such:

For low impacts the higher firmness of the stiffer apples is dominating the fact that stiffer apples lead also to a higher peak contact stress. For high impacts the opposite is true, here the higher peak contact stress dominates the higher firmness of the stiffer apples.

As a final remark it must be stated that although stiffer apples gave rise to higher peak contact forces when dropped from the same height, still an effect of acoustic stiffness on

[32] The physical definition of firmness is intended here: the maximum stress that a material can be deformed by before breakage

bruise volume could be identified when both acoustic stiffness and peak contact force were present in the statistical model. This must be explained as such: even for an equal peak contact force the peak stress can be higher, because besides peak contact force also the contact surface determines the peak stress ($\sigma_i = \frac{F_{\max}}{S}$), so even for equal peak contact force, the peak stress can be different.

It can be concluded that stiffer apples have a slightly higher threshold: they can be dropped from a slight higher height before they get bruised, but when dropped from high heights they contract larger bruises. This latter effect is more important for the overall bruise damage.

5.2.3.2 Bruise volume: Impact energy as independent variable

The discrete variable harvest date was made continuous by introducing dummy variables (see section 5.2.3.1). The significant main effects and interactions (up to three factorial level) between all variables (impact energy, temperature, harvest date, acoustic stiffness, radius of curvature and mass) were analyzed on the 95 % significance level. Using the backward stepwise (step-down) procedure, different linear and nonlinear statistical models were analyzed. Besides, different linear combinations of second and first order terms, also a power law dependency between impact energy and bruise volume in combinations with second and first order terms was analyzed. The following most relevant model was identified (P<0.0001):

$$BV = 478.067 + 3747.984Ei + 920.268X_1 + 375.446X_2 + 0.616T - 3.822w - 14.0111S - 4.016r + 519.564Ei \times X_1 - 629.776Ei \times X_2 - 52.894Ei \times T + 67.007Ei \times r - 0.789X_1 \times w - 24.541X_1 \times S - 11.978X_2 \times S + 0.142w \times S \quad (5.11)$$

$$R^2 = 0.934$$

with BV bruise volume [mm^3]
X_1 and X_2 dummy variable for harvest date
T temperature [°C]
Ei impact energy [J]
w apple mass [g]
S apple acoustic stiffness [Hz^2.kg$^{2/3}$]
r radius of curvature on location of impact [mm]

In Figure 5-10 the predicted bruise volume - measured bruise volume plot is presented for this model.

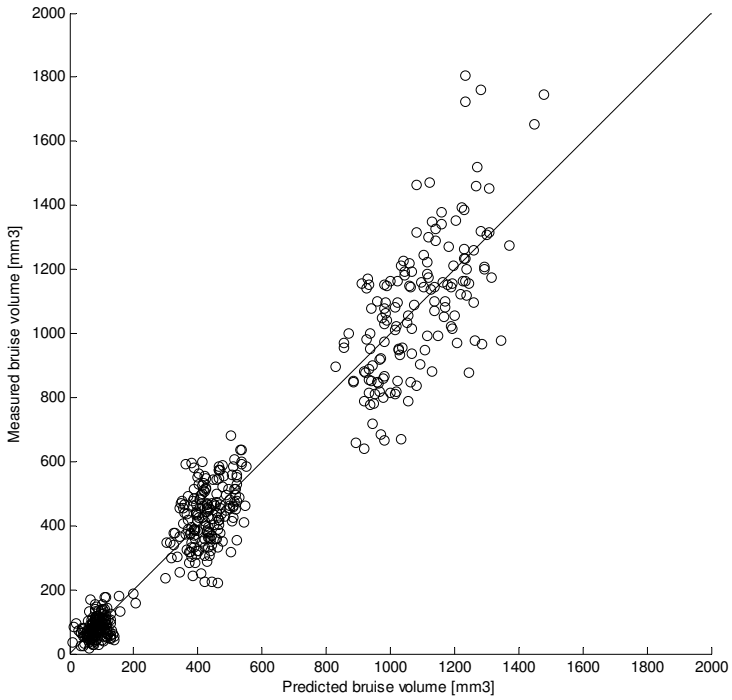

Figure 5-10. Model 5.11: Predicted value (p) – measured value (BV) plot of the bruise volume [mm^3]

A much more complex statistical model for impact energy was achieved compared to peak contact force. All measured parameters have a significant effect on the bruise volume. Unlike the statistical models with the peak contact force as independent variable all independent variables coexist in one model (model 5.11). Moreover, much more interactions are present and besides interactions with the fruit properties (temperature, harvest date, radius of curvature) and the impact energy also mutual interactions between fruit properties were identified. All this contribute to a much more complicated but more subtle statistical model.

In Table 5-3 the extra sum of squares of the remaining independent variables are given when the peak contact force is already in the model.

Table 5-4. Extra sum of squares for the remaining independent variables when the impact energy is already included in the model

Type I Extra sum of squares	*Absolute number*	$\left[SSR(X_2, X_2 \times X_1 \middle| X_1) / SSE(X_1)\right]*100$
$SSR(X_1, X_1 \times Ei \middle| Ei)$	$1.48*10^6$	15.2
$SSR(X_2, X_2 \times Ei \middle| Ei)$	$1.40*10^6$	14.3
$SSR(T, T \times Ei \middle| Ei)$	$1.18*10^6$	12.0
$SSR(r, r \times Ei \middle| Ei)$	$1.07*10^6$	11.0
$SSR(S, S \times Ei \middle| Ei)$	$9.94*10^5$	10.1

The third column indicates the coefficient of partial determination multiplied by 100. It indicates with how many percent the error sum of squares when only X_1 is in the model is further reduced when $X_2, X_2 \times X_1$ are added to the model

By far the most important factor in predicting the bruise volume is the impact energy. This can be seen from the low coefficients of partial determination of all the other independent variables if the impact energy is already included in the model (Table 5-4).
Nevertheless, a significant effect of all fruit properties was identified. According to Table 5.4 the following classification of their importance in explaining the overall variance in the bruise volume can be made:

1. Harvest date
2. Apple temperature
3. Radius of curvature at the location of impact
4. Acoustic stiffness

A sensitivity analysis was performed to obtain a more detailed understanding of the effect of the different independent variables on the bruise volume. The results of this analysis are presented below.

Effect of apple harvest date on bruise volume (model 5.11)

In contrast to the models including the peak contact force (models 5.4, 5.5 and 5.7) significant interactions between harvest date and acoustic stiffness were identified. For apples of average acoustic stiffness in the experiment (31 $Hz^2.kg^{2/3}$) the same conclusions can be drawn as for the model including the peak contact force (in absolute and relative value, transition of the effect is around 0.05 J).
The positive effect of late harvest was more pronounced for stiffer apples. For apples with low acoustic stiffness almost no effect of late harvest on bruise volume could be observed.

The negative effect of early harvest on bruise volume was higher for apples with low acoustic stiffness. For apples with high acoustic stiffness almost no effect of early harvest on bruise volume could be identified.

Effect of apple temperature on bruise volume (model 5.11)

The same conclusions can be drawn for the effect of apple temperature on bruise volume as for the model with the peak contact force as independent variable (section 5.2.2.1).

Effect of apple radius of curvature on bruise volume (model 5.11)

The same conclusions can be drawn as for the models with the peak contact force as independent variable (section 5.2.2.1). However in relative terms the effect of the radius of curvature was more pronounced. The effect of apple size was calculated for the extremes in commercialized apple sizes. Apples of diameter 65 mm compared to apples of diameter 90 mm contracted up to 50 % more bruise for small impacts (in absolute terms difference is very small!) and up to 9 % less bruise for high impacts (0.18 J, ≅ 100 N).

Effect of apple acoustic stiffness on bruise volume (model 5.11)

The conclusions for the effect of the acoustic stiffness on apple bruise volume are slightly different compared to the models with the peak contact force as independent variable. First of all, no interaction between impact energy and acoustic stiffness was identified. Stiffer apples gave rise to more bruise damage. The interaction with the harvest date indicated that the effect of the acoustic stiffness was not the same for all harvest dates. The effect of acoustic stiffness was the most pronounced for the optimal harvest date, less pronounced for the late harvest date and almost nonexistent for the early harvested apples. For the optimal harvest date and average apple size the difference in bruise volume between the extremes in acoustic stiffness in the measurement (28 $Hz^2.kg^{2/3}$and 35 $Hz^2.kg^{2/3}$) was 166 mm^3. The interaction term between apple weight and acoustic stiffness indicates that the effect of acoustic stiffness was more pronounced for larger apples.

Effect of apple mass on bruise volume (model 5.11)

The effect of apple mass on bruise volume was not identified for the models with the peak contact force as independent variable. It was noted that larger apples contracted more bruise

than smaller apples. This effect was fixed for each impact level (no interaction between apple mass and impact energy). The effect of apple mass was more pronounced for higher acoustic stiffness apples. For early harvested apples this effect was less pronounced than for optimum and late harvested apples. Most likely the effect of apple mass on bruise volume has to be explained by its positive correlation with radius of curvature.

5.2.4 Conclusions

The effect of the fruit properties on the bruise volume can be summarized in a simplified form in the following table:

Table 5-5. Simplified summary of effect of apple parameters on bruise volume

Factor	
Harvest date	Bruise volume decreases with increasing harvest date
Temperature	Bruise volume decreases with increasing temperature
Radius of curvature	Low impacts: r ↓→ bruising ↑ High impacts: r ↓→ bruising ↓ Average impacts: no effect
Apple acoustic stiffness	Acoustic stiffness ↑ → bruising ↑, most pronounced optimal harvest date

5.3 Bruise prediction models for tomatoes

5.3.1 Introduction

In contrast to apples no browning of damaged tomato tissue occurs, what makes objective measurement of tomato bruise damage very difficult. Until present no such method is available. The only method that was found in literature was a visual scoring of the degree of bruise damage (Sargent *et al.,* 1989). Because the lack of accurate bruise determination of tomatoes, the research about tomato bruise susceptibility is rare.

In this research *absorbed energy* has been used to quantify bruise damage. For one experimental object (one tomato of a certain ripeness at a certain temperature) most likely can be stated that higher absorbed energy indicates higher bruise damage. However, between tomatoes in a batch and even a single tomato at a different ripeness stage or temperature this is less obvious. After all, not all absorbed energy is transformed into plastic deformation (bruise). The absorbed energy can be divided into plastic and viscous energy. The viscous energy loss is due to the materials viscosity (see Chapter 2). The hypothesis was made that

within a cultivar higher absorbed energy of the tomato also indicates higher bruise damage when impacted by the same impact energy.

The hypothesis is true if the proportion between viscous and plastic energy at a given impact energy is constant regardless, for example, fruit ripeness or temperature or at least this proportion is not that influenced by fruit properties that higher absorbed energy at a given impact energy is entirely due to an increase in viscous energy. As soon as a method is available to measure tomato bruise damage objectively this hypothesis could be verified.

In anticipation of such a method a verification of the hypothesis on the energy level was executed.

Using the same batch of tomatoes that were used for the experiment to test tomato fruit properties on absorbed energy, outlined below, an experiment was executed to test the effect of fruit properties on plastic and viscous energy separately. The constant height multiple impact method (CHMI) described by Bajema and Hyde (1998) has been used for this experiment. However, the experiment was not conclusive because for none of the fruit properties a significant effect neither on plastic energy nor on viscous energy could be demonstrated (data not shown). Two reasons can be given for this result. First, the assumptions made by Bajema and Hyde (1998) are questionable and the validity of the method is never proved. Second, the variance within tested tomatoes with the same fruit properties (temperature, ripeness, etc.) was very high. Most likely this is due to (slight) differences in impact energy between repeated impacts on the same tomatoes leading to a high measuring error.

In the experiment to establish the bruise prediction models for tomatoes besides the absorbed energy also the restitution coefficient was used as dependent variable. The restitution coefficient is calculated as:

$$\mathrm{Re}\,s = \frac{E_e}{E_i} = \frac{\mathrm{v}_r}{\mathrm{v}_i} \qquad (5.12)$$

with E_e and E_i elastic and impact energy [J]

v_r and v_i rebound and impact velocity [m/s]

The restitution coefficient can be seen as an estimation of the degree of absorbed energy (*Res* of 0 indicates 100 % of the energy is absorbed and *Res* of 1 indicates 0 % of the impact energy is absorbed). Because of the complementary of the restitution coefficient with the absorbed energy, the results are not presented. Besides, for DEM simulations, the absorbed energy as estimation for bruise damage is more useful than restitution coefficient.

5.3.2 Materials and methods

5.3.2.1 Experimental setup

The tomato cultivar that was used for the experiments was 'Tradiro'. The tomatoes were obtained from the "proeftuin" in Sint-Katelijne-Waver, Belgium.
Tomatoes of the same greenhouse were picked in three different ripeness stages: green, pink and red. 360 tomatoes were used for the experiment. Each tomato was impacted two times on two different locations: compartment and partition. Whole tomatoes were mounted on the pendulum (see Chapter 3). Three impact levels were applied (low, moderate, high; Table 5-6).
For each ripeness-temperature-impact level 20 tomatoes were utilized (18x20=360 tomatoes in total).
The independent variables were:

- Impact energy or peak contact force
- Tomato temperature (15 °C and 20 °C)
- Acoustic stiffness (indication of ripeness)
- Colour (indication of ripeness)
- Radius of curvature on location of impact
- Location of impact: compartment or partition

Impact energy and *peak contact force* were logged to a data file for each impact. The tree impact levels that were used were:

Table 5-6. Overview of different impact levels used in the experiment.

	Peak contact force [N]	*Impact energy [J]*
Level 1	≅ 15	≅ 0.020
Level 2	≅ 30	≅ 0.087
Level 3	≅ 60	≅ 0.26

All three impact levels were recorded by the electronic fruit PMS-60 during harvest and sorting in greenhouses in Belgium, although impacts of level 3 were rare (Desmet *et al.,* 2004b).
To measure acoustic *stiffness* and *radius of curvature* of the tomatoes the same equipment was used as for the apples (section 5.2.2.1). Because the tomato is not a perfect sphere, the

harmonic average was calculated of the circumferential radius of curvature and the meridian radius of curvature (see section 3.5.2.1).

Measurement of tomato ripeness by acoustic stiffness and colour

Tomato *acoustic stiffness* is an estimation for tomato ripeness when measured within one cultivar. A higher acoustic stiffness indicates a lower ripeness. The acoustic stiffness is not a good measure for ripeness in the case all tomatoes are in the red mature stage (De Ketelaere, 2002). Since in this experiment tomatoes in green, orange and red stadium were used, the acoustic stiffness can be considered as an objective measurement of tomato ripeness.
The *colour* itself is a very good estimation of tomato ripeness and can be measured objectively by spectrophotometry. A Minolta® CR-300 (Konica Minolta Photo Imaging Europe GmbH, Langenhagen, Germany) spectrophotometer was utilized to perform the measurement (VCBT, K.U. Leuven). The spectrophotometer is able to do measurements of the colour in various accepted standards methods. Usually, the measurements of the colour are represented using the L^* a^* b^* colour system. This model was proposed by the CIE (Commission Internationale d'Eclairage) in 1931 as an international standard to measure the colour where L^* is lightness on a scale of 0 (black) to 100 (white), a^* is red-green share and indicates red tones when is positive and green tone when is negative, and b^* is blue-yellow share indicating positive values for yellow tones and negative values for blue tones. The scale of values for the a^* and b^* goes from -120 to +120.
The colorimetric coordinate a^* was taken as estimation of tomato ripeness because it indicates the transition from green to red colour (higher a^* value indicates redder colour).
The colour is a good indication for tomato ripeness within one cultivar. The colour is not a good measure for ripeness in the case all tomatoes are in the red mature stadium (De Ketelaere, 2002). Since in this experiment tomatoes of green, orange and red stadium were used the colour can be considered as an objective measurement of tomato ripeness.

5.3.2.2 Statistical analysis

The data were processed with the statistical software package SAS (SAS version 8.2, The SAS Institute Inc., Cary, NC, U.S.A.). A multifactor covariance analysis was setup (proc GLM) A backward stepwise (step-down) procedure was used to select the relevant independent variables and their interactions. The significance level for staying in the model was set at 0,05. Interaction terms were analyzed up to the three-factorial level. In contradiction to the statistical analysis for the apples (section 5.2), no dummy variables were

introduced for the discrete variables in the model (=regression formulation of covariance model). 2-factorial covariance analysis with different concomitant variables (continuous variables) was performed.

To facilitate the interpretation of the regression models, in particular the interactions in the model, the absorbed energy was estimated for different values of the independent variables using EXCEL.

5.3.3 Results and discussion

As stated in the introduction (section 5.3.1), besides the absorbed energy in absolute value also the coefficient of restitution can be used to measure the degree of absorbed energy. The models with the restitution coefficient as dependent variable gave more or less the same results as for the models with the absorbed energy as dependent variable. Because the models with the restitution coefficient as dependent variable are less suitable to be used for the DEM simulations they are not discussed here.

In Figure 5-11 a schematic overview is presented of all the relations between the variables in the experiment. The grouping of the variables in the figure can be explained by the design of the experiment. Although the variables impact energy and peak contact force are continuous variables they appear in three different data clouds because the pendulum rod was released from three different heights. The control of the impact height was sub-optimal. Nevertheless, this is not introducing errors in the data analysis, because the exact impact energy/peak contact force was measured for each impact and was treated as a continuous variable.

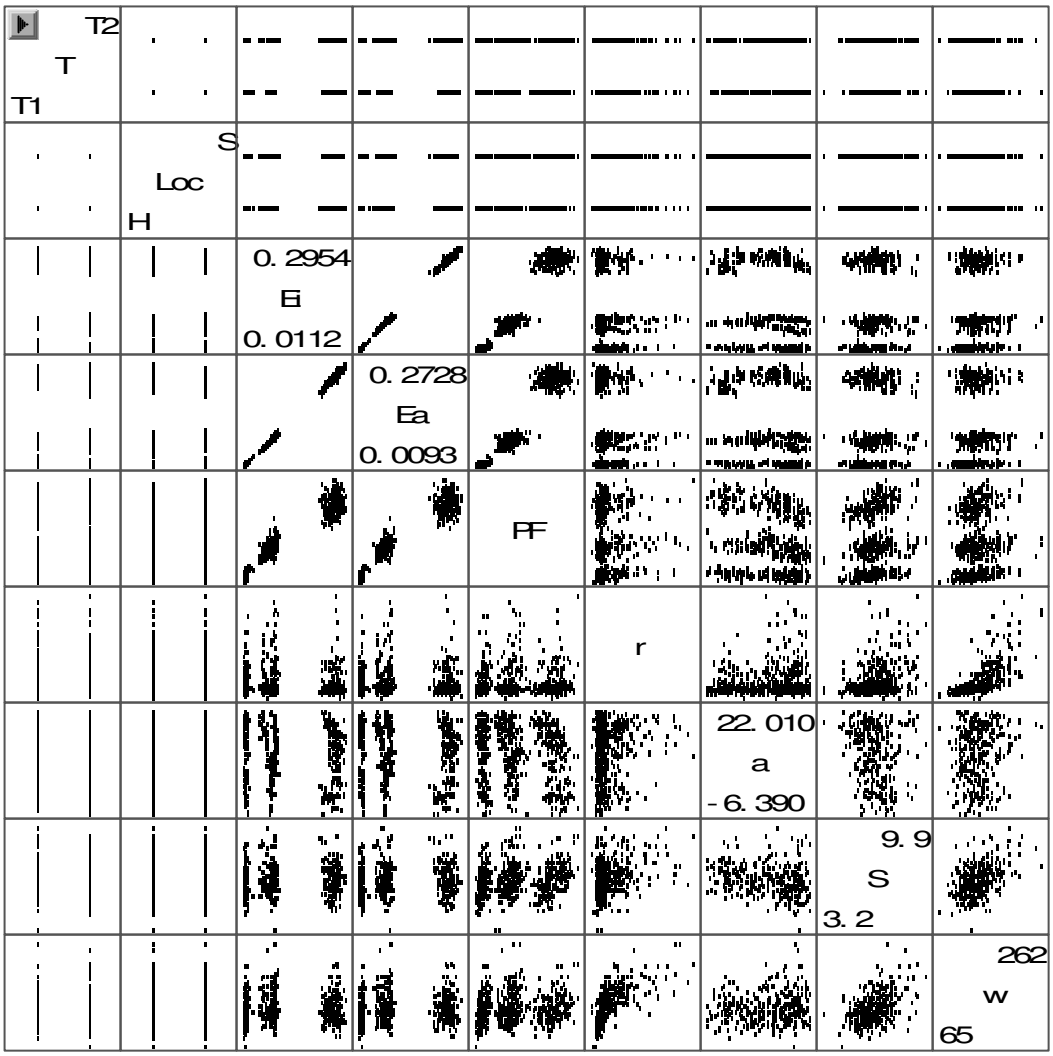

Figure 5-11. Overview of the different relations between independent/dependent variables in the experiment

Ea: Absorbed energy [J]; *T:* Temperature [°C]; *Loc*: Location of impact (compartment of partition); *Ei*: Impact energy [J]; *PF*: Peak force [N]; *r*: Radius of curvature at the location of impact [mm]; *a*: Colorimetric parameter a [-]; *S*: Acoustic stiffness [$Hz^2.kg^{2/3}$]; *w*: Weight [g]

5.3.3.1 Models with absorbed energy as dependent and peak contact force as independent variable

The significant main effects and interactions (up to three factorial level) between all variables (peak contact force, temperature, acoustic stiffness, colorimetric parameter, radius of curvature and mass) were analyzed on the 95 % significance level. Since colorimetric coordinate a^* and acoustic stiffness S are both an indication for the ripeness of tomatoes separate models were made with S and a^* as parameter for ripeness.

Using the backward stepwise (step-down) procedure, different linear and nonlinear statistical models were analyzed. Different linear combinations of second and first order terms were

analyzed. All variables were significant (P<0.05), except for the mass. The following most relevant models were identified (P<0.0001):

Treatment regression equations for the model with parameter *a* as indicator for ripeness

$$E_a(T_1) = -0.025387247 + 0.005161998 PF - 0.000337402 4a - 0.001364896 0r + 0.000042697 1 PF \times a$$
$$E_a(T_2) = -0.021957918 1 + 0.004765251 5 PF - 0.000337402 4a - 0.001364896 0r + 0.000042697 1 PF \times a$$
(5.13)

$R^2 = 0.947$

with E_a absorbed energy [J]

$T_{1/2}$ tomato temperature; T_1 is 15 °C and 20°C

PF peak contact force [N]

a colorimetric coordinate [-]

r tomato radius of curvature at place of impact [mm]

In Figure 5-12 the predicted absorbed energy - measured absorbed energy plot is depicted for this model.

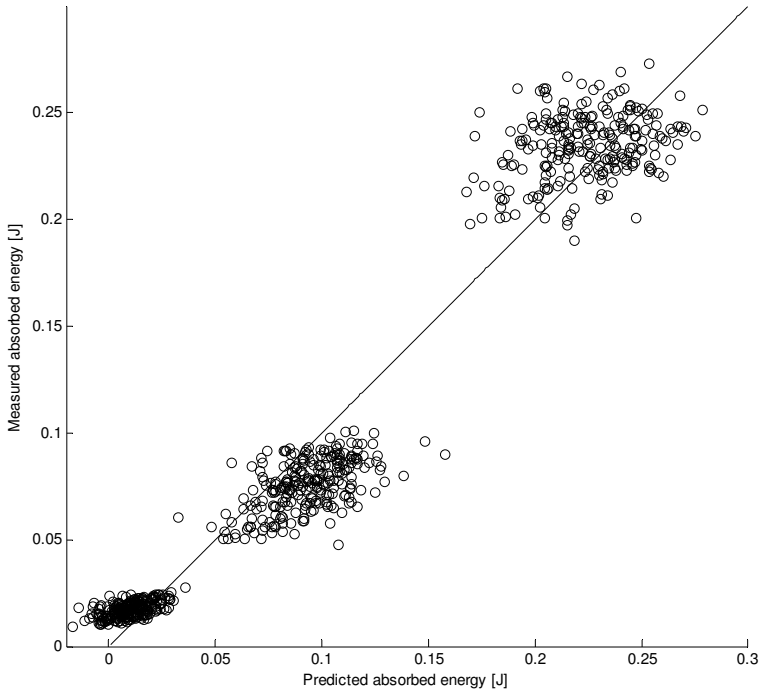

Figure 5-12. Model 5.13: Predicted value (p) – measured value (Ea) plot of the absorbed energy [J].

Treatment regression equations for the model with parameter *S* as indicator for ripeness

$$E_a(T_1) = -0.037639689 + 0.006574217PF - 0.0028789403S - 0.00050454821r - 0.000159254PF \times S$$
$$E_a(T_2) = -0.0317045639 + 0.0060022073PF - 0.0028789403S - 0.0005045482r - 0.0001592541PF \times S$$
(5.14)

$R^2 = 0.945$

with S acoustic stiffness [$Hz^2.kg^{2/3}$]

In Figure 5-13 the predicted absorbed energy - measured absorbed energy plot is presented for this model.

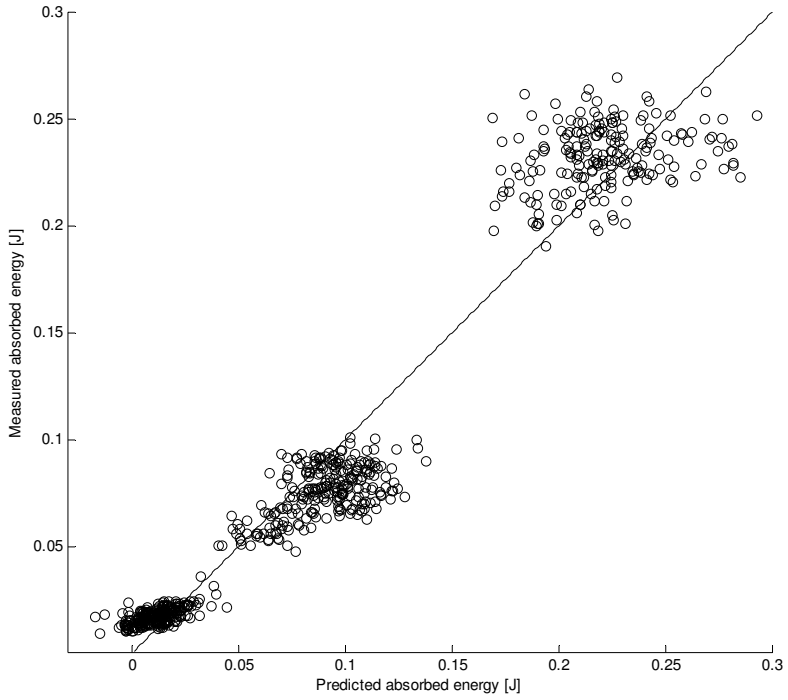

Figure 5-13. Model 5.14: Predicted value (p) – measured value (Ea) plot of the absorbed energy [J].

In Table 5-7 the extra sum of squares of the remaining independent variables are given when the peak contact force is already in the model.

Table 5-7. Extra sum of squares for the remaining independent variables when the peak contact force is already included in the model

Type I Extra sum of squares	*Absolute number*	$\left[SSR(X_2, X_2 \times X_1 \middle| X_1)/SSE(X_1)\right]*100$
$SSR(S, S \times PF \middle| PF)$	0.08	19.4
$SSR(a, a \times PF \middle| PF)$	0.07	15.6
$SSR(T, T \times PF \middle| PF)$	0.04	8.4
$SSR(r, r \times PF \middle| PF)$	0.02	4.6
$SSR(side, side \times PF \middle| PF)$	0.0008	0.2

The third column indicates the coefficient of partial determination multiplied by 100. It indicates with how many percent the error sum of squares when only X_1 is in the model is further reduced when $X_2, X_2 \times X_1$ are added to the model

By far the most important factor in predicting the absorbed energy is the peak contact force. This can be seen from the low coefficients of partial determination of all the other independent variables if the peak contact force is already included in the model (Table 5-7). According to Table 5.4 the following classification of their importance in explaining the overall variance in the absorbed energy can be made:

1. Acoustic stiffness
2. Colorimetric parameter $a*$
3. Tomato temperature
4. Radius of curvature at the location of impact
5. Side of the tomato (compartment/partition)

A sensitivity analysis was performed to obtain a more detailed understanding of the effect of the different independent variables on the absorbed energy. The results of this analysis are presented below.

Effect of tomato ripeness on absorbed energy

Both indicators of ripeness ($a*$ and S) indicate that energy absorption increases with ripeness. The interaction term between ripeness and peak contact force indicates that the difference in absolute value of the absorbed energy between ripe and unripe tomatoes increases with peak impact force. However, the relative difference decreases with increasing peak contact force. For the extremes in ripeness (upper and lower boundary of standard deviation, 5.5 and 7.5 $Hz^2.kg^{2/3}$ for acoustic stiffness, 3.21 and 18.17 for colorimetric coordinate $a*$) the difference in absorbed energy for unripe compared to ripe tomatoes goes from 40% for low impacts to 12 % for high impacts. These results are in agreement with the literature. Sargent *et al.* (1989)

and Sargent *et al.* (1992b) found that tomatoes are significantly less bruised in the mature green stage compared to the breaker stage (first appearance of external pink colour).
The effect of ripeness on bruise susceptibility is the opposite of the effect for Jonagold apples. Based on the findings in literature about apples, most likely the explanation for the effect is the decrease in tomato firmness with increasing ripeness. The positive correlation between firmness and acoustic stiffness (Duprat *et al.,* 1997) indicates that the firmness of the tomatoes was decreasing with increasing ripeness.
An apparent contradiction of the effect acoustic stiffness can be noted between (Jonagold) apples and tomatoes. In contrast to tomatoes, higher acoustic stiffness leads to more bruise damage for apples. As explanation was stated that higher acoustic stiffness leads to higher peak stress during impact. Also, for tomatoes this is the case. Higher tomato acoustic stiffness leads to a significantly higher peak contact force (peak stress) when impacted with the same impact energy. In our view the explanation lays in the difference in tomato firmness. Although a higher peak stress for stiffer unripe tomatoes is present, it doesn't lead to more bruise damage because the failure stress is also higher for the unripe tomatoes.

Effect of tomato temperature on absorbed energy

Tomatoes at room temperature absorb less energy than tomatoes at 15 °C. Although in absolute value the difference in absorbed energy between tomatoes at 15°C and room temperature increases with increasing peak contact force, in relative value the difference goes from 25 % for low impacts (15 N) to 12 % for high impacts (60 N). In literature no information about the effect of tomato temperature on bruise susceptibility is available. Probably, the same explanation for the effect of tomato temperature on absorbed energy can be stated as for the effect of tomato ripeness: the higher firmness of tomatoes of 20 °C leads to lower absorbed energy. Unexpectedly, it has been statistically indicated that tomatoes of 20 °C were stiffer than tomatoes of 15 °C (data not shown).

Effect of radius of curvature on absorbed energy

No interaction term between radius of curvature and peak contact force was present. This means a fixed effect of the radius of curvature on the absolute value of the absorbed energy. Tomatoes with small radius of curvature absorb more energy compared to a tomato with larger radius of curvature (at location of impact). The difference in relative terms for the extremes in tomato radius of curvature in the experiment (29.7 and 38.3 mm) is much higher for low impacts (136 %, 15 N), it decreases rapidly to barely 5 % for high impacts (60 N).

No data was found in literature about the effect of tomato radius of curvature on bruise susceptibility. An explanation of the effect of radius of curvature on absorbed energy could be that the higher peak contact stress for tomatoes with smaller radius of curvature is more important than the lower contact area during impact.

Effect of location of impact (compartment/partition) on absorbed energy

No significant effect of location of impact on absorbed energy could be demonstrated.
However for the statistical model including the impact energy (see section 5.3.3.2) a difference in absorbed energy between compartment and partition was identified. Probably the reason no effect of location of impact for the statistical model including the peak contact was identified, is the strong influence of location of impact on the peak contact force itself. After all, a statistical higher peak contact force was noted for the tomato partition compared to compartment. This is in agreement with the different contact force parameters for partition and compartment of the tomatoes (Chapter 3).

5.3.3.2 Models with absorbed energy as dependent and impact energy as independent variable

The significant main effects and interactions (up to three factorial level) between all variables (impact energy, temperature, acoustic stiffness, radius of curvature and mass) were analyzed on the 95 % significance level. Since colorimetric coordinate a^* and acoustic stiffness S are both an indication for the ripeness of tomatoes separate models were made with S and a^* as parameter for ripeness.
Using the backward stepwise (step-down) procedure, different linear and nonlinear statistical models were analyzed. Different linear combinations of second and first order terms were analyzed. The following most relevant models were identified ($P<0.0001$):

Treatment regression equations for the model with parameter *S* as indicator for ripeness

$$Ea_{T1/C} = -2.326*10^{-3} + 0.909Ei - 0.000263S + 5.76*10^{-5} r$$
$$Ea_{T1/P} = -1,455*10^{-3} + 0.909Ei - 0.000263S + 5.76*10^{-5} r$$
$$Ea_{T2/C} = 1.954*10^{-3} + 0.900Ei - 0.000263S - 6.74*10^{-5} r$$
$$Ea_{T2/P} = 2.824*10^{-3} + 0.900Ei - 0.000263S - 6.74*10^{-5} r$$

(5.15)

$$R^2 = 0.998$$

with E_a absorbed energy [J]

$T_{1/2}$ tomato temperature; T_1 is 15 °C and T_2 is room temperature [°C]

C and P are respectively indicating the compartment and partition of the tomato

Ei impact energy [J]

S acoustic stiffness [$Hz^2.kg^{2/3}$]

r tomato radius of curvature at place of impact [mm]

In Figure 5-14 the predicted absorbed energy - measured absorbed energy plot is given for this model.

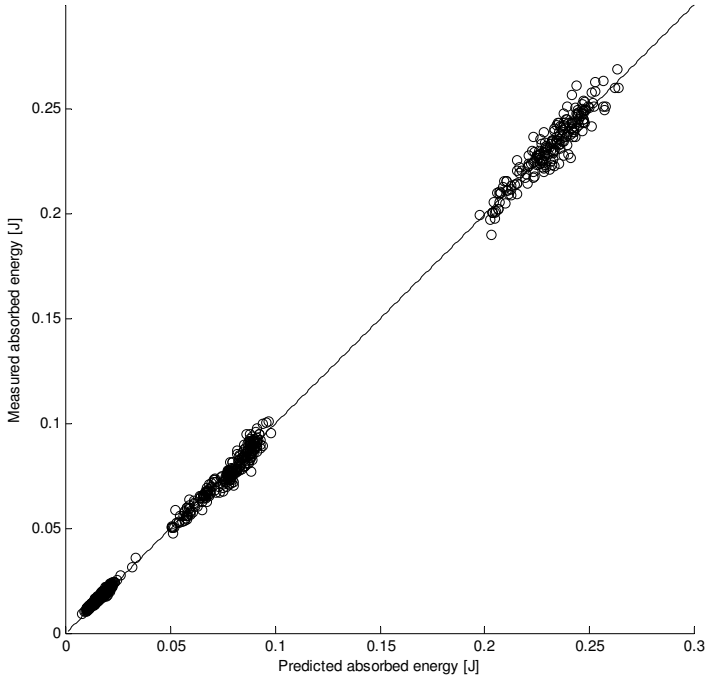

Figure 5-14. Model 5.15: Predicted value (p) – measured value (Ea) plot of the absorbed energy [J].

Treatment regression equations for the model with parameter *a* as indicator for ripeness

$$Ea_{T1/C} = -4.878*10^{-3} + 0.922Ei - 0.00000924a + 9.17*10^{-5}r + 0.00103Ei \times a - 0.000775Ei \times r$$
$$Ea_{T1/P} = -4.148*10^{-3} + 0.922Ei - 0.00000924a + 9.17 \times 10^{-5}r + 0.00103Ei \times a - 0.000775Ei \times r$$
$$Ea_{T2/C} = -6.64*10^{-4} + 0.922Ei - 0.00000924a - 4.83 \times 10^{-5}r + 0.00103Ei \times a - 0.000775Ei \times r$$
$$Ea_{T2/P} = 6.399*10^{-5} + 0.922Ei - 0.00000924a - 4.83 \times 10^{-5}r + 0.00103Ei \times a - 0.000775Ei \times r$$
(5.16)

$$R^2 = 0.999$$

with a colorimetric coordinate [-]

In Figure 5-15 the predicted absorbed energy - measured absorbed energy plot is depicted for this model.

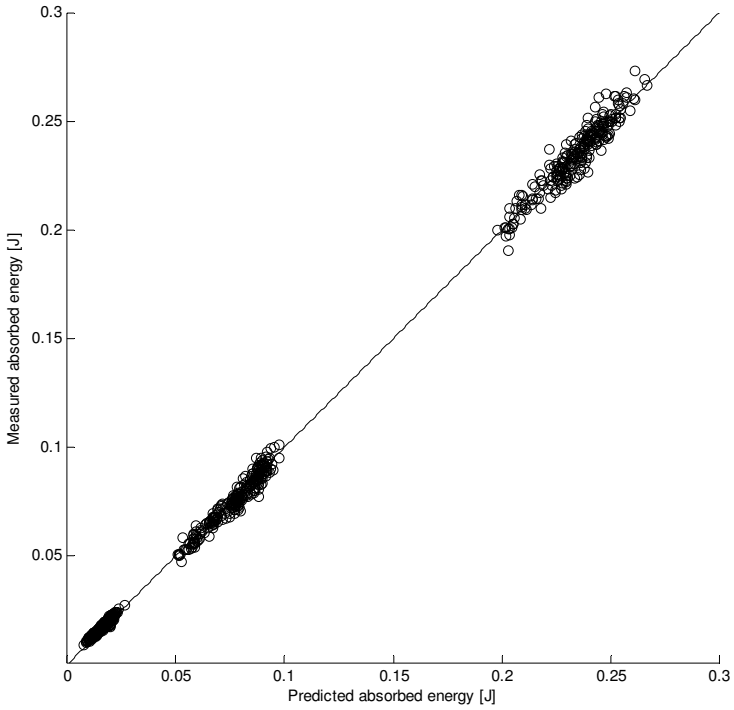

Figure 5-15. Model 5.16: Predicted value (p) – measured value (Ea) plot of the absorbed energy [J].

In Table 5-8 the extra sum of squares of the remaining independent variables are given when the impact energy is already in the model.

Table 5-8. Extra sum of squares for the remaining independent variables when the impact energy is already included in the model

Type I Extra sum of squares	*Absolute number*	$\left[SSR(X_2, X_2 \times X_1 \mid X_1) / SSE(X_1)\right]*100$
$SSR(a, a \times Ei \mid Ei)$	$9.6*10^{-4}$	9.6
$SSR(S, S \times Ei \mid Ei)$	$2.1*10^{-4}$	2.4
$SSR(T, T \times Ei \mid Ei)$	$2.0*10^{-4}$	1.9
$SSR(r, r \times Ei \mid Ei)$	$1.2*10^{-4}$	1.2
$SSR(side, side \times Ei \mid Ei)$	$7.3*10^{-5}$	0.8

The third column indicates the coefficient of partial determination multiplied by 100. It indicates with how many percent the error sum of squares when only X_1 is in the model is further reduced when $X_2, X_2 \times X_1$ are added to the model

By far the most important factor in predicting the absorbed energy is the impact energy. This can be seen from the low coefficients of partial determination of all the other independent variables if the impact energy is already included in the model (Table 5-8).
Nevertheless, a significant effect of all fruit properties was identified. According to Table 5.4 the following classification of their importance in explaining the overall variance in the absorbed energy can be made:

1. Colorimetric parameter $a*$
2. Acoustic stiffness
3. Tomato temperature
4. Radius of curvature at the location of impact
5. Side of the tomato (compartment/partition)

A sensitivity analysis was performed to obtain a more detailed understanding of the effect of the different independent variables on the absorbed energy. The results of this analysis are presented below.

Effect of tomato ripeness on absorbed energy

The same conclusion can be drawn as for the model including the peak contact force as independent variable. Ripe tomatoes absorb more energy than unripe tomatoes. However, the difference is much smaller compared to the model including the peak force. The maximum difference in absorbed energy between the ripeness extremes in the measurement (upper and

lower boundary of standard deviation of a^* and S, 5.5 and 7.5 $Hz^2.kg^{2/3}$ for acoustic stiffness S, 3.21 and 18.17 for colorimetric coordinate a^*) is barely 1.5 %.
This large difference between the models with the peak contact force as independent variable and the models with the impact energy as independent variable is due to the fact that the peak contact force itself is influenced by ripeness. A significant negative correlation between peak contact force and ripeness was noticed for the tomatoes in the experiment (data not shown).

Effect of tomato temperature on absorbed energy

The same conclusion can be drawn as for the model including the peak contact force as independent variable. Tomatoes at 15 °C absorb more energy than tomatoes at 20 °C. However, the difference is much smaller compared to the model including the peak contact force. The maximum difference is barely 1%. This large difference between both models is due to the contact force itself that is influenced by temperature. Unexpected, the peak contact force of tomatoes at 20 °C was significantly higher compared to tomatoes at 15 °C (data not shown).

Effect of tomato radius of curvature on absorbed energy

An interaction term between radius of curvature and temperature was noticed. For tomatoes at room temperature, at all impact levels, tomatoes with low radius of curvature absorb more energy than tomatoes with higher radius. This is in agreement with the model including the peak contact force. Although, the effect of contact radius is very small: the difference in absorbed energy between the extremes in the measurement (upper and lower boundary of radius of curvature standard deviation, 29.7 and 38.3 mm) is at maximum 1 %. For tomatoes at 15°C, the opposite effect was noticed: less energy absorption for lower radius of curvature. Once again, this effect is very small: even for the extremes in radius of curvature at maximum 2 %. Probably the opposite effect of radius of curvature for tomatoes of 15°C and 20 °C is due to their difference in acoustic stiffness (for tomatoes the positive correlation with firmness is important). Tomatoes of 20 °C have higher firmness (failure stress) and therefore the small radius of curvature give rise to higher peak stresses necessary to overcome the high failure stress. Tomatoes of 15 °C have a lower failure stress, with the consequence that the higher contact area of tomatoes with higher radius of curvature (see Hertz theory) becomes more important than the lower peak stress compared to tomatoes of lower radius of curvature (see Hertz theory).

Effect of location of impact (compartment/partition) on absorbed energy

Unlike the models including the peak contact force as independent variable, it was observed that the partition of a tomato absorbs significantly more energy compared to the compartment. The effect decreases from 4 % for low impacts (0.03 J ≅ 15N) to 0.5 % for high impacts (0.23 J ≅ 60 N).

This difference between models including peak contact force and impact energy as independent variable is due to the fact that the peak contact force itself is influenced by the location of impact. It was demonstrated that the peak contact force was significantly higher for partition compared to compartment when impacted by the same impact energy (data not shown). This is also in agreement with the different contact force model parameters between tomato partition and compartment (Chapter 3).

In the literature no data was found about differences in bruise susceptibility between compartment and partition of tomatoes.

5.3.4 Conclusions

The effect of the tomato fruit properties on the absorbed energy can be summarized in a simplified form in the following table:

Table 5-9. Simplified summary of effect for tomato parameters on absorbed energy

Factor	
Ripeness (determined by acoustic stiffness and colour)	Absorbed energy increases with increasing ripeness of tomato.
Location of impact	A tomato partition absorbs more energy than the compartment of the tomato
Radius of curvature[33]	15°C: r↑ → absorbed energy ↑ 20°C: r↑ → absorbed energy ↓
Temperature	Tomatoes at 20 °C absorb less energy compared to tomatoes at 15 °C

[33] Conclusions are valid for models including the impact energy. For models including peak contact force r↑ → absorbed energy ↓ for both temperatures.

5.4 Relation between bruising of Jonagold apples and packaging materials

5.4.1 Introduction

One of the basic roles of packaging is to protect the products from damage during handling and transportation and generally in the process chain between harvesting and reaching the end-consumer.

Therefore, one of the parameters under study in this work was the effectiveness of packaging materials. To predict performance, i.e. bruise protection, of packages, it is necessary to understand and quantify the effect of these factors in bruising. Package design can then proceed to minimize bruising and the performance of packages can be predicted before they enter the system. (Holt *et al*, 1981)

Regression models were constructed with both the impact energy and the peak contact force as independent variable. The impact energy as independent variable is most useful to make a classification of the packaging material in its effectiveness of diminishing the bruise development. The peak contact force as independent variable is most useful in combination with DEM, as described before. The impact time was analyzed in combination with the peak contact force; because it is known from literature it is also an important factor in determining the bruise damage (Chen en Yazdani, 1991). A regression equation with besides the peak contact force also the impact time as independent variable could be used to predict damage between apples and materials with different mechanical properties (stiffness and damping). The only condition is that the peak contact force and impact time have to be known. For DEM this information is captured in normal contact force model (Chapter 2 and 3)[34].

5.4.2 Materials and methods

5.4.2.1 Material

The effectiveness of different packaging materials used in the Belgium market for diminishing apple bruising was tested. The packaging materials that were tested are given below:

[34] The parameters of the contact force model for the different packaging materials were determined, but were not presented in Chapter 3 for two reasons. First of all, the method is not different from the one already presented in Chapter 3 for apples and tomatoes. Secondly, no DEM simulations with packaging materials could be done because of lack of time.

Table 5-10. Overview of the different packaging materials used in the experiment.

Type of packaging material	
Small packaging	Foam dish Carton dish
Standard packaging	Rippled pack paper Multilayer paper pack sheet

Pack sheets are sheets with pre-shaped holes (alveoli). The sheets exist in different number of holes, depending on diameter class of the apples being packed. Two types of pack sheets are used in Belgium: plastic- and multilayer paper pack sheets. Plastic pack sheets are always used in combination with rippled pack paper, because the damping characteristics of the plastic pack sheets are very low. Rippled pack paper is rippled paper without holes, used to absorb energy. Multilayer paper pack sheets have higher damping characteristics and are not used in combination with the rippled pack paper. The use of plastic pack sheets in combination with the rippled paper is drastically diminishing on the Belgian market in favor of the use of the multilayer paper pack sheet (VCBT, personal communication). The driving motivation for this is the lower environmental load of the multilayer paper pack sheets.
The Jonagold apples for this research were obtained from the 'Fruitteeltcentrum K.U. Leuven' in Rillaar. They were harvested on the same day in October 2002 and stored for 3.5 months in CA storage conditions (2.5 % CO_2; 1% O_2; 0.8 °C).

5.4.2.2 Methods

The pendulum device (Chapter 3) was utilized. Halves of an apple were mounted on the pendulum device and impacted with a round flat metal impactor (∅ 25 mm). A sample of ∅ 25 mm from the different packaging materials was glued on the metal flat impactor. The glue was only applied on the edges of the packaging sample to diminish interference of the damping properties of the glue.
The impact parameters logged to the computer were the impact energy, peak contact force and impact time. The bruise volumes were measured 24-72 hours later using the method described by Chen and Sun (1981).
Five impact energy levels were applied. The lowest impact energy class was at the edge of bruise measurability. The highest impact class was above the maximum damage class that was measured in Belgium (Van linden, unpublished). Besides the four different packaging materials being tested also the metal plate impact was taken as reference.

In total 30 apples were used for each (packaging) material. Because both halves of the apples were impacted, 60 impacts for each material were obtained. In total 5x30=150 apples were analyzed in this experiment.

5.4.2.3 Statistical analysis

The data were processed with the statistical software package SAS (SAS version 8.2, The SAS Institute Inc., Cary, NC, U.S.A.). A multiple linear or nonlinear regression model was setup (proc GLM or proc NLIN). A Gauss-Newton optimisation routine was applied and the coefficient of determination was calculated as: $1-\frac{SSE}{SSTO}$.

5.4.3 Results and discussion

5.4.3.1 Impact energy level

As far as known, only linear statistical models have been applied in literature to describe the relation between impact energy and bruise volume. However, such linear statistical models led to inferior data fitting results for all packaging materials. Besides linear models different nonlinear models were tested. It was concluded that the sigmoid function described most accurately the impact energy-bruise volume relationship. For the packaging materials the model improved considerably compared to the linear model. In case of the metal plate reference measurement, the model improvement was limited (R^2=0.866 compared to R^2=0.883 for the linear model).

The equation of the sigmoid function is given here:

$$BV = \frac{A}{1 + Be^{-CE_i}} \qquad (5.17)$$

with BV bruise volume [mm^3]

E_i, impact energy [J]

A, B and C parameters of the sigmoid function

Parameter *A* stands for the value of the upper asymptote of the sigmoid function, parameter *B* is a measure for the shift of the curve to the positive direction of the X-axis and parameter *C* is a measure for the slope of the sigmoid function.

The results of the nonlinear least squares parameter estimation using the Gausss-Newton optimisation method are presented in Table 5-11. In Figure 5-16 the sigmoid functions for the five tested materials are depicted.

Table 5-11. Overview of the estimation of the different parameters of the sigmoid curves of the different packaging materials

	Foam dish	*Carton dish*	*Ripple paper*	*Metal plate*	*Multilayer paper*
A	3911	5055	5056	6641	4377
B	1157	32.03	50.99	28.67	56.14
C	24.17	11.43	12.08	9.77	14.67
R^2	0.936	0.918	0.846	0.883	0.914

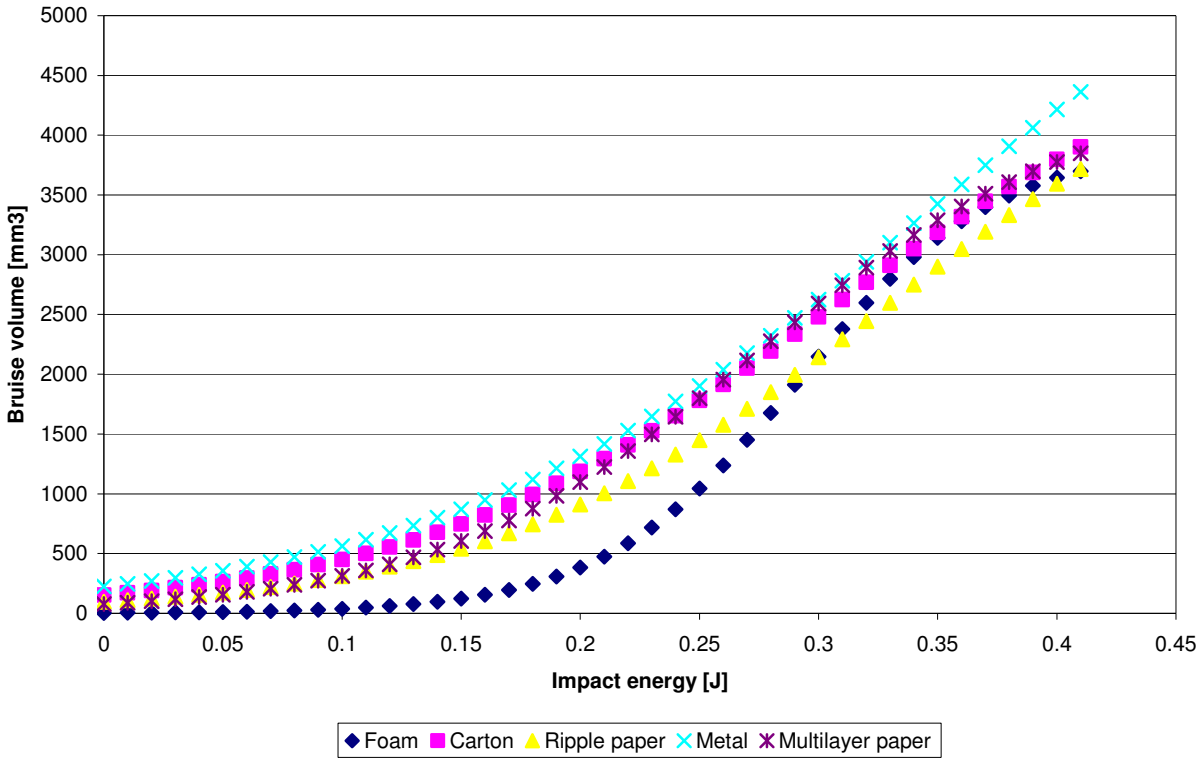

Figure 5-16. Plot of the sigmoid curves of the different packaging materials for the models including the impact energy.

In Figure 5-16, no threshold impact energy is noted, in contrast to linear models. In linear models the bruise volume becomes negative for low impact energies, indicating the absence of bruise damage. However, using these sigmoid models, even for impact energy of 0 J, some bruise damage was calculated. This can be seen as a drawback of these models. However, bruise volumes less than ≅ 100 mm^3 can be considered as theoretical bruise volumes, because they are not visible from the outsight and are difficult to measure (depth). However, for metal plate impact and carton dish impact the estimation of the bruise volumes for lowest impact energies is above the theoretical level of 100 mm^3. In addition, the model

showed a considerable overestimation of the bruise volumes for low impact energies for metal plate and carton dish. For DEM applications a solution for these artifacts is to set the bruise volume artificially on 0 mm^3 for impacts below the bruise threshold, obtained from linear models.

Some interesting practical conclusions can be drawn from Figure 5-16. A high difference between foam and carton dishes was noticed for their efficiency to diminish bruise damage with respect to low and average impacts. For high impacts this difference diminishes drastically. Most likely, the explanation therefore is that the damping efficiency decreases with increasing deformation of the foam. Statistically ($P<0.05$) only a difference in parameter *C* (slope) of the sigmoid curve between foam and carton could be demonstrated (data not shown).
For the standard packaging it was noticed that the rippled pack paper gave rise to less bruise than the multilayer paper pack sheets for higher impact only (>0.2 J). As a consequence the use of the more costly rippled pack paper is only justified for more roughly handled fruit. However, statistically on the 95 % significance level no difference between both types of packaging material could be demonstrated for all three parameters of the sigmoid curve (data not shown).

5.4.3.2 Peak contact force level

Also a sigmoid relation between bruise volume and peak contact force was identified. The results are given in Table 5-12 and Figure 5-17.

Table 5-12. Overview of the estimation of the different parameters of the sigmoid curves of the different packaging materials

	Foam dish	*Carton dish*	*Ripple paper*	*Metal plate*	*Multilayer paper*
A	4080	6078	4898	5471	4260
B	3936	61.6	140.2	71.2	260.8
C	0.0539	0.0229	0.0279	0.0237	0.0354
R^2	0.935	0.864	0.794	0.864	0.915

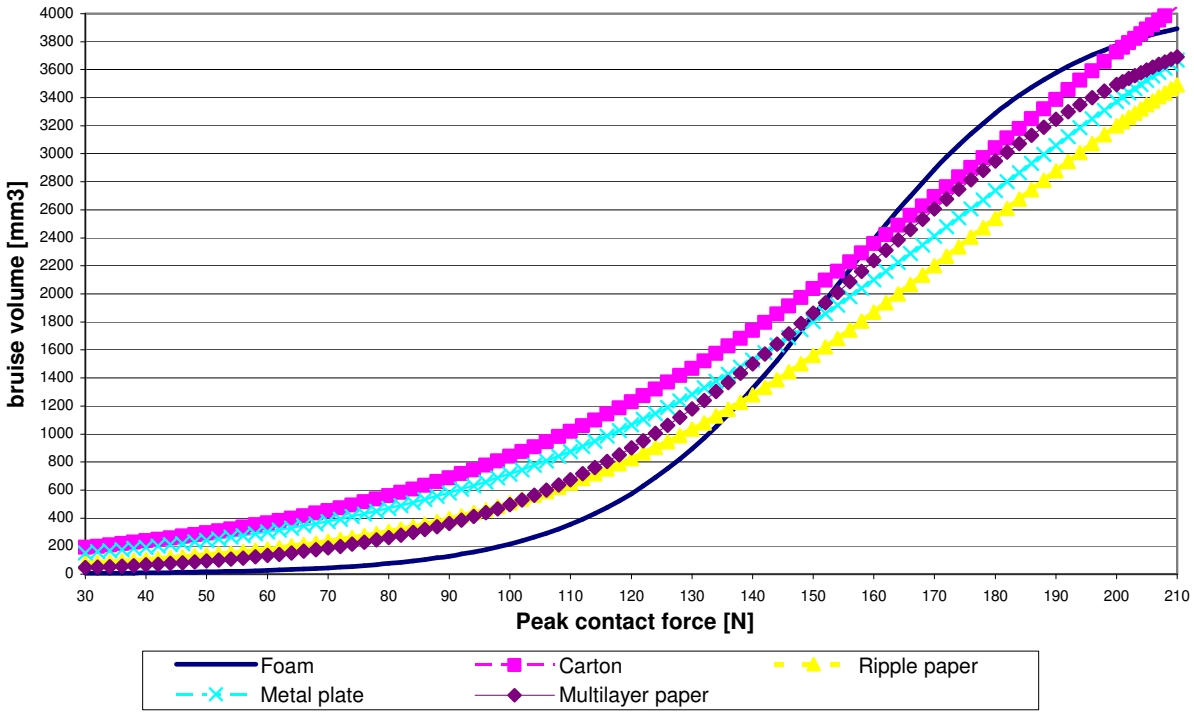

Figure 5-17. Plot of the sigmoid curves of the different packaging materials for models including the peak contact force

Two substantial differences with Figure 5-16 can be noted: 1) the sigmoid curve of the carton lies above the curve of the metal and 2) the curve for the foam for high peak forces is situated above all other curves. However, this may not lead to the wrong conclusion that carton give rise to more bruise damage than metal and foam give rise to more bruise damage than all other materials for higher impacts. The reason for the difference between Figure 5-16 and 5-17 is that the peak contact force is lower for carton (compared to metal) and for foam (compared to all other materials) at a given impact energy. Moreover, peak contact force is not the only parameter determining bruise damage. Also impact time is an important factor. Shorter apple impacts cause more bruise damage than longer impacts at the same peak contact force (Chen en Yazdani, 1991).

However, the fact that for peak contact forces starting from 160 N the curve of the foam lays above all other curves is a model artifact. It is not observed in the data point plot.

Based on this knowledge, a statistical model was made with the independent variables peak contact force and impact time. In this model no distinction was made between packaging materials and all the data was pooled. The model with the highest coefficient of determination is given below. In this model the effect of time was linearly added to factor B (shift to the right) of the sigmoid equation:

$$BV = \frac{3366}{1+(18.9+4.323t-0.0344t\times PF)e^{-0.0172PF}} \quad (5.18)$$

$R^2 = 0.867$

with *PF* peak force [N]

t time [s]

In figure 5-18 the fit of predicted bruise volume compared to measured bruise volume is presented.

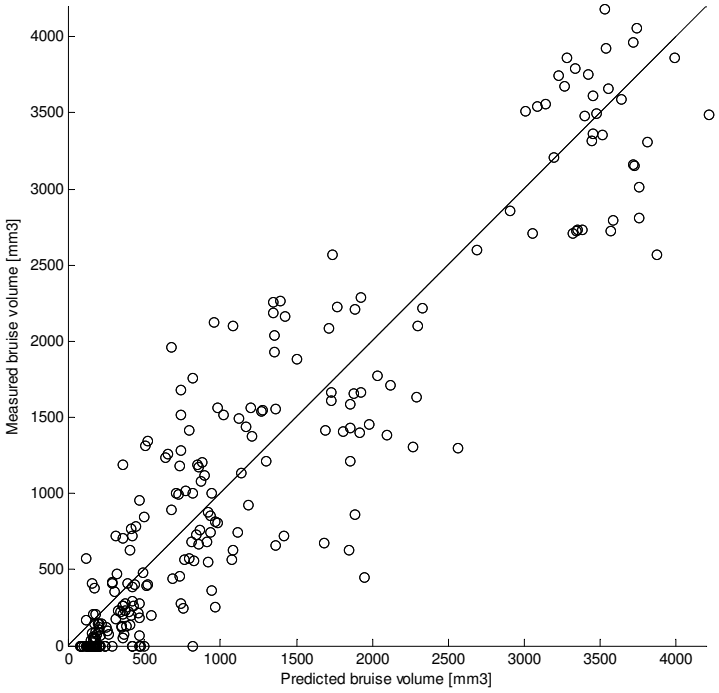

Figure 5-18. Model 5.18: Predicted value (p) – measured value (BV) plot of the bruise volume [mm^3].

In Table 5-13 this model is compared to other statistical models with lower coefficient of determination.

Table 5-13. Overview of other statistical models than model 5.18.

Model	*Model equation*	R^2
Time linear added to sigmoid model	$BV = \frac{2056}{1+216423e^{-0.0723PF}} - 57.24t + 1.3891t\times PF$	0.863
Sigmoid model with only peak force	$BV = \frac{4919}{1+145e^{-0.0296PF}}$	0.850
Linear model with peak force and time	$BV = -2128 + 22.5PF + 95.5t$	0.796
Linear model with only peak force	$BV = -1230 + 21.7PF$	0.789

Although a negative correlation existed between impact time and bruise damage ($r_{t,BV} = -0.22$) there can be noted a positive effect of impact time in the regression equations. This is due the negative correlation between impact time and peak contact force ($r_{t,PF} = -0.41$), leading to the effect of multicollinearity. The same was noted in the results of Chen and Yazdani (1991) and Timm *et al.* (1989). However, in the latter research linear regression equations were made with bruise diameter instead of bruise volume as dependent variable.

The research of Chen and Yazdani (1991) is the only research known from literature giving a relationship between bruise volume and peak contact force/impact time. In the research Golden Delicious apples were used and different thicknesses of a sponge cushion material were used to create the different impact times. A linear model with a coefficient of determination of 0.893 was obtained. However, in this model besides peak force and impact time three other independent variables were included. These parameters were 'maximum combined deformation of apple and cushioning material', 'combined absorbed energy' and 'maximum value of time rate of change of acceleration during an impact' (jerk, da/dt). In our model where only two compared to five independent variables were used, the coefficient of determination of 0.867 can be seen as a good result.

Caution has to be taken by using model (5.18) for the impact of Jonagold apples with a wide range of materials. A good procedure is to check the results experimentally. If the prediction of the bruise volume using equation (5.18) differs too much from the measured bruise volume, it is better to use a separate model for the impact pair being considered.

5.5 General conclusions

In this chapter bruise prediction models, essential for the applicability of DEM for the bruise damage problem, were outlined. Bruise prediction models relate the contact force during impact, as modelled by DEM trough the contact force models, with the real bruise damage. However the information in this chapter can also be seen as a contribution to the bruise damage problem apart from DEM. Besides bruise prediction models with the peak contact force as independent variable additional models were constructed with the impact energy as independent variable. Advantages and disadvantages of both models were discussed. Bruise prediction models were constructed for apple cultivar 'Jonagold' and tomato cultivar 'Tradiro'. The pendulum that was utilized has been described in Chapter 3. Multiple linear and nonlinear regression models were made to link 'fruit properties', like ripeness, acoustic stiffness, fruit temperature, radius of curvature, harvest date (only apples), location of impact (partition or compartment of tomato) with bruise damage. Bruise volume was taken as a

measure for apple bruising while absorbed energy was used as measure for bruising of tomatoes, since still no objective method is available to measure the bruise size of tomatoes.
Besides significant main effects also significant interactions between fruit properties were identified, that were not described in literature before. Mutual interactions between fruit properties (for example interaction between harvest date and stiffness for apples and interaction between radius of curvature and temperature for tomatoes) together with significant interactions between some fruit properties and the degree of bruising (measured by peak impact force or impact energy) were identified. Most of the effects of those fruit properties on bruise damage could be clarified by applying theoretical bruise models described in literature. A schematic overview of the effect of fruit properties on bruise damage is given in section 5.2.4 for the apples and section 5.3.4 for the tomatoes. Some of these findings could be reformulated to guidelines to reduce apple and tomato bruising in practice. In Chapter 7 the effect of these fruit properties on bruise damage is illustrated by means of simulations of apple and tomato transport.
An overview is given of the effect of the fruit properties on the bruise damage for apples and tomatoes. The overview that is presented here is the analysis with besides the fruit properties the impact energy as independent variable. It was argued that this analysis is to be preferred because in contrast to the peak contact force, impact energy is not influenced by the fruit properties.
For both apples and tomatoes it was identified that higher fruit *temperature* leads to more bruise damage. For apples the effect was most pronounced for high impacts: identical (heavy) mechanical treatment of apples at 1 °C gives 15 % more bruise damage than apples at 20 °C. Although a significant effect of temperature on tomato absorbed energy was identified, the difference between 15°C and 20 °C tomatoes was barely 1%.
An opposite effect of *acoustic stiffness* on bruise damage was identified for apples and tomatoes. Apples of acoustic stiffness of 35 $Hz^2.kg^{2/3}$ contract 166 mm^3, independent of impact level, more bruise damage during identical mechanical treatment than apples with acoustic stiffness of 28 $Hz^2.kg^{2/3}$. On the other hand, stiffer tomatoes absorb less energy. Nevertheless this effect is limited: tomatoes with acoustic stiffness of 7.5 $Hz^2.kg^{2/3}$ absorb 1.5 % less energy during identical mechanical treatment than tomatoes with an acoustic stiffness of 5.5 $Hz^2.kg^{2/3}$. For fresh harvested tomatoes, besides the stiffness also the color, measured by colorimetry, is an indication for tomato ripeness. The same effect of *tomato ripeness* on absorbed energy was identified when the acoustic stiffness or the colorimetric parameter a^*, indicating green/red color, was considered.
For apples the effect of the *radius of curvature* on the bruise damage depends on the level of impact: for small impacts smaller radius of curvature leads to more bruise damage, up to 50

% for the extremes in apple size : 32.5 mm and 45 mm radius of curvature. The opposite is true for high impact: up to 9 % less bruise damage for the extremes in apple size. For average impact levels no effect of the radius of curvature on the bruise damage was identified. For the tomatoes it was identified that the effect of radius of curvature depends on the temperature of the tomatoes. For tomatoes at 15°C, higher radius of curvature leads to more absorbed energy, the opposite is true for tomatoes at 20 °C. However the effect is small, for tomatoes at 15°C and 20°C for the extremes in size (radius of 29.7 mm and 38.3 mm) the effect is 1 and 2 % respectively.

For the effect of apple *harvest date* on bruise damage besides an interaction with the impact level also an interaction with the acoustic stiffness was identified. For apples of average acoustic stiffness (31 $Hz^2.kg^{2/3}$) late harvest leads to 10 % reduction in the bruise damage compared to apples harvested on the optimal harvest date. For early harvested apples of average acoustic stiffness (beyond 0.05 J) there is up to 9 % more bruise damage in the case of high impacts. The opposite effect is true for low impacts, however in absolute number this effect is small.

Some results of the effect of fruit properties on the bruise damage for both apples and tomatoes were explained by theoretical bruise models described in literature.

In addition the effectiveness of packaging materials, as used on the Belgian market, in reducing apple bruise damage was investigated. A sigmoid statistical relation between peak contact force/impact energy and bruise damage was identified for the impact of apples with the packaging materials. One of the most practical findings was that the application of more costly and more environmentally charging ripple pack paper in combination with plastic pack sheets is only justified for fruit submitted to high impacts (‘rough handling’) because no difference was noted for low impacts.

Since the impact of the apples with the packaging materials created a wide range of impact durations, a statistical model was constructed with the peak contact force as well as the impact duration as independent variable. It is known from literature that short duration impacts create more bruise damage than long duration impacts for identical peak contact force. The statistical model that was developed could be used in DEM simulations to predict the bruise damage for the impact of Jonagold apples with a wide range of materials. The only condition is of course that the parameters of the contact force model for each impact pair are known. The parameters of the contact force model for the impact apple - packaging materials were identified, but were not included in this work because no DEM simulations of packaging materials were executed (Van Zeebroeck *et al.,* unpublished).

Chapter 6

Validation of the Discrete Element Method to predict bruise damage to fruit

6.1 Introduction

The overall objective of the thesis was the development of the Discrete Element Method (DEM) for the simulation of the impact damage during transport and handling of fruit. In the previous chapters the methodology to measure the mechanical parameters, both for the contact force model and the bruise model, are outlined. Once these mechanical parameters are known, realistic DEM simulations can be performed.

Validation of the Discrete Element Method (DEM) for its applicability in predicting fruit bruise damage is an important step in the outline of the thesis. It shows to which degree the simulations by the Discrete Element Method match reality. In this respect, the results of several experiments were compared with the simulation results. The overall objective of the application of DEM in this thesis is the prediction of fruit bruise damage. For that reason bruise damage was taken as validation parameter: measured bruise damage was compared with simulated bruise damage. Bruise damage as validation was preferred above the comparison of the individual particle (fruit) trajectory between experiment, filmed by hi-speed imagery, and DEM simulation. However, the latter method is more common in DEM validation experiments of non-biological materials (Venugopal and Rajamani, 2001; Sakaguchi *et al.,* 2001; Tanaka *et al.,* 2002; Mishra, 2003b).

The prediction by DEM simulation of the contracted bruise damage of an individual fruit (apple) is the overall result of the application of the Discrete Element software

DEMeter++3.1 incorporating the contact force models and bruise models. These models itself incorporate certain material parameters.

If can be shown that DEM can predict fruit bruise damage in an acceptable way, a powerful tool is ready to get insight in bruise development in practice. Several scenarios could be tested by computer simulations, without any practical work. Testing these scenarios by real experiments are possibly very time consuming, unpractical or both. Moreover, simulations can bring to light information that is very difficult to extract from real experiments. An illustration of the possibilities of the Discrete Element Method will be presented in the next chapter (Chapter 7, Application of the DEM: shaking box).
As experimental setup for the DEM validations a "shaking box" was selected, i.e. a certain amount of apples in bulk were shaken for a certain period of time using a well defined acceleration signal. The bruise damage of (real) apples was compared with the calculated bruise damage from DEM simulations with identical initial conditions (the same amount of apples, similar stacking, the same acceleration signal, etc).
The use of a shaking box as validation experiment has the following advantages:

- The initial conditions of the shaking box are easy to match between the experiment and the simulation (size of the box, the applied vibration signal, etc.)
- A lot of randomness is incorporated in the experimental setup, for example, the apples can be in contact with a certain number of other apples and can contract multiple impacts in time.

6.2 Materials and methods

The experimental work can be divided in three parts:

- An experiment to determine the normal contact force model parameters of the apples used in the different shaking box validation experiments. These contact force model parameters are an essential input for the DEM simulations.
- An experiment to determine the statistical bruise model of the apples used in the different shaking box validation experiments. The statistical bruise model is essential for the calculation of the bruise damage from the DEM simulations.
- The shaking box validation experiments itself.

For all three experimental setups together 380 'Jonagold' apples of uniform size (diameter between 75 and 80 mm) were utilized. The apples were obtained from the Belgian auction

"Veiling Haspengouw". All apples were picked in the same orchard and were stored under identical conditions (stored in CA for ± 2 months until the measurement and storage at 3°C, 85% RH during the two weeks measurement period in the lab). The acoustic stiffness of the apples was 28.3 ± 1.1 $Hz^2.kg^{2/3}$ (determined on 20 apples taken at random). A certain amount of apples, to be utilized in the different kind of experiments, was selected at random from the batch of 380 apples.
The parameters of the normal contact force models and the coefficients of the statistical bruise models were determined specifically for the apples used in the shaking box validation experiments because these parameters are strongly dependent on the physiological condition of the fruit (fruit ripeness, storage conditions, etc.)

6.2.1 Validation experiments: shaking box

310 apples were randomly selected from the batch of 380 apples. An electro-hydraulic shaker (Hostens *et al.,* 2000) has been used for the shaking box experiments. The apples were piled up in bulk in a Plexiglas® box with dimensions 45x45x50 cm^3 (see Figure 6-1). As validation signal a vertical sinusoidal vibration signal was selected. This was chosen for the following reasons:

- The application of more complicated signals (for example multisine signal in xyz-direction) has no added value for validation purposes
- The simple vertical sinusoidal signal is easy to match between the validation experiment and the simulation

A sinusoidal vibration signal with a frequency of 4 Hz was applied on the electro-hydraulic shaker. The frequency of 4 Hz has been identified by own research (Deli *et al.,* unpublished) and literature (Timm *et al.,* 1998) as most critical for the mechanical damage of apples transported in bulk.
The acceleration amplitudes applied in the validation experiments were 12.56 m/s^2 (1.28 g), 14.22 m/s^2 (1.45 g) and 14.52 m/s^2 (1.48 g). These acceleration levels are just above the maximum accelerations occurring under field conditions. In comparison, maximum acceleration peaks measured on hardwood bulk bins transported on a fork-lift tractor in an orchard (Fruitteeltcentrum, K.U. Leuven, Rillaar) were 11.77 m/s^2 (1.20 g) (Deli *et al.,* unpublished). Still, shocks during transport (potholes, rough dropping of bulk bin, etc) can create accelerations peaks much higher than 1.20 g (7 g and higher; Peleg and Hinga, 1986).

Previous experiments (electro-hydraulic shaker) have shown that sinusoidal accelerations below 10.79 m/s^2 (1.10 g) provoke hardly detectable bruising. For validation purposes, it was preferred to induce clearly detectable and precisely measurable bruising. The validations experiments are summarized in Table 6-1.

Table 6-1. Overview of the different validation experiments.

Signal	*Vertical acceleration amplitude [g]*	*Number of apples*	*Time [min]*	*Stacking*
Signal 1	1.48	144	30	Forced
Signal 2	1.45	25	10	Natural
Signal 3	1.45	57	10	Natural
Signal 4	1.28	83	10	Natural

The vertical acceleration amplitudes were measured by an accelerometer (Kistler 83-05A2M2, Kistler Instrumente AG, Winterthur, Switzerland) mounted on the platform[35]. The measured vertical acceleration amplitudes have been applied in the DEM simulations.

The stacking of the apples in the 2nd, 3rd and 4th validation experiment was totally random. The apples were stacked by laying the apples carefully on each other (to prevent premature bruising). In the first experiment, however, the apples were stacked in a structured way by putting layers of 36 apples in 6x6 configurations. These apples were numbered to know the exact initial location of the apple in the stack.

Apple bruise was measured 24-72 hours later. The bruises on the outside were detected (visual inspection) and afterwards the bruise depth and diameter (if possible, see further) were measured by cutting the apple.

[35] The vertical acceleration amplitude has been measured because of differences between the theoretical acceleration amplitude, the acceleration amplitude that was applied to the electro-hydraulic shaker, and the actual vertical acceleration amplitude of the platform of the electro-hydraulic shaker

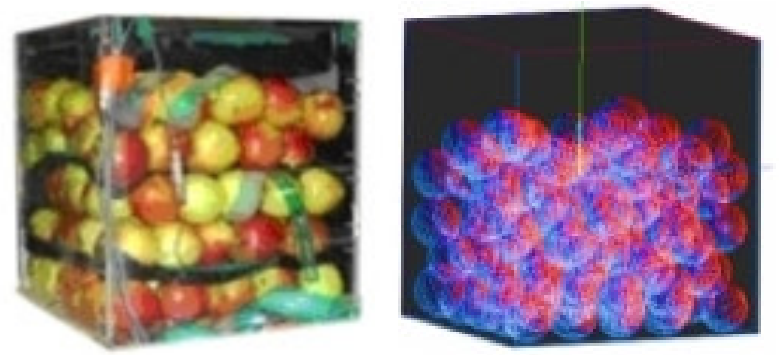

Figure 6-1. Photo of the Plexiglas® box used for the shaking box validation experiments (left) and the box of apples visualized by DEMeter++ (right)

6.2.2 Determination of the bruise model

Fifty "Jonagold" apples from the total batch of 380 apples have been utilized in the experiment. The red and green half of an apple was impacted, using the pendulum device (Chapter 3). The same experimental setup as described in Chapter 5 was applied. Five impact energy levels have been considered in the experiment, from impacts causing barely detectable bruising until impacts provoking clear bruising.

Unlike the bruise models of Chapter 5, besides bruise models with bruise volume as dependent variable, also models with bruise surface, bruise diameter and bruise depth as dependent variable were developed. The reason is that bruise volume as measure to express bruising is only applied in the academic world, but not in practice. In practice, bruise surface is used because this is the only parameter detectable by grading machines and customers. In addition, "the United States Standards for Grades of Apples" (USA, Department of Agriculture, 2002) only specify maximum bruise diameter or maximum bruise depth as parameters for apple grading.

The equation to calculate the bruise volume has been given before (equation 5.1 in Chapter 5). To calculate the bruise surface the following equation was used (Barreiro, 2004):

$$BS = \pi \frac{D}{2} d \qquad (6.1)$$

with BS bruise surface [mm^2]
D bruise diameter [mm]
d bruise depth [mm]

The data was analyzed by the General Linear Model procedure (Proc GLM) in SAS (SAS version 8.2, The SAS Institute Inc., Cary, NC, U.SA).

6.2.3 Determination of the normal contact force model parameters

Twenty apples were randomly selected from the batch of 380 apples to determine the normal contact force model parameters. In section 3.5.2 of Chapter 3, the experimental procedure to determine the normal contact force model parameters of the apples was described.

6.2.4 Computer simulations

For the validation simulations and the shaking box application (Chapter 7) a specific program was written using the C++ library DEMeter++3.1. The compiled program is only 1.6 Megabytes (MB) in size and the initial conditions and other simulation parameters can be defined by a simple text file (*.txt).
In the text file, the following initial conditions can be specified:

1. Number of particles (= apples or tomatoes).
2. The radius of the particles: uniform random distribution between a minimum and maximum value, or individually specified
3. The density of the particles. 800 kg/m^3 was taken as density of the apples (Mohsenin, 1986, p 787).
4. The dimensions of the box
5. Simulation time and time step. For apples a time step of 0.0005 s or less is necessary to obtain accurate integration results. Higher time steps decrease the integration accuracy[36]. The applied integration algorithm was an explicit time integration algorithm, named leap- frog (Tijskens *et al.,* 2003).
6. Initial positions of the particles in the box: randomly or individually defined. The initial positions of the particles, *before* falling in the box, were determined randomly but with the restriction of avoiding initial overlap.
7. Initial velocities of the particles. In the simulations the initial values were taken at zero.
8. The vibration signal: the displacement amplitude and angular velocity (frequency) of a vertical sine can be defined.
9. The grid for 'the smart contact detection algorithm' has to be specified. The algorithm decreases the simulation time considerably compared to pair wise contact detection. The smart contact detection algorithm is a binning algorithm that divides

[36] The maximum allowable time step for accurate integration results decreases with increasing stiffness of the materials

the space in different boxes. Contact detection is only needed between neighboring boxes. The grid has to be smaller than the size of the largest particle in the simulation (Tijskens, unpublished).

10. The colour of the particles, defined as intensity of red, green and blue (RGB)
11. The parameters of the contact force models (normal and tangential)

The data of the particles for each time step is saved is a binary file. This binary file can be read by MATLAB, utilizing MATLAB program files (m-files).
The following data is saved for *each time step*:

1. Position and velocity of the particles
2. The contact force for all the particle contacts in the time step

In MATLAB a program (m-file) was written to process the data for the bruise damage application. The peak force and impact time of each impact is calculated in MATLAB and saved in a data structure. This data is coupled with different bruise models and the results can be presented in different ways (see section 6.3.4).
The first part (1.5 s) of the particle contact forces, positions and velocities data was not analyzed in MATLAB. During this period the particles fell in the box so a natural stacking of the particles was obtained. The calculation of the bruise damage started when the stack was stabilized (after ≅ 1.5 s in the simulations) and movement of the particles was entirely due to the acceleration of the box.
A possibility was created to use bruise models taking in account the bruise sensitivity of the fruit, determined by fruit properties like:

1. Ripeness
2. Acoustic stiffness
3. Temperature
4. Radius of curvature

For the validation simulations, such bruise models, including the bruise sensitivity of the fruit, have not been used, but they were applied in the ‘shaking box’ application in Chapter 7.

6.2.5 Apple-apple impact vs. apple-hard plate impact

In this section, the physics of apple-apple impact is compared to apple-hard plate impact. When an apple falls from a certain height on a hard plate (metal plate, Plexiglas® plate or wooden plate) or on a second apple (apple of the same size and mechanical properties), the bruise damage of the apple will be lowest in the latter case. In the literature this is often explained by the damping effect of the two apples on each other and the fact that the bruise is distributed between both apples (Pang *et al.,* 1992). More fundamentally, the peak contact force during the contact apple-apple will be lower than in the case of the impact apple-hard plate.

The contact force model parameters that were measured with the pendulum in the case apple-metal plate were recalculated for the case apple-Plexiglas® (Plexiglas box was used as recipient during the validation measurements) and the case apple-apple. However, Plexiglas® can also be considered as a hard plate and consequently the same contact parameters can be applied as measured with the pendulum for the apple-metal plate impact.

The spring parameter for the impact apple-apple follows from Hertz contact theory: the spring parameter for the impact apple-apple is exactly half of the impact apple-hard wall. The derivation was outlined in Chapter 2 (section 2.3.3.1). The opposite is true for the damping parameter: the damping parameter for the contact apple-apple is exactly two times the damping parameter for the contact apple-Plexiglas®. This derivation is also outlined in Chapter 2 (section 2.3.3.2). The different damping and stiffness parameters between apple-Plexiglas® and apple-apple contact used in the simulations cause the lower peak contact force in the latter case.

In the validation simulations, the same statistical relationship between peak contact force and bruise damage was applied for the impact apple-Plexiglas® and impact apple-apple. However, critical reflections have to be considered. Besides the peak contact force also the impact time is an important parameter that determines the damage of the colliding objects (Chen and Yazdani, 1991). It must be stated that by applying the regression equations without the impact time as independent variable (Table 6-1), for the apple-apple contact, the bruise damage is somewhat overestimated. Experimentally it is known that longer impact times (apple-apple) lead to less bruise damage than shorter impact times (apple-hard plate) at identical peak contact force.

Pang *et al.* (1992) pointed out that the largest apple in the impact of two apples of unequal size is more damaged than the smaller one. This effect can also be incorporated in the simulations at the level of the statistical bruise model. In Chapter 5, it was demonstrated that the radius of curvature is proportional to the bruise damage. However, a relationship

between the radius of curvature and bruise damage for the apples used in the validation experiments was not developed. The reason therefore is that all the apples utilized in the validation shaking box experiments were almost of uniform size (equator radius of 0.0378 ± 0.001 m).

6.3 Results and discussion

6.3.1 Bruise models

Bruise models were developed with bruise volume, bruise surface, bruise diameter and bruise depth as dependent variables and peak force, impact time and impact side (red or green side of Jonagold apple) as independent variables. No significant effect (95 % level) of the impact side on the four dependent variables could be demonstrated.
The following regression equations were obtained (Table 6-2):

Table 6-2. Regressions equations

	R^2
$BV = 15.81 PF - 608.90$	0.90
$BDE = 5.67 \ln(PF) - 18.99$	0.89
$BDI = 11.40 \ln(PF) - 36.48$	0.86
$BS = 2.48 PF - 73.29$	0.92

with: *BV*: Bruise volume in [mm^3]; *BDE*: Bruise depth in [mm]; *BDI*: Bruise diameter in [mm]; *BS*: Bruise surface in [mm^2]; *PF*: Peak force in [N]

Figures 6-2 to 6-5, show the relation between peak contact force *PF* [N] on one hand and bruise volume *BV* [mm^3], bruise diameter *BDI* [mm], bruise depth *BDE* [mm] and bruise surface *BS* [mm^2] on the other hand.

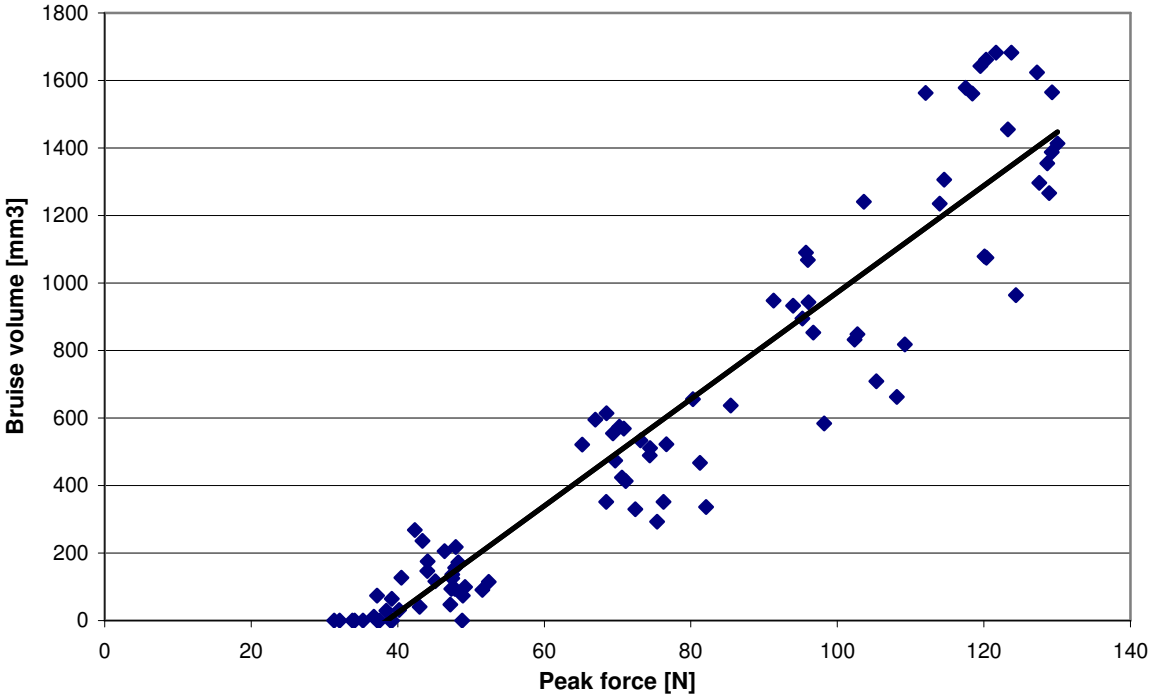

Figure 6-2. Relation between peak contact force [N] and bruise volume [mm^3] of the Jonagold apples

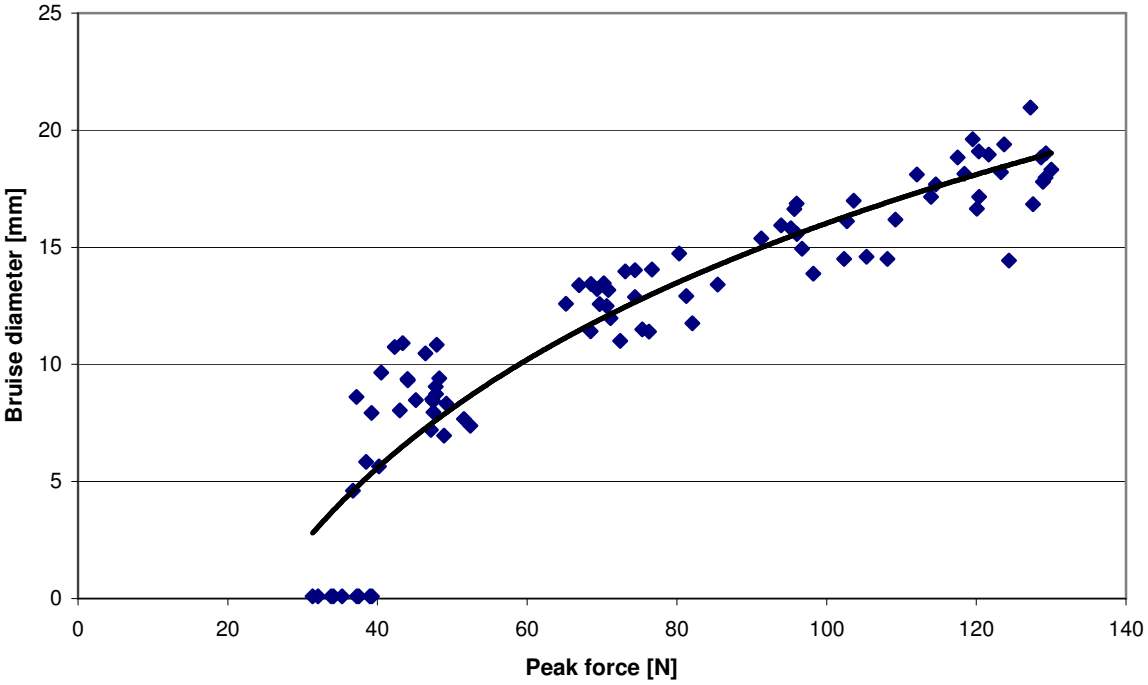

Figure 6-3. Relation between peak contact force [N] and bruise diameter [mm] of the Jonagold apples

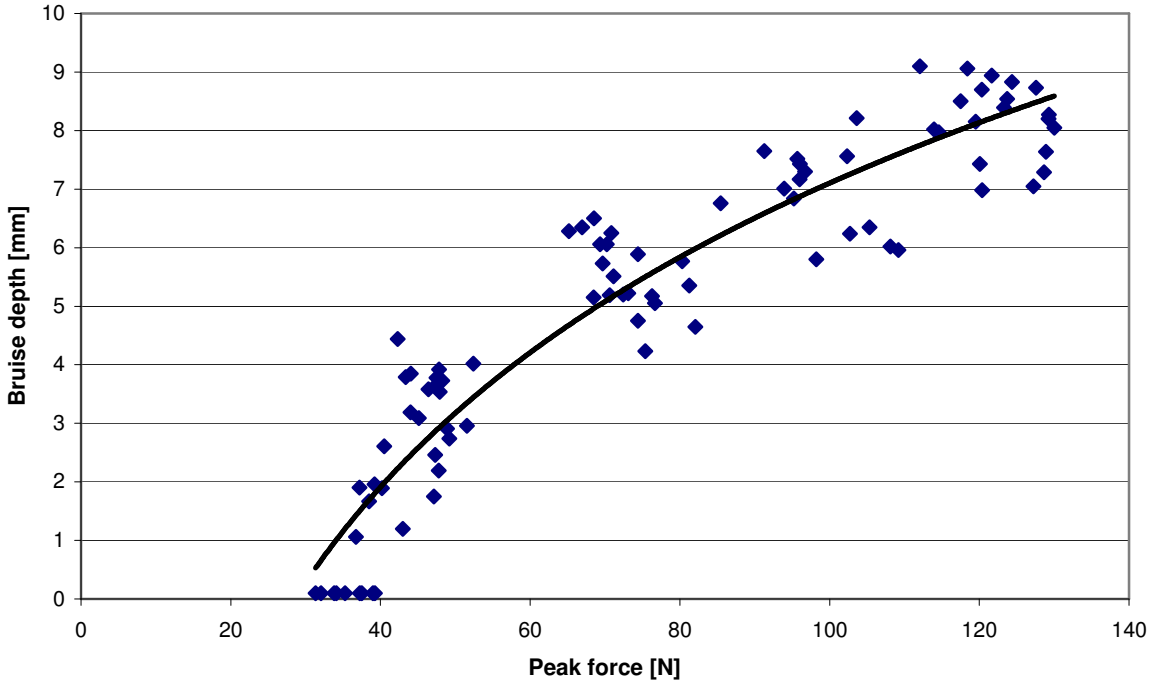

Figure 6-4. Relation between peak contact force [N] and bruise depth [mm] of the Jonagold apples

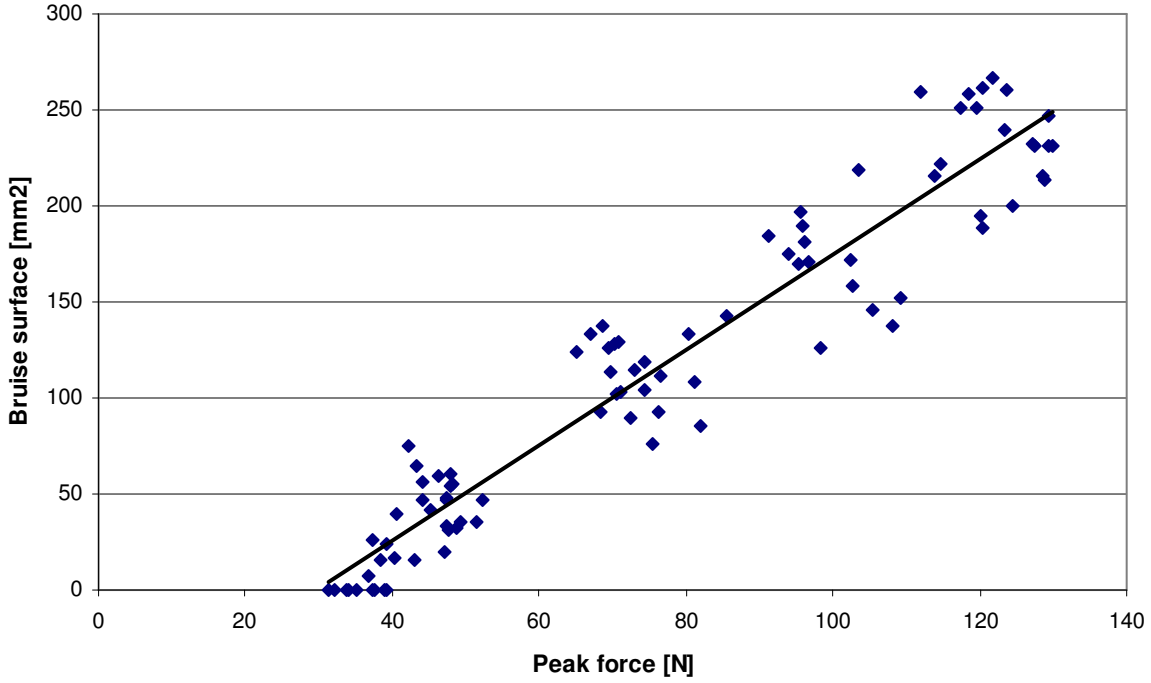

Figure 6-5. Relation between peak contact force [N] and bruise surface [mm^2] of the Jonagold apples

The fruit properties like ripeness and temperature were not included in the statistical models because these parameters were not different for the apples used in the validation experiments. The acoustic stiffness of the apples was 28.3 ± 1.1 $Hz^2.kg^{2/3}$, an indication for the uniform ripeness of the apples and the temperature during determination of the bruise models (pendulum) was the same as during the validation shaking box experiments.

6.3.2 Contact force model parameters

In section 3.5.2 of Chapter 3, the results of the normal contact force model parameters of the apples used in the validation shaking box experiments were presented.

In anticipation of the implementation in DEMeter++ of the viscoelastic extension of the Mindlin and Deresiewicz model (Chapter 4) a simplified tangential contact force model based on dry Coulomb friction was applied:

$$F_t = -\min(|\gamma_t \mathrm{v}_t|, |\mu F_N|).sign(\mathrm{v}_t) \qquad (6.2)$$

with F_t the tangential contact force [N]
γ_t a technical parameter [kg/s]
v_t the tangential velocity [m/s]
μ the dynamic friction coefficient
F_N the normal contact force [N]
$sign(\mathrm{v}_t)$ means the sign of the tangential velocity

The tangential force F_t defined by equation (6.2) cannot provide reversal of the tangential velocity v_t, like it can be the case in reality due to tangential stiffness, it can only slow down v_t down to zero. Without the term $|\gamma_t \mathrm{v}_t|$ in equation (6.2) the tangential force F_t, numerically jumps between positive and negative values when $\mathrm{v}_t = 0$ (discontinuity of Coulomb law) rather than $F_t = 0$. With the term $|\gamma_t \mathrm{v}_t|$ in the equation this can be avoided. The value of γ_t must be taken sufficiently high so that the case ($F_t = -\gamma_t \mathrm{v}_t$) occurs only for small v_t.

For the dynamic friction coefficient μ for apple-apple contact the experimentally measured friction coefficient of 0.27 was applied (Chapter 4). A dynamic friction coefficient of 0.27 (apple-aluminium contact, Chapter 4) was also assumed for apple-Plexiglas® contact, like aluminium Plexiglas® can be considered as a smooth surface.

6.3.3 Comparison of the results of validation shaking box experiments with DEMeter++ simulations

6.3.3.1 Introduction

The radius of curvature at the equator of the apples used in the validation experiments was equal to 0.0378 ± 0.001 m. In the DEM simulations, the radius of the particles (apples) was uniformly randomized between 0.0368 and 0.0388 m, lower and upper boundary of the standard deviation. Also the number of particles in the box and the acceleration signal (acceleration amplitude and frequency were matched between validation experiments and simulations.

The measured and simulated bruise damage can be expressed as bruise volume, -depth, -diameter, or -surface. However, the measurement of the bruises of the apples used in the validation experiments revealed that individual bruises were not always clearly distinctable, complicating the measurement of the bruise diameter and as a consequence the bruise volume and bruise surface. Surfaces of brown colouring were visible as the result of overlapping multiple impacts. In case of large brown spots on the apple surface, only the maximum bruise depth was measured. The bruise surface or diameter as a result of multiple impacts around the same location on the apple surface was not measured, because unambiguous measurement methods do not exist. Therefore, it can be stated that only the bruise depth is a reliable parameter to be compared between the validation experiments and simulations (experimental data is missing for multiple impact bruising for diameter, volume, and surface). In addition, bruise depth is the only parameter, at the present stage of the research that unambiguously can be calculated from the DEM simulations. This is explained below.

Theoretically, it must be possible using DEM simulations to calculate bruise surface and volume of overlapping impacts. This could be achieved by including a surface coordinate system for each particle. By means of coordinates, each impact location on the apple surface could be registered. Peak contact force information coupled with particle surface coordinates must allow calculating overlapping bruise surface and volume. At the present stage of research such a surface coordinate system was not included in the DEMeter++ *3D* software that was used in this work[37].

The original objective was that the DEM simulations could simulate the whole time period of the validation experiments (10 or 30 minutes real time). Practically, however, this was not possible. The reason is that the binary data file, containing the impact history, becomes too

[37] A particle coordinate system was already employed in a early *2D* version of the DEMeter++ software

large in size (for example, a 10-minute real time simulation of 142 particles creates a data file of 40 GB). In addition, MATLAB cannot handle such large data files. The maximum real time simulation that could be analyzed by MATLAB for 142 particles was three minutes. The solution to this problem is preprocessing of the data in C++ (DEMeter++) to decrease considerably the size of the data file to be analyzed in MATLAB or more drastically a complete analysis of the bruise problem in C++, so the data transfer to MATLAB can be avoided.

Fortunately, long simulation times appeared not to be necessary to model the bruise depth (the only parameters that could be compared with the validation experiments; see above).

The bruise damage of the apples expressed as bruise depth appeared not to differ between three minutes or 5 seconds real time simulation. Of course, the total number of impacts each particle encountered during the simulation is much higher for the three minutes simulation compared to the five seconds real time simulation. Nevertheless, this higher number of impacts was not translated into more bruise damage expressed as bruise depth (maximum bruise depth of one apple or even number of apples with maximum bruise damage within a certain damage class). This can be explained as follows:

- A sinusoidal signal with a period of 0.25 s was used. Each 0.25 s the acceleration pattern is repeated. Consequently, the magnitude of the accelerations is identical during 5 s or 3 minutes real time simulation.

- O'Brien (1963) experimentally demonstrated that the total bruise surface of a fruit is dependent on the time period of the acceleration (total acceleration time), however, the bruise depth is only defined by the magnitude of the acceleration pattern (acceleration amplitude)

In Figure 6-6 a typical graphical representation of the MATLAB bruise analyzing program is presented:

The figures provide information about:

1. **Total amount of bruise damage (for example bruise depth) of each particle (Figure 6-6 upper left)**. Without the use of the surface coordinates, it leads to a considerably overestimation of the bruise damage: Each impact, beyond the bruise threshold, is considered as a new bruise, whereas in reality the impact can be on the same spot on the apple surface as a previous impact.
2. **Maximum bruise (bruise depth, or bruise volume/surface of individual impacts) a particle encountered during the whole simulation time (Figure 6-6 upper right)**
3. **Histogram of total number of impacts in a certain damage class (Figure 6-6 down left).** Classes can be defined by the user.
4. **Histogram of the number of particles that encountered a bruise in a certain damage class (Figure 6-6 down right)**. Classes can be defined by the user. Since the surface coordinate system was not used, it is possible that in reality the smaller bruises are mimicked, as a second impact at the same spot provoked a larger bruise. In this respect it is also possible to interpret the histogram as such: **the number of particles that are showing bruises in the given damage class or above**

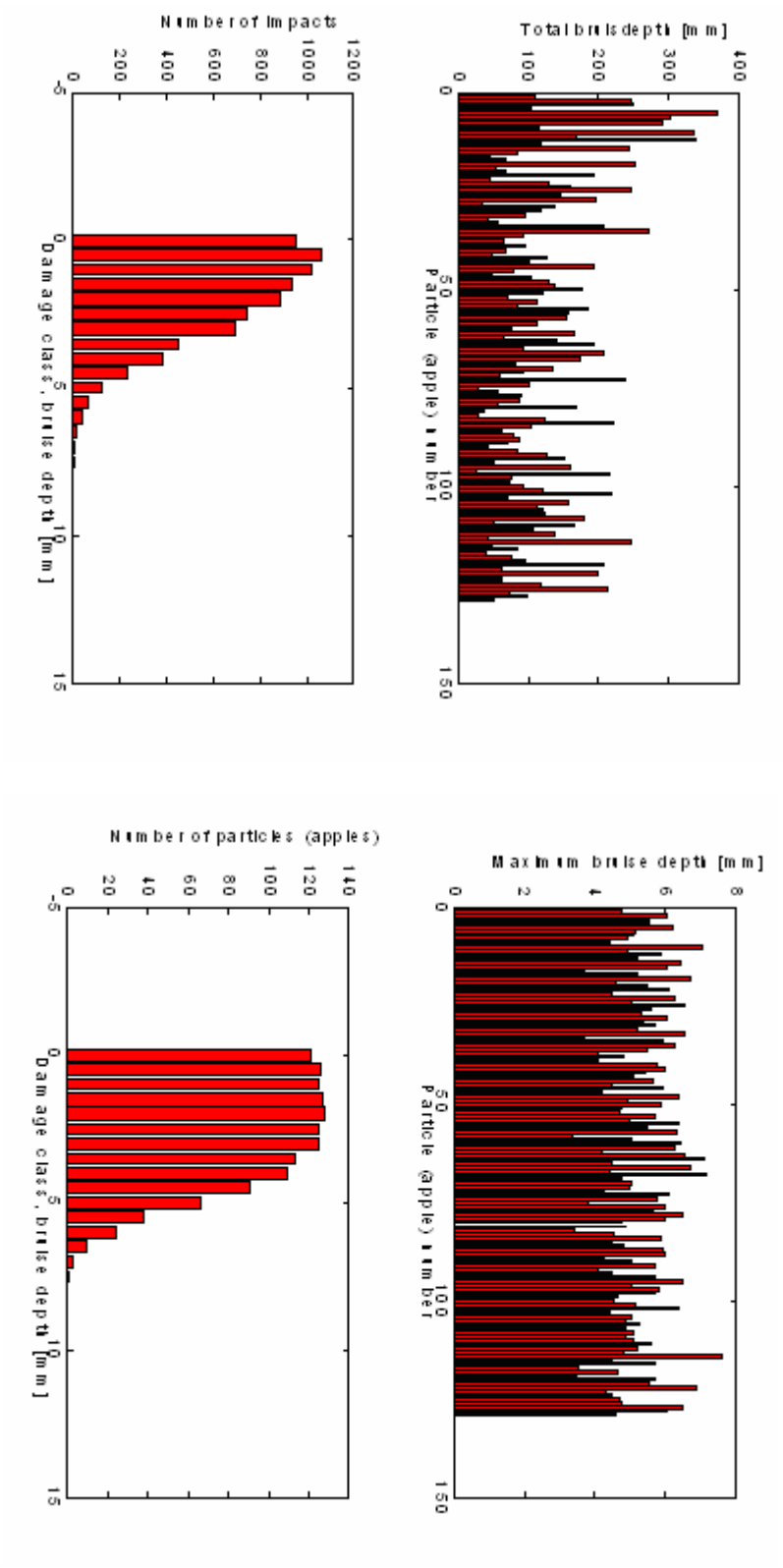

Figure 6-6. Overview of a typical output of the MATLAB bruise analyzing program. For an explanation see text

6.3.3.2 Comparison of validation experiment and simulation: acceleration signal 1

In Figure 6-7 the comparison between simulation and experiment is demonstrated in the histogram of the number of particles (apples) that encountered a maximum bruise depth in a certain damage class.

It can be concluded that the distribution of bruises is almost identical between simulation and validation experiment. However, the bruise depth in the simulation is systematically overestimated by 2.5 mm (100 to 300 % overestimation).

It could be concluded that DEM is unable to predict the mechanical damage of the apples sufficiently. However, further research (see below) pointed out that this difference is due to a difference in initial conditions. More specifically, the stacking of the apples in the experiment and the simulation were too different. In the experiment, the apples were ordered exactly as 36 apples per layer in 6x6 configurations. However in the simulation it was not possible to stack the apples in a structured way (this possibility is not yet included in the basic software). Only a natural stacking of the particles, a random stacking due to gravity, could be simulated. In the validation experiment the apples were *forced* in the desired 6 x 6 configuration. The fact that the damage of the apples in the experiment was less than in the simulation can be explained by the difference in the freedom of motion of the apples between simulation and experiment due to the difference in initial stacking (natural in simulation and forced in experiment).

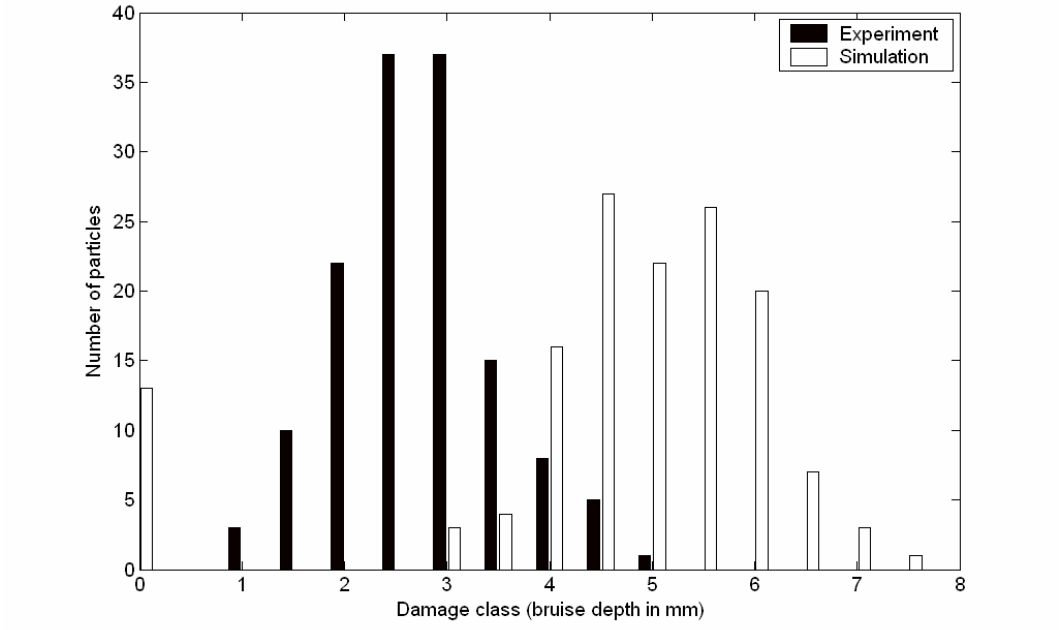

Figure 6-7. Histogram: Numbers of apples with a maximum bruise depth in a certain damage class. black: experiment, white: simulation

6.3.3.3 Comparison of validation experiment and simulation: acceleration signal 2

In Figure 6-8 the comparison between simulation and experiment is demonstrated in the histogram of the number of particles (apples) that encountered a maximum bruise depth in a certain damage class.

Contrary to the previous validation experiment (section 6.3.4.2), the apples were stacked in natural configuration in both validation experiment and simulation.

From Figure 6-8 can be concluded that simulation approximates the validation experiment quite well. However, the apple bruise damage was slightly overestimated by the simulation compared to the validation experiment. The average maximum bruise depth was overestimated by ± 1 mm (5.08 mm compared to 3.94 mm).

The peak acceleration of signal 2 (1.48 g) was almost identical to the peak acceleration of signal 1 (1.45 g). Therefore the average maximum bruise depth and the distribution of maximum bruise depth of both validation experiment and simulation using signal 2 was almost identical to the previous simulation result using signal 1 (section 6.3.3.2). The fact that the results of validation experiment and simulation using signal 2 were not similar to the result of the validation experiment using signal 1 (section 6.3.3.2) can be interpret as an extra proof that the lack of similarity between validation experiment and simulation using acceleration signal 1 (section 6.3.3.2) was due to their difference in apple stacking.

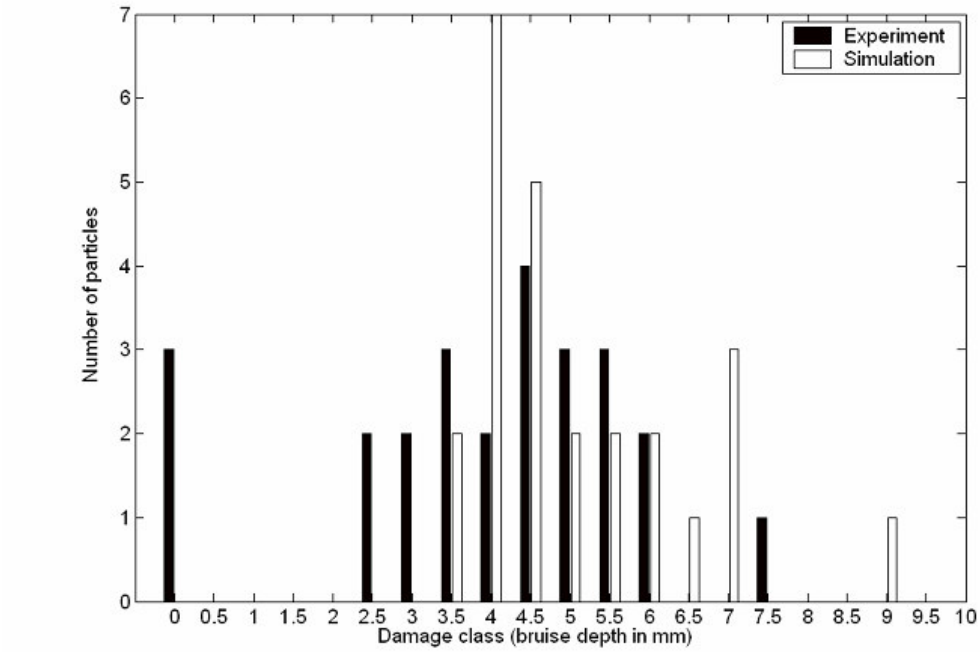

Figure 6-8. Histogram: Numbers of apples with a maximum bruise depth in a certain damage class. black: experiment, white: simulation

6.3.3.4 Comparison of validation experiment and simulation: acceleration signal 3

In Figure 6-9 the comparison between simulation and experiment is demonstrated in the histogram of the number of particles that encountered a maximum bruise depth in a certain damage class. Similar to acceleration signal 2 (section 6.3.3.3), the apples were stacked in natural configuration in both validation experiment and simulation. From Figure 6-9 can be concluded that the simulation approximates the validation experiment quite well.
However, the apple bruise damage was slightly overestimated by the simulation compared to the validation experiment. The average maximum bruise depth was overestimated by ± 0.8 mm (3.54 mm compared to 2.75 mm).
Acceleration signals 2 and 3 were identical. However, the average maximum bruise damage of the 25 apples in the validation experiment using acceleration signal 2 (section 6.3.3.3) was 1.2 mm higher than the average maximum bruise damage of the 57 apples in the validation experiment using signal 3. This can be explained by the fact that all 25 apples in the validation experiment using acceleration signal 2 were in contact with the Plexiglas® bottom plate and minimum 21 of the 57 apples in the validation experiment using acceleration signal 3 were not. As explained before (section 6.2.5), apples in contact with the bottom plate contract more damage than apples in contact with other apples. Because of that the *average* maximum bruise depth of the apples in the validation experiment using signal 2 was higher.

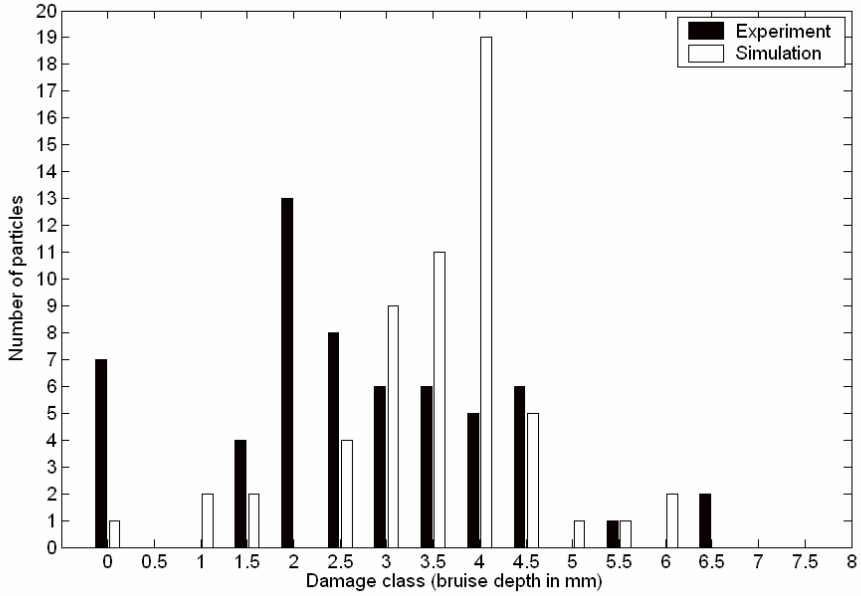

Figure 6-9. Histogram: Numbers of apples with a maximum bruise depth in a certain damage class. black: experiment, white: simulation

6.3.3.5 Comparison of validation experiment and simulation: acceleration signal 4

In Figure 6-10 the comparison between simulation and experiment is demonstrated in the histogram of the number of particles that encountered a maximum bruise depth in a certain damage class. Similar to acceleration signal 2 and 3 (section 6.3.4.3 and section 6.3.4.4), the apples were stacked in natural configuration in both validation experiment and simulation.

From Figure 6-10 can be concluded that the simulation approximates the validation experiment quite well. However, the apple bruise damage was slightly *underestimated* by the simulation compared to the validation experiment. The average maximum bruise depth was underestimated by ± 0.7 mm (1.08 mm compared to 1.77 mm).

It can be concluded there is no proof for a systematical error between validation experiments and simulations, because twice the bruise damage was overestimated (section 6.3.3.3 and section 6.3.3.4) and one time the bruise damage was underestimated.

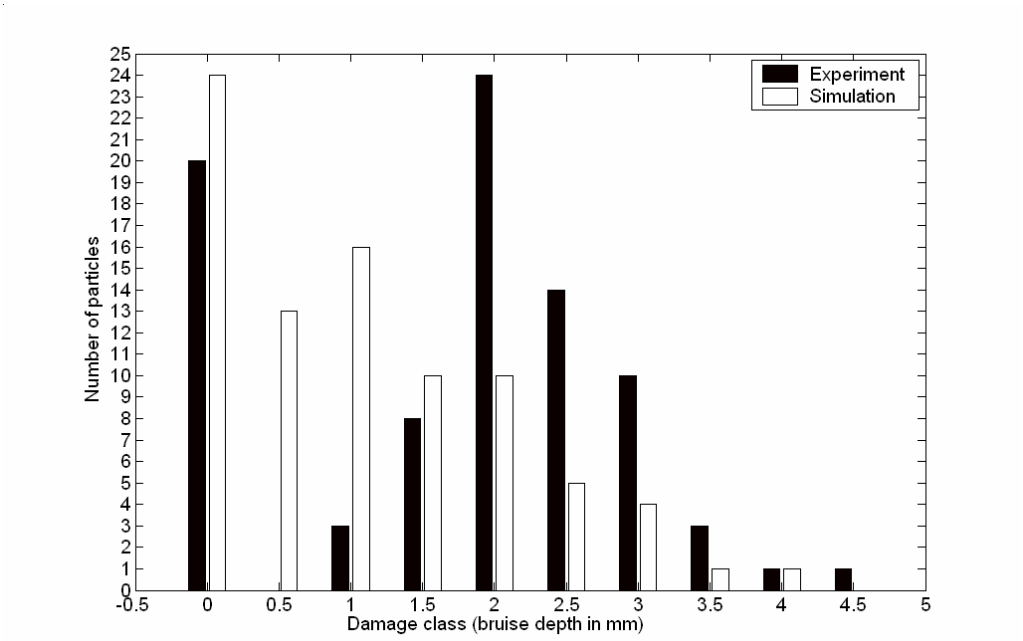

Figure 6-10. Histogram: Numbers of apples with a maximum bruise depth in a certain damage class. black: Experiment, white: simulation

6.4 Conclusions

In this chapter the applicability of DEM to predict the bruise damage has been validated for Jonagold apples. The validation was a crucial but necessary step in this work. 'Bruise damage' was preferred above the 'particle trajectory' as validation parameter. The bruise damage of apples in boxes that were shaken with a well defined vertical sinusoidal acceleration signal on an electro-hydraulic shaker was compared with the bruise damage calculated from DEM simulations with the same setup and initial conditions (identical acceleration signal, identical number of apples and size, etc.). The parameters for the contact force models, needed as input to the simulations, and the bruise model were determined on the same batch of apples used for the shaking validation experiments. For the simulations *3D* DEM application program named 'Shaking box' was compiled from the DEMeter++ library. Further analysis of the data for the bruise problem was performed in MATLAB. Due to some constraints in both validation experiments and the DEMeter++ application program, bruise depth was the only parameter that could be applied for bruise evaluation.

The comparison between simulation and validation experiment was demonstrated in the histogram of the number of particles (apples) that encountered a maximum bruise depth in a certain damage class. The validations indicated that DEM can predict in an acceptable way the apple bruise damage.

Chapter 7

Case study: DEM simulation of bruise damage during transport of apples and tomatoes

7.1 Introduction

In Chapter 6 it was demonstrated that DEM simulations can predict the bruise damage of apples in an acceptable way. This validation step was necessary to proceed to the next step: the execution of simulations without experimental validation to gain insight in the process of bruising during handling.

For the tomatoes the validation step was not carried out because an objective method to measure the bruise damage of tomatoes is not available. Nevertheless, it is believed that simulation results of tomatoes are reasonable because the same methodology was used as for the apples. As soon as an objective method to measure tomato damage becomes available a validation of the DEM for tomatoes would be very interesting.

A considerable amount of experimental work has been done in fruit bruise damage (mostly apples and peaches) due to vibration (both continuous and transient) (O'Brien *et al.*, 1963, 1965, 1969ab, 1972; O'Brien and Guillon, 1969; Chesson and O'Brien, 1971; O'Brien, 1974; Plumbee and Webb (1974); Schoorl and Holt, 1982a, 1985; Holt and Schoorl, 1985; Peleg and Hinga, 1986; Schulte-Pason *et al.*, 1989, 1990a; Armstrong *et al.*, 1991; Jones *et al.*, 1991; Hinsch *et al.*, 1993; Singh and Xu, 1993; Timm *et al.*, 1996; Timm *et al.*, 1998; Bollen *et al.*, 2001). However, some contradictions in the literature were noted (see further in this chapter).

Besides, extensive experimental work, few simulation models associated with some simple laboratory tests have been developed. The road-vehicle-load systems by Holt and Schoorl (1985) and Jones *et al.* (1991) using energy dissipation mechanism for modelling a single column apple pack seem valuable and pioneering. However, the difficulty in modelling such a system is increased when a large quantity of fruit is involved. In a attempt to resolve this problem pioneering research in DEM modelling of fruit bruise damage due to vibration has been executed by Rong (1993, 1994). Rong indicated that the experimental results by Holt and Schoorl (1985) could be reproduced by DEM. Only the effect of transient vibrations (shocks) on apple bruise damage, no continuous vibrations, were simulated. The simulation comprehended a simulation of 12 apples (three rows of four apples) in two dimensions. A linear contact force model was applied, with parameters estimated from apple material properties available in literature (Mohsenin, 1986).

In this chapter DEM simulation of fruit bruise damage due to continuous vibrations during transport is discussed. Simulations in three dimensions up to 1500 particles were executed. More in detail, the effect of *mechanical parameters* (vibration frequency, stack height, size of the fruit, etc.) and *fruit properties* (ripeness, acoustic stiffness, temperature, etc.) on fruit vibration damage is investigated.

In section 7.2 the materials and methods of the DEM simulations are discussed. In section 7.3 apple bruise damage in bulk bins due to continuous vibrations is discussed. In section 7.4 tomato bruise damage due to continuous vibrations in Expanded Polystyrene (EPS) crates is discussed. In section 7.5 conclusions are drawn for bruise damage due to vibrations for apples and tomatoes.

7.2 Materials and methods

As input for the simulations the regression equations of Chapter 3 of the Kuwabara and Kono normal contact force model parameters were used (apples: section 3.5.2; tomatoes: section 3.5.3). As tangential contact force model, the same model was applied as for the validation simulations (see section 6.3.2).

In the simulations to evaluate the effect of *mechanical parameters* on apple bruise damage, the statistical bruise model of Chapter 6 (Table 6-1), with bruise depth as dependent variable, was utilized. In the simulations to evaluate the effect of *fruit properties* on fruit bruise damage the regression equations of Chapter 5 were applied (apples: section 5.2.2.1; tomatoes: section 5.3.2.1) with bruise volume (apples) and absorbed energy (tomatoes) as dependent variable.

Although complex accelerations patterns in three dimensions occur in reality, simulations with a vertical sine as acceleration signal were executed.

To reduce the simulation time, reduced dimensions of an apple bulk bin were used in some simulations. Holt and Schoorl (1983a) showed that the total volume of bruised tissue in a package is independent of the package arrangement. Furthermore, the bruising in the various layers of the packs, measured as a percentage of the total bruise volume, is also independent of the package arrangement. Apples in packages will behave as if they were stacked in columns, with each apple vertically above the corresponding apple in the layer below. Based on the assumption that the behaviour of fruit can be modeled as a single column, the results of a bulk bin with reduced dimensions can be generalized to a full size bulk bin.

7.3 Simulation of apple bruise damage during transport

7.3.1 Effect of vibration frequency on apple bruise damage

Simulations were executed to quantify the effect of the vibration frequency on mechanical damage during the bulk transport of apples. In the simulations 100 particles (apples) with a radius of 0.038 m (diameter class 75/80) were used. The size of the box in the simulations was equal to 0.2x0.2x1 m leading to a stack height of ± 0.57 m, the maximum stack height of apples during bulk transport in Belgium. The vertical vibration signal used in the simulations was a sine with varying frequency but with a constant peak acceleration of 1.4 g. To achieve this constant peak acceleration, the vertical displacement amplitude was adapted for each frequency. The peak acceleration of 1.4 g in the simulations was 0.2 g higher than the maximum peak acceleration in the vertical direction that was measured on the fork-lift of a tractor during apple harvest at the Fruitteeltcentrum of the K.U. Leuven (Deli *et al.,* unpublished). Figure 7-1 depicts the results of the simulated average maximum bruise depth[38] of the apples for each frequency. It can be concluded that by far the most damage is contracted below the vibration frequency of 5 Hz.

[38] From all the bruises one particle contacted during the simulation, the maximum bruise depth was taken and an average was made for the 100 particles in the simulation

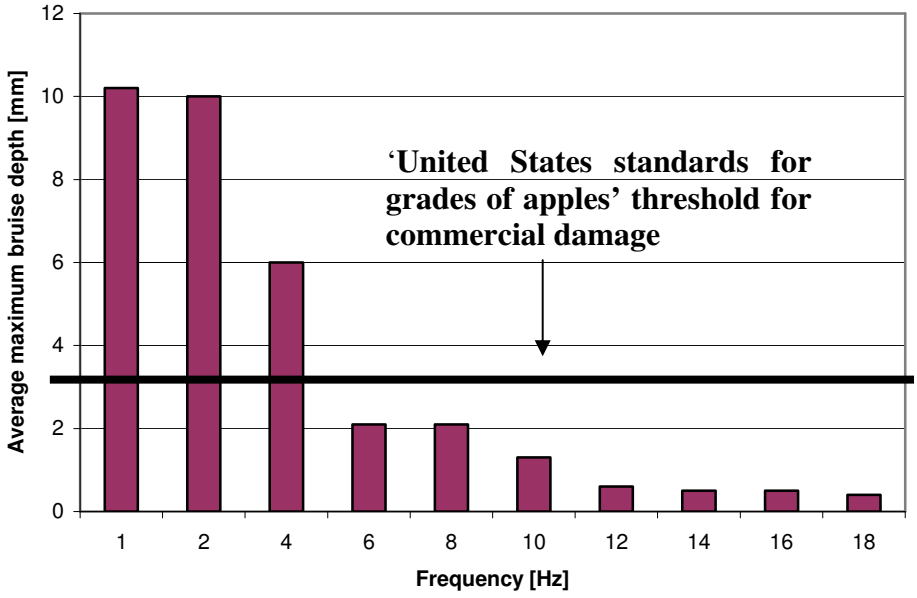

Figure 7-1. Effect of vibration frequency on the mechanical damage of apples at constant peak acceleration of 1.4 g.

Bruise depths of 3 mm and less are only visible from the outside with a trained eye (own experience). According to the United States Standards for Grades of Apples, bruise depths less than 1/8 inch (3.2 mm) are considered not to be leading to a quality reduction of the apple. For that reason this threshold was indicated in Figure 7-1.

By considering this threshold it can be concluded that frequencies above 5 Hz, even with a rather high peak acceleration of 1.4 g are not leading to damage visible by consumers. These results are in agreement with the literature. Timm *et al.* (1998) showed dominant force spectral densities[39] between 1-2 Hz and 3.5-4.5 Hz (measurement with force membranes during orchard bulk transport). Pressure spectral density analysis of the pressure data measured using Tekscan® tactile films during orchard bulk transport confirm these results (own research, Deli *et al.,* unpublished).

It can be interesting to reduce all the vibrations below 5 Hz to diminish the apple bruise damage during bulk orchard transport. This could be achieved by equipping the fork-lift of the tractor with a semi-active or active suspension. This type of suspension has to shift the energy in the 0-5 Hz domain to frequencies above 5 Hz.

Although the results of the simulations are in agreement with our field research (Deli *et al.,* unpublished) and the research by Timm *et al.* (1998), it is not in agreement with all the literature data. Some authors (O' Brien *et al.*, 1965; Chesson and O' Brien, 1971; Armstrong *et al.,* 1991) claimed that most mechanical damage to fruit must be found around the

[39] Fast Fourier Analysis of force levels measured in the time domain

resonance frequency of the fruit column. The resonance frequency of the fruits was determined using the equations for longitudinal vibration of a bar with one end fixed (O' Brien *et al.,* 1965):

$$f_n = \frac{1}{4\lambda}\sqrt{\frac{Eg}{\tau}} \qquad (7.1)$$

with f_n the resonance frequency [Hz]
E the column elasticity of fruit [Pa]
λ the stack height of fruit [m]
τ the bulk density of fruit [kg/m^3]
g the gravity force [9.81 m/s^2]

It would be expected that, when the resonance frequency for a given kind of fruit is in the middle of the range of that of the transport vehicle, resonant vibration will occur leading to peak acceleration- and displacement amplitudes depending on the fruit's freedom of motion. The freedom of motion is high for the upper layers but decreases rapidly with depth of the fruit in the stack. By applying equation (7.1) for the apples in the simulation, a resonance frequency around 14 Hz was calculated for the maximum stack height of 0.57 m. Experimental verification of the resonance frequency for apples was performed by Amstrong *et al.* (1991). Resonance was defined as the peak in visual movement (of the apples) around a certain frequency. Amstrong *et al.* (1991) showed, utilizing a video camera, a peak in the motion of the apples, primarily in the top layers, for hard wood bins at 11 Hz and for rigid (metal) bins at 14 Hz[40]. These results were confirmed by Timm *et al.* (1996). Nevertheless, in both studies no relationship was developed between the fruit column (resonance) frequency and the bruise damage.

In the data presented in Figure 7-1 no increase in the (average) bruise damage around the resonance frequency (14 Hz, because the box in the simulation is perfect rigid) could be noted. In later analysis of the distribution of the bruise damage in the bulk stacking (section 7.3.4) a small increase in the bruise damage around 14 Hz in the upper layers was noticed (see Table 7-9). This increase is very low compared to the bruise damage below 5 Hz. It can be concluded that for apples the phenomenon of resonance vibration, in contrast with other fruits like peaches (O'Brien *et al.,* 1965), is not important. This is because besides 'peak acceleration' also 'column weight' determines the bruise damage. This is discussed in more detail in section 7.3.4.

[40] The resonance frequency, although not included equation (7.1), is also dependent on the rigidity of the bulk bin. Higher rigidity leads to higher resonance frequency. For a perfect rigid bulk bin the resonance frequency is around 14 Hz (in simulation), for a hard wooden bulk bin this is around 11 Hz.

Analysis of the vibration simulator utilized by O'Brien and Guillou (1969) showed that also sinusoidal tests were performed by increasing the vibration frequency without adapting the displacement amplitude leading to increased acceleration amplitudes. To our opinion, this is not the right method to test the effect of the frequency itself on the mechanical damage because the effect of the frequency is mixed with the effect of peak acceleration. However, this led to the idea to perform DEM simulations to further investigate the effect of the resonance frequency on bruise damage by performing simulations at different vibration frequencies but constant displacement amplitude (leading to higher peak accelerations by increasing frequency). The results of these simulations are presented in Tables 7-1 and 7-2 for respectively a stack height of 0.57 and 0.292 m. As can be seen, the stack height of 0.57 m is leading to a maximum bruise depth around 14 Hz and according to equation (7.1) a lower stack height (0.292 m) is leading to a maximum bruise depth at a higher frequency (16 Hz). These simulations clearly demonstrate the theory of O'Brien of maximum bruise damage around the fruit column resonance frequency.
Nevertheless, the mechanical damage around the fruit column resonance frequency is not important for practice (at least for apples):

- The DEMeter++ simulations showed that a clear peak in apple bruise damage around the fruit column resonance frequency is only present at high acceleration levels, but these acceleration levels were not measured in practice (only shocks can lead to such high accelerations)

- In studies with realistic accelerations levels in which either the damage to the apples was directly measured or the pressure between the apples (directly correlated with damage) frequencies below 5 Hz were always most harmful to the apples (Deli *et al.*, unpublished; Timm *et al.,* 1998)

Table 7-1. Effect of vibration frequency on the mechanical damage of apples with varying peak acceleration. Maximum stack height of 0.57 m (100 particles).

Vibration frequency [Hz]	*Acceleration amplitude [g]*	*Average maximum bruise depth [mm]*
4	0.8	1.14
8	3.19	1.81
12	7.19	***2.890***
16	12.77	2.707
20	19.96	2.386
25	31.18	2.758
30	44.91	2.399
50	124.8	1.86

Table 7-2. Effect of vibration frequency on the mechanical damage of apples with varying peak acceleration. Stack height of 0.292 m (50 particles).

Vibration frequency [Hz]	*Acceleration amplitude [g]*	*Average maximum bruise depth [mm]*
4	0.8	0.0046
8	3.19	3.858
12	7.19	3.906
16	12.77	***4.193***
20	19.96	3.807
25	31.18	3.144
30	44.91	3.079

7.3.2 Effect of stack height on apple bruise damage

The effect of stack height during bulk transport (in orchard) on apple damage has been simulated. The simulations were performed with apples of middle diameter class (diameter class 75/80, uniform randomization of the radius between 0.0375 and 0.040 m). The size of the box in the simulation was 0.4x0.4x1.2 m. The vibration frequency was 4 Hz. The effect of stack height was tested at two different acceleration amplitudes: 0.5 and 0.8 g. 0.5 g is the minimum vertical acceleration measured during orchard bulk transport, 0.8 g is the average vertical acceleration amplitude during orchard bulk transport (Deli *et al.,* unpublished).

In a completely filled bulk bin used in Belgium, the stack height is around 0.57 m. Simulations with this stack height were taken as reference. Simulations were also performed with a bulk bin filled for 70 % (stack height 0.41 m) and stack height of 0.75 m (this means

in practice the use of higher bulk bins, although it is most unlikely in an industry which has standardized on the current bins).

The results are presented in Tables 7-3 and 7-4. In Table 7-3 the number of apples with bruise depths higher than 3 mm (the American commercial threshold) is presented. In Table 7-4 the highest bruise depth found for each simulation is given. Figures 7-2 to 7-7 depict the histogram of bruise depth for each simulation.

By analyzing the results of the simulations, it can be advised to keep the stack height at 0.57 m or to diminish the stack height. A substantial increase and decrease in bruise damage was noted for a stack height of 0.75 m and 0.41 m respectively. For higher peak acceleration (0.8 g compared to 0.5 g) the effect of stack height on apple bruise damage is more pronounced.

As a general remark, the relative importance of the stack height could be dependent on the vibration frequency and the size of the apples but this was not investigated.

Table 7-3. The number of apples with a bruise depth higher than 3 mm as a function of the stack height and acceleration amplitude (vibration frequency of 4 Hz).

Stack height / acceleration	*0.5 g*	*0.8 g*
0.41 m	2/150 (1.3 %)	9/150 (6.0 %)
0.57 m	16/200 (8.0 %)	65/200 (32.5 %)
0.75 m	69/260 (26.5 %)	153/260 (59 %)

Table 7-4. The highest bruise depth [mm] in the batch of apples as a function of the stack height and acceleration amplitude (vibration frequency of 4 Hz).

Stack height / acceleration	*0.5 g*	*0.8 g*
0.41 m	4.0	4.5
0.57 m	4.5	6.5
0.75 m	7.0	9.5

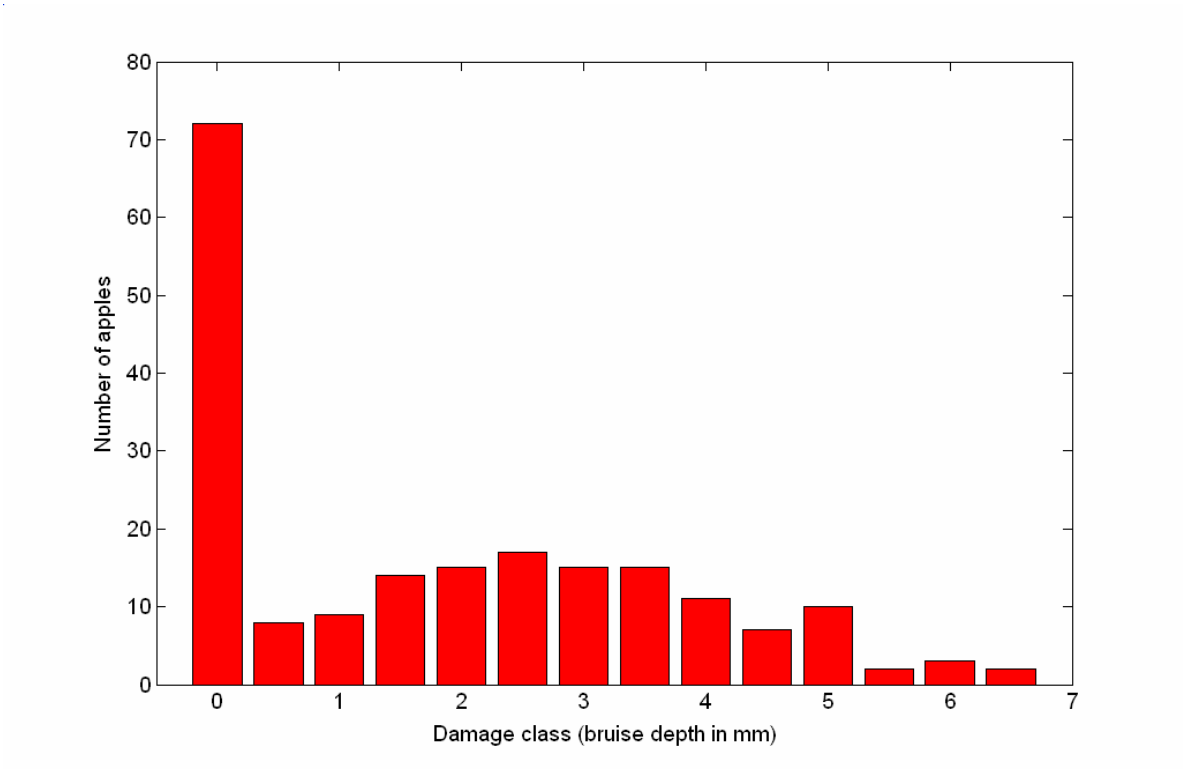

Figure 7-2. Histogram of bruise depth for stack height of 0.57m (200 particles), and acceleration amplitude of 0.8 g (vibration frequency of 4 Hz).

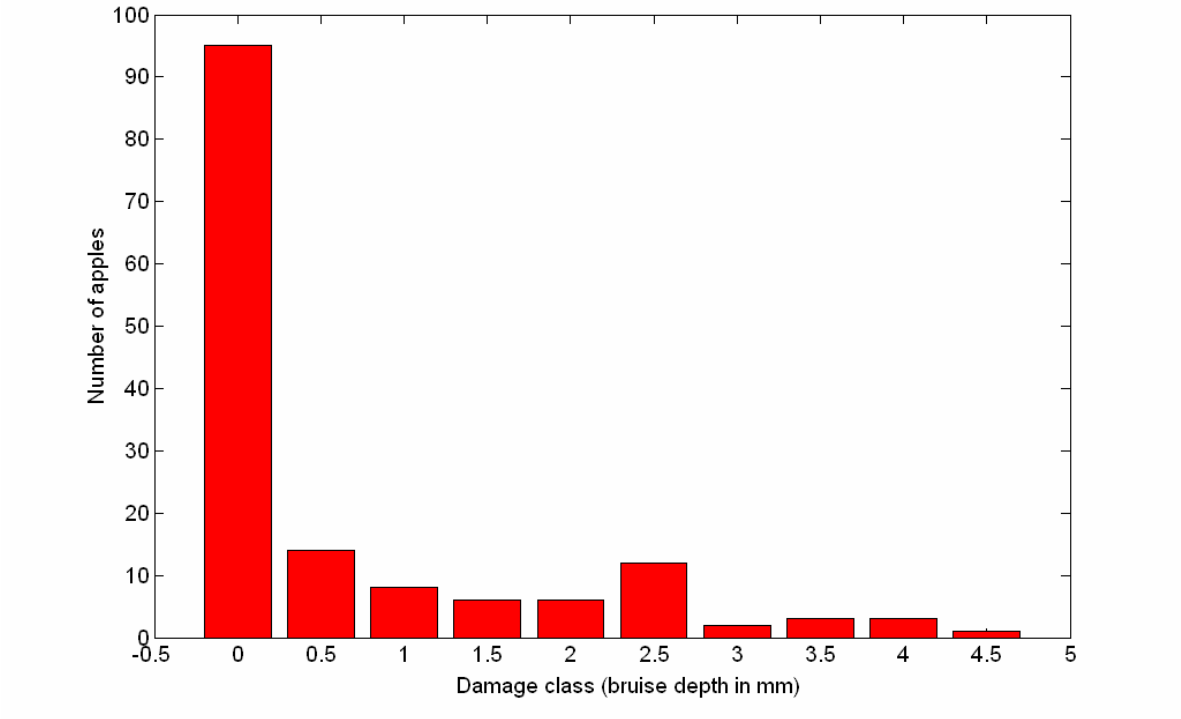

Figure 7-3. Histogram of bruise depth for stack height of 0.41m (150 particles), and acceleration amplitude of 0.8 g (vibration frequency of 4 Hz).

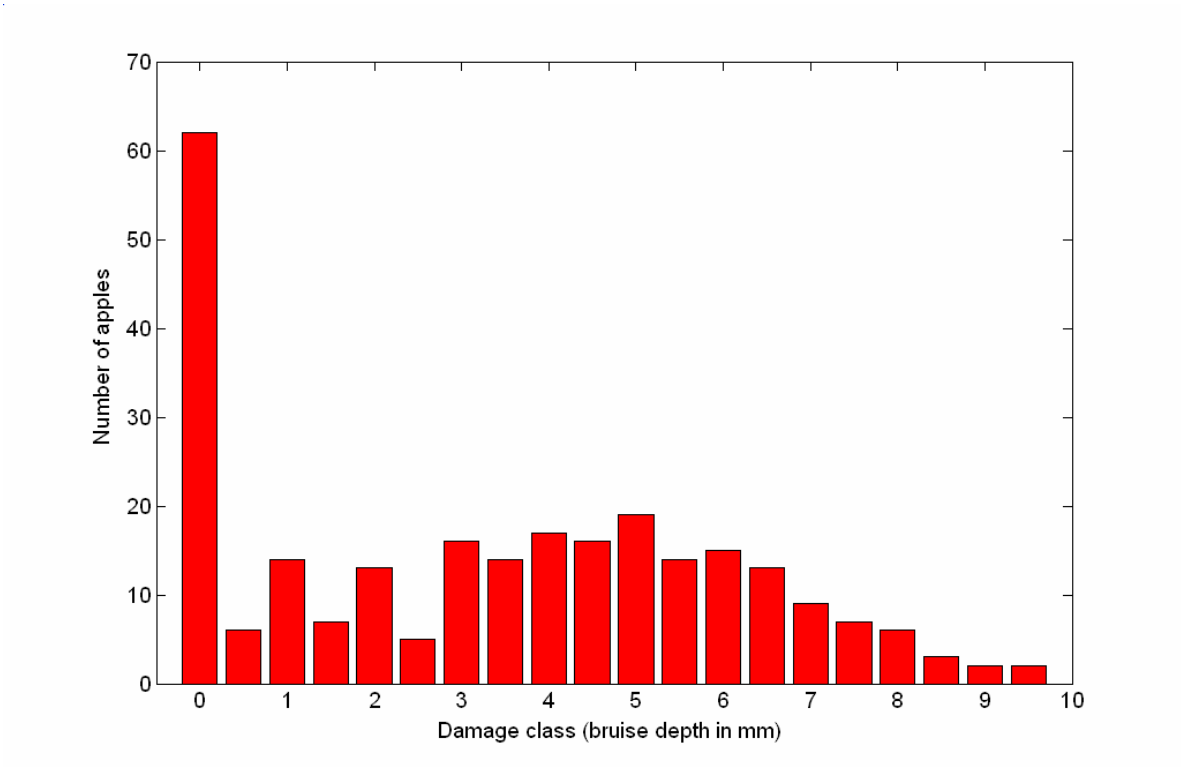

Figure 7-4. Histogram of bruise depth for stack height of 0.75m (260 particles), and acceleration amplitude of 0.8 g (vibration frequency of 4 Hz).

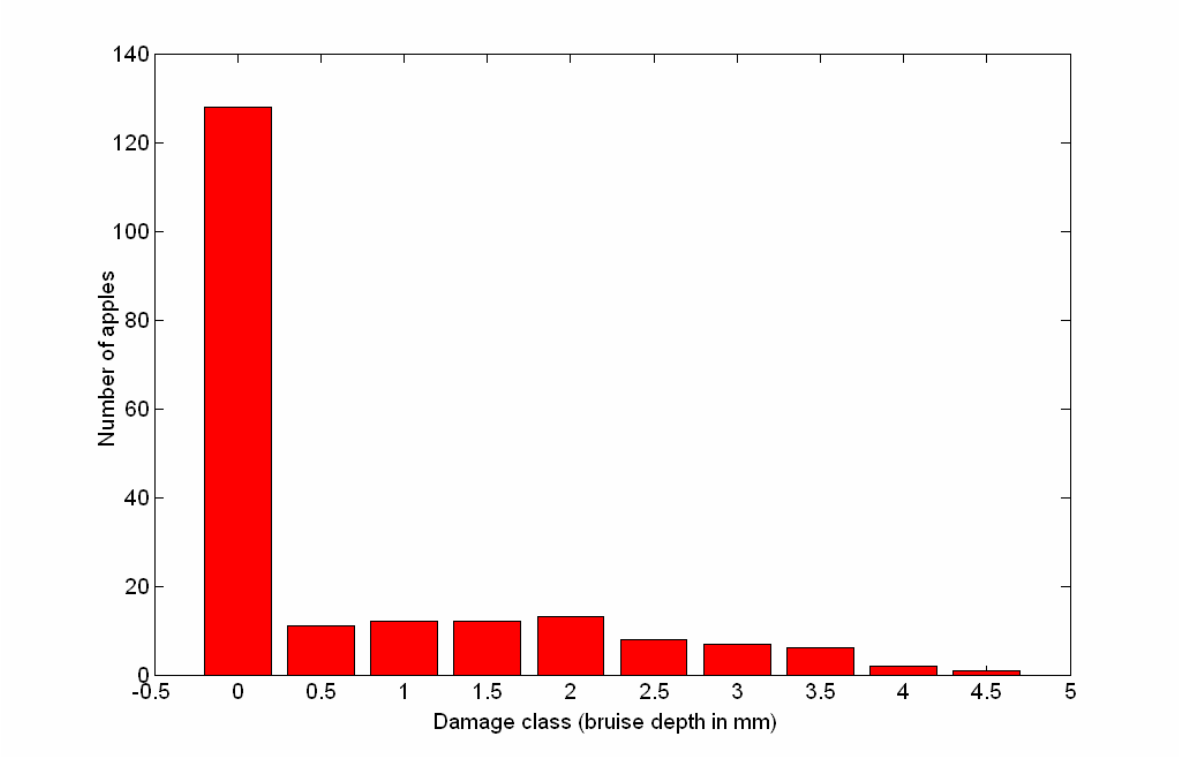

Figure 7-5. Histogram of bruise depth for stack height of 0.57m (200 particles), and acceleration amplitude of 0.5 g (vibration frequency of 4 Hz).

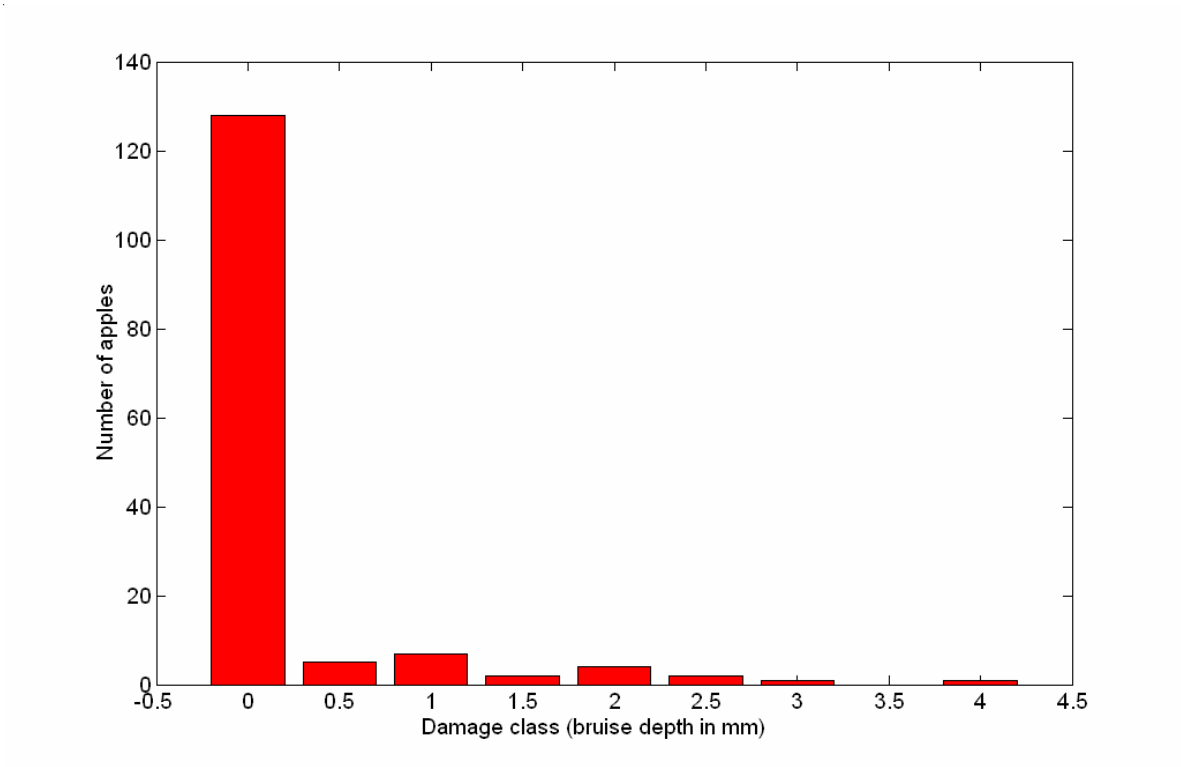

Figure 7-6. Histogram of bruise depth for stack height of 0.41m (150 particles), and acceleration amplitude of 0.5 g (vibration frequency of 4 Hz).

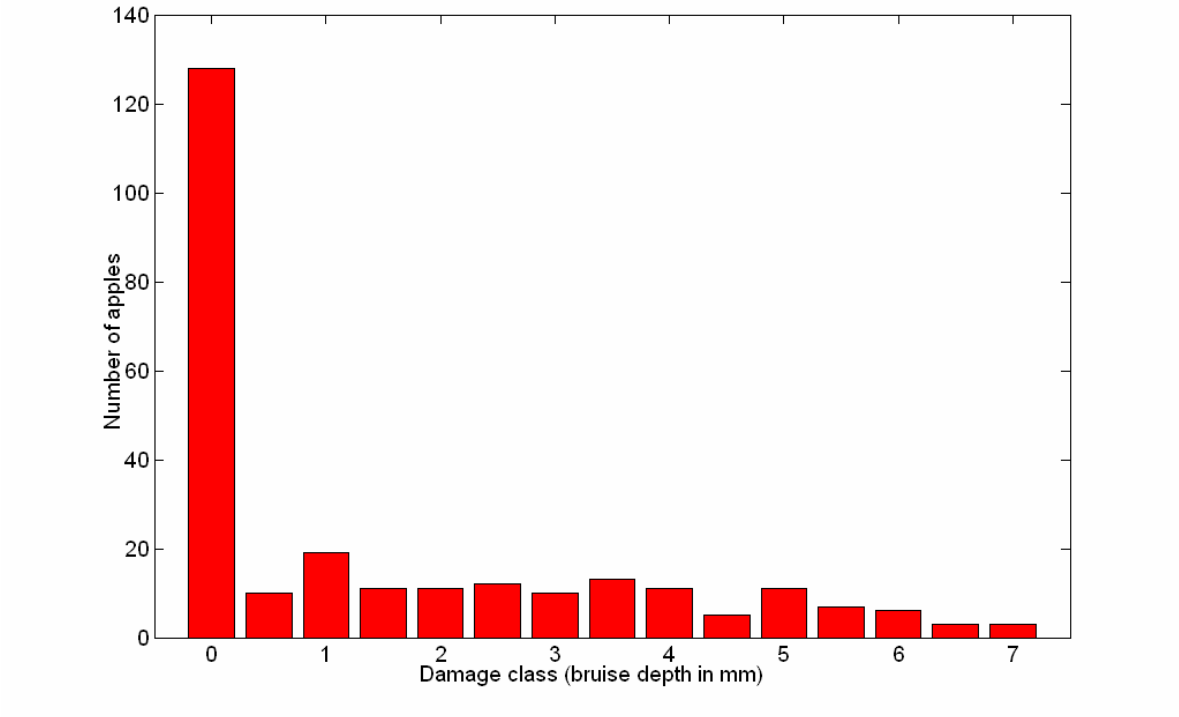

Figure 7-7. Histogram of bruise depth for stack height of 0.75m (260 particles), and acceleration amplitude of 0.5 g(vibration frequency of 4 Hz) .

7.3.3 Effect of apple size on bruise damage

The effect of apple size on apple damage during bulk transport was simulated. It was preferred to simulate the two extremes in apple size: small apples of diameter class 65/70 (radius of 0.0325 m) and large apples of diameter class 85/90 (radius of 0.045 m). The size of the box in the simulation was 0.4x0.4x1.2 m. The vibration frequency at all time was 4 Hz and the acceleration amplitude 0.7 g. For the simulations a stack height of 0.57 m (maximum stack height in Belgium) for both the small and large apples was chosen. In Table 7-5 and Figures 7-8 and 7-9 the results of the simulations are presented. In Table 7-5 the number of apples with a bruise depth beyond 3 mm is given. In Figures 7-8 and 7-9 the histograms of bruise depth are shown for small and large apples respectively. In percentage and even in absolute numbers, the small apples are less damaged than the large apples.

As a general remark, the relative importance of the apple size on bruise damage could be dependent on the vibration frequency, stack height and acceleration amplitude, but this was not investigated here.

Table 7-5. Number of apples with a bruise depth higher than 3 mm as a function of apple size (vibration frequency of 4 Hz and acceleration amplitude of 0.7 g).

Radius of the apples	*Number of apples with a bruise depth higher than 3 mm.*
0.0325 m (diameter class 65/70)	34/390 (9 %)
0.045 m (diameter class 85/90)	77/140 (55 %)

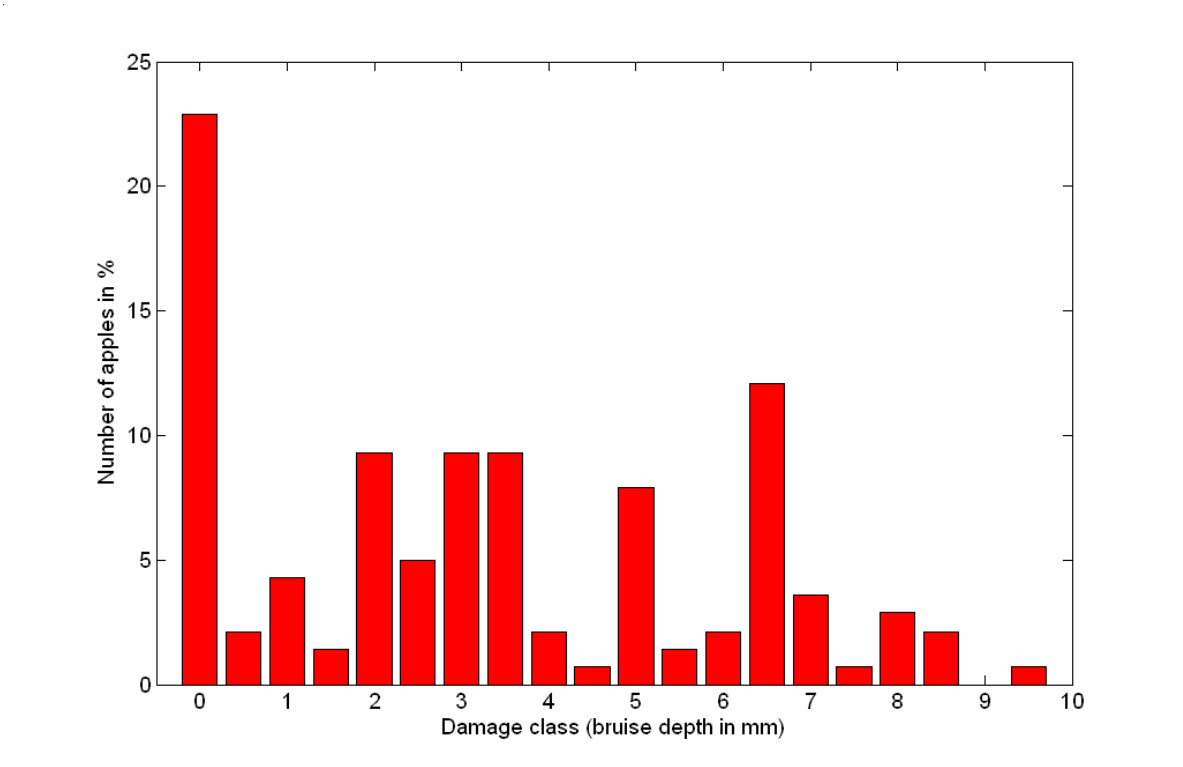

Figure 7-8. Histogram of bruise depth for diameter class 85/90 (140 apples), vibration frequency of 4 Hz and acceleration amplitude of 0.7 g.

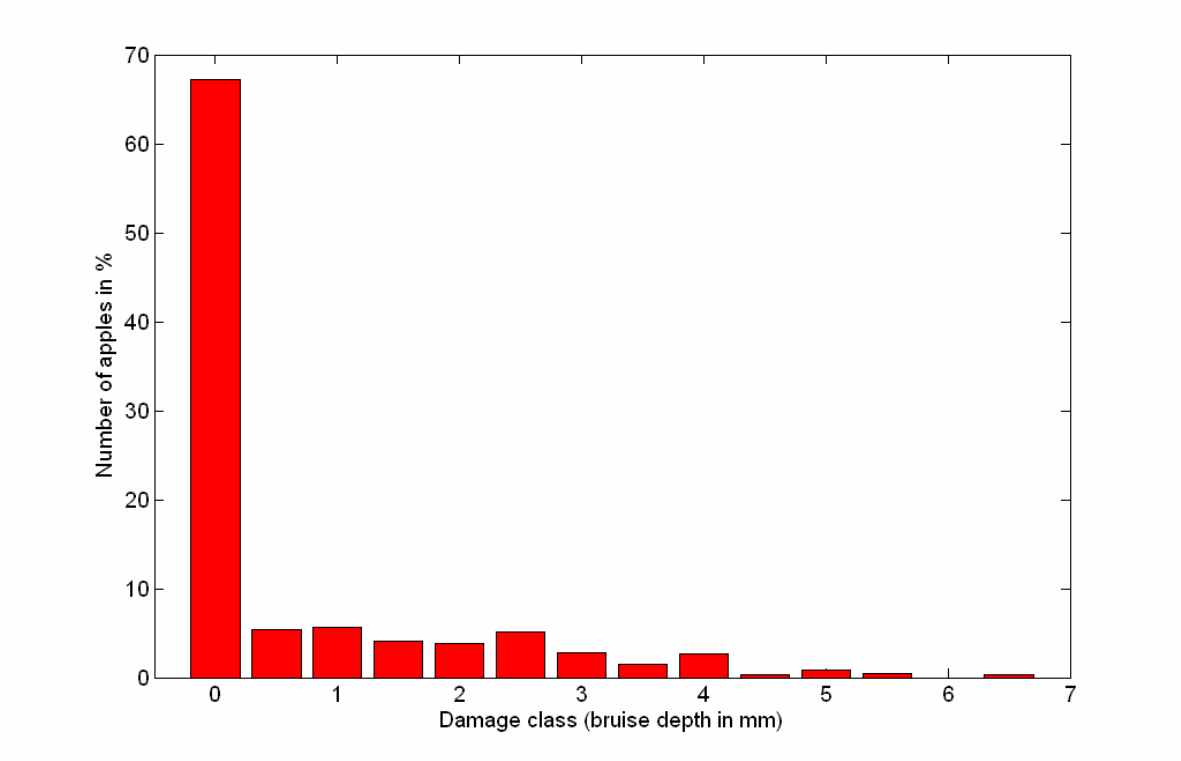

Figure 7-9. Histogram of bruise depth for diameter class 65/70 (390 apples), vibration frequency of 4 Hz and acceleration amplitude of 0.7 g.

7.3.4 Spatial distribution of apple damage in bulk bins

7.3.4.1 Introduction

From a scientific viewpoint and possibly also from a practical viewpoint, interest exists in the knowledge for the spatial distribution of mechanical damage in the bulk bins.
In literature some contradictory results concerning this topic were found. The results of Michael O'Brien are in contradiction with the results of other researchers.
O' Brien *et al.* (1965), cited by Mohsenin (1986), stated that fruit damage due to vibration gradually increases from the bottom layers to the upper layers. The work of O' Brien was based on peaches as experimental object, but his conclusions were extended to all fruit. On the other hand, other research groups (Plumbee *et al.,* 1974; Holt *et al.,* 1981, 1985; Armstrong *et al.,* 1991; Jones *et al.,* 1991) and research by Deli *et al.* (unpublished) found the opposite effect: fruit damage gradually decreases from the bottom layers to the top layers. Except for the work of Plumbee *et al.* (1974) where peaches were used, all the work was done using apples.
Simulations were executed in an attempt to clarify these contradictory results and to gain more insight in this topic.

7.3.4.2 Simulation of a real size bulk bin used in Belgium

In this simulation the vibration of a full size bulk bin (1.15x0.96x0.57m) was simulated, entirely filled with 1500 apples of diameter class 75/80.The applied input acceleration signal had a frequency of 4 Hz and an acceleration amplitude of 0.5; 0.7 and 1.1 g. In Table 7-6, the number of apples with a bruise depth beyond 3 mm is presented for all three acceleration amplitudes. Figures 7-10 to 7-12 depict the histogram of the bruise depth for all three acceleration amplitudes. In Figure 7-13 a spatial distribution is presented for apples with a minimum bruise depth of 4 mm subjected to 0.7 g acceleration amplitude. In Figures 7-14 and 7-15 a spatial distribution is depicted for apples with a minimum bruise depth of 5 mm subjected to 1.1 g acceleration amplitude with a bruise depth of 5 mm and more.
A first conclusion is that most apple damage can be found in the bottom layers and the side walls of the bulk bin confirming the experimental results of Armstrong *et al.* (1991). A second conclusion is the presence of series of apples with high damage in the core of the apple stack as seen in Figure 7-14. This calls to mind the phenomena of force chains, well known in stacking of granular materials described by for instance Cates *et al.* (1999).

Table 7-6. The number of apples with a bruise depth higher than 3 mm as a function of acceleration amplitude for a completely filled full size bulk bin (vibration frequency of 4 Hz).

Acceleration amplitude	*Apples with bruise depth above 3 mm*
0.5 g	98/1500 (6.5 %)
0.7 g	231/1500 (15.4 %)
1.1 g	1040/1500 (69.3 %)

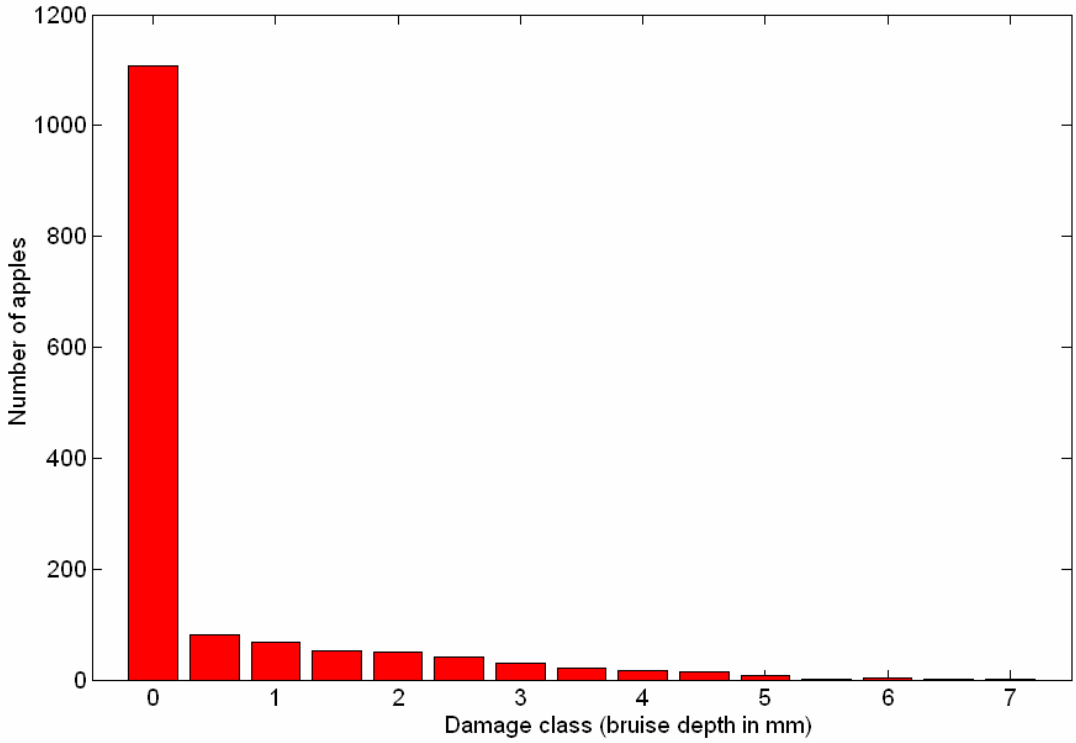

Figure 7-10. Histogram of maximum apple bruise depth for an acceleration amplitude of 0.5 g (vibration frequency of 4 Hz).

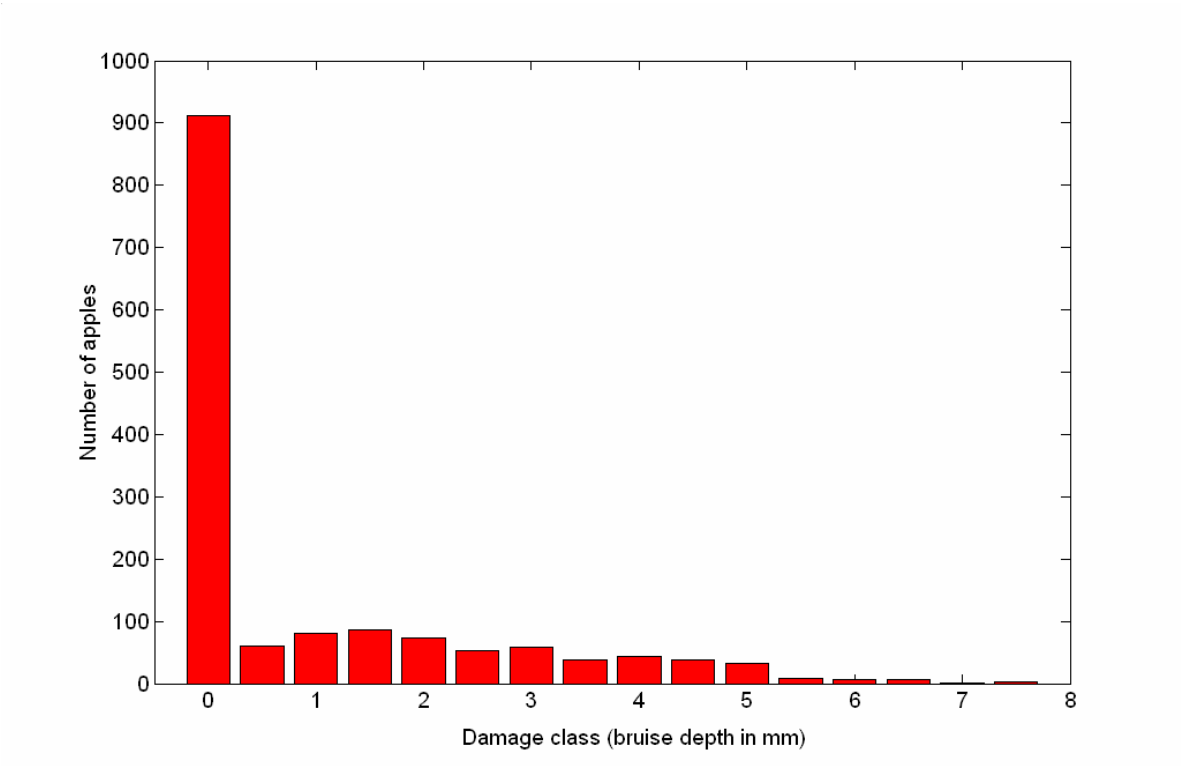

Figure 7-11. Histogram of maximum apple bruise depth for an acceleration amplitude of 0.7 g (vibration frequency of 4 Hz).

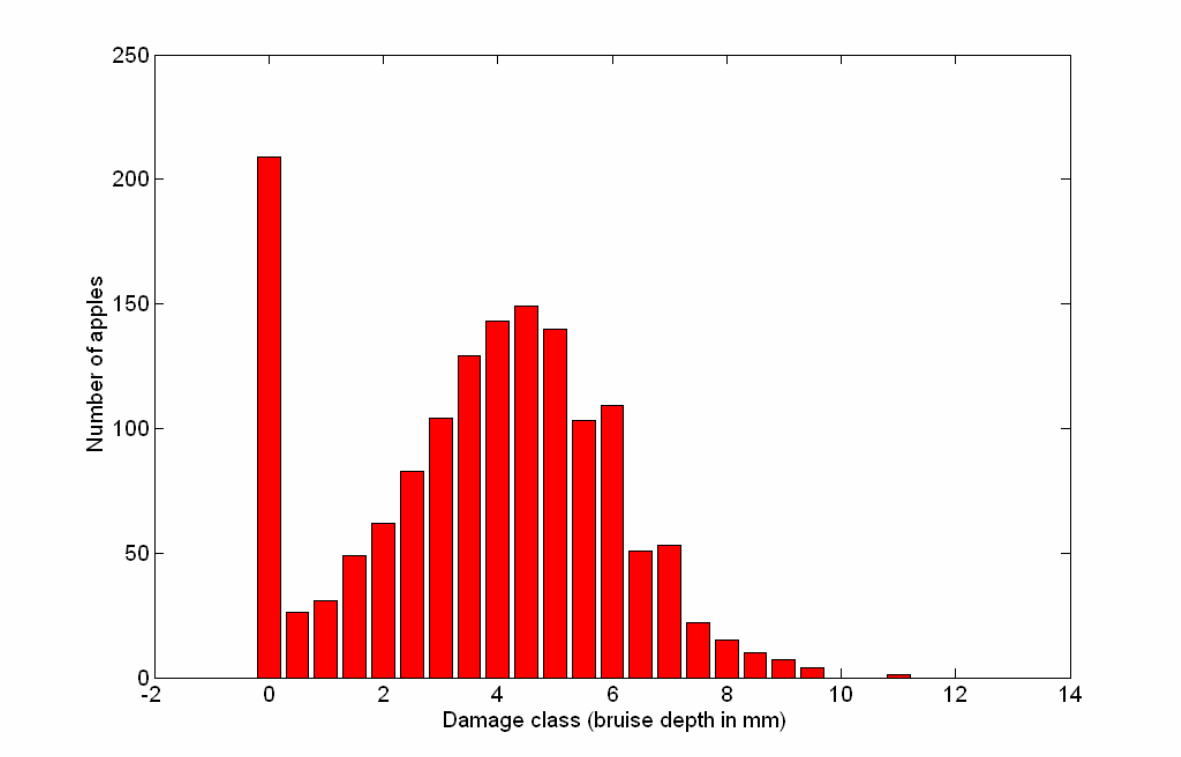

Figure 7-12. Histogram of maximum apple bruise depth for an acceleration amplitude of 1.1 g (vibration frequency of 4 Hz).

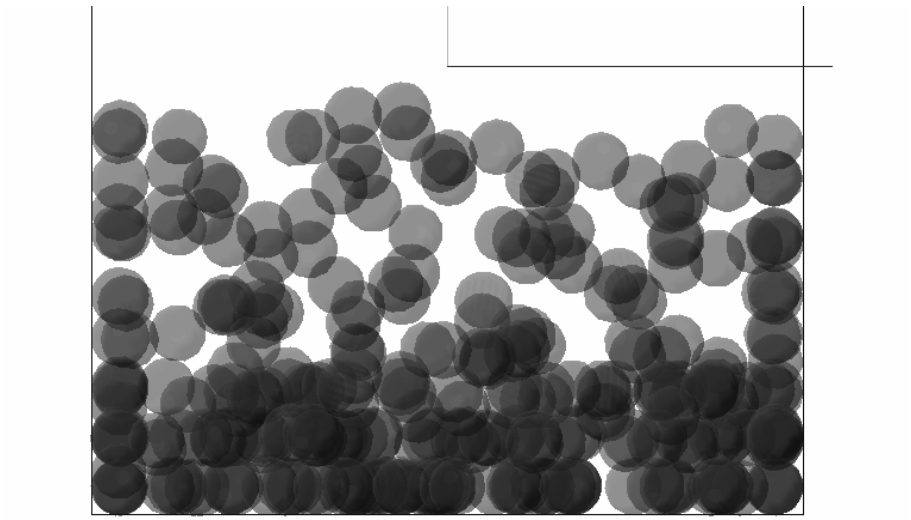

Figure 7-13. Spatial distribution of apples with a maximum bruise depth of 4 mm and higher subjected to a 0.7 g acceleration amplitude. Apples with a maximum bruise depth less than 4 mm are invisible.

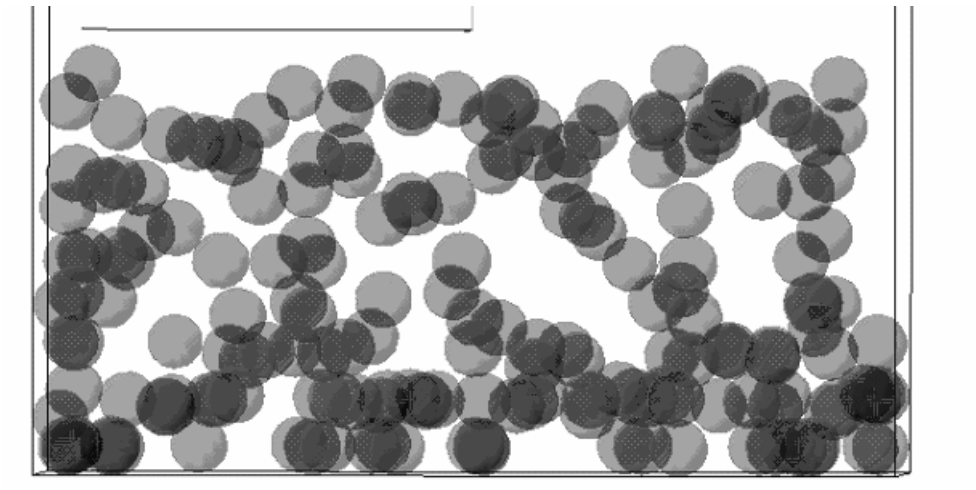

Figure 7-14. Spatial distribution of apples with a maximum bruise depth of 5 mm and higher for an acceleration amplitude of 1.1 g. Apples with a maximum bruise depth less than 4 mm are invisible.

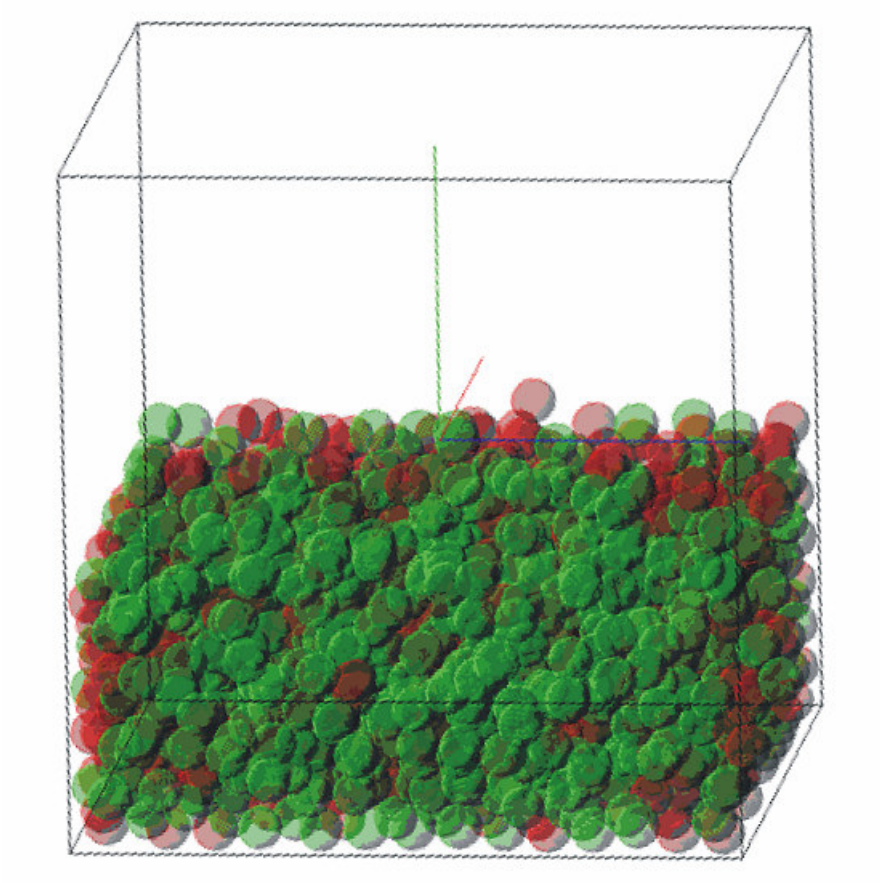

Figure 7-15. Spatial distribution of apples with a maximum bruise depth of 5 mm and higher for the acceleration amplitude 1.1 g. Red: apples with a maximum bruise depth more than 5 mm; Green: remaining apples.

7.3.4.3 Detailed study of the relation bruise damage - position

To perform the study of the relation between apple bruise damage and the position of the apple in the stack the bruise analyzing program in MATLAB (see Chapter 6) needed to be extended. The program divides the stack in 6 equal horizontal parts and calculates the average maximum bruise depth in each horizontal part. The size of the box in the simulations was 0.2x0.2x1 m. Simulations were performed with 50 and 100 particles. In the case of 100 apple simulations each horizontal part consisted out of two fruit layers. In the case of the 50 apples simulation each horizontal part consisted out of 1 layer. With 100 apples in the simulation the maximum stack height of 0.57 m was reached and with 50 apples the stack height of 0.297 m was obtained. The radius of the apples in all simulations was 0.033 m.
In Table 7-7 an 7-8 the effect of the acceleration amplitude on the spatial distribution of the average maximum bruise depth per part is presented for stack heights 0.57 m (100 apples) and 0.297 m (50 apples) respectively. The standard deviation of the maximum bruise depth for the bottom horizontal part was around 1 mm, for the other parts it was around 0.5 mm.

It can be concluded that bruise damage increases gradually from the upper layers to the bottom layers, but there are some exceptions. The top part contracted more bruise damage than the part just below it in the case of acceleration amplitudes of 1.3 g and higher. It can be noted that in case of 50 apples the differences between the layers is less pronounced than in the case of 100 apple simulation. In the case of the 50 apples simulation (situation of bulk bin filled for 50 %), starting from 1.5 g, the upper layer contracted as much bruise damage as the bottom layer while the layers in between contracted less bruise damage.

Besides the effect of the peak acceleration also the effect of the vibration frequency on spatial distribution of the apple bruise damage was investigated. Table 7-9 depicts the effect of vibration frequency on the spatial distribution of the apple bruise damage for acceleration amplitude of 1.4 g. Starting from a vibration frequency of 2 Hz the bruise damage is without exception increasing from the upper layers to the bottom layers. A vibration frequency of 1 Hz gave rise to a more or less equal distribution of the bruise damage.

Tables 7-10 and 7-11 show the effect of vibration frequency on the spatial distribution of the average maximum bruise damage per part for a constant displacement amplitude (=increasing acceleration amplitude with increasing frequency) for respectively 100 and 50 apples. The standard deviation of the maximum bruise depth for the bottom horizontal part was around 1 mm, for the other parts it was around 0.5 mm. Once again, without any exception the bruise damage is increasing from the upper layers to the bottom layers.

Remarkable is the conclusion of a different frequency for each layer where the fruit damage is at the maximum. The upper layers have a lower frequency where the fruit damage is at the maximum than the bottom layers. Even more, the frequency gradually increases from the upper layers to the bottom layers. As far as known, this phenomenon has not been described in literature before. Nevertheless, this is only of theoretical importance because most acceleration amplitudes as depicted in Tables 7-10 and 7-11 are unrealistic for field conditions.

The results of the apple bruise damage in the different simulations can be explained by two conflicting processes. These two processes are ‘peak acceleration’ and ‘weight pressure’. Higher acceleration levels of the individual particles will cause higher contact forces leading to higher damage. Higher weight pressure experienced by an individual particle (column weight) leads to higher contact forces (and damage) as well. It is known form literature (O’Brien *et al.,* 1965) and own research (Deli *et al.,* unpublished) that peak accelerations of the individual particles (apples) is increasing gradually from the bottom layers to the top layers. This peak acceleration argument has been described by O’Brien *et al.* (1965) as the only explanation for the higher mechanical damage in upper layers of peaches. However, the second process of ‘weight pressure’ is also an important factor determining mechanical fruit

damage. Bollen *et al.* (2001) mentioned this argument as the only explanation for the higher apple damage in the bottom layers, they stated that apples submitted to 'higher static forces also experience higher dynamic forces'.

In reality, both processes have their importance. Because 'peak acceleration' and 'weight pressure' are conflicting processes: peak acceleration increases with height and weight pressure decreases with height, the resulting fruit damage is highly dependent on the equilibrium of certain parameters. The conflicting results in literature are a result of this equilibrium.

The following parameters are important in this equilibrium:

1. Stack height (demonstrated)
2. Acceleration amplitude of vibration signal (demonstrated)
3. Vibration frequency (demonstrated)
4. Mass of individual particles (both intra and inter species differences)
5. Impact characteristics (spring-damper) (both intra and inter species differences)

Table 7-7. Simulation of 100 apples (stack height 0.57 m). Average maximum bruise depth [mm] per part as a function of acceleration amplitude. Sine with frequency of 4 Hz. Each part is representing two layers.

Acceleration amplitude [g]	*Part 1*[41] *(top)*	*Part 2*	*Part 3*	*Part 4*	*Part 5*	*Part 6 (bottom)*
0.8	0	0	0.067	0.635	2.699	3.494
0.9	0	0.021	0.765	1.393	2.404	3.222
1	0.004	0.038	0.814	0.974	2.400	3.796
1.1	0.289	0.373	0.666	2.335	4.666	5.311
1.2	1.547	1.678	1.444	2.758	3.989	5.468
1.3	***2.989***	2.521	3.215	4.024	5.312	6.748
1.4	***2.257***	1.974	2.330	3.266	4.873	7.123
1.5	***3.136***	3.032	3.471	4.692	6.084	7.302
1.6	***3.455***	2.932	3.592	5.317	5.437	7.401
1.7	***3.700***	3.231	3.778	4.825	6.145	8.037
2	***4.131***	3.741	4.623	5.342	6.858	7.532
3	***5.602***	5.289	6.0827	7.613	8.959	10.727

[41] In the case of the 100 particle simulation, the stacking was divided in six equal parts and each part existed out of two layers

Table 7-8. Simulation of 50 apples (stack height 0.297 m). Average maximum bruise depth [mm] per layer as a function of acceleration amplitude. Sine with frequency of 4 Hz.

Acceleration amplitude [g]	*Layer 1 (top)*	*Layer 2*	*Layer 3*	*Layer 4*	*Layer 5*	*Layer 6 (bottom)*
0.8	0	0	0	0	0.0711	0.00568
0.9	0	0	0	0	0	0
1	0	0	0	0	0.114	0.186
1.1	0.609	0.226	0.051	0	0.187	0.414
1.2	0	0	0	0.226	0.712	0.416
1.3	0.602	0.559	0.515	0.815	1.367	0.822
1.4	0.795	1.041	0.619	0.912	1.538	1.731
1.5	***4.047***	3.282	3.030	2.284	2.977	3.236
1.6	***3.551***	2.869	3.788	3.442	3.795	4.460
1.7	***4.056***	2.890	2.951	3.410	3.942	4.184
2	***5.674***	5.731	5.746	5.416	5.381	5.633

Table 7-9. Simulation of 100 apples (stack height 0.57 m). Average maximum bruise depth [mm] per part as a function of vibration frequency. Constant acceleration amplitude of 1.4 g. Each part is representing two layers.

Frequency [Hz]	*Displacement Amplitude [m]*	*Part 1 (top)*	*Part 2*	*Part 3*	*Part 4*	*Part 5*	*Part 6 (bottom)*
1	0.3478	9.92	10.28	10.30	9.37	8.55	11.69
2	0.0869	7.00	6.71	8.27	10.04	12.45	13.59
4	0.0217	2.07	4.41	4.62	5.87	6.62	9.52
6	0.0097	0.02	0.13	1.16	3.05	3.62	4.72
8	0.0054	0	0.19	1.31	2.93	3.52	4.41
10	0.0035	0	0	0.61	1.19	1.76	3.68
12	0.0024	0	0	0.17	0.49	1.07	1.98
14	0.0018	***0.12***	0	0.07	0.59	0.36	1.68
16	0.0014	0	0	0.67	0.63	0.32	1.12
18	0.0011	0	0	0.23	0.05	0.42	1.35

Table 7-10. Simulation of 100 apples (stack height 0.57 m). Average maximum bruise depth [mm] per part as a function of vibration frequency. Constant displacement amplitude (=varying acceleration amplitude). Each part is representing two layers.

Frequency [Hz]	*Acceleration amplitude*	*Part 1 (top)*	*Part 2*	*Part 3*	*Part 4*	*Part 5*	*Part 6 (bottom)*	*Average*
4	0.8	0	0	0.067	0.635	2.699	3.494	1.14
8	3.19	0.237	***0.980***	1.685	1.904	2.589	3.446	1.81
12	7.19	***0.296***	0.623	***1.881***	3.053	4.881	6.577	***2.890***
16	12.77	0	0.022	0.793	***3.578***	4.86	6.989	2.707
20	19.96	0	0	0.280	1.902	4.655	7.479	2.386
25	31.18	0	0.013	0.459	2.401	***5.431***	8.246	2.758
30	44.91	0	0	0.079	1.450	4.559	***8.304***	2.399
50	124.8	0	0	0	0.329	2.595	8.252	1.86

Table 7-11. Simulation of 50 apples (stack height 0.297 m). Average maximum bruise depth [mm] per layer as a function of vibration frequency. Constant displacement amplitude (=varying acceleration amplitude).

Frequency [Hz]	*Acceleration amplitude [g]*	*Layer 1 (top)*	*Layer 2*	*Layer 3*	*Layer 4*	*Layer 5*	*Layer 6 (bottom)*	*Average*
4	0.8	0	0	0	0	0.004	0.236	0.0046
8	3.19	***3.198***	2.943	3.048	3.76	4.305	5.893	3.858
12	7.19	2.427	***3.411***	3.104	4.192	4.73	5.569	3.906
16	12.77	1.189	2.491	***3.143***	***5.234***	5.976	7.122	***4.193***
20	19.96	0.365	1.707	2.886	4.525	***6.449***	6.909	3.807
25	31.18	0.262	0.716	0.791	2.977	5.833	***8.265***	3.144
30	44.91	0	0.158	1.454	3.200	6.097	7.565	3.079

7.3.5 Effect of fruit properties on apple bruise damage

7.3.5.1 Introduction

The statistical models of Chapter 5 were used to link peak contact force to bruise damage. In contrast to the previous simulations (section 7.3.1, section 7.3.2, section 7.3.3 and section 7.3.4), bruise *volume* instead of bruise *depth* is utilized as measure for the apple bruise damage. The reason therefore is that no statistical models were constructed to link the fruit properties with the bruise depth. In accordance with the 'maximum bruise depth of a particle (apple)' in the previous simulations 'maximum bruise volume of the particle' is used. However, because of the lack of a particle coordinate system as has been stated in the Chapter 6, the quantity 'maximum bruise volume' of a particle must be interpreted as the *single impact* maximum bruise volume. Moreover, repeated impact on a spot that was already damaged by a smaller impact will lead to a slightly larger bruise volume.

The coupling of the bruise volume with the peak contact force and the fruit properties was executed in MATLAB instead of DEMeter++. The contact force model parameters (Chapter 3) that were utilized in the DEMeter++ simulations were identical in all simulations. For example no distinction was made between the contact force model parameters of apples of 1 °C and 20°C. The influence of fruit properties (ripeness, fruit temperature, etc.) on the contact force model parameters has not been investigated. The errors made by ignoring the differences in contact force model parameters on the overall bruise damage are difficult to estimate. However, because the statistical bruise models with the impact energy and the peak contact force as independent variable indicated more or less the same effect of the fruit

properties on the apple bruise volume (see Chapter 5) simulations of apples with different fruit properties were considered meaningful.
In all simulations a full size bulk bin (1.15x0.96x0.57m) was used, filled to the maximum height with 1500 apples of diameter class 75/80. In all simulations a sine with a frequency of 4 Hz was applied.

7.3.5.2 Effect of apple temperature on bruise damage

In Chapter 5 a significant interaction between fruit temperature and peak contact force was indicated, therefore simulations were carried out using different acceleration amplitudes. The apple temperatures simulated were 1°C and 20°C and the acceleration amplitudes being applied 0.5 and 0.7 g. The simulations were performed with apples of the optimal harvest date.
In figures 7-16 until 7-19 the histogram of the maximum bruise volume is presented for all the temperature-acceleration amplitude combinations. Table 7-12 indicates the number of apples with a maximum bruise volume higher than 500 mm^3. From the simulations can be concluded that apples of 1 °C are more damaged than apples of 20 °C due to vibration during transport. This is in agreement with the results of Chapter 5. It can be concluded that at high acceleration amplitudes ('rough handling') the effect of temperature on the apple bruise damage is more pronounced.

Table 7-12. Numbers of apples with a maximum bruise volume higher than 500 mm^3 as a function of the acceleration amplitude and apple temperature.

Acceleration / fruit temperature	*1°C*	*20°C*
0.5 g	31/1500 (2.1 %)	24/1500 (1.6 %)
0.7 g	110/1500 (7.3 %)	77/1500 (5.1 %)

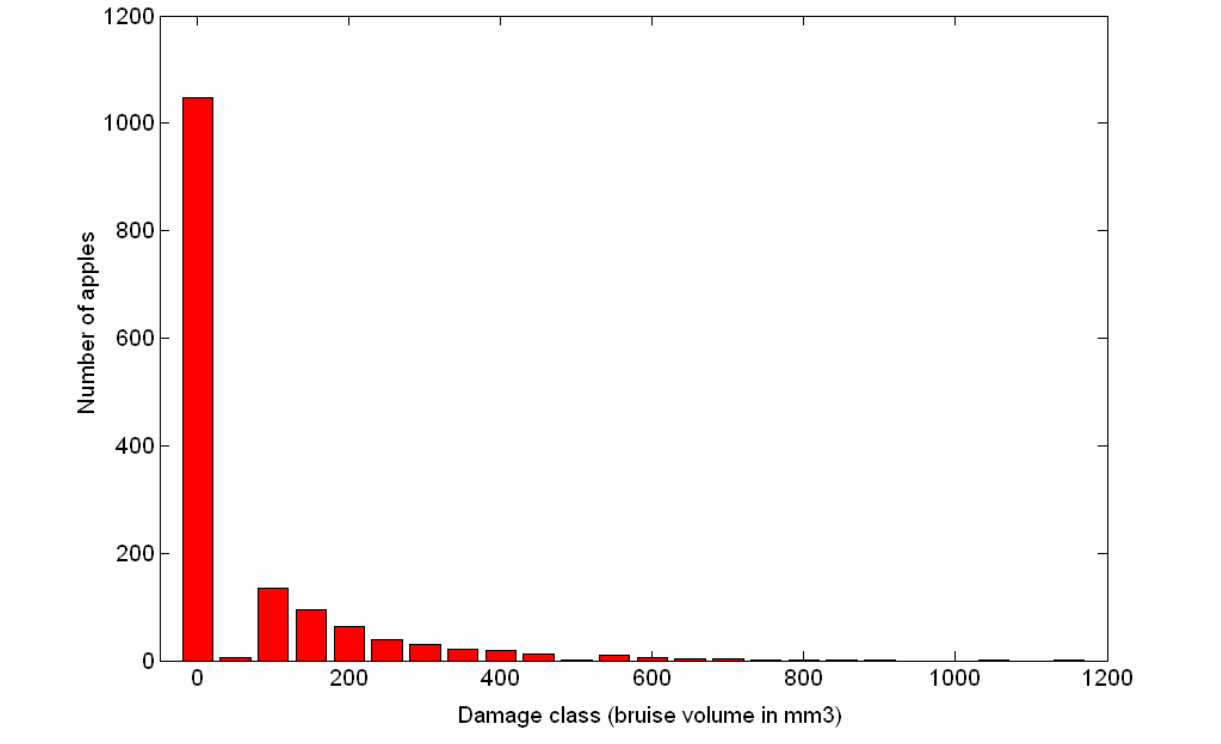

Figure 7-16. Histogram of maximum bruise volume of 1°C apples for acceleration amplitude 0.5 g.

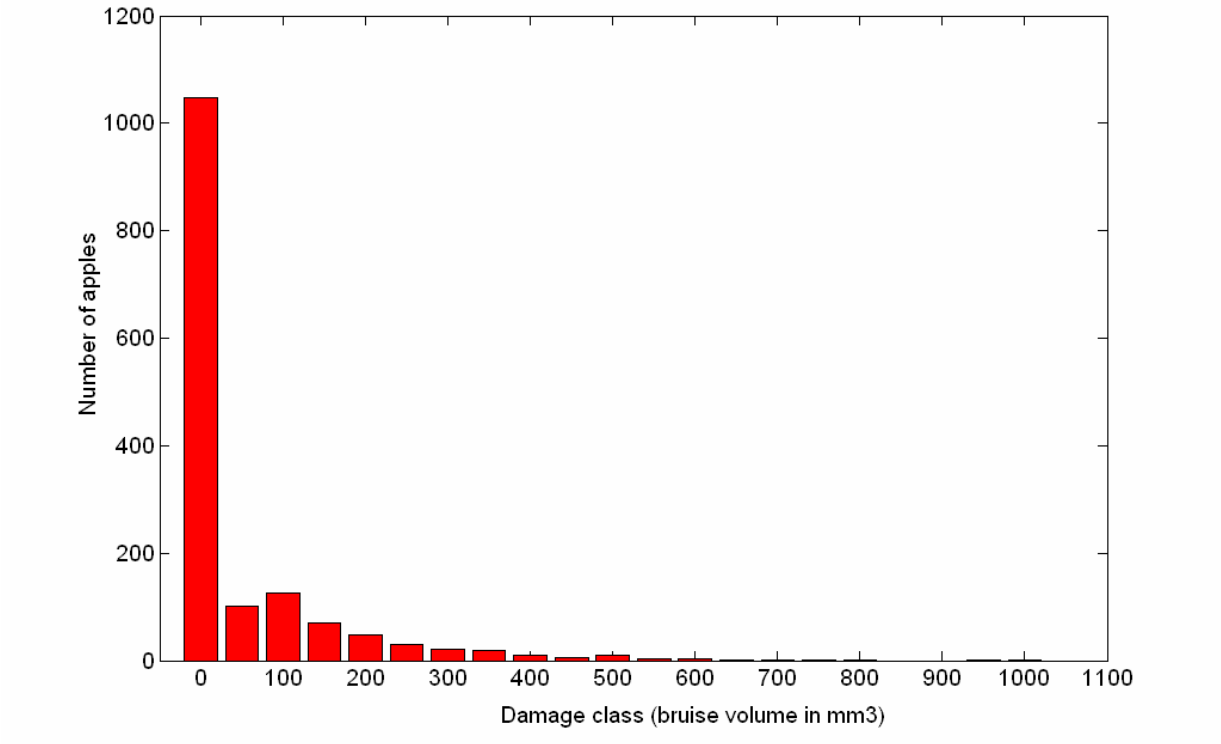

Figure 7-17. Histogram of maximum bruise volume of 20°C apples for acceleration amplitude 0.5 g.

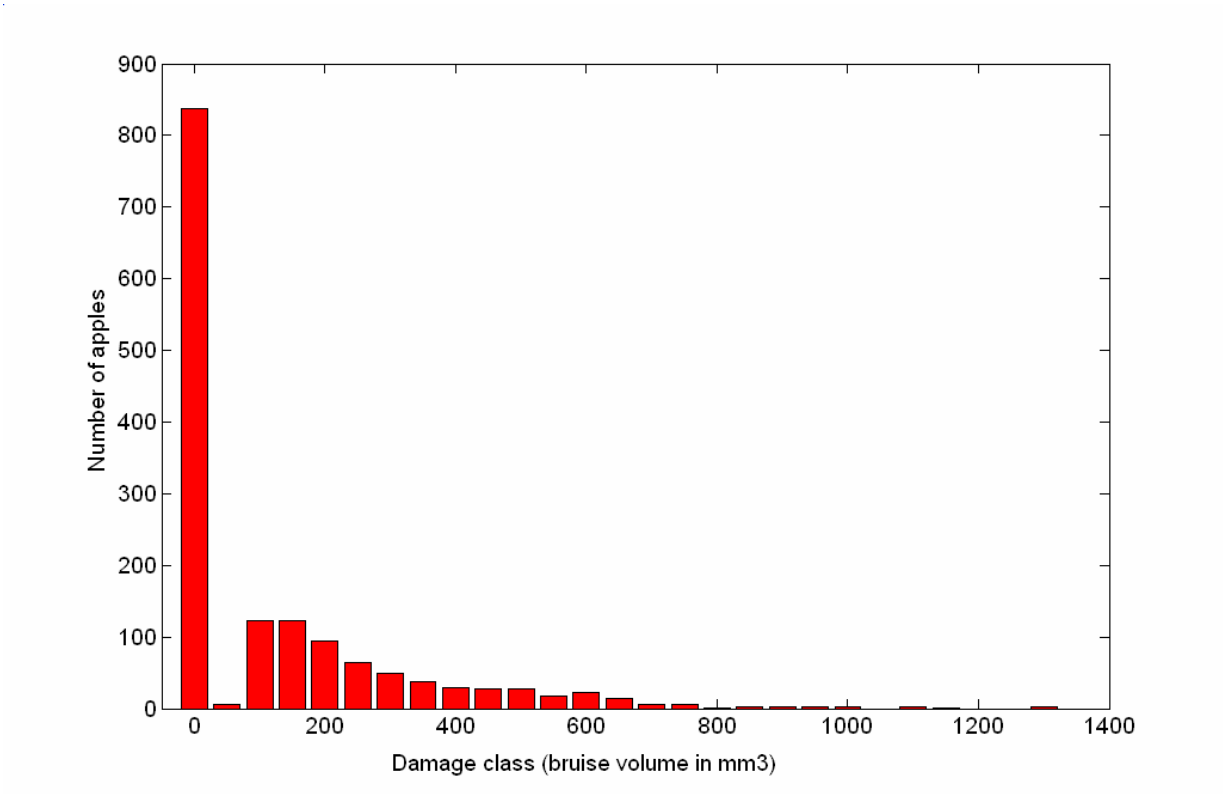

Figure 7-18. Histogram of maximum bruise volume of 1°C apples for acceleration amplitude 0.7 g.

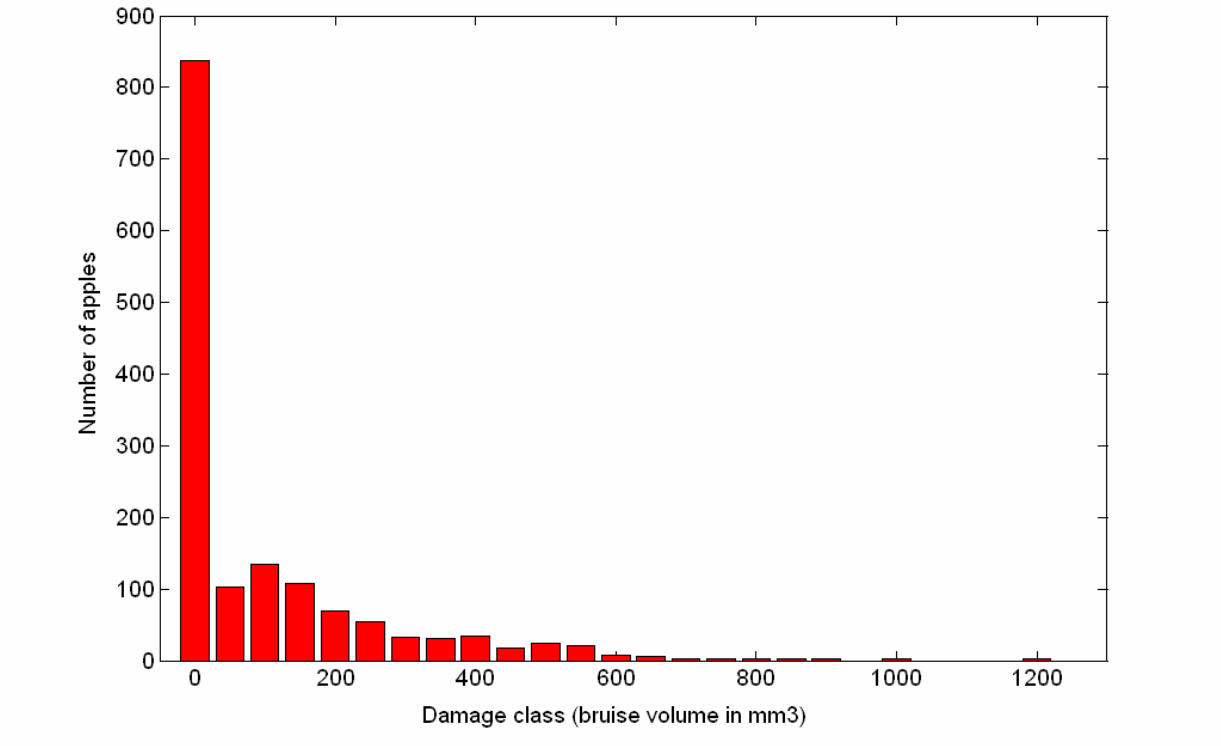

Figure 7-19. Histogram of maximum bruise volume of 20°C apples for acceleration amplitude 0.7 g.

7.3.5.3 Effect of harvest date on bruise damage

In Table 7-13, the effect of harvest date on the average maximum bruise volume is presented for three different harvest dates and two different acceleration amplitudes. Figures 7-20 and 7-21 illustrate the histogram of the maximum bruise volume at non optimal harvest date for 0.7 g acceleration amplitude. The apples in the simulation were at room temperature.

It can be concluded that early harvested apples are more easily damaged during transport, compared to apples harvested on the optimal harvest date (definition of optimal harvest date, see Chapter 5). The opposite is true for later harvested apples. The interaction of the harvest date with the peak contact force (see Chapter 5) is not pronounced because of the small difference between the acceleration amplitudes. The high standard deviation of the maximum bruise volume in Table 7-13 is due to the *bruise damage – apple position in the stack* relation described in section 7.3.4. Although the high standard deviation, significant differences in maximum bruise volume between the simulations were identified (Table 7-13).

Table 7-13. The average maximum bruise volume [mm^3] and the standard deviation of the maximum bruise volume [mm^3] as a function of harvest date and acceleration amplitude.

Acceleration	*10 days earlier*	*Optimal harvest date*	*10 days later*
0.5 g	69 (115 %)^{a} ± 135	60 (100 %)^{b} ± 122	50 (83 %)^{c} ± 107
0.7 g	128 (112 %)^{A} ± 193	114 (100 %)^{B} ± 177	96 (84 %)^{C} ± 158

a,b,c and A, B, C indicate significant difference on the 95 % level. The percentages are to compare the relative effect of early and late harvest date to the optimal harvest date (100%)

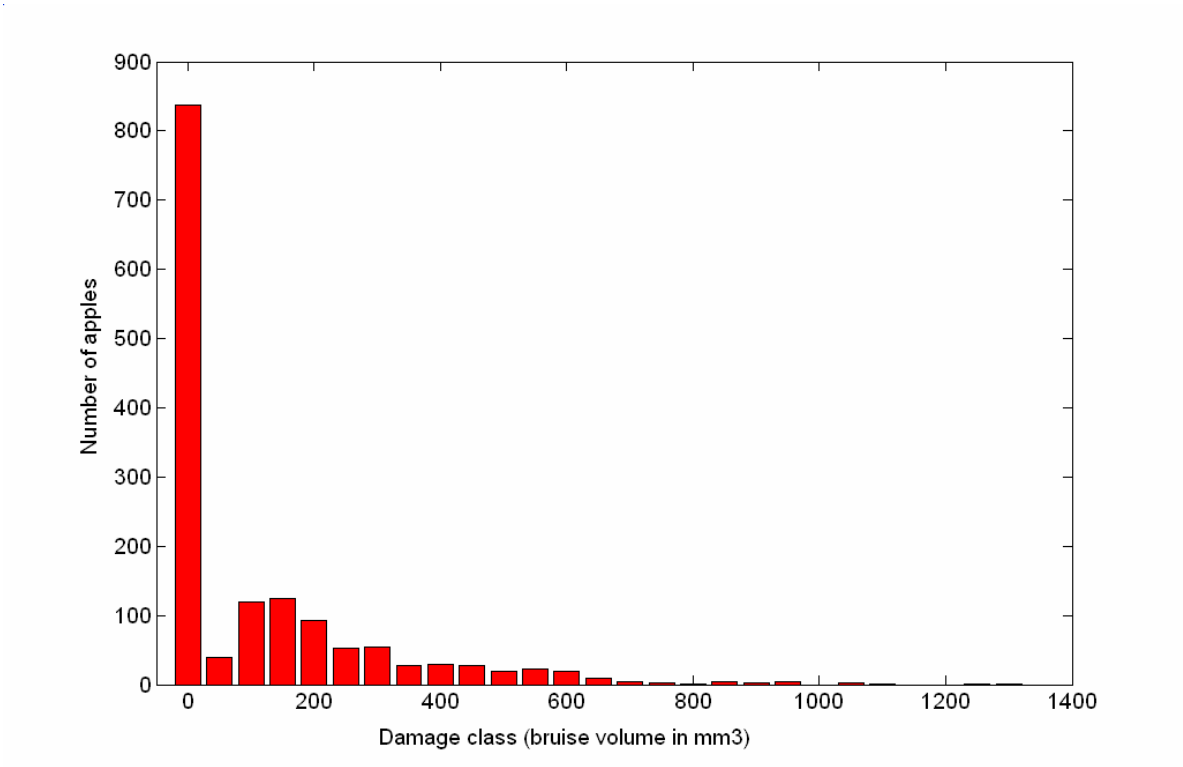

Figure 7-20. Histogram of maximum bruise volume [mm^3] for the optimum harvest date – 10 days and 0.7 g acceleration amplitude.

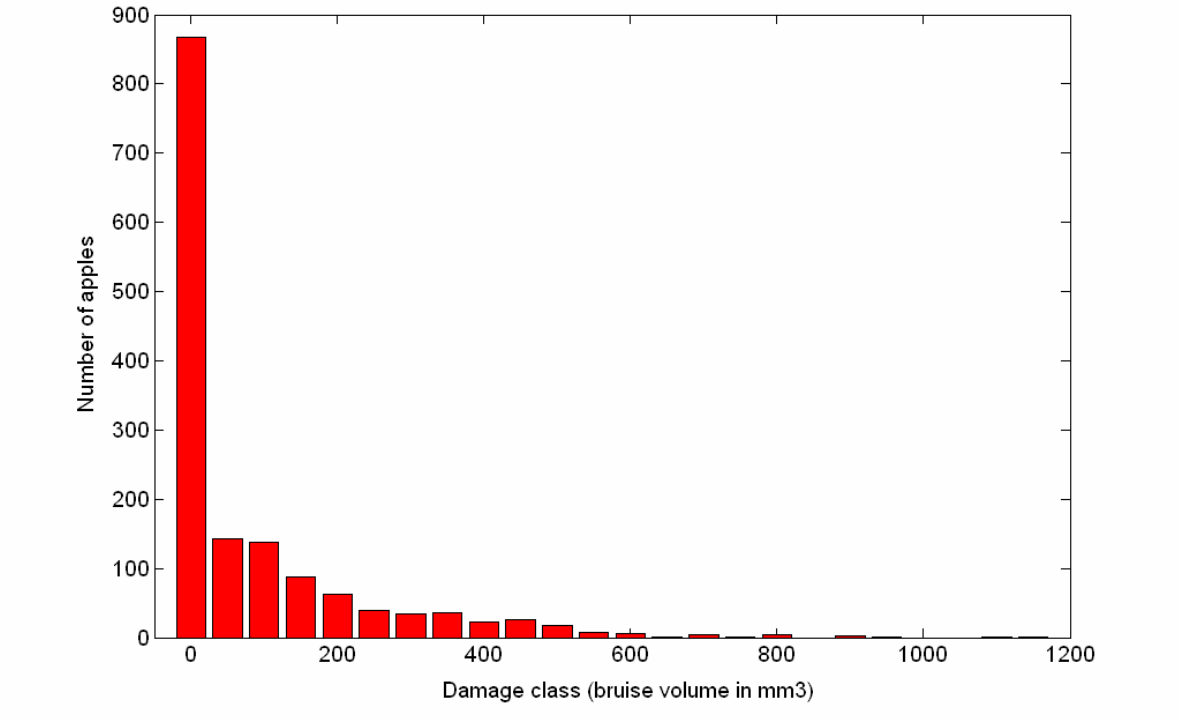

Figure 7-21. Histogram of maximum bruise volume [mm^3] for the optimum harvest date + 10 days and 0.7 g acceleration amplitude.

7.3.5.4 Effect of apple acoustic stiffness on bruise damage

In Table 7-14, the effect of acoustic stiffness on the average maximum bruise volume is presented for three different acoustic stiffness and two different acceleration amplitudes. The apples in the simulation were at room temperature and of optimal harvest date.

It can be concluded, stiffer apples at the acceleration amplitude of 0.5 g (gently handled apples) experience less bruise. In contrary, almost no effect of acoustic stiffness was noted for apples at the acceleration amplitude of 0.7 g (more roughly handled apples). This can be explained by the acoustic stiffness – peak contact force interaction of the bruise model (see Chapter 5). High acoustic stiffness has a positive effect on bruise damage for low impacts (0.5 g acceleration amplitude), for medium impacts (0.7 g) no effect of acoustic stiffness was identified. On the other hand, for high impacts the acoustic stiffness has a negative effect on bruise damage (> 0.7 g), however this has not been demonstrated here. The high standard deviation of the maximum bruise volume in Table 7-14 is due to the *bruise damage – apple position in the stack* relation described in section 7.3.4. No significant differences between the simulations were identified on the 95 % level.

Table 7-14. The average maximum bruise volume [mm^3] and the standard deviation of the maximum bruise volume [mm^3] as a function of acoustic stiffness and acceleration amplitude.

Acceleration / acoustic stiffness	*25 [$10^6 Hz^2 g^{2/3}$]*	*30 [$10^6 Hz^2 g^{2/3}$]*	*35 [$10^6 Hz^2 g^{2/3}$]*
0.5 g	75 (106 %)^a ± 137	71 (100 %)^a ± 141	67 (94 %)^a ± 147
0.7 g	134 (101 %)^A ± 187	133 (100 %)^A ± 200	131 (98 %)^A ± 214

a,A indicate no significant difference on the 95 % level. The percentages are to compare the relative effect of low and high acoustic stiffness to medium acoustic stiffness (100%)

7.3.6 Conclusions of the simulations of apple bruise damage during transport

The following conclusions can be drawn:

- Mainly, the frequency domain of 1-5 Hz is causing mechanical damage to the apples. Around the resonance frequency of 14 Hz, no peak in the mechanical damage of the apples could be observed for acceleration amplitudes occurring in practice.

- The stack height is an important factor in apple mechanical damage. A reduction of 30 % in stack height drastically decreases the overall bruise damage during bulk transport. High stack height (≅ 0.3 m and more) leads to an increase of apple bruise damage from top to bottom. Low stack height (≅ less than 0.3 m) leads to a more uniform spatial distribution of the bruise damage.

- Starting from acceleration amplitude of 1.3 g the apples of the top layer(s) contract more bruise damage than the apples in the layer(s) just below it.

- The diameter class (weight) of the apples is also an important factor in overall bruise damage during bulk transport. A bulk bin filled with small apples causes much less bruise damage than the box filled to the same height with larger apples.

- The existence of force chains (damage chains) in the core of the fruit stack has been identified.

- The positive effect of higher apple temperatures on bruise damage is more pronounced for high acceleration amplitudes (rough handling due to driver factor or bad road conditions)

- The respectively positive and negative effect of late and early harvest was illustrated for apple bulk transport.

- Stiff apples are less sensitive to bruise at low acceleration amplitudes (<0.7 g) and more sensitive at high acceleration amplitudes (>0.7 g)

7.4 Simulation of tomato bruise damage during transport

7.4.1 Introduction

Tomatoes in standard packaging (EPS crates, 27x36.5 cm) were used in the simulations since they are common practice in Belgium. The parameters of the Kuwabara and Kono normal contact force model for tomatoes as determined in Chapter 3 were applied in the simulations. The damping of the EPS crate was neglected, with the consequence that the absorbed energy of the tomatoes in the simulations was overestimated. In anticipation of the application of more complex (and accurate) tangential contact force models (Chapter 4) a simplified tangential contact force model was utilized (model 6.2, Chapter 6). In the simulations, until present, no distinction was made between the compartments and partitions of the tomatoes. The average normal contact force parameters of compartment and partition were applied (Chapter 3). Statistical models of Chapter 5 were utilized to link peak contact force and fruit properties with the absorbed energy as measure for the bruise damage. However, a drawback of using the statistical models including the peak contact force can be mentioned. In Chapter 5, it was demonstrated that peak contact force itself is highly influenced by tomato fruit properties, leading to a distorted influence of the fruit properties on the absorbed energy. The solution for DEM is to apply the contact force models with the parameters depending on the fruit properties. Research on this topic is still ongoing.
The application of statistical models including the impact energy is an alternative solution. However, the problem with these models, as stated before, is that they cannot be generalized to tomato-tomato impact and to impact with soft materials. An approach is proposed here that is a temporally solution until data about the dependency of contact force model parameters on tomato fruit properties become available. The normal contact force model parameters (Chapter 3) were determined on a batch of tomatoes in the red stage and the experiment was executed with tomatoes at room temperature[42]. As a consequence, the contact force model parameters used in the simulation are valid for tomatoes in the red ripeness stage at room temperature.

[42] Unfortunately, not the same batch of tomatoes was used for the determination of the statistical bruise model.

The following statistical relation between peak contact force and impact energy was derived, based on the data of Chapter 5 (statistical bruise model):

$$Ei = \frac{PF - 7.08 + 0.048a - 233r}{178.4 - 1.221a} \qquad (7.2)$$

with Ei impact energy [J]
PF peak contact force [N]
a colorimetric coordinate indicating tomato ripeness [-]
r tomato radius of curvature [m]

Equation (7-2) is valid for tomatoes at room temperature. Equation (7-2), with colorimetric parameter a^* of 18.17 (red tomatoes) and the radius equal to the tomatoes in the simulation, was applied to the peak contact force matrix obtained from the simulations to calculate the corresponding impact energies. The obtained impact energies are those for red tomatoes at room temperature. The statistical models including the impact energy were subsequently applied to this data to calculate the effect of tomato fruit properties on the absorbed energy. It must be noted that by this procedure, the impact energy is also corrected for tomato-tomato impact[43].

The results of the simulated effect of tomato fruit properties on absorbed energy are presented applying the statistical model including the peak contact force and the model including the impact energy. As mentioned above, equation (7-2) was utilized to obtain the impact energies for the latter statistical model.

Unless noted differently, a sine with a frequency of 4 Hz was applied in the simulations and the bruise damage of 50 tomatoes each with a diameter of 0.030 m was simulated. This is equal to ≅ 6 kg of tomatoes per EPS crate, which is common in Belgium.

In the simulations realistic radii of curvature of tomatoes and ripeness indication parameter colorimetric parameter a^* were utilized:

Table 7-15. Overview of realistic radii of curvature, colorimetric parameter a^* and acoustic stiffness S in the simulations.

Parameter	*Average and standard deviation*	*Lower limit*	*Upper limit*
r [m]	0.034 ± 0.0043	0.0297	0.0383
a^* [-]	10.69 ± 7.48	3.21	18.17

In this work no relationship between tomato absorbed energy and visible bruise damage was investigated (and also literature data are rare). Preliminary results of Van linden

[43] The peak contact force is calculated depending on tomato-tomato or tomato-wall impact by using mechanical contact theory, see Chapter 3

(unpublished) indicate the presence of visible damage (measured more than 24 h after impact) at the absorbed energy level of 0.02 J, although not for every tomato in a uniform batch. Own research (section 3.4) using the CHMI method indicated a shift in the force-time curve, possibly an indication of mechanical damage, starting from 0.01 J impact energy (≅ absorbed energy because the restitution coefficient is very low). The force-time shift was associated with a perceptible dent in the tomato, although it is not sure this dent is still present some time after the impact. Nevertheless, the preliminary knowledge of the relationship absorbed energy – tomato bruise damage is useful in interpreting the obtained tomato absorbed energy levels in the simulations.

7.4.2 Effect of tomato temperature on bruise damage (absorbed energy)

Tomatoes of average ripeness (a^*=10.69) were simulated. Since the statistical analysis elaborated in Chapter 5 indicated an interaction between temperature and peak contact force, the simulations were performed at different acceleration amplitudes. The results are given in Table 7-16. The high standard deviation of the maximum absorbed energy in Table 7-16 is due to the *bruise damage – tomato position in the stack* relation described in section 7.3.4 for apples.

Table 7-16. Average maximum absorbed energy of tomatoes [J] and the standard deviation of the maximum absorbed energy [J] as a function of temperature and acceleration amplitude for two different statistical models including the impact energy and the peak contact force.

	1.2 g		*1.5 g*	
Temperature / acceleration	*Peak contact force model*	*Impact energy model*	*Peak contact force model*	*Impact energy model*
15 °C	0.0055 J[a] ± 0.0082 J	0.0036 J[A] ± 0.0064 J	0.0158 J[a] ± 0.0154 J	0.0131 J[A] ± 0.0149 J
20 °C	0.0045 J[a] ± 0.0071 J	0.0036 J[A] ± 0.0064 J	0.0136 J[a] ± 0.0139 J	0.0131 J[A] ± 0.0149 J

a, A indicate no significant difference on 95 % level

No effect could be noticed of temperature on absorbed energy for the statistical model including the impact energy. This is in agreement with Chapter 5 where only a limited effect of tomato temperature was noticed for this model. However, for the model including the peak contact force a 15 % lower absorbed energy was noticed for the 20 °C tomatoes (not significant). Probably this effect is exaggerated because the contact force parameters (and as a consequence also the peak contact force) are different between 15°C and 20°C tomatoes. Another more general conclusion is that tomatoes of average size in an EPS crate absorb limited energy below 1.2 g peak acceleration.

7.4.3 Effect of tomato ripeness on bruise damage (absorbed energy)

This simulation were performed with tomatoes of 15 °C and two ripeness extremes were simulated Because the statistical analysis (Chapter 5) indicated an interaction between ripeness and peak contact force the simulations were performed at different acceleration amplitudes. The results are presented in Table 7-17. The high standard deviation of the maximum absorbed energy in Table 7-17 is due to the *bruise damage – tomato position in the stack* relation described in section 7.3.4 for apples.

Table 7-17. Average maximum absorbed energy of tomatoes and the standard deviation of the maximum absorbed energy [J] as a function of ripeness and acceleration amplitude for two different statistical models including the impact energy and the peak contact force.

	1.2 g		*1.5 g*	
acoustic stiffness / acceleration	*Peak contact force model*	*Impact energy model*	*Peak contact force model*	*Impact energy model*
3.21	0.0046 J[a] ± 0.0071 J	0.0036 J[A] ± 0.0064 J	0.0138 J[a] ± 0.0142 J	0.0131 J[A] ± 0.0148 J
18.17	0.0064 J[a] ± 0.0093 J	0.0036 J[A] ± 0.0064 J	0.0178 J[a] ± 0.0166 J	0.0132 J[A] ± 0.0150 J

a, A indicate no significant difference on 95 % level

No effect of ripeness on absorbed energy for the statistical model including the impact energy could be derived. This is in agreement with Chapter 5 where only a limited effect of tomato ripeness was identified for these models. However, for the model including the peak contact force a 25 % lower absorbed energy was noticed for the unripe tomatoes (not significant). Probably this effect is exaggerated because the contact force parameters (and as a consequence also the peak contact force) are also dependent on tomato ripeness.

7.4.4 Effect of tomato size on bruise damage (absorbed energy)

In the simulation tomatoes of average ripeness (a^*=10.69) and temperature of 15 °C were utilized. Simulations were performed with two extremes in tomato size, but the number of tomatoes was adapted to obtain the same mass of tomatoes in the EPS crate (5.9 kg). To achieve this 54 tomatoes of radius 0.0297 m were needed and 25 tomatoes of radius 0.0383 m. Table 7-18 describes the average maximum absorbed energy as a function of tomato radii. Figures 7-22 and 7-23 depict the histogram of the maximum absorbed energy for both simulations for the statistical model including the impact energy. The high standard

deviation of the maximum absorbed energy in Table 7-18 is due to the *bruise damage – tomato position in the stack* relation described in section 7.3.4 for apples.

Table 7-18. Average maximum absorbed energy of tomatoes and the standard deviation of the maximum absorbed energy [J] as a function of radius for two different statistical models including the impact energy and the peak contact force.

	1.2 g	
Radius / acceleration	*Peak contact force model*	*Impact energy model*
0.0297 m (54 tomatoes)	0.0029 J (100 %)[a] ± 0.0051 J	0.0013 J (100 %)[A] ± 0.0032 J
0.0383 m (25 tomatoes)	0.0248 J (855 %)[b] ± 0.0201 J	0.0230 J (1769 %)[B] ± 0.0210 J

a,b and A, B indicate significant difference between absorbed energy on the 95 % significance level. The percentages indicate the relative importance of the tomato radius on the absorbed energy

A substantial effect of tomato radius on absorbed energy was noticed for both statistical models. The effect of tomato radius on absorbed energy occurs at three levels:

1. Tomato radius has an effect on the tomato mass while the latter influences the magnitude of the contact forces
2. The contact radius has an effect on the contact force model parameters (see Chapter 3)
3. The contact radius has an effect on the statistical relation between peak contact force/impact energy and the absorbed energy (see Chapter 5)

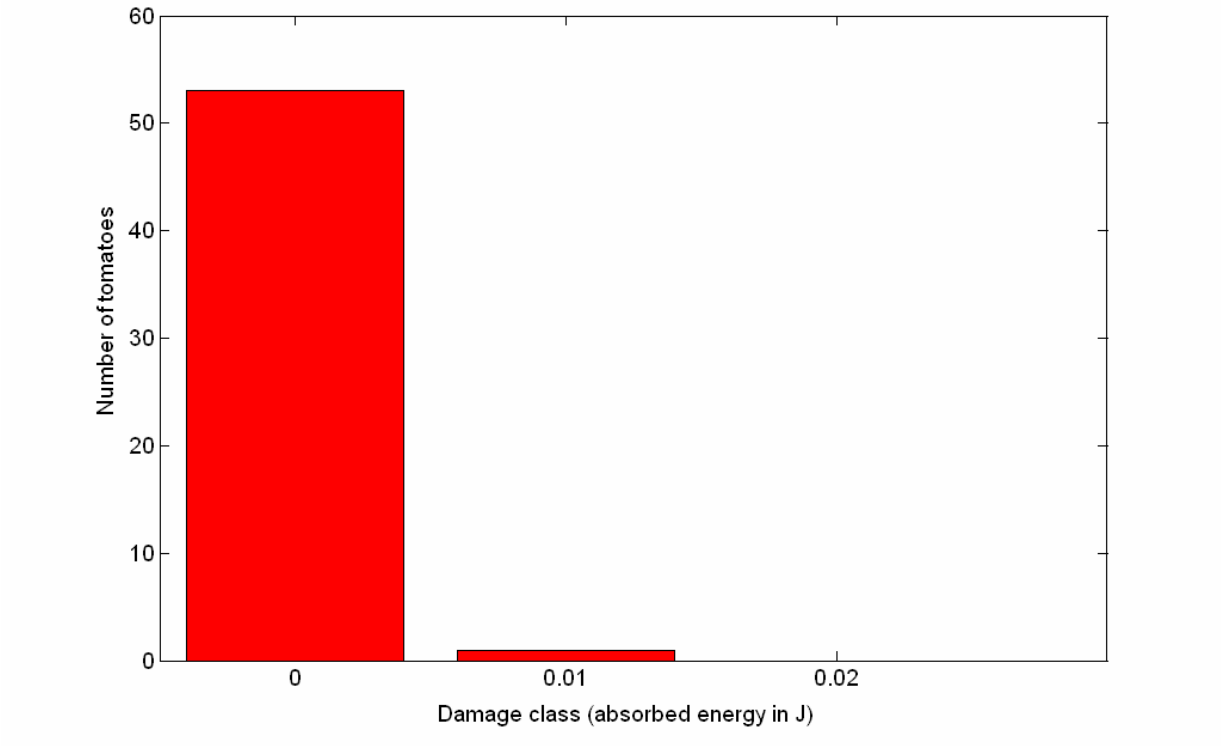

Figure 7-22. Histogram of maximum absorbed energy of tomatoes with radius of curvature 0.0297 m.

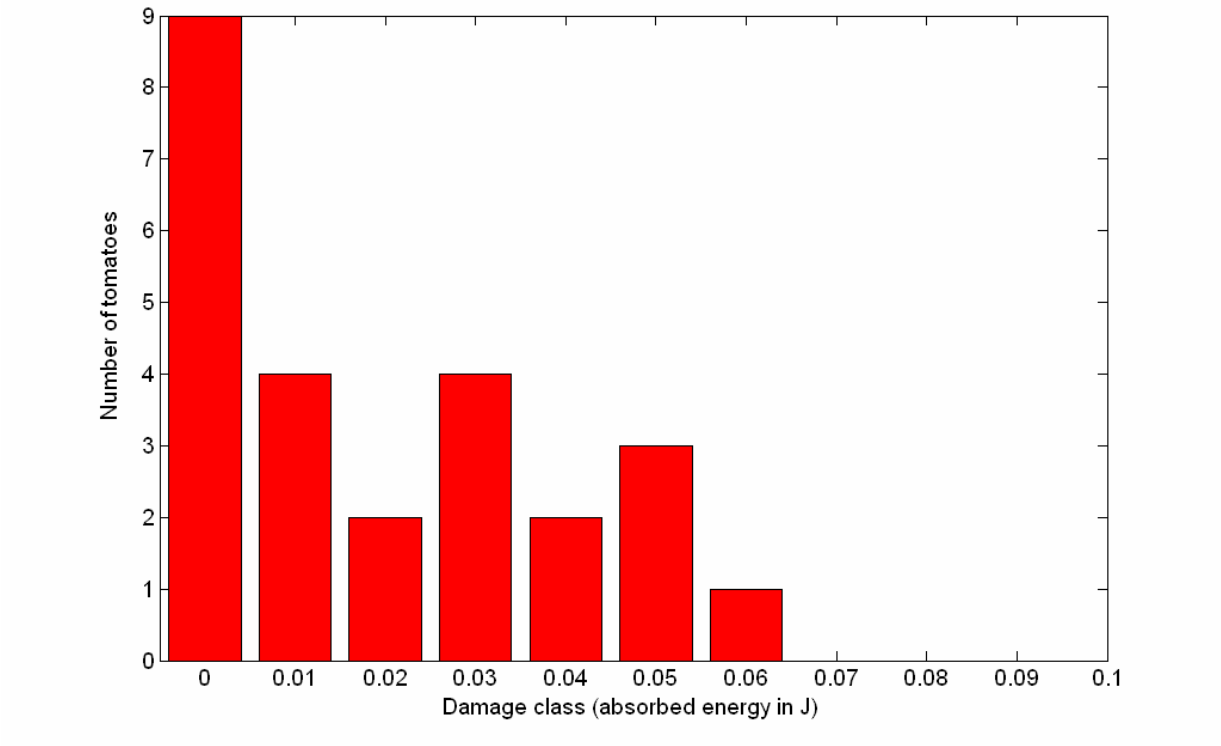

Figure 7-23. Histogram of maximum absorbed energy of tomatoes with radius of curvature 0.0383 m.

7.4.5 *Effect of vibration frequency on bruise damage (peak contact force)*

Unlike the previous simulations, the peak contact force was used to indicate tomato bruise damage. The acceleration amplitude in the simulations was 1 g. The results are represented in Figure 7-24.

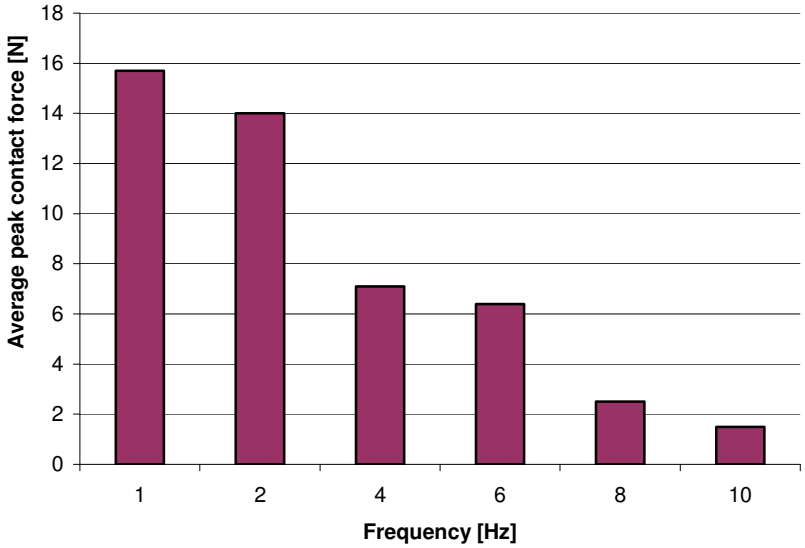

Figure 7-24. Average maximum peak contact force as a function of vibration frequency

It can be concluded that, in contrast to apples (Figure 7-1), frequencies higher than 4 Hz still have a considerable effect on the peak contact force and therefore also on the bruise damage. Beyond 8 Hz the effect on the peak contact force also declines for tomatoes.

7.4.6 *Conclusions of simulations of tomato bruise damage during transport*

- The effect of the tomato temperature and tomato ripeness on tomato bruise damage is limited.

- On the other hand a huge effect of the size of the tomatoes on the tomato bruise damage was identified: larger tomatoes absorb much more energy than smaller tomatoes. The effect of size is more pronounced for tomatoes than for apples.

- Vibration frequencies up to 8 Hz are mostly damaging the tomatoes.

7.5 General conclusions

This chapter was dedicated to a case study in which both the influence of mechanical parameters and fruit properties on vibration damage of apples and tomatoes were investigated. More specifically, the influence of bulk transport of apples in bins and EPS crates of tomatoes on bruise damage was investigated. As acceleration input a sine in the vertical direction was utilized. The same 'shaking box' DEMeter++ application was used as for the validation purposes in Chapter 6. Appropriate contact force model parameters and bruise prediction models described in previous chapters have been applied. The investigated mechanical parameters were peak acceleration and frequency of the vibration signal, stack height and size of the apples and tomatoes. The fruit properties under research were temperature, ripeness, acoustic stiffness and harvest date (only apples). It was identified that lowering the stack height of the apples below the commercial stack height leads to a strong reduction in the bruise damage.

Both for apples and tomatoes a strong effect of the fruit size on the bruise damage was identified. A 18 times higher average maximum absorbed energy was simulated for a EPS crate that was filled with 6 kg large tomatoes (radius of curvature of 0.383 m), compared to the crate filled with 6 kg small tomatoes (radius of curvature of 0.297 m). The EPS crate was shaken with a sine with a peak acceleration of 1.2 g. For a bulk bin, vibrated by a vertical sine with peak acceleration of 0.7 g, that was entirely filled with large apples (radius of curvature of 0.045 m) 55 % of the apples had a bruise depth beyond 3 mm, compared to only 9 % for a bulk bin entirely filled with small apples (radius of curvature of 0.0325 m).

Simulations indicated that vibration frequencies beyond 5 Hz for the apples and 8 Hz for tomatoes are not very harmful to the fruits.

In contrast to the mechanical parameters only slight effects of the fruit properties on the fruit vibration damage were identified, especially for the tomatoes.

A schematic overview of the effect of mechanical parameters and fruit properties on apple bruise damage is described in section 7.3.6 and for tomatoes in section 7.4.6.

For apples a more detailed study was performed. In the case of acceleration amplitudes occurring in practice (below 2 g), the apple bruise damage gradually decreases with increasing vibration frequency. This statement is confirms most studies described in literature. The phenomenon of a resonance frequency (described for most fruits by O'Brien, 1965, except apples) was only clearly identified for high acceleration amplitudes not occurring in practice.

In addition a study was performed to investigate the relation between apple positions in the stack and bruise damage. It was demonstrated that the position - bruise damage relation

depends on the acceleration amplitude, vibration frequency and stack height. Due to the effect of the stack height on the distribution of the bruise damage, simulations were performed with the maximum bulk bin stack height (0.57m) and simulations with half-full bins (stack height 0.257m). For full bulk bins the apple bruise damage gradually increased from top to bottom for peak acceleration below 1.3 g for all frequencies. For higher peak accelerations (rare in practice) the top layers contracted slightly more bruise damage than the layers just below. The apple bruise damage of the other layers, however, still gradually increased from top to bottom. On the other hand a more or less uniform distribution of the apple bruise damage was identified in the half-full bins. The distribution of the bruise damage can be explained by the balance between two conflicting processes: the column weight of the apples and the peak acceleration of the individual apples.

It has been argued that extrapolation of results concerning the relation position - bruise damage found for one fruit type to other fruit types (as it is done in literature before) is not allowed since behaviour (and damage) is dependent on the mass and impact characteristics (stiffness and damping) of the considered fruit. The existence of damage chains within the core of the apple stack was also identified. This is in accordance with the well-known force chains in bulk materials.

Chapter 8

General conclusions and future work

8.1 General conclusions

For most fruit types, including apples and tomatoes, bruise is the most common type of postharvest mechanical injury. Besides the direct effect of fruit bruising on fruit quality, and, hence, the visual quality appreciation by the consumer, an important indirect effect can be identified as damaged tissue is a good avenue for entrance of decay organisms, which decrease the shelf-life of the fruit drastically.

Forty years of research on the problem have been performed, and although the incidence of bruising has decreased compared to forty years ago, the problem is still one of the major problems in the fruit business. The reason for this is that the causes and mechanisms of impact and vibration damage are complex and interrelated: There is (1) the source, magnitude and nature of the impact and vibration input, (2) the influence of the fruit environment, like containers and packaging materials, (3) the influence of individual and neighboring fruit in modifying the impact or vibration input and (4) the susceptibility of the fruit to damage, as a function of maturity, size, temperature, etc.

Almost all research done so far was concentrated on a subcategory of one of these four aspects. Very few studies were performed using an integrated approach[44]. As a consequence of the ignorance of the interrelated aspects, frequently researchers obtained conflicting results and industry experience of bruising and scientific study also leaded to inconsistent

[44] Schoorl and Holt (1982ab) and Jones *et al.* (1991) used an integrated approach for the vibration damage during transport

results (reducing the credibility of both groups in the other eyes) (based on Hilton, 1994, Studman, 1997).
In this work the Discrete Element Method (DEM), a particle based simulation technique, was applied to investigate the fruit bruise damage during transport and handling. DEM can be considered as an integrated approach in the study of the fruit bruise problem.

In a first chapter, the state of the art of the apple and tomato bruising in general and DEM in agriculture and food industry was outlined. It can be concluded that although DEM has been used to a large extent for engineering materials (and is now in a "booming phase"), its application for agricultural materials is very limited especially for soft materials like fruits. Due to the viscoelastic nature, DEM of fruits is in fact more complicated than for most engineering materials. A major part of this work was an attempt to cope with the viscoelastic nature of the fruits for its use in DEM.

In Chapter 2 a general description of DEM was presented and the structure of a typical algorithm was outlined. However, the main focus of this chapter was on contact force models, an essential part of DEM. It was indicated that the Kuwabara and Kono (1987) normal contact force model for viscoelastic spheres, further developed by Brilliantov *et al.* (1996ab), is the most appropriate normal contact force model to date for DEM simulation of fruits. The Kuwabara and Kono model for viscoelastic spheres is the most physically correct model for the impact of apples and tomatoes below the bioyield point (= contact pressure beyond plastic deformation starts to occur). Also beyond the bioyield point the Kuwabara and Kono model is still capable to describe the real impact behaviour because the damping parameter can capture besides the viscous dissipation also the plastic dissipation. However, in the latter case (combination of viscous and plastic dissipation) a physical link of the damping parameter with material properties is missing. In addition, in this chapter an extension of the Kuwabara and Kono normal contact force model for impact of spheres with non identical material properties (different elasticity and viscosity) was presented.
The physically most realistic tangential contact force model for elastic spheres of Mindlin and Deresiewicz (1953) was extended to viscoelastic spheres by adding a viscous term. More details of this model are provided in Dintwa *et al.*(2004ab).

In Chapter 3 the pendulum device, based on the construction of Baheri (1997), was outlined. The pendulum was upgraded to measure impact quantities (contact force, displacement and displacement rate) needed to determine the normal contact force model parameters. It was indicated that direct measurement of the displacement during impact by an optical

incremental encoder is more accurate than double integration of the acceleration signal. An experimental technique was developed for fruits to derive the parameters (damping and stiffness) of the Kuwabara and Kono contact force model. The technique was a nonlinear least squares data fitting technique, determining the parameters by minimizing the error between the experimental impact quantities measured by the pendulum device (contact force, displacement and displacement rate) and those determined by solving the Kuwabara and Kono equation of motion. It was demonstrated that both the effective radius of curvature at the location of impact and impact velocity have a significant effect on the model parameters.

In Chapter 4 an experimental technique was described to determine the model parameters of a viscoelastic extension of Mindlin and Deresiewicz (1953) tangential contact force model. The material parameters of apples needed for the model (shear modulus, dissipative parameter, and dynamic friction coefficient between apples) were determined by use of a rheometer, a device normally intended to measure viscoelastic properties of fluids and semi-fluids. In addition, by means of a rheometer also the viscoelastic extension of the Mindlin and Deresiewicz tangential contact force model has been validated.

In Chapter 5 bruise prediction models, essential for the utility of DEM in the bruise damage problem, were described. Bruise prediction models relate the contact force during impact, as modelled by DEM, with the real damage. Chapter 5 is the only chapter that also provided a contribution to the bruise damage problem apart from DEM. The bruise susceptibility of apples cultivar ‘Jonagold’ and tomatoes cultivar ‘Tradiro’ was determined using the pendulum device, described in Chapter 3. Multiple linear and nonlinear regression models were developed to link ‘fruit properties’, like ripeness, acoustic stiffness, fruit temperature, radius of curvature, harvest date (only apples), location of impact (partition or compartment of tomato) with the bruise damage. Bruise volume was taken as a measure for apple bruise. Absorbed energy was taken as a measure for bruising of tomatoes, because no objective method is available yet to measure the bruise size of tomatoes.
Besides significant main effects also significant interactions between fruit properties were identified, that were not described in literature before. Besides the mutual interactions between fruit properties also significant interactions between some fruit properties and the degree of bruising (measured by peak impact force or impact energy) were identified. Possibly the mutual interactions between the fruit properties (for example interaction between harvest date and stiffness for apples and interaction between radius of curvature and temperature for tomatoes) on the one hand and the interactions between the degree of bruising and the fruit properties on the other hand are the main reason for most of the

contradictory results found in literature regarding the effect of fruit properties on bruise damage. In this context, the critics of Studman (1997) can be quoted that most of research on fruit properties was performed in laboratories at impact energies much higher than the impact energies in practice and this is probably the reason for the inconsistent results between some studies and the knowledge 'from practice'. For that reason in this study, the influence of fruit properties on bruise susceptibility was measured at a wide range of impact energies, including low impact energies at the edge of bruise detection ability.
Multiple linear and nonlinear regression models were preferred above the use of theoretical bruise models because the first mentioned models are able to describe the bruise damage more accurately (Siyama *et al.,* 1988).
Also the effectiveness of packaging materials, as used on the Belgian market, in reducing apple bruise damage was investigated. It can be stated that the use of the more costly and more environmentally charging ripple pack paper in combination with the plastic pack sheet is only justified for fruit submitted to high impacts ('rough handling') because no difference was noted between multilayer paper pack sheets and rippled pack paper in combination with the plastic pack sheets for low impacts.

In Chapter 6, the validity of DEM as a tool to predict the bruise damage has been validated for Jonagold apples. The validation was the crucial but necessary step in this work. 'Bruise damage' was preferred above the 'particle trajectory' as validation parameter. The bruise damage of apples in boxes shaken with a well defined acceleration signal on an electro-hydraulic shaker was compared to the bruise damage calculated from DEM simulations with the same setup and initial conditions. The parameters for the contact force models, needed as input for the simulations, were determined on the same batch of apples, used for the shaking experiments. The measurement procedures described in Chapters 3 and 4 were applied to determine these parameters. A simple bruise model was also constructed utilizing the same batch of apples. No fruit properties needed to be included in the model because uniform fruit properties of the apples in the batch were assumed. For the validation simulations a special *3D* DEM application program named 'Shaking box' was compiled from the DEMeter++ library. Further analysis of the data for the bruise problem was performed in MATLAB. The validations indicated that DEM can predict in acceptable way apple bruise damage. However, due to the lack of the possibility of saving the impact positions on the apple surface by means of a coordinate system no prediction of multi impact bruise surface and bruise volume could be accomplished.

Chapter 7 was dedicated to a case study in which both the influence of mechanical parameters and fruit properties on vibration damage of apples and tomatoes was investigated. More specifically, the bulk transport of apples in bins and EPS crates of tomatoes was investigated. As acceleration input a sine in the vertical direction was used. The same 'shaking box' DEMeter++ application was used for the validation purposes. Appropriate contact force model parameters and bruise prediction models described in previous chapters have been applied. The investigated mechanical parameters were peak acceleration and frequency of the vibration signal, stack height and size of the apples and tomatoes. The fruit properties under research were temperature, ripeness, acoustic stiffness and harvest date (only apples). As a general conclusion can be stated that major influences of mechanical parameters on the vibration damage were identified, in particular stack height and fruit size, and minor influences of fruit properties. In case of apples a detailed study was performed to investigate the relation between apple positions in the stack and bruise damage. It was demonstrated that the position - bruise damage relation depends on the acceleration amplitude, vibration frequency and stack height. Some contradictions concerning position - bruise damage relation in literature were clarified. Extrapolation of results concerning the relation position - bruise damage to other fruit types (like it is done in literature before) is not allowed because fruit behaviour (and damage) is dependent on the mass and impact characteristics (stiffness and damping). The existence of damage chains within the core of the apple stack was also identified, that is in accordance with the well-known force chains in bulk materials.

8.2 Future work

From the results of this work, research in the areas of programming, experiments and theoretical modelling related to bruising of harvested produce can be further explored.

Suggestions are made for improvements of the DEMeter++ code and the development of new applications from the DEMeter++ library. They are described here systematically:

- Integration of the viscoelastic extension of the Mindlin and Deresiewicz model (Chapter 4) in the DEMeter++ code and comparison of the particle behaviour with more simple tangential contact force models.

- Integration in DEMeter++ of the different normal contact force model parameters identified between the compartment and partition of tomatoes (Chapter 3).

- Integration in DEMeter ++ of a surface coordinate system (see Chapter 6) that enables modelling of bruise surfaces and volumes as a result of repeated impact. Using the 'surface coordinate system', it must also be possible to model repeated impact more realistically. Firstly, the contact parameters could be made dependent of the level of damage. Secondly, also the bruise model could be extended to count for additional bruising on already damaged tissue. Including these improvements in the DEM simulations will necessitate more experimental work on repeated impacts. However, first must be decided if this model improvement is necessary for the overall purpose of the use of DEM in the research of fruit bruising.

- In Chapter 6 was stated that the simulation time is limited because the size of the data transfer between DEMeter++ (C++) and MATLAB is restricted. Therefore it is suggested that partially or all data analysis is performed in C++ instead of MATLAB.

- More realistic shape representation algorithms could be applied. By this the simulations become more realistic since the effective radius of curvature at the location of impact can be calculated more accurately. In Chapter 3 was demonstrated that the effective radius of curvature has an effect on the normal contact force model parameters. A more realistic shape representation also leads to a more realistic tangential behaviour since most tangential contact force models depend on the contact radius (the contact radius depends on the effective radius of curvature). A

drawback of the use of more complex shape representation algorithms is that it also necessitates the application of more complex contact detection algorithms.

- More complex continuous vibration patterns could be integrated in the shaking box application. Data of vibration patterns of road transport and orchard (field) transport are available for six degrees of freedom (three translational and three rotational).

- Until now, only a continuous vibration pattern has been utilized in the shaking box application. It is known from literature that discrete inputs like potholes and bumps, curbs and ramps are also harmful to transported fruits. Potholes and bumps can be approximated by an impulse input, a curb by a step input and a ramp by a ramp input (Rong *et al.,* 1993).

- Many other DEM applications could be developed from the DEMeter++ library. Suggestions are the simulation of the 'turnover of bulk bins before sorting', the 'simulation of some critical stages during the fruit sorting process' and 'the simulation of the effect of packaging materials on fruit bruising'. An expected difficulty for the simulation of packaging materials (paper pack sheets for example) is its shape representation and the implementation of a realistic mechanical behaviour. The normal and tangential contact force model parameters of some packaging materials common in Belgium were determined (Van Zeebroeck*,* unpublished).

- The ultimate objective of applying DEM, as stated in the introduction, was to optimize the process and design parameters with a view to minimize the bruise damage. Until now DEM has not been integrated in an optimisation algorithm. Suggested applications are the optimisation of packaging materials and suspensions.

Besides programming work, also some further experimental work could be accomplished.

- In this respect, an important issue is the development of an objective method to measure the degree of bruising (bruise size) of tomatoes. The bruise size of tomatoes as a measure for bruise damage is superior to the use of 'absorbed energy'. It is not only necessary to develop a physical or biochemical method to detect the presence or absence of bruising, but also the degree of bruising has to be quantified. Fortunately, for this application, in contrast to tomato sorting purposes, no instantaneous detection method is mandatory. As soon as a physical or biochemical tomato bruise

measurement method becomes available, experiments to test the effect of tomato parameters (ripeness, etc.) on bruise damage could be repeated.

- Experiments could be done to validate the DEM for tomatoes, once an objective method of measuring the bruise damage becomes available.

- Further research is currently performed to identify the effect of fruit properties like tomato ripeness on the normal contact force model parameters.

The applied contact force models could be improved. Research on this topic is currently performed based on finite element modelling of viscoelastic impacts (Dintwa, unpublished).

- Research for a physically correct viscoelastic-plastic normal contact force model could be executed. The objective of the new model is to simulate viscoelastic-plastic impacts more realistically, with energy dissipation separated in viscous and plastic energy loss, without the need for the dependency of the contact force model parameters on the degree of impact (impact velocity).

- Research for a more rigorous derivation of the combined damping parameter in the Kuwabara and Kono model for the collision of spheres with different viscosity that can be used instead of the heuristic equation (equation (2.49)) proposed by Pöschel and Schwager (2005).

Abbreviations

ANOVA	: Analysis of variance
BD	: Bruise Depth
BDI	: Bruise Diameter
BS	: Bruise surface
BV	: Bruise Volume
C	: Cost function (Chapter 3)
	: Compartment of tomato (other chapters)
CA	: Controlled atmosphere
CHMI	: Constant Height Multiple Impact
DEM	: Discrete Element Method
DYP	: Dynamic Yield Pressure
EPS	: Expanded Polystyrene
FEM	: Finite Element Modelling
G	: Green side of apple
GD	: Granular Dynamics
IS	: Instrumented Sphere
MD	: Molecular Dynamics
MLRA	: Multiple Linear Regression Analysis
ODE	: Ordinary Differential Equation
P	: Partition of tomato
PBS	: Particle Based Simulation
PF	: Peak (contact) Force
R	: Red side of apple
RH	: Relative humidity
SAS	: Statistical Analysis System
SSE	: Error sum of squares
SSTO	: Total sum of squares
UTS	: Universal Testing Machine
VCBT	: Vlaams Centrum Bewaring van Tuinbouwproducten

Notation

Latin symbols

A	Dissipative material parameter = dissipative parameter [s]
a	- Colorimetric coordinate [-] (*Chapter 5*) - Contact radius [m] (*other chapters*)
A^*	Equivalent dissipative material parameter = dissipative parameter [s]
a_i	Translational acceleration i-th particle [m/s^2]
BDE	Bruise depth [mm]
BDI	Bruise diameter [mm]
BS	Bruise surface [mm^2]
BV	Bruise volume [mm^3]
c	Damping parameter [kg/s or kg.m$^{-1/2}$.s^{-1}]
c_t	Tangential damping [kg/s]
d	- Deformation depth from the contact plane to a fixed plane in the interior of the sphere where the viscous force becomes zero [m] (*Chapter 4*) - Bruise depth [m] (*other chapters*)
D	Bruise diameter [m]
e	Normal coefficient of restitution [-]
E	- Column elastic modulus [Pa] (*Chapter 7*) - Elastic modulus [Pa] (*other chapters*)
E^*	Equivalent elastic modulus [Pa]
$E_{a(bsorbed)}$	Absorbed energy [J]
$E_{i(mpact)}$	Impact energy [J]
E_{kin}	Kinetic energy [J]
$E_{e(lastic)}$	Elastic energy [J]
F	Normal/tangential contact force [N]
F^*	Maximum force during loading [N]
F_c^*	Experimental contact force [N]
F_{ci}	Contact force acting on particle i due to c-th contact [N]

$F_{\max}$	Maximum contact force [N]
F_{mt}	Magness-Taylor force, 11.1 mm probe [kg]
F_N	Normal force [N]
F_t	Tangential force [N]
F_v	Viscous damping force [N]
F_y	Critical force [N]
g	Gravity = 9.81 m/s^2
G	Shear modulus [Pa]
G^*	Complex modulus [Pa]
G'	Storage modulus [Pa]
G''	Loss modulus [Pa]
G_i	Body force vector i-th particle [N]
h	Drop height [m]
h_c	Critical drop height [m]
H_i	Body moment vector of i-th particle [N.m]
I_i	i-th particle inertia tensor [$kg.m^2$]
I	Inertia [$kg.m^2$]
k	Spring parameter [N/m or $N/m^{3/2}$]
k_t	Tangential spring parameter [N/m]
l	Length of pendulum rod [m]
M	Mass of pendulum rod [kg]
m	Mass [kg]
m_{eff}	Effective mass [kg]
m_i	Mass i-th particle [kg]
M_s	Critical torque [N.m]
M_z	Torque in z-direction [N.m]
PF	Peak force [N]
p_y	Critical pressure [Pa]
R	- Radius of curvature [m] (*Chapter 2*) - Coefficient of correlation [-](*other chapters*)
r	Radius of curvature [m]

R^*	Effective radius of curvature [m]
r_{ci}	Position vector of the c-th contact relative to the i-th particle centre of mass [m]
r_g	Distance of the rotating axis of the pendulum rod to the centre of gravity of the rod [m]
r_i	Radius of i-th particle [m]
R_p^*	Effective radius of curvature of deformed spheres (spheres with plastic deformation) [m]
S	Acoustic stiffness [$Hz^2.kg^{2/3}$]
S_t	Tangential stiffness [N/m]
t	(impact) time [s]
T	- Time period of pendulum rod [s] (*Chapter 3*) - Temperature [°C] (*other chapters*)
v	Impact velocity [m/s]
v_i	Impact velocity [m/s]
v_r	Rebound velocity [m/s]
v_y	Critical impact velocity, velocity above plastic deformation starts [m/s]
w_δ	Weight corresponding to displacement δ [-]
$w_{\dot{\delta}}$	Weight corresponding to displacement rate $\dot{\delta}$ [-]
w_F	Weight corresponding to contact force F [-]
x_i	Position of the centre of the i-th particle [m]

Greek symbols

α_i	Angular acceleration i-th particle [rad/s^2]
α	Empirical constant [-]
δ	Displacement or approach [m]
β	Angular displacement [rad]
δ_i	Displacement at time I [m]
$\dot{\delta}_i$	Displacement rate at time i [m/s]
δ_m	Maximum deformation [m]
δ_o	Permanent deformation [m]
δ_p	Permanent deformation [m]
δ_y	Displacement at critical force F_y [m]
ω	Angular velocity [rad/s]
ν	Poisson's ratio [-]
μ	(Dynamic) friction coefficient [-]
μ_d	Dynamic friction coefficient [-]
η	(Steady shear) viscosity [Pa.s]
$\eta_{1/2}$	Viscous constants (relation between dissipative stress tensor and deformation rate tensor) [Pa.s]
γ	Correction factor [-]
γ_t	Technical parameter [kg/s]
η'	Dynamic viscosity [Pa.s]
θ	Angle between impactor rod and direction of gravity [rad]
$\ddot{\theta}$	Angular acceleration of pendulum rod [rad/s^2]
γ_0	Strain amplitude [-]
$\dot{\gamma}$	Shear rate [1/s]
σ_i	Peak contact stress [Pa]
σ_f	Failure stress [Pa]
λ	Stack height of fruit [m]
τ	Bulk density of a stack [kg/m^3]

Bibliography

Abbott, J.A., Lu, R. 1996. Anisotropic mechanical properties of apples. Transactions of the ASAE, 39(4), 1451-1459.

Adegoroye, A.S., Eniayeju, D.E. 1988. Technical note: Influence of container material and shape on impact-induced damage to tomatoes in transit. International journal of food science and technology, 23, 633-637.

Allende, A., Desmet, M., Vanstreels, E., Verlinden, B.E., Nicolaï, B.M. 2004. Micromechanical and geometrical properties of tomato skin related to differences in puncture injury susceptibility. Postharvest biology and technology, 34, 131-141.

Armstrong, P.A., Timm, E.J., Schulte, N.L. 1991. Apple Bruising in bulk bins during road transport. ASAE paper no 91-1020, St. Joseph, Michigan.

Arnold, P. C., Mohsenin, N. N. 1971. Proposed techniques for axial compression tests on intact agricultural products of convex shape. Transactions of the ASAE, paper no 71-0055.

Baheri, M. 1997. Development of a method for prediction of potato mechanical damage in the chain of mechanized potato production. PhD thesis, Faculty of agricultural and applied biological sciences, K.U.Leuven, Belgium.

Bajema, R. W., Hyde, G. M. 1998. Instrumented pendulum for impact characterization of whole fruit and vegetable specimens. Transactions of the ASAE, 41(5), 1399-1405.

Bajema, R., Hyde, G. M. 1992. Multiple-Impact Technique for determining bruise resistance. ASAE paper no. 92-1513, St. Joseph, Michigan.

Bajema, R.W., Baritelle, A.L., Hyde, G.M, Pitts, M.J. 1999. Factors influencing dynamic mechanical properties of red 'Delicious apple' tissue. ASAE paper no 99- 6002, St. Joseph, Michigan.

Bajema, R.W., Hyde, G.M., Peterson, K. 1998. Instrumentation design for dynamic axial compression of cylindrical tissue samples. Transactions of the ASAE, 41, 747-754.

Baritelle, A., Hyde, G.M. 2000. Commodity conditioning to reduce impact bruising. ASAE paper no 00-6059, St. Joseph, Michigan.

Baritelle, A., Hyde, G.M. 2001. Commodity conditioning to reduce impact bruising. Postharvest biology and technology, 21, 331-339.

Barnes, H.A. 2000. A handbook of elementary rheology. University of Wales Aberystwyth, Aberystwyth.

Barreiro, P. 2004. Detailed procedure for fruits damaging, ASTEQ publication. http://www.inapg.inra.fr/ens_rech/siab/asteq/some.htm#DPFD.

Bilanski, W.K. 1966. Damage resistance of seed grains. Transactions of the ASAE, 9, 360-363.

Blahovec, J. 1999. Bruise resistance coefficient and bruise sensitivity of apples and cherries. International agrophysics, 13, 315-321.

Bollen, A.F., Dela Rue, B.T. 1990. Handling impacts for kiwifruit, Asian peers and apples. ASAE paper no. 90-6005, St. Joseph, Michigan.

Bollen, A.F., Timm, E.J., Dela Rue, B.T. 2001. Relation of individual forces on apples and bruising during orchard transport of bulk bins. Applied engineering in agriculture, 17(2), 193-200.

Brilliantov, N.V., Pöschel, T. 2000. Diffusion in granular gases of viscoelastic particles. In: Freund; J.A., Pöschel, T. Granular gases, Lecture notes in physics, 557. 107-120, Springer, Berlin.

Brilliantov, N.V., Spahn, F., Hertzsch, J-M, Pöschel, T. 1996a. The collision of particles in granular systems. Physica A, 231, 417-424.

Brilliantov, N.V., Spahn, F., Hertzsch, J-M, Pöschel, T. 1996b. Model for collisions in granular gases. Physical review E, 53(5), 5382-5392.

Brillinatov, N.V., Pöschel, T. 2001. Granular gases with impact-velocity- dependent restitution coefficient. In: Pöschel, T., Luding, S. Granular gases, Lecture notes in physics, 564. 100-124, Springer, Berlin.

Brown, G. K., Schulte-Pason, N. L., Timm, E. J. 1990. Impact classification using the instrumented sphere. ASAE paper no 90-6001, St. Joseph, Michigan.

Brown, G.K., Segerlind, L.J. 1975. Location probabilities of surface injuries for some mechanical harvested apples. Transactions of the ASAE, 18(1), 57-61.

Brusewitz, G. H., Bartsch J. A. 1989. Impact parameters related to post harvest bruising of apples. Transactions of the ASAE, 32(3), 953-957.

Burton, C.L., Brown, G.K., Schulte-Pason, N.L., Timm, E.J., Marshall, D.E. 1989. Apple bruising related to picking and hauling impacts. ASAE paper no 89-6049, St. Joseph, Michigan.

Cates, M.E., Wittmer, J.P, Bouchaud, J-P, Claudin, P. 1999. Jamming and stress propagation in particulate matter. Physic A, 263, 354-361.

Chen, H. 1993. Analysis of the acoustic impulse resonance of apples for non-destructive estimation of fruit quality. PhD thesis, Faculty of agricultural and applied biological sciences, K.U.Leuven, Belgium.

Chen, H., De Baerdemaeker, J. 1995. Optimisation of impact parameters for reliable excitation of apples during firmness monitoring. Journal of agricultural engineering research, 61, 275-282.

Chen, P., Sun, Z. 1981. Impact parameters related to postharvest bruising of apples. ASAE paper no 81-3041, St. Joseph, Michigan.

Chen, P., Tang, S., Chen, S. 1985. Instrument for testing the response of fruits to impact. ASAE paper no 85-3537, St. Joseph, Michigan.

Chen, P., Yazdani R. 1989. Prediction of apple bruising due to impact on different surfaces. ASAE. paper no 89-6501, St. Joseph, Michigan.

Chen, P., Yazdani, R. 1991. Prediction of apple bruising due to impact on different surfaces. Transactions of the ASAE, 34(3), 956-961.

Chesson, J.H., O'Brien, M. 1971. Analysis of mechanical vibration of fruit during transportation. Transactions of the ASAE, paper no 69-628.

Cox, M.A., Zhang, M.I.N., Willison, J.H.M. 1996. Apple bruise assessment through electrical impedance measurements. Journal of horticultural science, 68(3), 393-398.

Cundall, P.A., Strack, O.D.L. 1979. A discrete numerical model for granular assemblies. Géotechnique, 29, 47-65.

De Baerdemaeker, J., Lemaitre L., Meire, R. 1982. Quality detection by frequency spectrum analysis of the fruit impact force. Transactions of the ASAE, paper no 79-3060.

De Baerdemaeker, J., Segerlind, L.J., Murase, H., Merva, G.E. 1978. Water potential effect on tensile and compressive failure stresses of apple and potato tissue. ASAE paper no 78-3057, St. Joseph, Michigan.

De Baerdemaeker, J.G. 1975. Experimental and numerical techniques related to the stress analysis of apples under static loads. PhD dissertation, Michigan State University, East Lansing, Michigan, USA.

De Baerdemaeker, J.G., Segerlind, L.J. 1976. Determination of the viscoelastic properties of apple flesh. Transactions of the ASAE, 346-353.

De Ketelaere, B. 2002. Data analysis for the non-destructive quality assessment of agro-products using vibration measurements. PhD thesis, Faculty of agricultural and applied biological sciences, K.U.Leuven, Belgium.

De Ketelaere, B., De Baerdemaeker, J. 2001. Advances in spectral analysis of vibrations for non-destructive determination of tomato firmness. Journal of agricultural engineering research, 78(2), 177-185.

Deli, V., Van Zeebroeck, M., Anthonis, J., Deprez, K., De Baerdemaeker, J., Ramon, H. Extraction of parameters influencing fruit bruising during transportation. Postharvest biology and technology. Submitted.

Desmet, M., Lammertyn, J., Scheerlinck, N., Verlinden, B.E., Nicolaï, B.M. 2003. Determination of puncture injury susceptibility of tomatoes. Postharvest biology and technology, 27, 293-303.

Desmet, M., Lammertyn, J., Van linden, V., Verlinden, B.E., Darius, P., Nicolaï, B.M. 2004a. The relative influence of stem and fruit properties on stem puncture injury in tomatoes. Postharvest biology and technology, 33, 101-109.

Desmet, M., Van linden, V., Hertog, M.L.A.T.M. Verlinden, B.E., De Baerdemaeker, J., Nicolaï, B.M. 2004b. Instrumented sphere prediction of tomato stem-puncture injury. Postharvest biology and technology, 34, 81-92.

Diehl, K.C., Hamann, D.D. 1979. Structural failure in selected raw fruits and vegetables. Journal of texture studies, 10, 371-400.

Diener, R.G., Elliott, K. C., Nesselroad, P. E., Ingle, M., Adams, R. E., Blizzard, S.H. 1979. Bruise Energy of peaches and apples. Transactions of the ASAE, paper no 77-1029.

Dintwa, E., Van Zeebroeck, M., Tijskens, E., Ramon, H. 2004a. Torsional stiffness of viscoelastic spheres in contact. European physical journal B, 39, 77-85.

Dintwa, E., Van Zeebroeck, M., Tijskens, E., Ramon, H. 2004b. Determination of parameters of a tangential contact force model for spheroids (fruits) using a rheometer device. Proceedings of AgEng 2004, September 12-16, Leuven, Belgium. paper no 94-w3-564.

Doraiswamy, D., Mujamdar, A.N., Tsao, I., Beris, A.N., Danforth, S.C., Metzner, A.B., 1991. The Cox-Mertz rule extended: A rheological model for concentrated suspensions and other materials with a yield stress. Journal of rheology, 35, 647-685.

Duprat, F., Grotte, M., Pietri, E., Loonis, D. 1997. The acoustic impulse response method for measuring the overall firmness of fruit. Journal of agricultural engineering research, 66, 251-259.

Faik, S., Witteman, H. 2000. Modelling of impact dynamics: a literature survey. Proceedings of international ADAMS user conference.

Falcon, E., Laroche, C., Fauve, S., Coste, C. 1998. Bouncing of one elastic ball bouncing repeatedly off the ground. The European physical journal B, 3, 45-57.

Fekete, A. 1994. Elasticity characteristics of fruits. International agrophysics, 8, 411-414.

Finney, E.E., Massie, D.R. 1975. Instrumentation for testing the response of fruits to mechanical impact. Transaction of the ASAE, 18, 1184-1187.

Fluck, R.C., Ahmed, E.M. 1972. Impact testing of fruits and vegetables. Transactions of the ASAE, 16, 660-666.

Fridley, R.B., Gohlich, H., Claypool, L.L, Adrian, P.A. 1964. Factors affecting impact injury to mechanically harvested fruit. Transactions of the ASAE, 7, 408-411.

Galili, N., De Baerdemaeker, J. 1996. Performance of acoustic test methods for quality evolution of agricultural products. ISMA conference, September 1996, Leuven, Belgium.

Gao, Q., Pitt, R.E. 1991. Mechanics of parenchyma tissue based on cell orientation and microstructure. Transactions of the ASAE, 34(1), 232-238.

Garcia, J.L., Barreiro, P., Ruiz-Altisent, M., Vicente, M. 1994. Use of electronic fruits to evaluate fruit damage along the handling process. Proceedings of AgEng 1994, August 29- September 01, Milano, Italy, paper no 94-G-045.

Garcia, J.L., Ruiz-Altisent, M., Barreiro, P. 1995. Factors influencing mechanical properties and bruise susceptibility of apples and pears. Journal of agricultural engineering research, 61, 11-18.

Geyer, M., Herold, B., Studman, C. J. 1998. Fruit contact pressure distributions. Proceedings of AgEng 1998, August 24-27, Oslo, Norway, paper no 98-F-001.

Golacki, K., Stropek, Z. 2002. Viscoelastic properties of Jonagold apple flesh. Electronic journal of polish agricultural universities. 4(2).

Gran-Mor, S., Galili, N. 2000. Rheological model of fruit collision with an elastic plate. Journal of agricultural engineering research, 75, 139-147.

Hamann, D. D. 1970. Analysis of stress during impact of fruit considered to be viscoelastic. Transactions of ASAE, paper no 68-812.

Hammerle, J.R., Mohsenin, N.N. 1966. Some dynamic aspects of fruit impacting hard and soft materials. Transactions of the ASAE, paper no 65-320.

Hatton, T.T., Reeder, W.F. 1963. Effect of field and packinghouse handling on bruising of Florida tomatoes. Proceedings of the Florida state horticultural society, 76, 301-304.

Haug, E.J. 1992. Intermediate dynamics. Prentice-Hall Inc., New Jersey, USA.

Hay, J.L., Wolf, P.J. 2001. Small correction required when applying the Hertzian contact model to instrumented indentation data. Journal of material research, 16(5), 1280-1286.

Herold, B., Siering, G., Truppel, I. 1993. Comparison of measuring spheres as means to determine mechanical stress on fruits during handling. Proceedings of the fourth international symposium on fruit, nut and vegetable production engineering, March 22-26, Valencia-Zaragoza, Spain, 2, 35-42.

Herold, B., Oberbarnscheidt, B., Jakovac, F., Borsa, B., Kovacs, L. 2001. Mechanical load on tomatoes during mechanical harvest and transport. Proceedings of 6th international symposium on fruit, nut, and vegetable production engineering, September 11-14, Potsdam, Germany.

Herold, B., Truppel, I., Siering, G., Geyer, M. 1996. A pressure measuring sphere for monitoring handling of fruit and vegetables. Computers and electronics in agriculture, 15, 73-88.

Hertog, M.L.A.T.M., Ben-Arie, R., Roth, E., Nicolaï, B.M. 2004. Humidity and temperature effects on invasive and non-invasive firmness measures. Postharvest biology and technology, 33, 79-91.

Hertz, H. 1881. Über die Berührung fester elastischer Körper. J.f. reine u. angewandte Math, 92, 156.

Hertzsch, J-M, Spahn, F., Brilliantov, N.V. 1995. On low-velocity collisions of viscoelastic particles. Journal of physics II France, 5, 1725-1738.

Hertzsch, J-M. 2002. A model for surface effects in slow collisions of icy grains. Planetary and space science, 50, 745-755.

Hilton, D. J. 1994. Impact and vibration damage to fruit during handling and transportation. In: Champ, B.R., Highley, E., Johnson, G.I. Post-harvest handling of tropical fruits. Australian centre for international agricultural research, Canberra, Australia.

Hinsch, R.T., Slaughter, D.C., Craig, W.L., Thompson, J.F. 1993. Vibration of fresh fruits and vegetables during refrigerated truck transport. Transactions of the ASAE, 36(4), 1039-1042.

Hoag, D.L. 1972. Properties related to soybean shatter. Transactions of the ASAE, 15, 494-497.

Holst, J.M.F.G., Ooi, J.Y., Rotter, M., Rong, G.H. 1999a. Numerical modelling of silo filling. I: Continuum analysis. Journal of engineering mechanics, 125, 94-103.

Holst, J.M.F.G., Ooi, J.Y., Rotter, M., Rong, G.H. 1999b. Numerical modelling of silo filling. II: Discrete element analysis. Journal of engineering mechanics, 125, 104-110.

Holt, J.E., Schoorl, D. 1977. Bruising and energy dissipation in apples. Journal of texture studies, 7, 421-432.

Holt, J.E., Schoorl, D. 1982. Mechanics of failure in fruits and vegetables. Journal of texture studies,13, 83-97.

Holt, J.E., Schoorl, D. 1983a. The robustness of a model predicting bruising in impacted multilayered apple packs. Journal of agricultural engineering research, 28, 97-105.

Holt, J.E., Schoorl, D. 1983b. Fracture in potatoes and apples. Journal of materials science, 18, 2017-2028.

Holt, J.E., Schoorl, D. 1984a. Package protection and energy dissipation in apple packs. Scientia horticulturae, 24, 165-176.

Holt, J.E., Schoorl, D. 1984b. Mechanical properties and texture of stored apples. Journal of texture studies, 15(4), 377-394.

Holt, J.E., Schoorl, D. 1985. A theoretical and experimental analysis of the effects of suspension and road profile on bruising in multilayered apple packs. Journal of agricultural engineering research, 31, 297-308.

Holt, J.E., Schoorl, D., Lucas, C. 1981. Prediction of bruising in impacted multilayered apple packs. Transactions of the ASAE, 24, 242-247.

Holt, J.E., Schoorl, D., Muirhead, I. F. 1983. Post-harvest quality control strategies for fruit and vegetables. Agricultural Systems, 10, 23-37.

Horsfield, B.C., Fridley, R.B., Claypool, L.L. 1972. Application of theory and elasticity to the design of fruit harvesting and handling equipment for minimum bruising. Transactions of the ASAE, 15(4), 746-750.

Hostens, I., Anthonis, J., Kennes, P., Ramon, H., 2000. Six-degrees-of-freedom test rig design for simulation of mobile Agricultural machinery vibrations. Journal of agricultural engineering research, 77(2), 155-169.

Hunt, K.H., Crossley, F.R.E. 1975. Coefficient of restitution interpreted as damping in vibroimpact. Journal of applied mechanics, 440-445.

Hyde, G.M., Bajema, R.W., Zhang W. 1993. Measurement of impact damage thresholds in fruits and vegetables. Proceedings of 4th international symposium on fruit, nut, and vegetable production engineering, March 22-26, Valencia-Zaragoza, Spain.

Hyde, G.M., Baritelle, A.L., Varith, J. 2001. Fruit and vegetable conditioning to improve impact bruise threshold. Proceedings of 6th international symposium on fruit, nut, and vegetable production engineering, September 11-14, Potsdam, Germany.

Jackman, R.L., Stanley, D.W. 1995. Creep behaviour of tomato pericarp tissue as influenced by ambient temperature ripening and chilled storage. Journal of texture studies, 26, 537-552.

Jarimopas, B., Sarig, Y., Peiper, U.M., Manor, G. 1990. Instrumentation for measuring the response of apples subjected to impact loading. Computation and electronics in agriculture, 5, 255-260.

Jindal,V.K., Mohsenin, N.N. 1976. Analysis of a simple pendulum impacting device for determining dynamic strength of selected food materials. Transactions of the ASAE, 19(4), 766-770.

Jofriet, J.C., Negi, S.C., Lu, Z. 1997. A numerical model for flow of granular materials in silos part 3: Parametric study. Journal of agricultural engineering research, 68, 237-246.

Johnson, D.S., Dover, C.J. 1990. Factors influencing the bruise susceptibility of Bramley's seedling apples. Proceedings of the European workshop on impact damage of fruits and vegetables, Zaragoza, Spain, 87-93.

Johnson, K.L., 1985. Contact mechanics, 2nd ed. Cambridge University Press, New York.

Jones, C.S., Holt, J.E., Schoorl, D. 1991. A model to predict damage to horticultural produce during transport. Journal of agricultural engineering research, 50, 259-272.

Jourdain, J. M., Vaysse, P., Mora, P., Cammal, P., Villes, C. 1993. Apple bruise damage evaluation op packing lines using an instrumented sphere. Proceedings of the 4th international symposium on fruit, nut and vegetable production engineering, March 22-26, Valencia-Zaragoza, Spain, 2, 99-106.

Khan, A.A., Vincent, J.F.V. 1990. Anisotropy of apple parenchyma. Journal of the science of food and agriculture, 52, 455-466.

Khan, A.A., Vincent, J. F.V. 1993a. Anisotropy in the fracture properties of apple flesh as investigated by crack-opening tests. Journal of materials science, 28, 45-51.

Khan, A.A., Vincent, J.F.V. 1991. Bruising and splitting of apple under uni-axial compression an the role of skin in preventing damage. Journal of texture studies, 22, 251-263.

Khan, A.A, Vincent, J.F.V. 1993b. Compressive stiffness and fracture properties of apple and potato parenchyma. Journal of texture studies, 24, 423-435.

Klein, J.D. 1987. Relationship of harvest date, storage conditions and fruit characteristics to bruise susceptibility. Journal of the American society of horticultural science, 112(1), 113-118.

Knee, M., Miller, A.R. 2002. Mechanical injury. In: Knee, M. Fruit quality and its biological basis. Sheffield Academic press, Sheffield, 157-179.

Kopec, K. 1979. Texture changes in ripening of stored tomatoes. Acta horticulturae Proceedings of symposium on quality of vegetables, June 11- 15, Lund, Sweden. 331-334.

Kremmer, M., Favier, J.F. 1999. Multi-body dynamics simulation using ReDem (the reverse engineered Discrete Element Method). ASAE paper no 99-3301, St. Joseph, Michigan.

Kuwabara, G., Kono, K. 1987. Restitution coefficient in a collision between two spheres. Japanese journal of applied physics, 26(8), 1230-1233.

Lammertyn, J., Nicolaï, B., Ooms, K., De Smedt, V., De Baerdemaeker, J. Non-destructive measurement of acidity, soluble solids, and firmness of Jonagold apples using NIR-spectroscopy. Transactions of the ASAE, 41(4), 1089-1094.

Landahl, S., De Belie, N., De Baerdemaeker, J., Peirs, A., Nicolaï B. 2000. Non-destructive and destructive firmness measurements on apples and peaches. International conference on modelling and control in agriculture, horticulture and post-harvested processing. July 10-12, Wageningen, the Netherlands.

Landahl, S., Herppich, W.B., Herold, B., Geyer, M., De Baerdemaeker, J. 2004. A comprehensive evaluation of the interactions between produce elasticity and water status. European journal of horticultural science, 69(6), 250-257.

Lankarani, H., Nikravesh, P.E. 1994. Continuous contact force models for impact analysis in multibody systems. Nonlinear dynamics, 5, 193-207.

Lankarani H.M., Nikravesh, P.E. 1990. A contact force model with hysteresis damping for impact analysis of multibody systems. Journal of mechanical design, 112, 369-376.

Li, Q., Rudolph, V., Wang, F.Y, Kajikawa, S-I, and Horio, M. 2001. Axial porosity distribution in a packed bed of deformable particles – a numerical study based on DEM, In: Levy, A., Kalman, H. Handbook of conveying and handling of particulate solids, Elsevier Science, the Netherlands.

Lichtensteiger, M.J. 1982. Impact analysis of viscoelastic spheres, fruits and vegetables with rigid plane surfaces. PhD thesis, department of agricultural engineering, North Carolina state university, Raleigh, USA.

Lichtensteiger, M.J., Holmes, R.G., Hamdy, M.Y., Blaisdell, J.L. 1988a. Evaluation of Kelvin model coefficients for viscoelastic spheres. Transactions of the ASAE, 31(1), 288-292.

Lichtensteiger, M.J., Holmes, R.G., Hamdy, M.Y., Blaisdell, J.L. 1988b. Impact parameters of spherical viscoelastic objects and tomatoes. Transactions of the ASAE, 31(2), 595-602.

Lu, R., Puri, V.M. 1991. Characterization of nonlinear behaviour of apple and potato flesh under creep. ASAE paper no 91-6023, St. Joseph, Michigan.

Lu, Z., Negi, S.C., Jofriet, J.C. 1997. A numerical model for flow of granular materials in silos part 1: model development. Journal of agricultural engineering research, 68, 223-229.

Luan, J-M, Rohrbach, R.P. 1989. Measurements of contact pressure during fruit impact. ASAE paper no 89-6025, St. Joseph, Michigan.

Lubkin, J.L., 1951. The torsion of elastic spheres in contact. ASME journal of applied mechanics, 18, 183-187.

Martinez, V.Y., Nieto, A.B., Viollaz, P.E., Alzamora, S.M. 2002. Viscoelastic properties of fresh and thermally treated apple tissue. Proceedings of annual meeting and food expo, Anaheim, California.

Menesatti, P., Paglia, G. 2001. Development of a drop damage index of fruit resistance to damage. Journal of agricultural engineering research, 80(1), 53-64.

Menessatti, P., Paglia, G., Solaini, S., Zanella, A., Stainer, R., Costa, C., Cecchetti, M. 2002. Nonlinear multiple regression models to estimate the drop damage index of fruit. Biosystems engineering, 83(3), 319-326.

Mindlin, R.D., 1949. Compliance of elastic bodies in contact. ASME journal of applied mechanics, 16, 259-268.

Mindlin, R.D., Deresiewicz, H. 1953. Elastic spheres in contact under varying oblique forces. ASME journal of applied mechanics, 20, 327-344.

Mishra, B.K. 2003a. A review of computer simulation of tumbling mills by discrete element method Part I-contact mechanics. International journal of mineral processes, 1635, 1-21.

Mishra, B.K. 2003b. A review of computer simulation of tumbling mills by discrete element method Part II practical applications. International journal of mineral processes, 1634, 1-18.

Mishra, B.K., Thornton, C. 2002. An improved contact model for ball mill simulation by discrete element method. Advanced Powder Technology, 13(1), 25-41.

Mohsenin, N. N., Jindal, V. K., Manor A. N. 1978. Mechanics of impact of a falling fruit on a cushioned surface. Transactions of the ASAE, 21, 245-247.

Mohsenin, N.N. 1977. Characterization and failure in solid foods with particular reference to fruits and vegetables. Journal of texture studies, 8, 169-193.

Mohsenin, N.N. 1986. Physical properties of plant and animal materials. Gordon and Breach science publishers, New York.

Molema, G-J. 1999. Mechanical force and subcutaneous tissue discolouration in potato. PhD thesis, Wageningen University, Wageningen, The Netherlands.

Mowatt, C.M. 1997. Factors influencing the bruise susceptibility of apples. PhD thesis, Massey university, New Zealand.

Musiol, C., Harty, D. 1991. The use of numerical integration for the estimation of displacement from an accelerometer signal. Application note 12, nCode International Ltd.

N.N. 1999. ASAE S368.3 MAR95 Compression test of food materials of convex shape. In: ASAE standards 1999 46th Ed., Standards engineering practices and data adopted by the American society of agricultural engineers, American society of agricultural engineers, St. Joseph, Michigan 49085.

N.N. 2002. The United States Standards for Grades of Apples. Department of Agriculture, USA.

Negi, S.C., Lu, Z., Jofriet, J.C. 1997. A numerical model for flow of granular materials in silos Part 2: Model validation. Journal of agricultural engineering research, 68, 231-236.

Nelson, C.W., Mohsenin, N.N. 1968. Maximum allowable static and dynamic loads and effect of temperature for mechanical injury in apples. Journal of agricultural engineering research, 13, 305-317.

Nigg, B.M., Liu, W. 1999. The effect of muscle stiffness and damping on simulated impact force peaks during running. Journal of biomechanics, 32, 849-856.

O'Brien, M. 1974. Damage losses in handling processing tomatoes in bulk. Transactions of ASAE, 17(3), 583-586.

O'Brien, M., Claypool, L.L., Leonard, S.J., York, G.K., McGillivray, J.H. 1963. Causes of Fruit Bruising on Transport Trucks. Hilgardia, 35 (6), 113-124.

O'Brien, M., Goddard, W.B., Gyasi, S. 1972. Tomato damage during harvesting and handling. Transactions of the ASAE, 15(4), 653-655.

O'Brien, M., Pearl, R.C., Vilas, E.P., Dreisbach, R.L. 1969. The magnitude and effect of in-transit vibration damage of fruits and vegetables on processing quality and yield. Transactions of the ASAE, paper no 68-382.

O'Brien, M., Guillon, R. 1969. An in-transit vibration simulator for fruit-handling studies. Transactions of the ASAE, paper no 68-119.

O'Brien, M., Gentry, J.P., Gibson, R.C. 1965. Vibrating characteristics of fruit as related to in-transit injury. Transactions of the ASAE, 8(2), 241-243.

Olorunda, A.O., Tung, M.A. 1985. Simulated transit studies on tomatoes, effect of compressive load, container, vibration and maturity on mechanical damage. Journal of food technology, 20, 669-678.

Pang, D.W., Studman, C.J., Banks, N.H., Baas, P.H. 1996. Rapid assessment of the susceptibility of apples to bruising., 64, 37-48.

Pang, W., Studman, C.J., Ward, G.T. 1992. Bruising damage in apple-to-apple impact. Journal of agricultural engineering research, 52, 229-240.

Pang, W., Studman, C.J., Banks, N. H. 1991. Use of an instrumented sphere for assessing apple bruising thresholds. ASAE paper no 91-6596, St. Joseph, Michigan.

Park, D. 1963. The resistance of potatoes to mechanicaldamage caused by impact loading. Journal of agricultural engineering research, 8, 173-177.

Peleg, K. 1981. Package product interaction in corrugated containers for fresh produce. Transactions of the ASAE, paper no 794800.

Peleg, K. 1984. A mathematical model of produce damage mechanisms. Transactions of ASAE, 27(2), 287-293.

Peleg, K., Hinga, S., 1986. Simulation of Vibration damage in produce transportation. Transactions of the ASAE, 29 (2), 633-641.

Pitt, R.E. 1982. Models for the rheology and statistical strength of uniformly stressed vegative tissue. Transactions of the ASAE, 25(6), 1776-1784.

Pitt, R.E., Chen, H.L. 1983. Time-dependent aspects of the strength and rheology of vegative tissue. Transactions of the ASAE, 26(4), 1275-1280.

Plumbee, T. W, Webb, B. K. 1974. Effects of frequency and acceleration on peach bruising during transit. ASAE paper no 74-3514.

Pöschel, T, Schwager, T. 2005. Granular dynamics: Models and Algorithms, Springer, Berlin.

Pöschel, T., Brilliantov, N.V. 2001. Chains of viscoelastic spheres. In: Pöschel, T., Luding, S. Granular gases, Lecture notes in physics, 564, 203-212, Springer, Berlin.

Pöschel, T., Brilliantov, N.V., Schwager, T., 2003. Long-time behaviour of granular gases with impact-velocity dependent coefficient of restitution, Physica A, 274-283.

Pöschel, T., Saluena, C., Schwager, T. 2001. Scaling properties of granular materials. Physical reviews E. 64(1), art no-011308 part1.

Puchalski, C., Gorzelany J. 1992. Testing apple resistance to dynamic loading. Trends in agricultural engineering, 15-18 September, Prague.

Pulchalski, C., Brusewitz, G.H. 2001. Fruit ripeness and temperature affect friction coefficient of McLemore and Gala apples. International agrophysics, 15, 109-114.

Ragni, L., Berardinelli, A. 2001. Mechanical behaviour of apples, and damage during sorting and packaging. Journal of agricultural engineering research, 78(3), 273-279.

Raji, A.O., Favier, J.F. 1998. Discrete element modelling of deformation in particulate agricultural materials under bulk compressive loading. Proceedings of AgEng 1998, Augustus 24-27, Oslo, Norway, paper no 98-F-045.

Raji, A.O., Favier, J.F. 1999. Discrete element modelling of the compression of an oil-seed bed. ASAE paper no 99-6109, St. Joseph, Michigan.

Raji, A.O., Favier, J.F. 2004a. Model for the deformation in agricultural and food particulate materials under bulk compressive loading using discrete element method I: Theory, model development and validation. Journal of food engineering, 64, 359-371.

Raji, A.O., Favier, J.F. 2004b. Model for the deformation in agricultural and food particulate materials under bulk compressive loading using discrete element method II: Compression of oilseeds. Journal of food engineering, 64, 373-380.

Ramirez, R., Pöschel T., Brilliantov, N.V., Schwager, T. 1999. Coefficient of restitution of colliding viscoelastic spheres. Physical review E, 60(4), 4465-4472.

Rong, G.H. 1994. DEM for flow of particulate materials in bins. PhD thesis University of Guelph, Canada

Rong, G.H., Negi, S., Jofriet J.C.1995. Simulation of flow behaviour of bulk solids in bins, Part 1: model development and validation. Journal of agricultural research. 62, 247-256.

Rong, G.H., Negi, S.C., Jofriet, J.C. 1993. DEM simulation of in-transit fruit damage. ASAE paper no 93-6503.

Roudot, A.C., Duprat, F., Wenian, C. 1991. Modelling the response of apples to loads. Journal of agricultural engineering research, 48, 249-259.

Rumsey, T.R. Fridley, R.B. 1977. Analysis of viscoelastic contact stresses in agricultural products using a finite-element method. ASAE paper no 74-3513, St. Joseph, Michigan.

Sakaguchi, E. Favier, J.F. 1998. Analysis of the shear behaviour of a grain assembly using DEM simulation. Proceedings of ICPAFP'98, International conference on physics of agro- and food products .

Sakaguchi, E., Kawakami, S., Tobita, F. 1994. Simulation on flowing phenomena of grains by distinct element method. Proceedings of AgEng 1994, August 29- September 01, Milano, Italy, paper no 94-G-025.

Sakaguchi, E., Suzuki, M., Favier, J.F., Kawakami, S. 2001. Numerical simulation of the shaking separation of paddy and brown rice using the discrete element method. Journal of agricultural engineering research, 79(3), 307-315.

Sakaguchi, E., Kawakami, S., Suzuki, M., Urakawa, T., Favier J.F. 1998. Effective use of DEM simulation for development of grain processing technology. Proceedings of AgEng 1998, August 24-27, Oslo, Norway, paper no 98-F-021.

Saltveit, M. 1984. Effects of temperature on firmness and bruising of Starkrimson Delicious and Golden Delicious apples. Horticultural science, 19(4), 550-551.

Sargent, S.A., Brecht, J.K., Zoellner, J.J. 1989. Assessment of mechanical damage in tomato packing lines. ASAE paper no 89-6060, St. Joseph, Michigan.

Sargent, S.A., Brecht, J.K., Zoellner, J.J. 1992. Instrumented sphere impact analyses of tomato and bell pepper packing lines. Applied engineering in agriculture, 8, 76-83.

Sargent, S.A., Brecht, J.K., Zoellner, J.J. 1992a. Instrumented sphere impact analysis of tomato and bell pepper packing lines. Applied engineering in agriculture, 8, 76-83.

Sargent, S.A., Brecht, J.K., Zoellner, J.J. 1992b. Sensitivity of tomatoes at mature-green and breaker ripeness stages to internal bruising. Journal of the American society of horticultural science, 117(1), 119-123.

Sargent, S.A., Brown, G.K., Burton, C.L., Schulte-Pason, N.L., Timm, E.J., Marshall, D.E.. 1986. Damage assessment for apple harvest and transport. ASAE paper no 87-6517, St. Joseph, Michigan.

Sarig, Y. 1991. Review: Impact loading associated with agricultural products. International journal of impact engineering, 11(3), 251-275.

Schäfer, J., Dippel, S., Wolf, D.E. 1996. Force schemes in simulations of granular materials. Journal of physics I France, 6, 5-20.

Schembri, M.G., Harris, H.D. 1996. Modelling impact on a biological material (sugar cane) using the discrete element method, AgEng 1996, September 23-26, Madrid, Spain, paper no 96F-072.

Schoorl, D., Holt, J.E. 1977. The effects of storage time and temperature on the bruising of Jonathan, Delicious and Granny Smith apples. Journal of texture studies, 8, 409-416.

Schoorl, D., Holt, J.E. 1980. Bruise resistance measurements in apples. Journal of texture studies, 11, 389-394.

Schoorl, D., Holt, J.E. 1982a. Road-vehicle-load interaction for transport of fruit and vegetables, Agricultural systems, 8, 143-155.

Schoorl, D., Holt, J.E. 1982b. Impact bruising in 3 apple pack arrangements. Journal of agricultural engineering research, 27, 507-512.

Schoorl, D., Holt, J.E. 1982c. Fresh fruit and vegetable distribution – management of quality. Scientia horticulturae, 17, 1-8.

Schoorl, D., Holt, J.E. 1985. Verification of a model for predicting damage to horticultural produce during transport. Agricultural systems, 16, 67-83.

Schoorl, D., Holt, J.E. 1986. Post-harvest energy transformations in horticultural produce. Agricultural systems, 19, 127-140.

Schoorl, D., Holt, J.E., 1974. Bruising and acceleration measurements in apple packs. Journal of agriculture and animal science, 31(1), 83-92.

Schotte, S., De Belie, N., De Baerdemaeker, J. 1999. Acoustic impulse-response technique for evaluation and modelling of firmness tomato fruit. Postharvest biology and technology, 17, 105-115.

Schulte-Pason, N.L., Brown, G.K., Timm, E.J. 1992. Apple impact damage thresholds. Applied engineering in agriculture, 8, 55-60.

Schulte-Pason, N.L., Timm, E.J., Brown, G.K. 1990b. Apple, peach and pear damage thresholds. ASAE paper no 90-6002, St. Joseph, Michigan.

Schulte-Pason, N.L., Timm, E.J., Brown, G.K., Marshall, D.E., Burton, C.L. 1989. Apple damage assessment during intrastate transportation. ASAE paper no 89-6051, St Joseph, Michigan.

Schulte-Pason, N.L., Timm, E.J., Brown, G.K., Marshall, D.E., Burton, C.L. 1990a. Apple damage assessment during interstate transportation. Applied engineering in agriculture, 6(6), 753-758.

Schwager, T., Pöschel, T. 1998. Coefficient of normal restitution of viscous particles and cooling rate of granular gases. Physical review E, 57(1), 650-654.

Sears, F.W., Zemansky, M.W. 1963. University physics. Addison-Wesley pub., Boston, USA.

Segerlind, L.J., Fabbro, I.D. 1978. A failure criterion for apple flesh. ASAE paper 78-3556, St. Joseph, Michigan.

Simpson, J.B. 1971. Forces, pressures, and apple damage during cushioned impact. PhD thesis, Department of Agricultural engineering, Cornell university, Ithaca, USA.

Singh, S.P., Xu, M. 1993. Bruising in apples as a function of truck vibration and packaging. Applied engineering in agriculture, 9(5), 455-460.

Siyami, S. Brown G. K. Burgess G. J. Gerrish J. B. Tennes B. R. Burton C. L. Zapp R. H. 1988. Apple Impact Bruise Prediction Models. Transactions of the ASAE, 31(4), 1038-1046.

Sober, S. S. Zapp H. R. Brown G. K. 1989. Simulated packing line impacts for apple bruise prediction. ASAE paper no 89-6047, St. Joseph, Michigan.

Sober, S. S. Zapp H. R. Brown G. K. 1990. Simulated packing line impacts for apple bruise prediction. Transactions of the ASAE, 33(2), 629-636.

Srivastava, A.K., Herum, F.L., Stevens, K.K. 1976. Impact parameters related to physical damage to corn kernel. Transactions of the ASAE, 19, 1147-1151.

Studman, C. 1997. Factors affecting the bruise susceptibility of fruit. In: Jeronimidis, G.J., Vincent, J.F.V. Plant Biomechanics 1997 Conference Proceedings I, University of Reading, 273-281.

Studman, C.J., Pang, W. 1990. Mechanics of fruit damage. Project report to New Zealand Apple and Pear marketing board. Massey university, Palmerston North, New Zealand.

Studman, C.J., Brown, G.K., Timm, E.J., Schulte, N.L., Vreede, M.J. 1997. Bruising on blush and non-blush sides in apple-to-apple impacts. Transactions of the ASAE, 40(6), 1655-1663.

Tabor, D. 1951. Hardness of metals. Oxford University Press, London.

Taguchi, Y.H. 1992. Powder turbulence-direct onset turbulent-flow. Journal de physique II, 2, 2103-2114.

Tanaka, K., Nishida, M., Kunimochi, T., Takagi, T. 2002. Discrete element simulation and experiment for dynamic response of two-dimensional granular matter to the impact of a spherical projectile. Powder technology, 124, 160-173.

Tennes, B.R., Zapp, H.R., Marshall, D.E., Armstrong, P.R. 1990. Apple handling impact data acquisition and analysis with an instrumented sphere. Journal of agricultural engineering research, 47, 269-276.

Thomson, G.E., Cotter, D.F. , Daly, P.A. 1996. Temperature effects on bruise darkness of 'Granny Smith', 'Golden Delicious', and 'Jonathan' apples. New Zealand journal of crop and horticultural science, 24(1), 99-101.

Thornton, C., Ning, Z., Wu, C-y, Nasrullah, M., Li, L-y. Contact mechanics and coefficient of restitution. 2001. In Pöschel, T., Luding, S. Granular gases, Lecture notes in physics, 564, 184-194, Springer, Berlin.

Thornton, C., Ning, Z. 1998. A theoretical model for the stick/bounce behaviour of adhesive, elastic-plastic spheres. Powder technology, 99, 154-162.

Tijskens, E., Loodts, J., Van Zeebroeck, M., Van Liedekerke, P., Dintwa, E., Ramon, H. 2004. Particle simulations with DEMeter++. Proceedings of 2004, September 12-16, Leuven, Belgium, paper no 04-w3-568.

Tijskens, E., Ramon, H., De Baerdemaeker, J., 2003. Discrete Element Modelling for Process Simulation in Agriculture. Journal of sound and vibration, 266, 493-514.

Tijskens, E., Van Zeebroeck, M., Ramon, H., De Baerdemaeker, J., Van Canneyt, T. 2002a. DEM modelling of agricultural processes: an overview of recent projects. In: H. Konietzky (Ed) Numerical Modelling in micromechanics via particle methods. A.A. Balkema, Rotterdam, The Netherlands, 87-92.

Tijskens, E., Van Zeebroeck, M., Ramon, H., De Baerdemaeker, J, Van Canneyt. 2002b. DEM modelling for agricultural processes: an overview of recent projects. First International PFC Symposium, November 6-8, Gelsenkirchen, Germany.

Tijskens, E., Van Zeebroeck, M., Van linden, V., Van Liedekerke, P., Ramon, H., De Baerdemaeker, J. 2001. DEM modelling of agricultural processes: an overview of recent projects. Proceedings of the fourth international conference on mathematical modelling an simulation in Ago- and Bio-industries. June 12-14, Haifa, Israel.

Timm, E.J., Bollen, A.F., Dela Rue, B.T., Woodhead, I.M. 1998. Apple damage and compressive forces in bulk bins during orchard transport. Applied engineering in agriculture, 14(2), 165-172.

Timm, E.J., Brown, G.K., Armstrong, P.R. 1996. Apple damage in bulk bins during semi-trailer transport. Applied engineering in agriculture, 12(3), 369-377.

Timm, E.J., Schulte-Pason, G.K., Bown, G.K, Burton C.L. 1989. Apple and impact surface effects on bruise size. ASAE paper no 89-6048, St. Joseph, Michigan.

Timoshenko, S., Goodier, J.N. 1951. Theory of elasticity. 3rd Edn. McGraw-Hill, New York.

Tsuji, Y., Kawaguchin T., Tanaka, T. 1993. Discrete particle simulation of two-dimensional fluidized bed. Powder technology, 77, 79-87.

Tsuji, Y., Tanaka, T., Ishada, T. 1992. Langrangian numerical simulation of plug flow of cohesionless particles in a horizontal pipe, Powder technology, 71, 239-250.

Van Lancker, J. 1979. Bruising of unpeeled apples and potatoes in relation with temperature and elasticity. Lebensmittel wissenscchaft und technologie, 12, 157-161.

Van Lancker, J., Kermis, L., De Bruyn, De Smey, F., Ottermans, G. 1975. Reologie en schuifspanningen bij aardappelen. Het ingenieursblad, 10.

Van linden, V., Van Zeebroeck M, Deli, V., Ramon, H. De Baerdemaeker, J. 2002a. Blutsschade van Jonagold: waar knelt het?, Belgische fruitrevue. Vakblad voor pomologische verenigingen en B.F.O., 54(4), 20-22.

Van linden, V., Van Zeebroeck, M., Deli, V., Ramon, H., De Baerdemaeker, J. 2002b. Blutsgevoeligheid: waar knelt het?, Fruitteeltnieuws, Maart 2002.

Van Woensel, G. De Baerdemaeker J. 1983. Mechanical properties of apples during storage. Lebensmittel wissenschaft und technologie, 16, 367-372.

Van Zeebroeck, M., Dintwa, E., Tijskens, E., Deli, V., Loodts, J., De Baerdemaeker, J., Ramon, H. 2003a. Determining tangential contact force model parameters for viscoelastic materials (apples) using a rheometer. Proceedings of the 4th plant biomechanics conference, July 20-25, East Lansing, USA.

Van Zeebroeck, M., Dintwa, E., Tijskens, E., Deli, V., Loodts, J., De Baerdemaeker, J., Ramon, H. 2004a. Determining tangential contact force model parameters for viscoelastic materials (apples) using a rheometer. Postharvest biology and technology, 33, 111-125.

Van Zeebroeck, M., Tijskens, E., Van Liedekerke, P., Deli, V., De Baerdemaeker, J., Ramon, H. 2003b. Determination of the dynamical behaviour of biological materials during impact using a pendulum device. Journal of sound and vibration, 266, 465-480.

Van Zeebroeck, M., Tijskens, E., Dintwa, E., De Baerdemaeker, J., Ramon, H. 2004b. The Discrete Element Method (DEM) to simulate fruit mechanical damage during transport: validation by shaking experiments. Proceedings of AgEng 2004, September 12-16, Leuven, Belgium, paper no 04-w4-513.

Van Zeebroeck, M., Tijskens, E., Dintwa, E., Loodts, J., De Baerdemaeker, J., Ramon, H. 2005. The Discrete Element Method (DEM) to simulate fruit mechanical damage during transport: effect of vibrations during transport on bruise damage. Acta horticulturae Proceedings of Model-it, May 29- June 03, Leuven, Belgium. Accepted.

Venugopal, R., Rajama, I.R.K. 2001. 3D simulation of charge motion in tumbling mills by the discrete element method. Powder Technology, 155, 157-166.

Verstreken, E., Garcia, J. L., Ruiz-Altisent, M., De Baerdemaeker, J. 1995. Controlling moisture loss as a tool to reduce bruise susceptibility. 1 St IFAC/CIGR/EURAGENG/ISHS Workshop on Control Applications in Post-Harvest and Processing Technology (CAPPT'95), June 1-2, Ostend, Belgium.

Vincent, J. F. V. 1989. Relationship between density and stiffness of apple flesh. Journal of the science of food and agriculture, 47, 443-462.

Vincent, J.F.V. 1990. Fracture properties of plants. Advances in botanical research, 17, 235-287.

Vu-Quoc, L., Zhang, X. 1999. An accurate and efficient tangential force-displacement model for elastic frictional contact in particle-flow simulations. Mechanics of materials, 31, 235-269.

Vu-Quoc, L., Zhang, X., Lesburg, L. 2001. Normal and tangential force-displacement relations for frictional elasto-plastic contact of spheres. International journal of solids and structures, 38, 6455-6489.

Vu-Quoc, L. Zhang X. Walton O. R. 2000. A 3-D discrete-element method for dry granular flows of ellipsoidal particles. Computer methods in applied mechanics and engineering, 187, 483-528.

Vu-Quoc, L., Zhang, X. 1999. An elastoplastic contact force-displacement model in the normal direction : displacement-driven version. Proceedings of the royal society of London series A, 455, 4013-4044.

Walton, O.R., Braun, R.L. 1986. Viscosity, granular-temperature, and stress calculations for shearing assemblies of inelastic, frictional disks. Journal of rheology, 30(5), 949-980.

Wilson, L.G., Boyette, M.D., Estes, E.A. 1999. Part III: Handling. In: Postharvest handling and cooling of fresh fruits, vegetables, and flowers for small farms, North Carolina cooperative extension service, Horticulture information leaflet 804.

Wright, R.S., Splinter, W.E. 1967. The mechanical behaviour of sweet potato under slow loading rates and impact loading. Transactions of the ASAE, 12, 765-770.

Wu C-y, Li, L-y, Thornton, C. 2003. Rebound behaviour of spheres for plastic impacts. International journal of impact engineering, 28, 929-946.

Wu, N., Pitts, M.J., Davis, D.C., Cavalieri, R.P. 1994. Modelling mechanical behaviour of apple with the finite element method. ASAE paper no 94-3585, St. Joseph, Michigan.

Zapp, H.R., Ehlert, S.H., Brown, G.K., Armstrong, P.R., Sober, S.S. 1989. Instrumented sphere performance: dynamic measurements and demonstration. ASAE paper no 89-0008, St. Joseph, Michigan.

Zapp, H.R., Ehlert, S.H., Brown, G.K., Armstrong, P.R., Sober, S.S. 1990. Advanced instrumented sphere (IS) for impact measurements. Transactions of ASAE, 33(3), 955-960.

Zhang, D., Whiten, W.J. 1998a. An efficient calculation method for particle motion in discrete element simulations. Powder technology, 98, 223-230.

Zhang, D., Whiten, W.J. 1998b. Contact modelling for discrete element modelling of ball mills. Mineral engineering, 11(8), 689-698.

Zhang, D., Whiten, W.J. 1996. The calculation of contact forces between particles using the spring and damping models. Powder technology, 88, 59-64.

Zhang, D., Whiten, W.J. 1999. A new calculation method for particle motion in tangential direction in discrete element simulations. Powder Technology, 102, 235-243.

Zhang, X, Vu-Quoc L. 2002a. A method to extract the mechanical properties of particles in collision based on a new elasto-plastic normal force-displacement model. Mechanics of materials, 34, 779-794.

Zhang, X. Vu-Quoc L. 2000. Simulation of chute flow of soybeans using an improved tangential force-displacement model, 32, 115-129.

Zhang, X., Vu-Quoc, L. 2002b. Modelling the dependence of the coefficient of restitution on the impact velocity in elasto-plastic collisions. International journal of impact engineering, 27, 317-341.